United States Department of Commerce
Technology Administration
National Institute of Standards and Technology

NIST Special Publication 850

4th International Colloquium on Atomic Spectra and Oscillator Strengths for Astrophysical and Laboratory Plasmas

POSTER PAPERS

Jack Sugar and David Leckrone, Editors

The National Institute of Standards and Technology was established in 1988 by Congress to "assist industry in the development of technology . . . needed to improve product quality, to modernize manufacturing processes, to ensure product reliability . . . and to facilitate rapid commercialization . . . of products based on new scientific discoveries."

NIST, originally founded as the National Bureau of Standards in 1901, works to strengthen U.S. industry's competitiveness; advance science and engineering; and improve public health, safety, and the environment. One of the agency's basic functions is to develop, maintain, and retain custody of the national standards of measurement, and provide the means and methods for comparing standards used in science, engineering, manufacturing, commerce, industry, and education with the standards adopted or recognized by the Federal Government.

As an agency of the U.S. Commerce Department's Technology Administration, NIST conducts basic and applied research in the physical sciences and engineering and performs related services. The Institute does generic and precompetitive work on new and advanced technologies. NIST's research facilities are located at Gaithersburg, MD 20899, and at Boulder, CO 80303. Major technical operating units and their principal activities are listed below. For more information contact the Public Inquiries Desk, 301-975-3058.

Technology Services
- Manufacturing Technology Centers Program
- Standards Services
- Technology Commercialization
- Measurement Services
- Technology Evaluation and Assessment
- Information Services

Electronics and Electrical Engineering Laboratory
- Microelectronics
- Law Enforcement Standards
- Electricity
- Semiconductor Electronics
- Electromagnetic Fields[1]
- Electromagnetic Technology[1]

Chemical Science and Technology Laboratory
- Biotechnology
- Chemical Engineering[1]
- Chemical Kinetics and Thermodynamics
- Inorganic Analytical Research
- Organic Analytical Research
- Process Measurements
- Surface and Microanalysis Science
- Thermophysics[2]

Physics Laboratory
- Electron and Optical Physics
- Atomic Physics
- Molecular Physics
- Radiometric Physics
- Quantum Metrology
- Ionizing Radiation
- Time and Frequency[1]
- Quantum Physics[1]

Manufacturing Engineering Laboratory
- Precision Engineering
- Automated Production Technology
- Robot Systems
- Factory Automation
- Fabrication Technology

Materials Science and Engineering Laboratory
- Intelligent Processing of Materials
- Ceramics
- Materials Reliability[1]
- Polymers
- Metallurgy
- Reactor Radiation

Building and Fire Research Laboratory
- Structures
- Building Materials
- Building Environment
- Fire Science and Engineering
- Fire Measurement and Research

Computer Systems Laboratory
- Information Systems Engineering
- Systems and Software Technology
- Computer Security
- Systems and Network Architecture
- Advanced Systems

Computing and Applied Mathematics Laboratory
- Applied and Computational Mathematics[2]
- Statistical Engineering[2]
- Scientific Computing Environments[2]
- Computer Services[2]
- Computer Systems and Communications[2]
- Information Systems

[1] At Boulder, CO 80303.
[2] Some elements at Boulder, CO 80303.

NIST Special Publication 850

4th International Colloquium on Atomic Spectra and Oscillator Strengths for Astrophysical and Laboratory Plasmas

POSTER PAPERS

at the National Institute of Standards and Technology, Gaithersburg, Maryland
September 14–17, 1992

Jack Sugar and David Leckrone,* Editors

Atomic Physics Division
Physics Laboratory
National Institute of Standards and Technology
Gaithersburg, MD 20899

*NASA/Goddard Space Flight Center
Greenbelt, MD

April 1993

U.S. Department of Commerce
Ronald H. Brown, Secretary
National Institute of Standards and Technology
Raymond G. Kammer, Acting Director

National Institute of Standards
and Technology
Special Publication 850
Natl. Inst. Stand. Technol.
Spec. Publ. 850
199 pages (Apr. 1993)
CODEN: NSPUE2

U.S. Government Printing Office
Washington: 1993

For sale by the Superintendent
of Documents
U.S. Government Printing Office
Washington, DC 20402

Sponsors

National Institute of Standards and Technology
National Aeronautics and Space Administration
Naval Research Laboratory
U.S. Department of Energy, Office of Fusion Energy
National Science Foundation
Computer Sciences Corporation
IBM

Program Committee

D. Leckrone (Chairman), NASA, Goddard Space Flight Center, Greenbelt, MD
S. Adelman, CITADEL, Charleston, SC
R. C. Elton, Naval Research Laboratory, Washington, D.C.
J. E. Hansen, Zeeman Laboratory, University of Amsterdam
S. Johansson, University of Lund, Sweden
R. McKnight, U.S. Department of Energy, Germantown, MD
D. Morton, Herzberg Institute of Astrophysics, NRC, Ottawa, Canada
J. Sugar, NIST, Gaithersburg, MD

Organizing Committee

J. Sugar (Chairman), NIST, Gaithersburg, MD
R. Bell, University of Maryland, College Park, MD
L. Curtis, University of Toledo, Toledo, OH
G. Doschek, Naval Research Laboratory, Washington, D.C.
D. Leckrone, NASA, Goddard Space Flight Center, Greenbelt, MD
W. Wiese, NIST, Gaithersburg, MD

Colloquium Description

This was the fourth in a series of colloquia begun at the University of Lund, Sweden in 1983 and subsequently held in Toledo, Ohio and Amsterdam, The Netherlands. The purpose of these meetings is to provide an international forum for communication between major users of atomic spectroscopic data and the providers of these data. This affords an opportunity for the users to review their present and future needs and the providers to review their laboratory capabilities, new developments in data measurement, and improved theoretical capabilities. These data include atomic wavelengths, line shapes, energy levels, lifetimes, and oscillator strengths. Speakers were selected from a wide variety of disciplines including astrophysics, laboratory plasma research, spectrochemistry, and theoretical and experimental atomic physics.

Contact between data users and providers has grown even more critical today with the prolific acquisition of data from space-based astrophysical observatories, with high temperature laboratory experiments in fusion energy and x-ray lasers, and with the demands for higher accuracy and large quantities of data from neutral to highly ionized atoms. The means of delivery of these data with new light sources such as the tokamak, the electron beam ion trap (EBIT), laser-generated plasmas, inductively-coupled plasmas (ICP), and with new techniques such as laser-induced fluorescence and fourier transform spectroscopy, has advanced considerably.

These colloquia assist in matching these resources with the current and anticipated demands for atomic data.

Format

The program consisted of presentations by invited speakers and poster sessions. One session was devoted to an informal workshop at which users of data briefly described their most immediate needs and providers of data give brief summaries of work currently in progress. The invited papers will be published in a topical issue of Physica Scripta.

Table of Contents

Lifetimes-theory

Lifetimes – measurements

Sun and Stars

Laboratory Sources

Atomic Structure-theory

Databases

Lifetimes-theory

Transition Rates in the $3d^2$ Configuration of the Calcium Isoelectronic Sequence

E. Biémont[1,*], J.E. Hansen[2], P. Quinet[3,$] and C.J. Zeippen[4]

1 Institut d'Astrophysique et Institut de Physique Nucléaire Expérimentale, Université de Liège, B-4000 Liège, Belgium.

2 Van der Waals-Zeeman Laboratorium, Universiteit van Amsterdam, NL-1018 XE Amsterdam, The Netherlands.

3 Faculté des Sciences, Université de Mons-Hainaut, B-7000 Mons, Belgium.

4 UPR 261 du CNRS et DAMAp, Observatoire de Paris, F-92195 Meudon, France.

Abstract

Transitions emitted from the $3d^n$ configurations are important in hot plasmas of low electron density (i.e. in astrophysical objects or in Tokamak devices) where magnetic dipole (M1) or electric quadrupole (E2) transitions become observable due to low collisional rates for the deexcitation from metastable levels. In this work, we concentrate on the study of the forbidden (M1 and E2) transitions appearing in the $3d^2$ ground configuration of the Ti III to Ag XXVIII Ca-like ions. Three different theoretical methods (MCDF, HFR and SST) taking configuration interaction into account are compared with respect to their ability to predict energy levels and radiative transition rates for the forbidden lines considered. The probabilities for the $3d^2$-3d4s transitions, which might significantly contribute to the depopulation processes of the 3d4s levels are also predicted. It is shown that the methods considered in our work are basically equivalent, in their respective range of applicability, for the prediction of accurate oscillator strengths.

* Senior Research Associate of the Belgian FNRS.

$ Holder of an IRSIA Fellowship.

Oscillator strengths of astrophysical interest for OI-sequence

K S Baliyan* and A K Bhatia

Laboratory for Astronomy and Solar Physics, NASA/Goddard Space Flight Center
Greenbelt, Maryland 20771 USA

X-ray and UV emission lines due to the transitions in the ions of oxygen iso-electronic sequence are frequently observed in the spectra of astrophysical objects, such as solar flares, active Sun, supernova remnants and other stellar objects. Many of these lines are listed by Acton et al. [1] and Doschek and Cowan [2] for the 10- 200 Å range and recently by Feldman and Doschek [3] for 910- 1200Å range. Most of the lines in this spectral region are from the transitions in the highly ionized atoms. This spectral information may be used to determine the gas temperature and the density of the emitting plasma through diagnostic emission line ratios. To evaluate these quantities accurate oscillator strengths and electron- excitation rates are required.

Here we report oscillator strengths for several transitions among the ground and excited states of the oxygen-like Ca XIII ion. We will also discuss intercombination transition OI($^3P^e - 2s^2 2p^3 3s\ ^5S^o$). Extensive configuration interaction wavefunctions have been used for the states involved in the transitions. The calculations are performed in both, the LS and the intermediate coupling schemes. In a configuration interaction calculation, the atomic wavefunctions have a form of a configuration state function superposition,

$$\Phi_j(\mathrm{LS}) = \sum_{i=1}^{m} a_{ij}\phi_i(\alpha_i \mathrm{LS}) \tag{1}$$

in the LS coupling or

$$\Phi_j(\mathrm{J}) = \sum_{i=1}^{m} a_{ij}\phi_i(\alpha_i \mathrm{L_i S_i J}) \tag{2}$$

in the Breit-Pauli approximation. For a given set of $\{\phi_i\}$, the variationally optimal values of the mixing coefficients a_{ij} are the components of the eigenvectors of the Hamiltoinian matrix. The configuration state functions $\{\phi_i\}$ are built using the one electron orbitals:

$$u_{nlm_l m_s}(r) \ = \ \frac{1}{r} P_{nl}(r) Y_l^{m_l}(\theta,\phi)\chi^{m_s}(s) \tag{3}$$

and radial functions are expressed in analytic form as:

$$P_{nl}(r) = \sum_{i=1}^{k} c_i r^{p_i} \exp(-\zeta_i r). \tag{4}$$

Several choices of the orbital basis set were considered. The final CI calculation has been performed using an orthogonal basis set,

$$\{1s, 2s, 2p, 3s, 3p, 3d, 4s, 4p, 4d, 5s, 5p\}.$$

The 1s,2s and 2p orbitals were taken from tables of Clementi and Roetti [4] given for the

*NAS-NRC Research Associate

ground state $2s^2 2p^4\ ^3P^e$. The radial functions for the rest of the orbitals are obtained by using CIV3 [5] program. The 3s radial functions were obtained by minimizing 3s $^3S^o$ state energy. Since 3s function in 3s $^5S^o$ is different from the one in 3s $^3S^o$, we used 4s orbital to optimize on

Table 1

Transition	Oscillator strength			
i-f	L(CI1)	V(CI1)	L(CI2)	V(CI2)
$2s^2 2p^4\ ^3P$- $2p^3 3s\ ^3S^o$	4.1697(-2)	4.0866(-2)	4.169(-2)	4.166(-2)
$2s^2 2p^4\ ^3P$- $2p^3 3d\ ^3S^o$	1.7528(-1)	1.5496(-1)	1.7657(-1)	1.5019(-1)
$2p^3 3s\ ^3S^o$- $2p^3 3p\ ^3P^e$	2.5036(-1)	2.4638(-1)	2.8110(-1)	3.4670(-1)
$2s^2 2p^4\ ^3P$- $2p^3 3s\ ^3D^o$	6.3385(-2)	6.1239(-2)	6.0918(-2)	5.9899(-2)
$2s^2 2p^4\ ^3P$- $2p^3 3d\ ^3D^o$	2.8840(-1)	2.7423(-1)	2.9629(-1)	2.7486(-1)
$2s^2 2p^4\ ^3P$- $2p^3(^2D^o)3d\ ^3D^o$	5.1729(-1)	4.8677(-1)	5.2596(-1)	4.8658(-1)
$2s^2 2p^4\ ^3P$- $2s2p^5\ ^3P^o$	1.0997(-1)	9.8608(-2)	1.1008(-1)	9.5607(-1)
$2s^2 2p^4\ ^3P$- $2p^3 3s\ ^3P^o$	3.6415(-2)	3.7456(-2)	3.5578(-2)	3.744(-2)
$2p^3 3s\ ^3P^o$- $2p^3 3p\ ^3S^e$	2.7871(-2)	2.9125(-2)	2.6894(-2)	2.8229(-2)
$2s2p^5\ ^3P^o$- $2s2p^4 3s\ ^3S^e$	1.5507(-2)	1.6761(-2)	1.5236(-2)	1.7036(-2)
$2s^2 2p^4\ ^1D^e$- $2s2p^5\ ^1P^o$	1.4075(-1)	1.0441(-1)	1.3985(-1)	1.0278(-1)
$2s^2 2p^4\ ^1D^e$- $2p^3 3s\ ^1P^o$	3.0290(-2)	3.2023(-2)	2.9394(-2)	3.2165(-2)
$2s^2 2p^4\ ^1D^e$- $2p^3 3s\ ^1D^o$	1.0115(-1)	9.8737(-2)	9.6989(-2)	9.5700(-2)
$2p^3 3s\ ^5S^o$- $2p^3 3p\ ^5P^e$	2.9207(-1)	2.8546(-1)	2.9628(-1)	2.8180(-1)
$2p^3 3p\ ^5P^e$- $2s2p^4 3p\ ^5S^o$	1.8533(-2)	1.2398(-2)	1.8638(-2)	1.3560(-2)

the energy of 3s $^5S^o$ state. The 5s orbital parameters were obtained on the average energy of 4s $^3S^o$ and 4s $^5S^o$ states. The 3p orbital was obtained minimizing ground state energy and 4p was subsequently optimized on the 3p $^3P^e$ state. The average energy of 4p $^3P^e$ and 4p $^5P^e$ was used to obtain parameters for the 5p orbital. The 3d and 4d orbitals were obtained minimizing 3d $^3D^o$ and 4d $^5D^o$ states respectively. In all 1221 configurations were formed for 21 even and odd parity symmetries using these orbitals in CI1 calculation while a limited set of configurations ($a_{ij} > 0.005$) was retained in CI2 calculation (see table 1).

In general, there is a good agreement between the calculated energies of the states and the values given by Sugar and Corliss [6]. These CI wavefunctions are used to calculate oscillator strengths in the dipole length and velocity formulation. Most of the length and velocity f-values agree within 10%. But for some of the transitions they differ by as much as 50%. This is mainly due to the use of common basis orbital set. These transitions need be considered separately. The intermediate coupling f-values are obtained by including the spin-orbit (S-O), spin spin (SS), spin-other orbit(S-O-O), mass correction and Darwin terms of the Breit-Pauli operator in the non-relativistic Hamiltonian. These calculations were performed using the configurations of the CI2 model. The f-values for some transitions calculated in the LS and intermediate coupling are given in tables 1 and 2, respectively. It was observed that S-O-O term plays very important role in the case of intercombination transitions. The inclusion of this term reduces the f-value for these transitions by a factor of half while it has little effect on the spin allowed transitions.

The ground state intersystem transitions of OI at 1355.6 and 1358.5Å are important probe of the oxygen abundance in interstellar medium and are potentially observable in the high resolution spectra of stars (Leckrone and Adelman [7]). We used an extensive CI basis and obtained 4.28×10^{-6} as gf-value for $^3P_2$ - $2p^3 3s\ ^5S^o_2$ transition in OI. The detailed results will be presented at the conference.

Table 2

Transition *i-f*	Oscillator strength L	V
$2s^2 2p^4\ ^3P_2$- $2s2p^3 3s\ ^3S^o_1$	4.4074(-2)	4.5300(-2)
$2s^2 2p^4\ ^3P_1$- $2s2p^3 3s\ ^3S^o_1$	3.4895(-2)	3.4984(-2)
$2s^2 2p^4\ ^3P_0$- $2s2p^3 3s\ ^3S^o_1$	4.0848(-2)	4.0149(-2)
$2s^2 2p^4\ ^3P_2$- $2s2p^3 3s\ ^5S^o_2$	5.7436(-4)	5.7590(-4)
$2s^2 2p^4\ ^3P_1$- $2s2p^3 3s\ ^5S^o_2$	1.3444(-4)	1.3510(-4)
$2s^2 2p^4\ ^3P_2$- $2s2p^3 3s\ ^3D^o_3$	4.8491(-2)	4.9174(-2)
$2s^2 2p^4\ ^3P_2$- $2s2p^3 3s\ ^3D^o_2$	2.0743(-2)	2.1229(-2)
$2s^2 2p^4\ ^3P_2$- $2s2p^3 3s\ ^3D^o_1$	8.5226(-4)	8.6304(-4)
$2s^2 2p^4\ ^3P_1$- $2s2p^3 3s\ ^3D^o_2$	2.6739(-2)	2.6185(-2)
$2s^2 2p^4\ ^3P_1$- $2s2p^3 3s\ ^3D^o_1$	2.3912(-2)	2.3767(-2)
$2s^2 2p^4\ ^3P_0$- $2s2p^3 3s\ ^3D^o_1$	3.6865(-2)	3.5418(-2)
$2s^2 2p^4\ ^3P_1$- $2s2p^3 3s\ ^3P^o_2$	2.7642(-2)	2.8159(-2)
$2s^2 2p^4\ ^3P_2$- $2s2p^3 3s\ ^3P^o_1$	4.4341(-3)	4.5546(-3)
$2s^2 2p^4\ ^3P_1$- $2s2p^3 3s\ ^3P^o_1$	7.1692(-3)	7.4349(-3)
$2s^2 2p^4\ ^3P_1$- $2s2p^3 3s\ ^3P^o_0$	1.2015(-2)	1.2366(-2)
$2s2p^5\ ^3P^o_0$- $2s2p^3 3p\ ^3P_1$	2.7593(-4)	2.9368(-4)
$2s^2 2p^4\ ^1D_2$- $2s2p^5\ ^3P^o_2$	2.6433(-3)	2.6984(-3)
$2s2p^3 3s\ ^5S^o_2$- $2s2p^3 3p\ ^5P_2$	9.9538(-2)	9.3898(-2)
$2s2p^3 3s\ ^5S^o_2$- $2s2p^3 3p\ ^5P_1$	5.9212(-2)	5.6578(-2)
$2s2p^3 3s\ ^5S^o_2$- $2s2p^3 3p\ ^3P_2$	1.7761(-3)	1.6263(-3)

We wish to thank Dr D S Leckrone for helpful discussions. This work was funded by NASA-RTOP-188-38-53-14 grant. One of us (KSB) is thankful to NRC for research associateship.

1. Acton LW, Bruner ME and Brown WA 1985 Ap J **291** 865.

2. Doschek GA and Cowan RD 1984 Ap J (suppl) **56** 67.

3. Feldman U and Doschek GA 1991 Ap J(suppl) **75** 925.

4. Clementi E and Roetti C 1974 At. Data Nucl. Data Tables **14** 177.

5. Hibbert A 1975 Comput.Phys.Commun.**9** 141.

6. Sugar J and Corliss C 1985 J. Phys. Chem. Ref. Data **14** (suppl.2).

7. Leckrone DS and Adelman SJ 1986 in 'New Insights in Astrophys.' ed EJ Rolfe, p 65.

Radiative data for Si-like ions: Si^0, S^{2+}, A^{4+}, Ca^{6+}

Sultana N. Nahar and Anil K. Pradhan
Dept of Astronomy, The Ohio State University, Columbus, OH 43210

Radiative data such as photoionization cross sections, oscillator strengths, energy levels for Si - like ions, Si^0, S^{2+}, A^{4+} and Ca^{6+} are obtained as a part of the Opacity Project (OP) [1]. Calculations are carried out in the close coupling (CC) approximation using the R-matrix method [2]. Partial photoionization cross sections of the ^3P ground state of each ion into various excited states of the residual ion are obtained.

Large number of bound states with $n \leq 10, \iota \leq 5$ are considered, amounting to a few hundred excited states for each atom and ion. Table I shows number of bound $SL\pi$'s and the corresponding number of excited bound states for each ion. All calculated energies for Si^0, S^{2+}, A^{4+} and Ca^{6+} agree in less than 5% with the observed values except for a few excited states of Si^0. Table I presents observed and calculated ionization energies (I.P.) of the ^3P ground state of each ion.

Detailed photoionization cross sections, including autoionizing resonances, of all the excited bound states, N_{bnd}, for each ion are obtained. Photoionization cross sections of the ^3P ground state of Si-like ions are presented in the lowest panels of Figs. 1(a) - (d). Presence of a wide resonance near the threshold for Si^0 can be observed in Fig. 1(a). The upper panels of Figs.1(a) - (d) exhibit partial photoionization cross sections of the ground state in to various exctied thresholds of the residiual ion. Partial cross sections are important in the determination of level populations under non-LTE conditions. The excited state photoionization cross sections usually show nonhydrogenic behavior. Excited states that are coupled to the ground state of the residual ion show wide PEC (photoexcitation-of-core) resonances in the cross section profile. PEC's are due to excitation of the core to dipole allowed states while the outer electron remain as a spectator. The PEC resonances can enhance the background cross sections significantly. Example of PEC features will be illustrated in poster presentation. Except for a number of states of Si^0, the photoionization cross sections detailed with autoionizing resonances and for a large number of states of S^{2+}, A^{4+} and Ca^{6+} are obtained for the first time as known to the authors.

Dipole oscillator strengths for transitions among all bound states with $n \leq 10$ are obtained in LS multiplets. Table I shows the number of oscillator strengths obtained for each ion. A short comparison is made with the available theoretical and experimental values in Table II. Oscillator strengths of Si^0 show good agreement with the values mesasured recently using laser induced flourescence, so are the oscillator strengths of S^{2+} with a number of measured values obtained using beam-foil technique. Good comparison of oscillator strengths of A^{4+} and Ca^{6+} is also found with the very little available data.

References

1. "Atomic Data for Opacity Calculations" XVI, Sultana N. Nahar and Anil K. Pradhan, J.Phys. B (submtted).
2. M. J. seaton, J. Phys. B **20**, 6363 (1987); K.A. Berrington, P.G. Burke, K. Butler, M.J. Seaton, P.J. Storey, K.T. Taylor, and Yu Yan, J. Phys. B **20**, 6379 (1987).
3. T.R. O'Brian and J.E. Lawler, Phys. Rev. A 44, 7134 (1991).
4. U. Becker, H. kerhoff, M. Kwiatkowski, M. Schmidt, U. Teppner and P. Zimmermann, Phys. Rev. Lett. 76A, 125 (1980).
5. Berry H G, Schectman R M, Martinsen I, Bickel W S, and Bashkin S J, J. Opt. Soc. Am. **60**, 335 (1970).
6. Livingston A E, Dumont P D, Baudinet-Robinet Y, Garnir H P, Biemont E, and Grevesse N, in "Beam-Foil Spectroscopy", eds. I.A. Sellin and D.J. Pegg, (Plenum, New York), p. 339, 1976.
7. Ryan L J, Rayburn L A, and Cunningham A J, J. Quant. Spectrosc. Radiat. Transfer **42**, 295 (1989).
8. Irwin D J G, Livingston A E and Kernahan J A, Nucl. Inst. Meth. **110**, 111 (1973).
9. Biemont E, J. Opt. Soc. Am. B **3**, 163 (1986).

* This work has been carried out on the Cray Y-MP at the Ohio Supercomputer Center and is supported partially by a grant from NSF (PHY- 9115057).

Table I: Ionization potential, I.P., of the ions; $N_{SL\pi}$ is the total number of bound symmetries and N_{bnd} is the corresponding number of bound states with $n \leq 10$ and $l \leq 5$ for each ion; N_f is the number of oscillator strengths obtained for each ion.

Ion	I.P.(Ry) obs	I.P.(Ry) cal	$N_{SL\pi}$	N_{bnd}	N_f	Ion	I.P.(Ry) obs	I.P.(Ry) cal	$N_{SL\pi}$	N_{bnd}	N_f
Si^0	0.598	0.601	27	218	3149	A^{4+}	5.515	5.499	36	342	7863
S^{2+}	2.573	2.574	31	236	3973	Ca^{6+}	9.389	9.364	40	497	16961

Table II: Oscillator strengths of Si^0, S^{2+}, A^{4+}, and Ca^{6+}.

Transition		Si^0 f OP	Si^0 f expt	Transition		S^{2+} f OP	S^{2+} f expt
$3p^2$ - 3p4s	^3P - $^3P^o$	0.236	0.211[3]	$3p^2$ - 3s3p^3	^3P - $^3D^o$	0.024	0.022±.002[5],.022[6]
	^1D - $^1P^o$	0.195	0.163[3],0.170[4]		^3P - $^3P^o$	0.043	0.036[6]
	^1S - $^1P^o$	0.101	0.0913[3],0.098[4]		^1D - $^1D^o$	1.02	0.99±0.10[8]
$3p^2$ - 3p3d	^3P - $^3P^o$	0.053	0.0513[3]	$3p^2$ - 3p3d	^3P - $^3D^o$	1.670	0.96±0.19[7]
	^1D - $^1P^o$	0.0056	0.0029[3],0.0036[4]		^1D - $^1D^o$	0.021	0.0167±0.0005[5]
	^1D - $^1D^o$	0.041	0.040[3]	3p4p - 3p4d	^3D - $^3F^o$	0.947	0.685±0.05[5]
	^1D - $^1F^o$	0.358	0.318[3]	$3p^2$ - 3p4s	^1D - $^1P^o$	0.094	0.07±0.04[7]
	^1S - $^1P^o$	0.409	0.331[3],0.355[4]		^1S - $^1P^o$	0.066	0.08±0.05[7]
$3p^2$ - 3s3p^3	^3P - $^3D^o$	0.051	0.056[3]				

		A^{4+} OP	A^{4+} expt			Ca^{6+} OP	Ca^{6+} Ref. 9
$3p^2$ - 3s3p^3	^3P - $^3P^o$	0.061	0.057±0.002[8]	$3p^2$ - 3s3p^3	^3P - $^3S^o$	0.268	0.249
	^3P - $^3S^o$	0.306			^1D - $^1P^o$	0.250	0.236
	^3P - $^3D^o$	0.042			^1D - $^1D^o$	0.088	0.096
$3p^2$ - 3p3d	^3P - $^3P^o$	0.581			^1S - $^1P^o$	0.175	0.191
	^3P - $^3D^o$	1.411		$3p^2$ - 3p3d	^3P - $^3D^o$	1.133	1.082
	^1D - $^1F^o$	1.212			^3P - $^3P^o$	0.460	0.399
	^1S - $^1P^o$	2.270			^1D - $^1D^o$	0.678	0.504
$3p^2$ - 3p4s	^3P - $^3P^o$	0.147			^1D - $^1F^o$	0.974	0.896

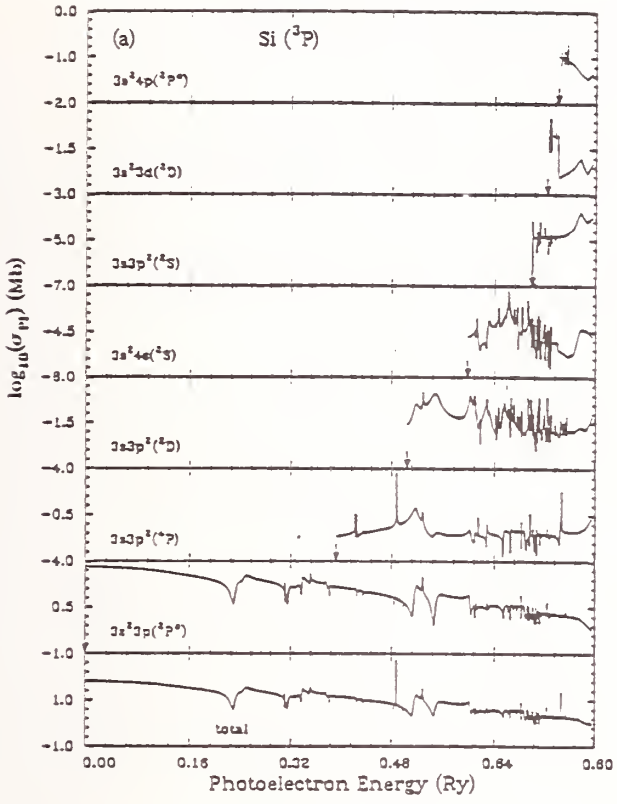

Fig. 1(a)

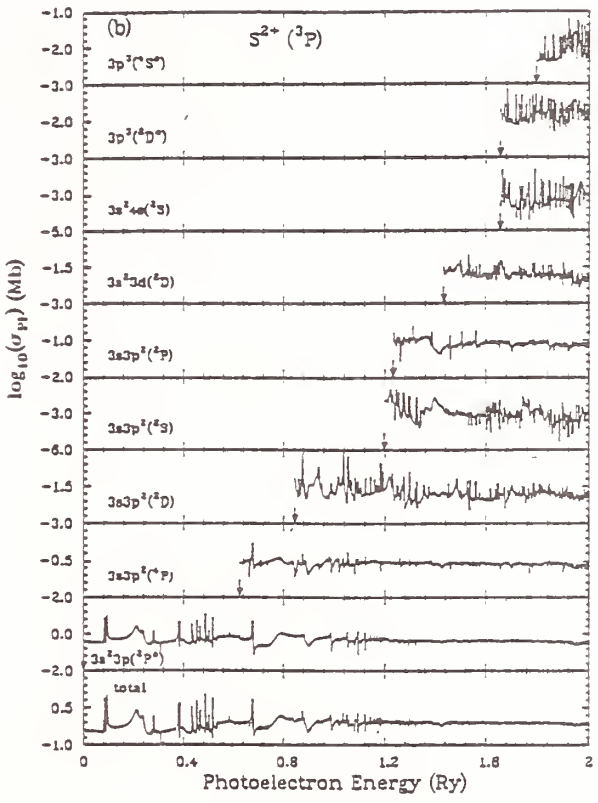

Fig. 1(b)

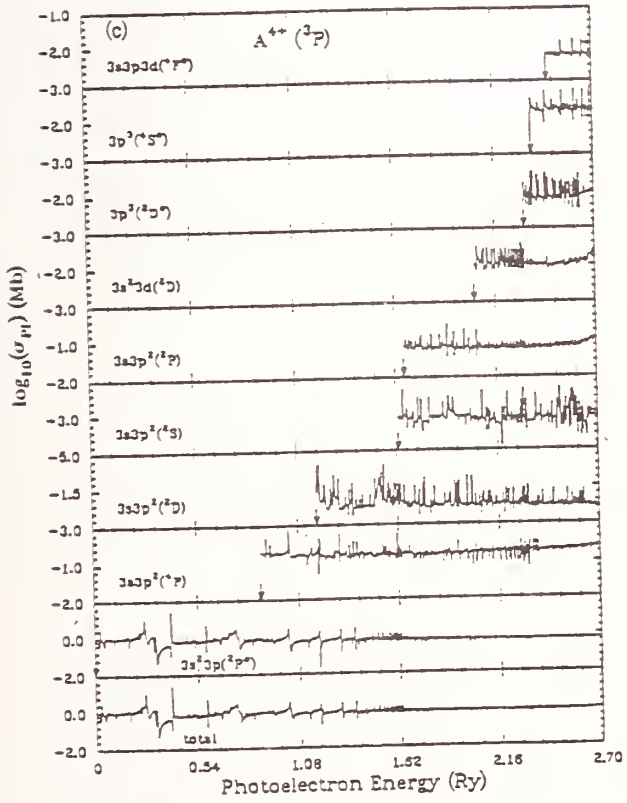

Fig. 1(c)

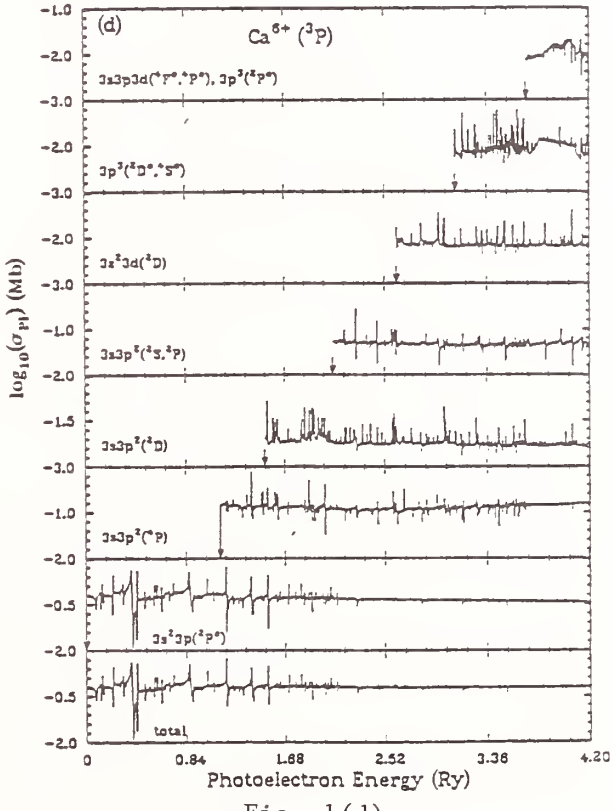

Fig. 1(d)

Fig.1 Partial photoionization cross sections of the ground state of Si-like ions into various excited states of the residual ions.

Large scale radiative and collisional calculations for Fe II

Sultana N. Nahar and Anil K. Pradhan
Dept of Astronomy, The Ohio State University, Columbus, Ohio 43210

Large scale computations are in progress to obtain radiative data for energy levels, oscillator strengths and photoionization cross sections, and for collision strengths of Fe II. Calculations are carried out in the close coupling (CC) approximation using the R-matrix method.

We define the atomic or ionic system as (N+1) electron system, and the residual ion or the target as the N-electron system. In CC approximation, the wave function of the (N+1) electron system is expanded in terms of target states as

$$\Psi^{SL\pi}(E) = A \sum_{i=1}^{I} \chi_i(r^{-1})\theta_i + \sum_{j=1}^{J} c_j \Phi_j, \qquad (1)$$

where $\chi_i(r^{-1})$'s are the target states, and $\theta_i(r)$'s are the free electron wave functions, Φ_j's are square-integrable correlation type function for the bound states of the (N+1) electron system, and c_j's are variational parameters.

COLLISIONAL CALCULATIONS: Two sets of CC calculations, (1) a 38-term expansion in LS coupling and (2) a 41-level fine structure calculations in the Breit-Pauli approximation have been carried out for detailed collision strengths, Ω, including resonance structures. The first set includes the quartet and sextet terms and Ω's for 703 transitions in LS coupling are obtained. The second set includes a number of important fine structure levels from the quartet and sextet multiplets and Ω's for 820 transitions are obtained. The autoionizing structures enhance the background significantly. Computations are under progress now to carry out collision strength calculations using the 38-state LS exapnsion split into 142 J values for fine sructure transitions by algebraic transformations. This will result in collision strengths and rates for about 10,000 fine structure transitions of Fe II.

RADIATIVE CALCULATIONS: The complication in computation of Fe II radiative data arises because of large number of closely spaced energy levels of the "target" or residual ion Fe III requiring large CC expansions for Fe II system. Studies of effect of correlations were made using several sets of CC expansions. In the present calculations, a total of 83 Fe III states have been included to carry out CC calculations of Fe II. Table I shows number of target states, N_{CC}, that are included in CC expansion for each type of symmetry. $N_{SL\pi}$, the number of $SL\pi$, that form bound states and total number of corresponding bound states for each type of symmetry of Fe II are also given in the Table. Photoionization cross secitons are obtained for all bound states. Cross sections for photoionization of $3d^5 4s\ ^6D$ ground state of Fe II are presented in Fig. 1.

Present calculations are carried out in LS coupling. Table II shows number of oscillator strengths obtained for allowed bound-bound transitions for each kind of symmetry. The f-values or the oscillator strengths obtained in LS multiplet are now being converted to fine structure transitions using relative line strength scheme. The accuracy of fine structure f-values are improved by use of observed energies in JJ. Present results are compared with the observed values[1] as well as those of Kurucz[2] in Table II.

References:
1. J.R. Fuhr, G.A. Martin and W.L. Wiese, J. Phys. Chem. Ref. Dt. 17 (AIP, 1988).
2. R.L. Kurucz, "Semiempirical calculation of gf values: Fe II", Smithsonian Astrophysical Observatory Special Report 390 (Cambridge, 1981).

Table I: N_{CC} is the number of target states in the CC expansion, $N_{SL\pi}$ is the number of bound symmtries and N_{bnd} is the corresponding number of bound states ($n \le 10$, $\iota \le 7$). N_f is the number of oscillator strengths in LS multiplet. * implies partial data from ongoing work.

Symmetry	N_{CC}	$N_{SL\pi}$	N_{bnd}	N_f	Symmetry	N_{CC}	$N_{SL\pi}$	N_{bnd}	N_f
Octets	2	4	6	8	Quartets	58	19	305	9755
Sextets	21	19	200	4127	Doublets	62	12*	196*	4860*

Table II: Fine structure f-values for allowed transtions of Fe II.

Transition	$2J_i+1$	$2J_f+1$	f_{if} Present (OP)	f_{if} Expt[1] (NIST)	f_{if} Kurucz[2] (1981)
^6D - $^6P^o$			0.12633		
	10	8	0.1264	0.11	0.144
	8	8	0.0449	0.051	0.0624
	6	8	0.0099	0.036	0.0401
	8	6	0.0814	0.091	0.0901
	6	6	0.0771	0.10	0.1035
	4	6	0.0377		
	6	4	0.0396	0.032	0.0437
	4	4	0.0887	0.087	0.1137
	2	4	0.1263	0.13	0.194
^6D - $^6D^o$			0.2936	0.26	
	10	10	0.2400	0.22	0.262
	10	8	0.0548	0.065	0.0736
	8	10	0.0675	0.043	0.0456
	8	8	0.1313	0.11	0.135
	8	6	0.0948	0.099	0.117
	6	8	0.1248	0.084	0.088
	6	6	0.0502	0.045	0.052
	6	4	0.1176	0.11	0.133
	4	6	0.1748	0.12	0.133
	4	4	0.0032	0.0037	0.004
	4	2	0.1144	0.10	0.119
	2	4	0.2275	0.18	0.187
	2	2	0.0652	0.050	0.059
^6D - $^6F^o$			0.3976		
	10	12	0.3425		0.37
	10	10	0.0527	0.028	0.038
	10	8	0.0043		
	8	10	0.2888	0.27	0.349
	8	8	0.0968	0.089	0.100
	8	6	0.0122		
	6	8	0.2431	0.20	0.287
	6	6	0.1313	0.12	0.142
	6	4	0.0227	0.019	0.019
	4	6	0.2031	0.19	0.249
	4	4	0.1610	0.14	0.181
	4	2	0.0314	0.031	0.0316
	2	4	0.1747	0.19	0.216
	2	2	0.2199	0.21	0.254

* This work is being carried out on the Cray Y-MP at the Ohio Supercomputer Center and is supported partially by a grant from NSF (PHY- 9115057).

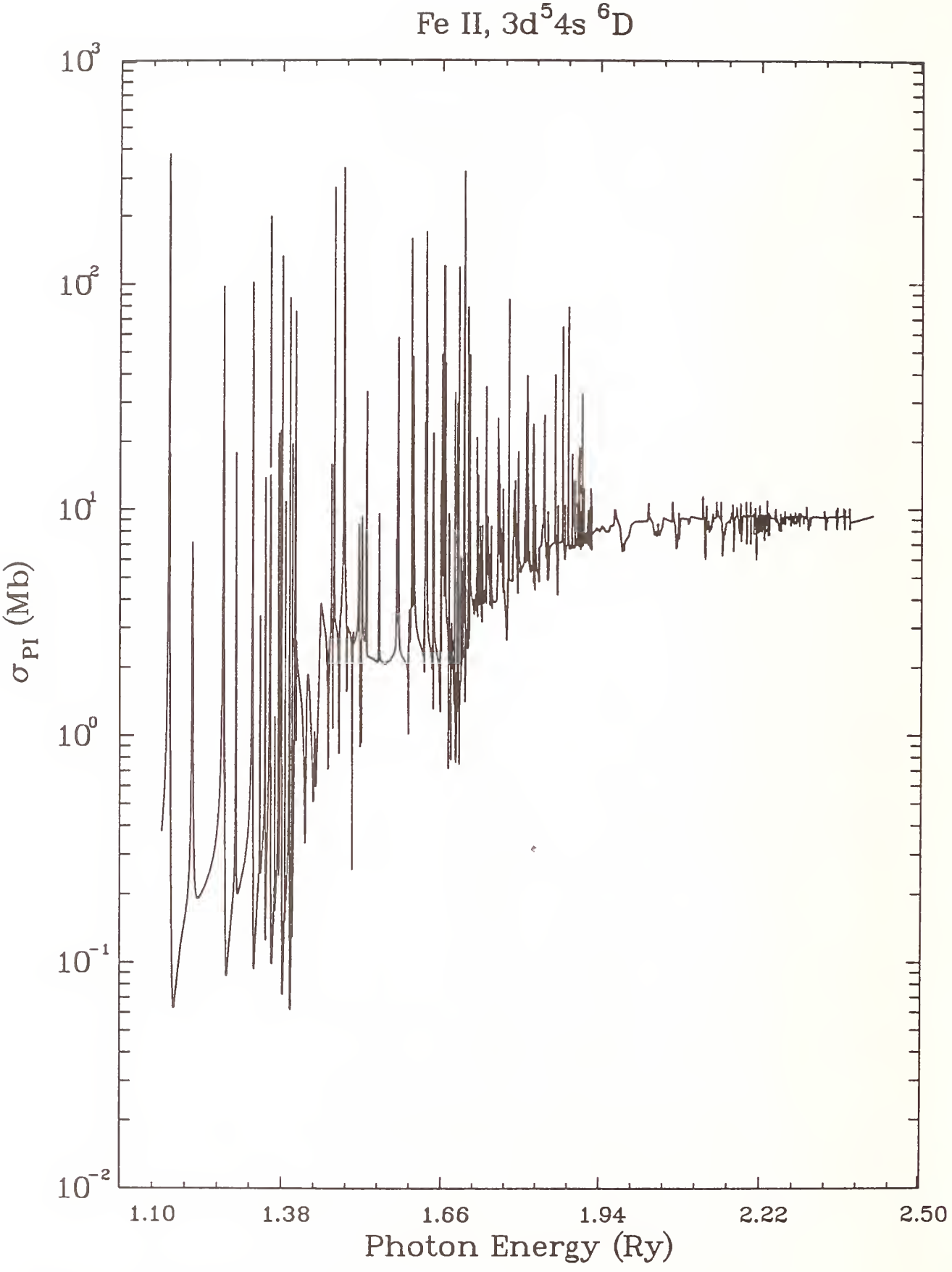

Fig. 1. Photoionization of ^{6}D ground state of Fe II.

Calculation of Oscillator strengths in Hg III

P.H.M.Uylings[1], A.J.J.Raassen[1], A.A. Joueizadeh[2], J.O.Ekberg[2], Se. Johansson[2] and J.-F. Wyart[3]

[1] Van der Waals-Zeemanlaboratorium, Universiteit van Amsterdam, Valckenierstraat 65-67, 1018XE Amsterdam, The Netherlands
[2] Atomic Spectroscopy, Department of Physics, University of Lund, Sölvegatan 14, 223 62 Lund, Sweden
[3] Laboratoire Aimé Cotton, CNRS II, Bât 505, Centre Universitaire, 91405 Orsay, France

Abstract
Log(gf) values for the $5d^{10}+5d^{9}6s+5d^{8}6s^{2}$ - $5d^{9}6p+5d^{8}6s6p$ transition array of Hg III have been calculated by means of several methods. Eigenvectors of the even and odd systems are obtained from diagonalizing a model-Hamiltonian. The radial factors in the Hamiltonian are either taken from ab initio calculations (HXR,HFR) or treated as parameters (fitting the eigenvalues towards the experimental energies). The angular factors of the Hamiltonian are either conventional (Slater-Condon) operators extended with effective operators using Cowan's programs, or orthogonal operators the associated parameters of which have a minimum correlation. The results of the various approaches are compared to each other.

Introduction
The development of Space laboratories, like IUE and HST, has on the one hand side enlarged the accessibility of the wavelength region in the vacuum ultra violet while on the other hand the resolving power of astrophysical observations has increased tremendously. This calls for more and accurate data in the VUV region for all elements of stellar interest. Traditionally, the emphasis lies on the lighter elements but recent observations by the Hubble Space Telescope have indicated very clearly the presence of heavy elements, as Pt and Hg (belonging to the 5d-sequence), in stellar objects, e.g. χ Lupi [1]. These new developments imply the need of accurate data of the heavier elements, which up to now were hardly considered to be of astrophysical interest. It concerns here especially the lower ionization stages: the I-, II- and III-spectra, with a nuclear charge of about 80. Recently the spectrum of Pt III was analyzed by Ryabtsev etal [2], while the analysis of the spectrum of Hg III was extended to higher configurations [3]. For the latter log(gf) values have been calculated and are presented in this poster.

Methods of calculation

The log(gf) values have been calculated in four ways. All four are based on the principle of parametric fitting to experimental level values. Two of them (marked 'HXR' and 'HFR') are obtained from coefficient files produced by Cowan's programs [4]. Both the transition integrals and the interaction integrals R^2(5d5d,6s6s) and R^2(5d5d,5d6s) [the latter scaled down to 80% of their original value], have been calculated by means of Cowan's program in the Hartree-plus-statistical-exchange (HXR) as well as in the Hartree-Fock (HFR) mode including relativistic corrections to the wavefunctions. The values of the interaction integrals were subsequently fixed in the fitting procedure. The other parameters were free to vary. Therefore the difference between the two fits is a result of the different values for the interaction integrals. The eigenvector compositions obtained from the fits were used to calculate the log(gf) values, with HXR or HFR radial transition integrals, respectively. For both calculations the interaction of the even configurations ($5d^{10}$, $5d^96s$ and $5d^86s^2$) was included while for the odd parity a single configuration approach (i.e. only $5d^96p$) was applied.

The two other fits were carried out with an orthogonal operator set [5], including the configuration interaction of the three even configurations. Unless enlarged with additional operators for higher order magnetic or correlation effects, this set gives in principle a description equivalent to the Cowan set or the Slater Condon set. However, the orthogonal set is more stable in the fitting procedure and therefore more suited to extend with operators that describe smaller effects. In the even system (i.e. $5d^96s$), our orthogonal operator set was extended with the Electrostatic Spin-orbit parameter Amso. Next to the usual spin orbit coupling constant ζ_{5d} this parameter describes the strength of the operator $\mathbf{s}_{6s}.\mathbf{l}_{5d}$. In the odd system the parameter set is enlarged with the pendants of the Amso, Z_3 and Z_4, which give the strengths of the operators $\mathbf{s}_{5d}.\mathbf{l}_{6p}$ and $\mathbf{s}_{6p}.\mathbf{l}_{5d}$. Using the orthogonal operator set two calculations were made; one without and one with the interaction with the $5d^86s6p$ configuration.

For the sake of completeness the results of an ab-initio calculation, using Cowan's program in the relativistic mode is given.

[1] D.S. Leckrone, G.M. Wahlgren and Se. Johansson, Astrophys. J. Letters **373**, L33 (1991)

[2] A.N. Ryabtsev, J.-F. Wyart, Y.N. Joshi, A.J.J. Raassen and P.H.M. Uylings, Phys. Scripta (submitted)

[3] J.-F. Wyart, A.J.J. Raassen, Y.N. Joshi and P.H.M. Uylings, Journ. de Physique **2**, 895 (1992)

[4] R.D. Cowan, The Theory of Atomic Structure and Spectra, University of California Press 1981

[5] J.E. Hansen, P.H.M. Uylings and A.J.J. Raassen, Phys. Scripta **37**, 664 (1988)

J.E. Hansen, A.J.J. Raassen, P.H.M. Uylings and G.M.S. Lister, Nucl. Instr. Meth. Phys. Res. **B35**, 134 (1988)

λ_{vac}(Å)	log(gf)					Even Lev		Odd Lev	
	HXR	HFR	OFIS	OFII	ab-in				
3090.93			-3.624	-2.939	-3.289	0	158909	1	126556
2725.23				-2.174	-2.125	4	97893	3	134588
2481.39			-4.923	-3.498	-3.464	0	158909	1	118607
2354.95	-1.926	-1.903	-1.856	-1.753	-1.668	2	61085	2	103549
2245.07	-1.884	-1.863	-1.717	-1.597	-1.436	2	61085	3	105627
2215.15	-2.931	-2.908	-2.895	-2.872	-2.733	1	58405	2	103549
1740.27	-0.560	-0.581	-0.901	-0.994	-2.456	2	61085	2	118548
1738.53	-0.802	-0.778	-0.907	-0.881	-1.220	2	46029	2	103549
1738.47	-0.573	-0.536	-0.589	-0.552	-0.732	2	61085	1	118607
1677.90	0.176	0.200	0.183	0.228	0.248	2	46029	3	105627
1671.06	-0.247	-0.224	-0.173	-0.100	-0.071	2	61085	2	120927
1662.73	-0.341	-0.318	-0.429	-0.447	-0.805	1	58405	2	118548
1661.09			-3.008	-3.406	-2.039	1	58405	1	118607
1652.45	-1.511	-1.490	-1.282	-1.213	-1.110	2	61085	3	121602
1647.47	0.222	0.245	0.235	0.288	0.309	3	42850	2	103549
1599.44	-0.206	-0.183	-0.144	-0.089	0.046	1	58405	2	120927
1592.93	0.023	0.046	0.030	0.056	0.023	3	42850	3	105627
1527.40	-0.115	-0.147	-0.140	-0.096	-0.054	2	61085	1	126556
1467.34	-0.644	-0.620	-0.615	-0.581	-0.498	1	58405	1	126556
1383.19	-0.360	-0.336	-0.351	-0.292	-0.288	1	58405	0	130702
1378.96	0.109	0.132	0.183	0.257	0.359	2	46029	2	118548
1377.83	-0.013	0.010	0.007	0.065	0.109	2	46029	1	118607
1360.50	0.479	0.503	0.486	0.531	0.526	2	61085	3	134588
1352.94	-0.676	-0.653	-0.672	-0.636	-0.594	2	61085	1	134998
1335.14	-0.162	-0.137	-0.278	-0.258	-0.755	2	46029	2	120927
1330.77	0.607	0.631	0.620	0.658	0.661	3	42850	4	117994
1326.38	0.101	0.124	0.107	0.170	0.198	2	61085	2	136479
1323.23	0.088	0.111	0.089	0.124	0.080	2	46029	3	121602
1321.04	-0.946	-0.923	-0.972	-0.869	-1.045	3	42850	2	118548
1305.60	0.048	0.071	0.058	0.111	0.087	1	58405	1	134998
1280.85	-0.009	0.014	0.010	0.051	0.013	1	58405	2	136479
1280.78	-0.970	-0.945	-1.115	-1.094	-1.616	3	42850	2	120927
1269.81	0.296	0.319	0.311	0.368	0.390	3	42850	3	121602
1241.82	-0.480	-0.455	-0.517	-0.497	-0.832	2	46029	1	126556
1129.20			-0.962	-0.949	-0.701	2	46029	3	134588
1123.98			-1.216	-1.258	-1.027	2	46029	1	134998
1105.59			-1.318	-1.265	-1.192	2	46029	2	136479
1090.06			-2.045	-1.921	-1.798	3	42850	3	134588
1068.05			-1.919	-1.969	-1.729	3	42850	2	136479
843.12	-1.322	-1.383	-1.393	-1.327	-1.052	0	0	1	118607
790.16			0.030	0.030	-0.018	0	0	1	126556
740.75			-0.576	-0.587	-0.473	0	0	1	134998

OFIS: Orthogonal fit, even system with configuration interaction, odd system without configuration interaction

OFII: Orthogonal fit, configuration interaction included in the even as well as the odd system

Transitions in neutral chromium

D.J.R. Robinson and A. Hibbert

Department of Applied Mathematics and Theoretical Physics, Queen's University, Belfast, BT7 1NN, N. Ireland.

Introduction

Knowledge of the oscillator strengths in neutral chromium is required for impurity diagnostics in the JET plasma, in particular for the transitions

$$\begin{aligned} 3d^5 4s\ a^{7,5}S &\rightarrow 3d^5 4p\ z^{7,5}P^o \\ &\rightarrow 3d^4 4s 4p\ y^{7,5}P^o \end{aligned}$$

A CI calculation of the septet transitions was undertaken by Hibbert *et al* [1]. Quite good agreement with experiment was obtained for the oscillator strength of the $a - z$ transition, and between the length (f_l) and velocity (f_v) forms. But for the $a - y$ transition, f_l and f_v differed by 30% (though the geometric mean of the two agreed well with experiment).

Present work

One of the major difficulties in obtaining accurate oscillator strengths for the septet transitions is that the radial functions of the $3d$ and $4p$ orbitals vary considerably from state to state. A more accurate representation of these transitions would be

$$\begin{aligned} 3d_1^5 4s\ a^{7,5}S &\rightarrow 3d_2^5 4p_2\ z^{7,5}P^o \\ &\rightarrow 3d_3^4 4s 4p_3\ y^{7,5}P^o \end{aligned}$$

where different subscripts denote different but not orthogonal orbitals. For singly occupied orbitals such as $4p$, it is in principle quite a simple matter to write $4p_3$ as a linear combination of $4p_2$ and another p-function (which below we label $5p$) orthogonal to $4p_2$. Hence the difference between the $4p$ functions for different states can be treated by conventional orthogonal CI. However, in the case of multiply occupied orbitals such as the $3d$ orbital in these transitions, linear combinations of different d-orbitals would require very extensive CI (because of the many angular momentum couplings of the open d-subshells). Moreover, some electron correlation would also be effectively introduced, though not in a systematic way. Thus, in calculation D of [1], with the $3d$ function determined as $3d_3$, the configuration $3d^4 4d 4p$ was included to act as a first-order correction to $3d^5 4p$, i.e. to $3d_2$ being different from $3d_3$. This configuration also partially incorporates $4s - 4d$ correlation in the $y\ ^7P^o$ state.

Prior to embarking on a non-orthogonal orbital approach to this problem, we have undertaken a series of calculations with the code CIV3 [2] in which the orthogonal orbitals arising in the configurations are optimised in different ways on the energies of different states, and again in which various choices of configurations are employed.

We show in Table I two such calculations. Calculation 1 coincides with Calculation D of [1]. The orbitals are represented as sums of normalised Slater-type orbitals (STOs). Those which differ in the two calculations were chosen as follows. In Calculation 1, $3d$ was first fixed as the Hartree-Fock orbital of $3d^4 4s^2\ ^5D$, after which the $4d$ and $5p$ were optimised of a^7S and y^7P^o respectively. The $3d$ was then reoptimised

on y^7P^o. Finally, the coefficients of the STOs of $4d$ were recomputed to ensure orthogonality of $3d$ and $4d$. In Calculation 2, the same configurations were used as in Calculation 1, but $3d$, $4d$, $5p$ were optimised on y^7P^o, a^7S, y^7P^o *in that order*. The CI expansion coefficients do not differ greatly in the two calculations: typically by less than 5%.

In order to compare the contributions to the oscillator strength from individual configurations, it is convenient to define for the length form

$$F_{ij} = \left(\frac{2}{3}\frac{\Delta E}{g_i}\right)^{1/2} a_i b_j \, |\langle \phi_i | \mathbf{r} | \chi_j \rangle|$$

(with an equivalent expression for the velocity form) in terms of the CI wave functions of the two states in the transition:

$$\Psi_i = \sum_i a_i \phi_i; \qquad \Phi_j = \sum_j b_j \chi_j$$

Then, in either form, the oscillator strength is

$$f = \left(\sum_i \sum_j F_{ij}\right)^2$$

Table I. F_{ij} and f-values for septet transitions

		$a - z$				$a - y$			
		Calc. 1		Calc. 2		Calc. 1		Calc. 2	
i	j	f_l	f_v	f_l	f_v	f_l	f_v	f_l	f_v
$3d^54s$	$3d^54p$	0.758	0.718	0.748	0.729	0.555	0.440	0.594	0.483
	$3d^44s4p$	-0.098	-0.319	-0.104	-0.350	0.163	0.447	0.160	0.450
	$3d^44s5p$	-0.034	-0.158	-0.038	-0.216	0.038	0.150	0.039	0.186
	$3d^44s4f$	-0.013	-0.154	-0.013	-0.151	-0.017	-0.162	-0.018	-0.178
$3d^44d4s$	$3d^44s4p$	-0.120	0.116	-0.098	0.095	0.201	-0.163	0.150	-0.122
	$3d^44s5p$	-0.003	0.070	-0.006	0.078	0.004	-0.070	0.007	-0.067
	$3d^44d4p$	0.112	0.106	0.087	0.085	0.075	0.059	0.064	0.052
$3d^44p4f$	$3d^54p$	-0.015	0.178	-0.015	0.178	-0.011	0.109	-0.012	0.118
	Others	-0.028	0.009	-0.019	0.005	-0.025	0.009	-0.022	0.011
	Total F_{ij}	0.559	0.566	0.542	0.453	0.983	0.819	0.962	0.933
	f-value	0.313	0.321	0.294	0.205	0.967	0.671	0.926	0.870
	Expt.		0.255 [4]; 0.254 [5]				0.884 [4]; 0.856 [5]		

The main F_{ij} are shown in Table I. For the $a - z$ transition, the total F_{ij} in length form is little different in the two calculations, but in the velocity form the total F_{ij} changes by 20%, resulting in a 35% change in f_v. This is partly due to changes in $4d$, but more to changes in $5p$, brought about by the way in which the $3d$ was optimised. Thus the length and velocity agreement achieved for $a - z$ in Calculation 1 is lost in Calculation 2.

For the $a - y$ transition, the situation is reversed: the poor agreement in Calculation 1 is much improved in Calculation 2, and the resulting f_l and f_v lie close to the experimental values.

We have made extensive sets of calculations of these transitions, by varying the way these orbitals are optimised and by increasing the number of configurations. In all this work, we find that in any one calculation, we can achieve good agreement with experiment and between f_l and f_v for either $a-z$ or $a-y$, but not for both transitions simultaneously.

Non-orthogonal approach

Accordingly, we have embarked on a calculation of these transitions using non-orthogonal orbitals. We have incorporated into CIV3 the non-orthogonal angular momentum package of [3] and have made the necessary (and extensive) changes to the radial part of the code. Calculations of these oscillator strengths in this formalism have begun and will be reported later.

Quintet transitions

Some calculations have also been made for the quintet transitions, using the same configurations as, but more angular momentum couplings than, the septet transitions. This work reveals much less CI cancellation than in the septet transitions. All our calculations yield results similar to those of Table II. The calculated energies agree well with experiment, as does the oscillator strength of the $a-z$ transition. Length and velocity forms agree quite well. However, our oscillator strength for $a-y$ differs markedly from experiment. The lack of any cancellation in $a-y$ suggests that the experimental value may be too low. A further experimental determination would be helpful.

Table II. f-values for quintet transitions

	$a-z$			$a-y$		
	ΔE (a.u.)	f_l	f_v	ΔE (a.u.)	f_l	f_v
Our work	0.0824	0.610	0.586	0.0971	0.094	0.105
Expt.	0.0875	0.64 [4]		0.1006	0.034 [6]	

References

1. Hibbert, A., Tait, J.H., Summers, H.P. and Burke, P.G., Nucl. Inst. Meth. **B31**, 276 (1988).
2. Hibbert, A., Comput. Phys. Commun. **9**, 141 (1975).
3. Hibbert, A., Froese Fischer, C. and Godefroid, M.R., Comput. Phys. Commun. **51**, 285 (1988).
4. Huber, M.C.E. and Sanderman, R.J., Proc. Roy. Soc. **A357**, 355 (1977).
5. Blackwell, D.E., Menon, S.L.R. and Petford, A.D., Mon. Not. R.A.S. **207**, 535 (1984).
6. Penkin, N.P., J. Quant. SPect. Rad. Transf. **4**, 41 (1964).

RCI calculation of energy levels and oscillator strengths in highly ionized atoms

Takashi Kagawa, Yoshie Honda and Shuji Kiyokawa

Department of Physics, Nara Women's University
Nara 630, Japan

Structures for highly ionized atoms have attracted interest not only in relativistic atomic physics but also other related fields such as astrophysics and plasma physics. X-ray spectra emitted from highly ionized atoms immersed in various plasmas such as solar, stellar and laboratory ones have been used for diagnosing and modelling them. However, these spectra observed usually are very complex because they consist of a large number of lines due to multiplet terms in the energy levels for ions in various charge states. So in the analysis of such complex spectra, it is desired to calculate transition energies and oscillator strengths for ions systematically.

Recently we have developed the relativistic configuration interaction (RCI) theory for atomic systems with analytical relativistic Hartree-Fock-Roothaan (RHFR) basis functions [1]. The basis set for constructing configuration state functions (CSF's) consists of all real and virtual RHFR one-electron functions expanded in terms of Slater-type orbitals. The Breit interaction operator is treated by the first-order perturbation theory. The lowest-order quantum electrodynamics (QED) corrections for the self-energy and vacuum polarization terms are taken into account in the RCI calculation as a first-order perturbation energy by use of Mohr's numerical results for hydrogenic systems [2,3]. Present RCI method has a merit that one can save much computation time when obtaining a large number of multiplet states in atomic systems because of an analytical form of the basis set.

The numerical application of the method to neonlike systems is carried out to see the effectiveness of the theory. Here we show the calculated results on the Z dependence of the transition frequencies and oscillator strengths for the $E1$ transition from the ground state to singly excited ones in neon isoelectronic sequence. In Fig. 1, the variation of the order of the excited levels for odd-parity states with $J = 1$ in the isoelectronic sequence is shown.

It is seen from the figure that many level crossings apprear when Z increases. In Fig. 2 and 3, variation of the oscillator strengths for the $n = 2 \rightarrow 3$ and $n = 2 \rightarrow 4$ $E1$ transitions in the isoelectronic sequence are shown. One sees anormaly in the Z dependent behavior of the oscillator strengths in which they suddenly increase or decrease in a position of a specific atomic system with Z. If one compares Fig. 2 and 3 with Fig. 1, the anormaly can clearly be explained as the CI effects in the oscillator strengths, since one can find in Fig. 1 that the level crossing for excited levels related to the transitions under consideration occurs at a position close to a specific ion in the isoelectronic sequence so that the wavefunctions between these states in the system mix largely. The atomic data containing such Z dependent behavior for the transition frequencies and optical oscillator strengths will be very useful in the identification of the spectra observed.

References

[1] T. Kagawa, Y. Honda and S. Kiyokawa, Phys. Rev. A44, 7092 (1991).
[2] P. J. Mohr, AT. Data and Nucl. Data Tables 29, 453 (1983).
[3] P. J. Mohr and Y.-K. Kim, Phys. Rev. A45, 2727 (1991).

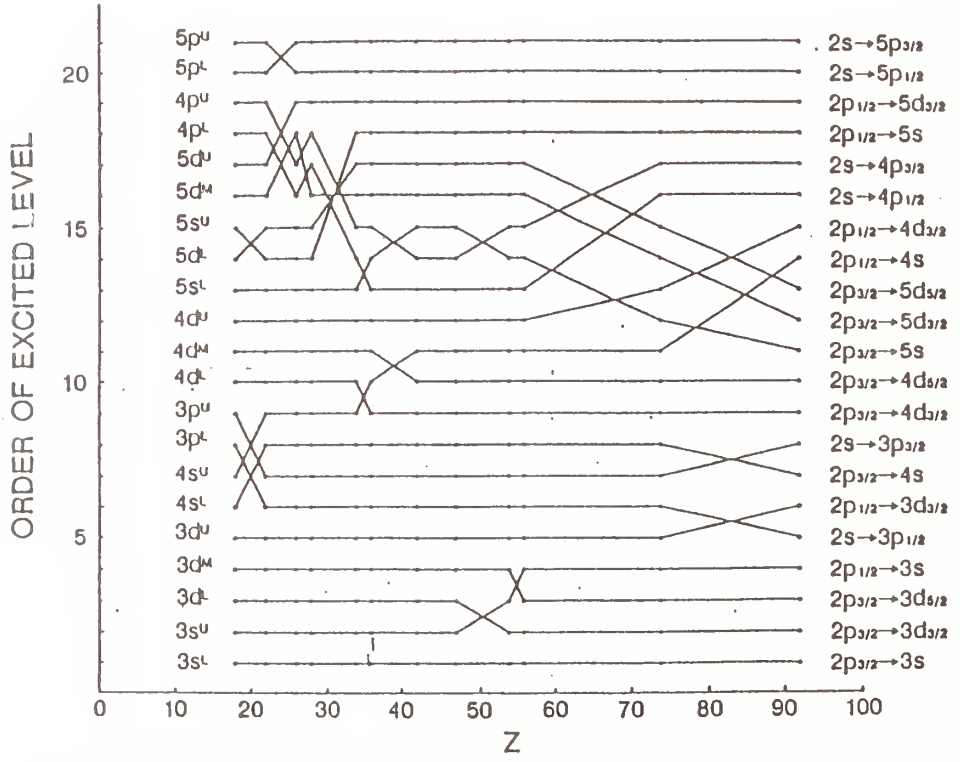

Fig. 1 Order of odd parity states with J=1 in Ne-like systems.

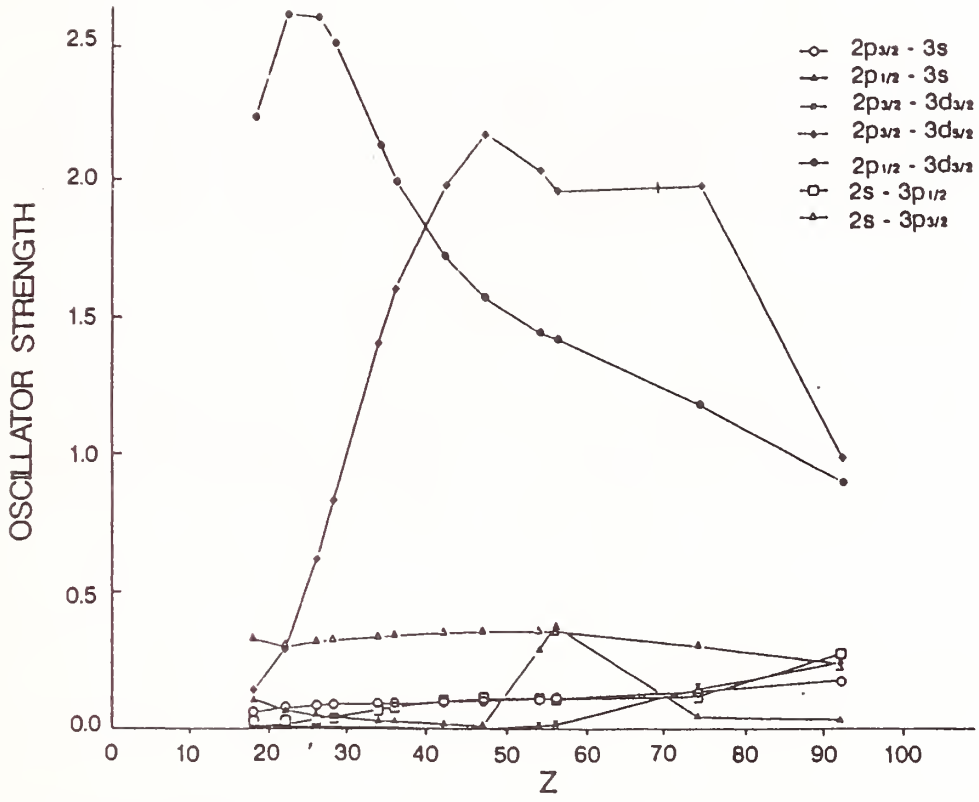

Fig. 2. Oscillator strengths for n=2-3 transitions in Ne-like systems.

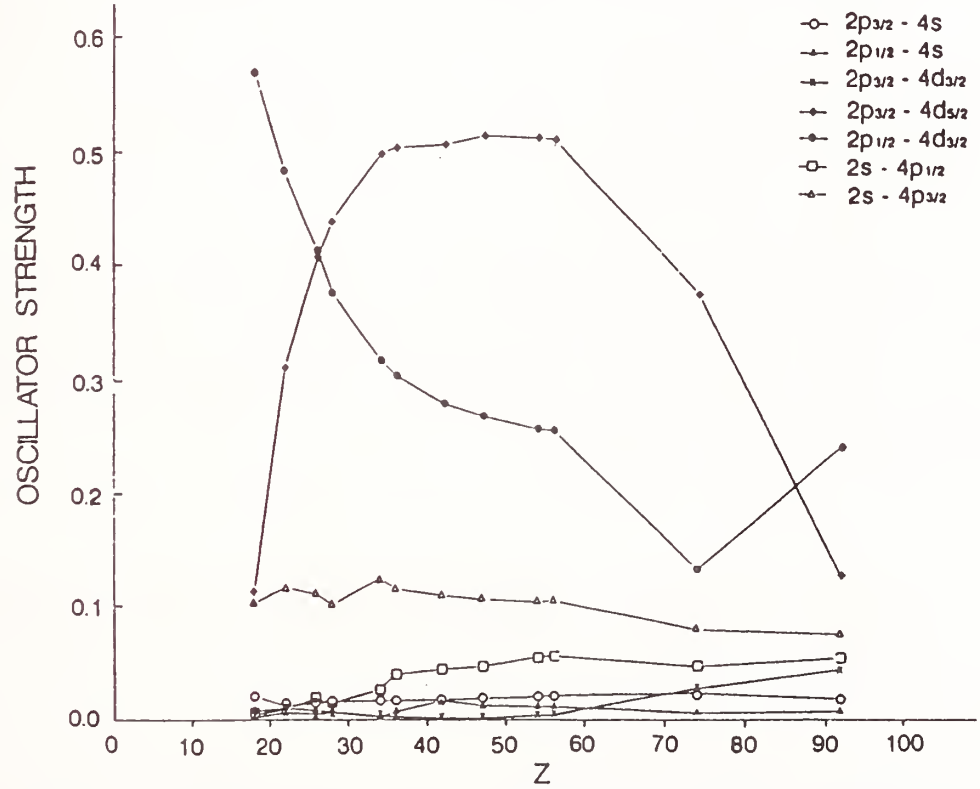

Fig. 3. Oscillator strengths for n=2-4 transitions in Ne-like systems.

A DENSITY-MATRIX DESRIPTION FOR THE BROADENING OF SPECTRAL LINES BY AUTOIONIZATION, RADIATIVE TRANSITIONS, AND COLLISIONS*

V. L. Jacobs

Complex Systems Theory Branch, Code 4694
Condensed Matter And Radiation Sciences Division
Naval Research Laboratory
Washington, D. C. 20375-5000

ABSTRACT

A density-matrix description has been developed to investigate the broadening of atomic spectral lines by autoionization processes, radiative transitions, and electron-ion collisions in a high-temperature plasma. Using Liouville-space projection-operator techniques, collisional and radiative relaxation processes are incorporated on an equal footing with autoionization and radiative stabilization. Particular interest is directed at the precise determination of the spectral line shapes for dielectronic recombination satellite transitions.

* SUPPORTED BY THE DEPARTMENT OF ENERGY

Developments in computation of form factors

C. T. Chantler
Quantum Metrology Division, National Institute for Standards and Technology,
Gaithersburg, MD 20899, U.S.A.

Abstract

Imaginary parts of atomic form factors are scaled total photoionisation and photoexcitation cross-sections. This relates directly to summed oscillator strengths for the excitation to continua or bound states for levels involved. Hence calculations of form factors, oscillator strengths and absorption edge energies are intrinsically related. Form factors are the fundamental unit in calculations of diffraction effects and shifts, involved in most X-ray spectral analysis, which is a further incentive for investigation.

Tables for form factors and anomalous dispersion are of wide general use in the UV, X-ray and γ-ray communities, and have existed for several decades. They have, perhaps, been dominated by the theoretical work of Cromer, Mann and Liberman (1968, 1970a, 1970b, 1981) and the experimental syntheses of Henke and co-workers (1982), with recent developments of Doolen and Liberman (1987) and Henke et al. (1988). The generality of these works has entailed numerous simplifications compared to detailed relativistic S-matrix calculations (Kane, 1986). However, the latter calculations do not appear to give convenient tabular application for the range of Z and energy of general interest, whereas the former tables have large regions of limited validity throughout the range of Z and energies, and in particular have limitations with regard to extrapolation to energies outside tabulated ranges.

Several *a priori* assumptions limit the applicability of theoretical form factor computations. Chief of these is the independent particle approximation, treating adjacent atoms as independent and effectively restricting consideration to 10 eV - 100 eV and higher energies. However, intermediate theoretical and procedural assumptions further limit the precision and applicability of available tabulations and procedures. This poster identifies regions of Z and energy where these secondary assumptions fail and the improvement which can be achieved by their avoidance, both in tabulated ranges and by extrapolation.

Particular concern involves the application of the dispersion relation to derive Re(f) from photoelectric absorption cross-sections. Revised formulae can lead to significant qualitative and quantitative improvement, particularly above 30-60 keV energies (Fig. 1), near absorption edges (Fig. 2), or at 30 eV to 6 keV energies (Fig. 3). Current experimental syntheses are not superceded by this approach, but examples are given where predictions underlying revised theoretical tables are in qualitative agreement with experiment

as opposed to results in available syntheses. Recent theoretical discussion involving small corrections to earlier form factors are confused if the relatively large corrections discussed herein are not included.

References:

Brennan S. (1991) private communication.

Cromer D. T. and Liberman D. (1970a) *J. Chem. Phys.* **53,** 1891-1898.

Cromer D. T. and Liberman D. (1970b) *Los Alamos internal report* LA-4403 UC-34, 163 pages.

Cromer D. T. and Liberman D. A. (1981) *Acta Cryst.* **A37,** 267-268.

Cromer D. T. and Mann J. B. (1968) *Acta Cryst.* **A24,** 321-324.

Doolen G. and Liberman D. A. (1987) *Physica Scripta* **36,** 77-79.

Henke B. L., Lee P., Tanaka T. J., Shimabukuro R. L., Fujikawa B. K. (1982) *At. Dat. Nucl. Dat. Tab.* **27,** 1-144.

Henke B. L., Davis J. C., Gullikson E. C., Perera R. C. C. (1988) *Lawrence Berkeley Laboratory report* LBL-26259 UC-411, 376 pages.

Kane P. P., Kissel L., Pratt R. H., Roy S. C. (1986) *Phys. Rep.* **140,** 75-159.

Perera R. C. C. and Gulliksen E. (1991) private communication.

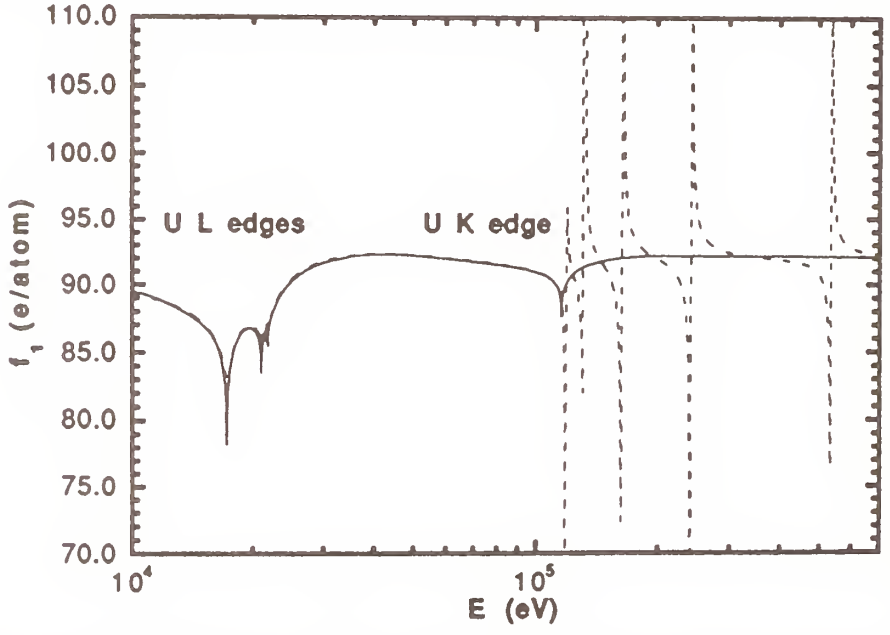

Figure 1: Form factor f_1 for uranium near K and L-edges indicating above-edge errors from standard formulae (Cromer et al., 1970a, 1970b, 1981; Brennan, 1991). (Solid line indicates revised formulation.)

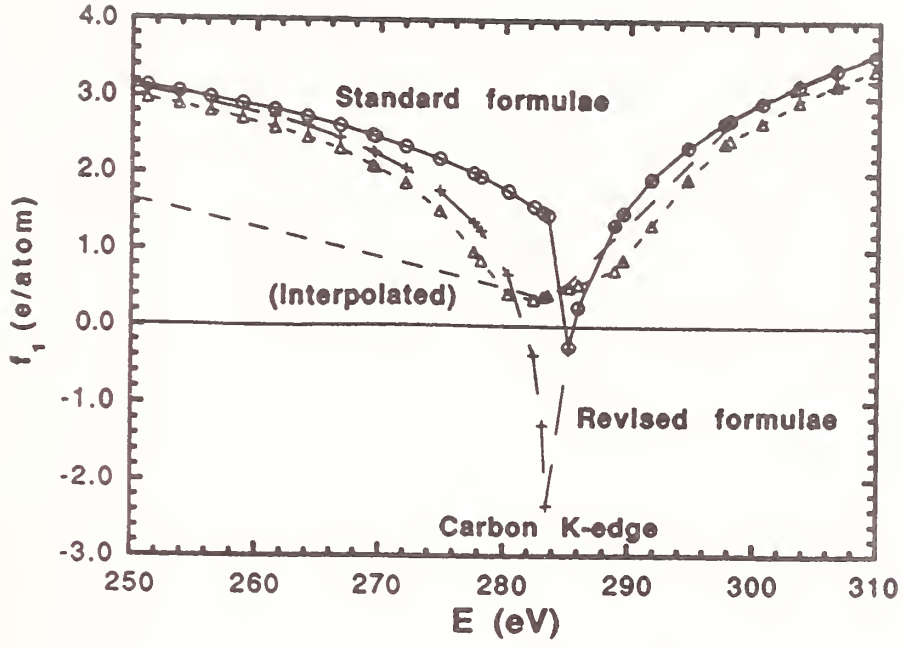

Figure 2: Form factor f_1 for carbon near K-edge indicating asymmetry and discontinuity produced by standard formulae ('o', Cromer (1981)), and inadequacy of synthesised data (dash, Henke (1982); triangles, Perera (1991)), versus the revised formulation ('+').

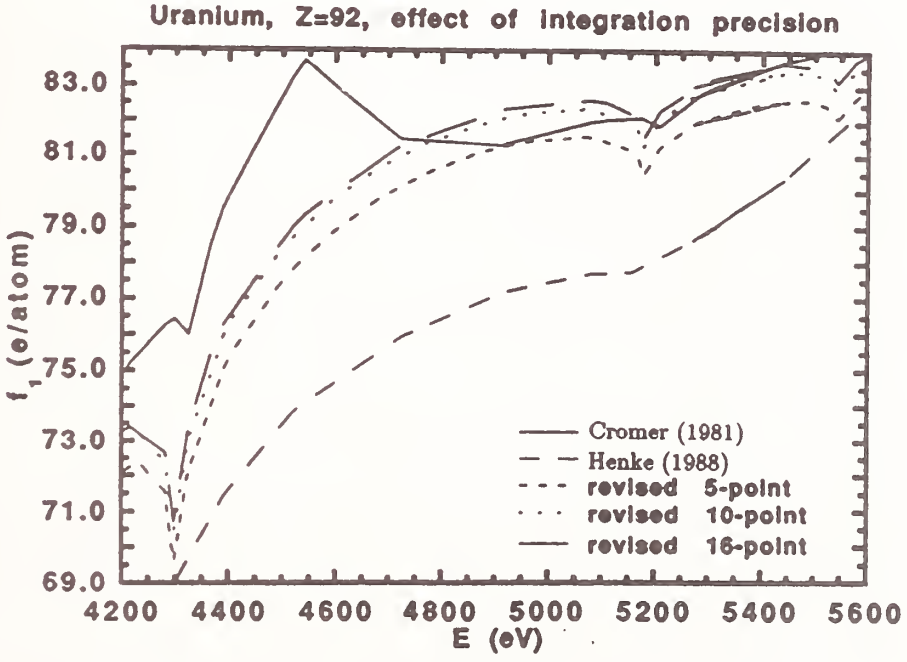

Figure 3: Form factor f_1 for uranium M_I - M_{III} edges showing importance of higher precision integration and the use of revised formulae versus earlier methods (Cromer, 1981) and synthesised data (Henke, 1988; Perera, 1991).

Accurate oscillator strengths for neutral carbon and astrophysical implications

E. Biémont[1], A. Hibbert[2], M.R. Godefroid[3] and N. Vaeck[4]

1 Institut d'Astrophysique, University of Liège, B-4000 Liège, Belgium.

2 Department of Applied Mathematics, Queen's University, Belfast, N. Ireland.

3 Laboratoire de Chimie Physique Moléculaire, CP 160/09, Université Libre de Bruxelles, B-1050 Bruxelles, Belgium

4 van der Waals-Zeeman Laboratory, University of Amsterdam, NL-1018 XE Amsterdam, The Netherlands

The calculation

Recently we embarked on a major study of transitions in neutral carbon, nitrogen and oxygen in order to provide a new determination of the solar content of these elements. Our transition probabilities in N I and O I [1] were used [2] to obtain solar abundances which were in excellent agreement with those obtained from an investigation of molecules in the Sun [3].

We have very recently completed a similar calculation of transition probabilities in C I [4]. The determination of the solar abundance of carbon is in progress [5]. C I is observed in the visible part of the solar spectrum but appears predominantly in the infrared region. Consequently it is necessary to consider all states of the form $2s^22p^2$, $2s2p^3$, $2s^22p3l$ (l=0,1,2), $2s^22p4l$ (l=0,1,2,3), $2s^22p5s$.

The calculation of transition probabilities was undertaken using the configuration interaction (CI) code CIV3 [6] with an extensive set of orbitals whose radial functions, chosen to represent both spectroscopic and correlation orbitals, were optimised variationally on the energies of various different LS states. The details are given in ref. [4]. The 57 even and 76 odd parity configurations gave rise to a total of over 4000 LSJ couplings. This calculation is then much more extensive than the earlier structure calculation of Nussbaumer and Storey (NS) [7].

Oscillator strengths of C I have also been obtained from close coupling (CC) calculations by Nussbaumer and Storey [7] and more recently by Luo and Pradhan (LP) [8] using the R-matrix method.

Discussion of the accuracy of LS oscillator strengths

It is appropriate to compare our results with the above-cited calculations in order to assess their accuracy. We give in Table I those of our LS-coupled results for which comparison is possible for the principal transitions contributing to the carbon abundance calculation. Oscillator strengths are calculated in length (f_l) and velocity (f_v) forms. LP also give both forms, whereas NS give only the length form.

It is clear that our length values agree very closely with the SUPERSTRUCTURE (SS) length values of NS. Hence, with two quite independent atomic structure codes, very good agreement is achieved. The collisional calculations yield length values which are generally in good agreement with the structure calculations, but there are some exceptions.

Table I. Multiplet oscillator strengths

		This work		LP*		NS(CC)†	NS(SS)†
		f_l	f_v	f_l	f_v	f_l	f_l
$3s-3p$	$^3P^o$–^3D	0.536	0.507	0.497	0.548	0.507	0.526
	$^3P^o$–^3P	0.378	0.336	0.360	0.371	0.356	0.375
	$^3P^o$–^3S	0.113	0.081	0.107	0.109	0.107	0.110
	$^1P^o$–^1D	0.656	0.709	0.637	0.672	0.624	0.657
	$^1P^o$–^1P	0.277	0.201	0.252	0.271	0.267	0.278
	$^1P^o$–^1S	0.125	0.105	0.121	0.120	0.117	0.122
$3p-3d$	^3D–$^3F^o$	0.797	0.809	0.813	0.677	0.783	0.787
	^3D–$^3D^o$	0.142	0.131	0.149	0.108	0.143	0.141
	^3P–$^3P^o$	0.301	0.276	0.301	0.232	0.265	0.304
	^1P–$^1P^o$	0.336	0.297	0.316	0.0243	0.301	0.332
	^1S–$^1P^o$	0.348	0.321	0.501	0.314	0.591	0.380
$3p-4s$	^3D–$^3P^o$	0.154	0.138	0.162	0.128	0.161	0.159
	^1D–$^1P^o$	0.232	0.220	0.227	0.195	0.250	0.226
	^1P–$^1P^o$	0.0066	0.0069	0.0233	0.0303	0.0510	0.0106

*: Ref. [8] †: Ref. [7]

In particular, the $3p\ ^1P-4s\ ^1P^o$ transition is a weak transition with some cancellation due to the CI mixing of $4s$ and $3d\ ^1P^o$ states, and the oscillator strength is very sensitive to the accuracy of that mixing. We note that, when we include relativistic effects, our f_l and f_v each increase from 0.007 to 0.009. This variation is small compared with the discrepancy between the various theoretical results. In our calculations, we made small adjustments to the diagonal elements of the Hamiltonian matrix, in order to reproduce experimental energy separations and thereby refine the CI mixing coefficients. This does not seem to have been done in the other calculations.

It is more surprising to find the structure and collisional calculations disagreeing for the length form of the $3p\ ^1S-3d\ ^1P^o$ transition, which has a large oscillator strength. The same $3d-4s$ mixing which led to cancellation effects in the transition considered above gives rise to an enhancement of the oscillator strength in this case. Normally such enhancement situations are rather insensitive to the accuracy of the mixing. However, we note that in some rather simple CI calculations we have made for other purposes, the oscillator strength of this particular transition can vary markedly from what we believe is a reasonably accurate value as given by our result in Table I.

The other possible comparison is between length and velocity forms. From Table I, we see that for the $3s-3p$ transitions, the agreement between f_l and f_v is better in the calculations of LP than in ours. However, for the $3p-3d$ and $3p-4s$ transitions, our results show much better agreement than theirs.

J-dependent effects

The calculations of LP are in LS coupling. We find that for some transitions, there are substantial departures from the standard statistical weight dependence of the $J-J'$

lines in a multiplet. We show in Table II the A-values of individual lines in the $2p^2\ ^3P - 2p4s\ ^3P^o$ multiplet, comparing our values ("actual") with what would be obtained if our LS A-value of $9.17 \times 10^7 s^{-1}$ were distributed according to "statistical" factors. The "ratio" column shows that the inclusion of spin-orbit mixing, principally that of $2p4s\ ^3P^o$ and $2p3d\ ^3D^o$ (which lie close in energy), both reduces the "multiplet" value and also creates substantial deviation from the "statistical" values.

Table II. Transitions in the $2p^2\ ^3P - 2p4s\ ^3P^o$ multiplet

		A-values (in $10^8 s^{-1}$)		
J	J'	Actual	Statistical	Ratio
2	2	0.616	0.688	0.90
1	2	0.321	0.229	1.40
2	1	0.348	0.382	0.91
1	1	0.183	0.229	0.80
0	1	0.334	0.306	1.09
1	0	0.845	0.917	0.92

Acknowledgements

It is a pleasure to thank Dr. W.L. Wiese for his interest and critical analysis of our results. The Belgian National Fund for Scientific Research (FRFC Convention 2.4533.91) and NATO (Collaborative research grant CRG 890225) are acknowledged for their financial support.

References

1. Hibbert, A., Biémont, E., Godefroid, M.R. and Vaeck, N., Astron. Astrophys. Suppl. Ser. **88**, 505 (1991); J. Phys. B. **24**, 3943 (1991).

2. Biémont, E., Froese Fischer, C., Godefroid, M.R., Vaeck, N. and Hibbert, A., *Atomic Spectra and Oscillator Strengths for Astrophysics and Fusion Research*, (ed: J.E. Hansen), 59 (1990); Biémont, E., Hibbert, A., Godefroid, M.R., Vaeck, N. and Fawcett, B.C., Astrophys. J. **375**, 818 (1991).

3. Grevesse, N., Lambert, D.L., Sauval, A.J., Van Dishoeck, E.F., Farmer, C.B. and Norton, R.H., Astron. Astrophys. **232**, 225 (1990); Astron. Astrophys. **242**, 488 (1991).

4. Hibbert, A., Biémont, E., Godefroid, M.R. and Vaeck, N., submitted to Astron. Astrophys. (1992).

5. Biémont, E., Hibbert, A., Godefroid, M.R. and Vaeck, N., to be submitted to Astrophys. J. (1992).

6. Hibbert, A., Comput. Phys. Commun. **9**, 141 (1975); Glass, R. and Hibbert, A., Comput. Phys. Commun. **16** 19 (1978).

7. Nussbaumer, H. and Storey, P.J., Astron. Astrophys. **140**, 383 (1984).

8. Luo, D. and Pradhan, A.K., J. Phys. B. **22**, 3377 (1989).

Relativistic study of lifetimes for the $ns^2np^k(n+1)s$ levels in heavy systems

Jacek R. Bieroń

Institute of Physics, Jagellonian University
30-059 Kraków, Reymonta 4, Poland.

Jacek Migdałek

Institute of Physics and Computer Science
Pedagogical Academy, 30-084 Kraków, Podchorążych 2, Poland.

We report on the theoretical study of E1 transitions from the levels of $ns^2np^k(n+1)s$ configurations in heavy systems. The following spectra are analysed: GeI, SnI, PbI, AsII, SbII, BiII for k=2; AsI, SbI, BiI for k=3 and SeI, TeI, PoI for k=4. Multiconfiguration Dirac–Fock computer code of Oxford group /1/ has been used to obtain wavefunctions and energy structure. The multiconfiguration basis set includes configurations from within the Layzer complex as well as several additional configurations, whose considerable interaction with the reference configuration had been established earlier.

Various options of MCDF code has been tested and their influence on the calculated electronic structure and radiative properties has been analysed. These include the possible choice of energy functional to be minimized, the model of the nucleus and the QED corrections /2/.

The modification of configuration interaction approach proposed recently /3/ has been employed. It is, basically, a combination of the standard multiconfiguration (MCDF) method with the configuration interaction (CI) approach. The attempt is made to benefit both from more accurate MCDF formulation and from relatively fast and easily convergent CI approach.

The computed lifetimes have been compared with other available theoretical and experimental data.

1. Grant I.P., McKenzie B.J., Norrington P.H., Mayers D.F., Pyper N.C., 1980 Comput. Phys. Commun. **21**, 207

2. McKenzie B.J., Grant I.P., Norrington P.H., 1980 Comput. Phys. Commun. **21**, 233

3. Bieroń J.R., Marcinek R., Migdałek J., 1991 J. Phys. B: At. Mol. Opt. Phys. **24**, 31

Oscillator strengths for the transitions in singly ionized KrII

P Anantha Lakshmi* and K S Baliyan†

*School of Physics, University of Hyderabad, Hyderabad 500 134, INDIA

†Laboratory for Astronomy and Solar Physics

NASA/Goddard Space Flight Center, Greenbelt Md 20771

Owing to its application in defining the unit of length 'meter', the neutral krypton attracted a lot of attention resulting in considerable amount of atomic data in the form of energy levels, collision cross sections etc. The motive was to determine a set of energy levels of Kr^{86} that could be used to establish a set of standard wavelengths. Relatively less attenion was focussed on ionized krypton as opposed to the neutral krypton. The spectrum of singly ionized krypton was analysed as early as in 1933 by de Bruin et al.[1], followed by Boyace[2] and Minnhagen et al.[3] and Bredice et al.[4]. Most of these levels have been tabulated by Sugar and Musgrave [5]. Here we intend to present preliminary results of the calculation of oscillator strengths among the various levels of Kr II ion.

The oscillator strengths and lifetimes of the ions of krypton are of considerable importance for their application in astrophysics, laser and plasma physics. In this study we use configuration interaction wavefunctions to calculate f-values for some transitions. The wavefunctions are generated by making use of atomic structure program written by A Hibbert [6] which incorporates electron correlation effects via configuration interaction. These CI wavefunctions may be expressed as,

$$\Phi_j(\mathrm{LS}) = \sum_{i=1}^{m} a_{ij}\phi_i(\alpha_i \mathrm{LS}) \tag{1}$$

in the LS coupling, or

$$\Phi_j(\mathrm{J}) = \sum_{i=1}^{m} b_{ij}\phi_i(\alpha_i \mathrm{L_i S_i J}) \tag{2}$$

in the Breit-Pauli approximation. For a given set of $\{\phi_i\}$, the variationally optimal values of the mixing coefficients a_{ij}/b_{ij} are the components of the eigenvectors of the Hamiltoinian matrix. The configuration state functions $\{\phi_i\}$ are built using the one electron orthogonal orbitals:

$$u_{nlm_l m_s}(r) \;=\; \frac{1}{r} P_{nl}(r) Y_l^{m_l}(\theta,\phi)\chi^{m_s}(s) \tag{3}$$

and radial functions are expressed in analytic form as:

$$P_{nl}(r) = \sum_{i=1}^{k} c_i r^{p_i} \exp(-\zeta_i r). \tag{4}$$

The orbital parameters $\{ c_i\}$, $\{p_i\}$ and $\{\zeta_i\}$ are obtained variationally.

We use 1s, 2s, 2p, 3s, 3p, 3d, 4s, and 4p orbitals published by Clementi and Roetti [4] for the ground state $4s^2 4p^5\ ^2P^o$ of the singly ionized Kr II ion. In addition to these, 4d, 4f, 5s, 5p, 5d, 5f and 6d orbitals are used in this calculation, parameters of which are obtained by the optimization procedure using CIV3 code. In this procedure we minimized the energy of $4p^4 4d\ ^4D^e$ to obtain radial function parameters for the 4d orbital. The 5s orbital parameters were obtained by minimising the energy of $4p^4 5s\ ^2P^e$ while those of 5p were obtained using $4p^4 5p\ ^4P^o$ state. The 5d orbital was optimized on the energy of $4p^4 5d\ ^4F^e$ state. The ground state energy was used to optimise the parameters of 4f and 5f orbitals. The radial orbital parameters of 6d orbital were obtained on the ground state keeping 4d and 5d configurations.

Table 1

Transition i - f		$\triangle$E au	Oscillator strength Length	Velocity	Trans.Prob. s^{-1}
$4s^2 4p^5\ ^2P^o$	$4s4p^6\ ^2S$	0.4620	1.4431(-2)	2.3635(-2)	2.9688(8)
	$4s^2 4p^4 4d\ ^2S$	0.7781	2.8124(-1)	2.2900(-1)	1.6411(10)
	$4s^2 4p^4 5d\ ^2S$	0.8913	2.8148(-1)	1.7507(-1)	2.1555(10)
$4s^2 4p^4(^3P)5p\ ^2P^o$	$4s^2 4p^4 5d\ ^2S$	0.1786	1.8697(-2)	1.2467(-2)	5.7456(7)
	$4s4p^5 5p\ ^2S$	0.5634	1.7497(-1)	1.3189(-1)	5.3538(9)
$4s^2 4p^4(^1D)5p\ ^2P^o$	$4s^2 4p^4 4d\ ^2S$	0.0110	2.1799(-2)	1.8537(-2)	2.5610(5)
	$4s^2 4p^4 5d\ ^2S$	0.1243	1.4458(-1)	8.4774(-2)	2.1533(8)
	$4s4p^5 5p\ ^2S$	0.5092	7.5274(-3)	8.2210(-3)	1.8811(8)
$4s4p^6\ ^2S$	$4s^2 4p^4 4f\ ^2P^o$	0.4002	6.0631(-3)	5.0257(-3)	1.0402(7)
$4s^2 4p^5\ ^2P^o$	$4s^2 4p^4(^3P)4d\ ^2D$	0.6704	1.0601(-1)	9.5208(-2)	9.1844(8)
	$4s^2 4p^4(^1D)4d\ ^2D$	0.7487	7.7252(-1)	6.4013(-1)	8.3490(9)
	$4s^2 4p^4(^3P)5d\ ^2D$	0.8150	3.9959(-2)	3.2391(-2)	5.1170(8)
	$4s^2 4p^4(^1S)4d\ ^2D$	0.8486	6.1375(-1)	4.8676(-1)	8.5203(9)
	$4s^2 4p^4(^1D)5d\ ^2D$	0.8806	9.4155(-1)	6.5340(-1)	1.4076(10)
	$4s^2 4p^4(^3P)4d\ ^2P$	0.6532	3.6733(-3)	3.0360(-3)	5.0351(7)
	$4s^2 4p^4(^1D)4d\ ^2P$	0.7634	4.2599(-1)	3.5138(-1)	7.9771(9)
	$4s^2 4p^4(^3P)5d\ ^2P$	0.8281	2.2805(-1)	1.8181(-1)	5.0246(9)
	$4s^2 4p^4(^1D)5d\ ^2P$	0.8876	6.5659(-1)	4.3569(-1)	1.6622(10)
	$4s4p^5 5p\ ^2P$	1.2708	1.1930(-4)	1.3898(-4)	6.1906(6)

Now the major problem in applying the configuration interaction method lies in the choice of the configuration state functions. Since Kr II is an almost neutral open shell ion, one should normally include the three major correlation effects: internal, semi-internal and all external. However, a very extensive configuration set would result with this prescription which is prohibitively difficult from the computational viewpoint. We therefore restrict ourselves to keeping a minimum of 1-electron in 4s shell and 3-electrons in 4p shell and use a very limited 'all external' correlation configuration set. A more elaborate set with all major configurations is still under consideration. It is observed that there is a strong mixing between the configurational states. In the event of almost equal mixing coefficients coming from two configurations, it is difficult to label the state. For the relativistic calculation, we

have included spin-orbit, spin-spin, spin-other-orbit, mass correction and Darwin term of the Breit-Pauli operator.In the intermediate coupling different LS states couple with large mixing coefficients for a particular value of J. This mixing allows the transitions which are otherwise forbidden in LS coupling.

These wavefunctions are used to calculate the dipole oscillator strengths for the transitions between the initial and final states of the singly ionized krypton. The expression for the oscillator strengths in length and velocity forms can be written as

$$f_l^{if} = \frac{2(E_f - E_i)}{3g_i} | < \Psi_i | \sum_{p=1}^{N} r_p | \Psi_f > |^2 \tag{5}$$

$$f_v^{if} = \frac{2}{3g_i(E_f - E_i)} | < \Psi_i | \sum_{p=1}^{N} \nabla_p | \Psi_f > |^2 \tag{6}$$

where $g_i = (2L_i+1)(2S_i+1)$ is the statistical weight of the initial state and the summation is over all the N electrons of the ion. The initial and final states must be of different parity. The calculations have been performed in both the length and velocity forms of the dipole operator which should give identical results for allowed transitions in LS coulpling provided exact wavefunctions are used. For approximate wavefunctions agreement between these two is a measure of the accuracy of the wavefunctions used. The f-values obtained in the present calculation for some of the transitions are given in table 1. The details will be presented at the conference.

1. de Bruin TL, Humphreys CJ and Meggers WF 1933 J Res. Nat. Bur. Stand.(US) **11** 409.

2. Boyce JC 1935 Phys. Rev **47** 718.

3. Minnhagen L, Strihed H and Petersson B 1969 Ark Fys **39** 471.

4. Bredice F, Raineu M, Reyna Almandos J And Gallardo M 1988 Spectrosc Lett **21** 11

5. Sugar J and Musgrave A 1991 J. Phys. Chem. Ref. Data **20** 875.

6. Hibbert A 1975 Comput.Phys.Commun.**9** 141.

7. Clementi E and Roetti C 1974 At. Data Nucl. Data Tables **14** 177.

Lifetimes-measurements

Transition Probabilities and Line Shapes: Usage and Needs at the University of Illinois

Alexander Scheeline* and Cheryl A. Bye, (Dept. of Chemistry)
1209 W. California St., Urbana, IL 61801
Herman Krier, Jyotirmoy Mazumder, Xiangli Chen, Tom Duffey, Sudhir Tewari, and David Zerkle (Dept. of Mechanical and Industrial Engineering), Mark J. Kushner (Dept. of Electrical Engineering)

The authors of this paper are consumers of fundamental atomic and molecular reference data. Assorted research which uses transition probabilities and other reference data is presented, highlighting current sources of information, adequacies and limitations of the data, and suggesting areas for additional measurement or calculation.

1. Pulsed Discharge Plasma Diagnostics: Sparks and Theta Pinches

In pulsed discharges used for elemental analysis, sampled species are excited by collision with an ambient plasma (usually argon or helium, but sometimes nitrogen or air). Excitation varies as a function of space, time, support gas impurities, sampled species identity and concentration, and interactions among sampled species. If excitation behavior is understood, internal standard lines can be chosen, interferences anticipated, and measurement quality assured. Our work has focused on pulsed discharges in argon, sampling ferrous alloys, copper and its alloys, aluminum, and aluminum oxide ceramics. Wavelength and linewidth data are important, but the major limitation in elucidating the behavior of the plasmas has been access to adequate transition probability data.

Because of the availability of plentiful and precise transition probabilities for Mo I[1], we have on occasion used Mo as a proxy for ferrous alloys. Were data available for Mo II to the same degree as Mo I, this would be an ideal material for study of spark discharges since both Mo I and Mo II have rich spectra in the UV and visible spectral regions. NIST 1265 electrolytic iron is a frequently used sample, because transition probabilities for iron are also readily available[2]. Copper and aluminum data are helpful because of the massive amount of research since 1961 on sparks to their alloys, and the common use of Al_2O_3 as a proxy for many refractory compounds. The most common source is the NIST/CRC tabulation[3], now also available in computer-readable form[4].

Typically, analyte is excited to a lower temperature than the support gas. Ar I data in the near UV and visible are now in reasonable order[5]. Ar II transition probabilities[3,6,7,8] have not been as well characterized, though new data will appear shortly[9]. The next step in extending Ar I and Ar II data should be in increasing wavelength coverage, particularly between 190 nm and 260 nm. Additional highly useful data would come from a re-examination of Cu I and Cu II, and perhaps a thorough survey of Cr I. With Cr data, together with Fe and the well-studied Ni system[10], one would be in a strong position to study Ar plasma interactions with stainless steel. For examining refractory materials, SiO_2 can be used[11] instead of aluminum, but the spectrum is sparse, meaning that line interferences (of which there are several with Ar) can reduce the number of useful lines below that needed to determine if Boltzmann plots are linear.

2. Laser-Supported Plasmas for Space Propulsion

A spin-off from the Strategic Defense Initiative was the design of spacecraft propulsion systems based on large, orbiting lasers whose output would be used to remotely heat gases carried by small satellites. The heated gas would then steer the small satellites[12,13]. For this idea to work, efficient lasers and efficient conversion of light to kinetic energy are necessary. Atomic gases are preferred, so that energy is not consumed by molecular internal degrees of freedom. One desires a highly non-LTE system. To date, argon has been the most studied support species. The comments made about the need for additional Ar I and Ar II data in connection with sparks and pinches holds here for many of the same reasons. While existing data[3,7,8,9] are adequate when experiment bandwidth limits observation to only a few lines, wider-bandwidth detection becoming available with charge-transfer detectors will facilitate measurements for which adequate supporting data are note available.

3. Laser Cladding of Nb-Al Alloys on Niobium Substrate

Laser-ablation is used to create to a plasma of Nb or Hf, which are then vapor deposited on Nb-Al alloys. Ideally, one would like to know the absolute concentration of atomic species in the laser-generated plasma. This requires knowledge of transition probabilities for both Nb and Hf. Data are available for Nb I[14].

4. Laser-Ablation Generation of Nanocrystalline Powder

Nanocrystalline materials are a current subject of intense study for their structural, catalytic, electronic, and optical properties. In our particular case, an excimer laser ablates Nb and Al targets. The atoms condense on a collection plate, forming mixed Nb-Al alloys. In addition to Nb and Al atomic data, molecular data on Nb_2, NbO, $NbAl_3$ and Nb_3Al are required. The literature is devoid of data on any of these species except NbO, and those data[15,16,17] are quite old and fragmentary. Any data on wavelengths, level identifications, term symbols, and vibration/rotation constants would be an improvement.

5. Laser CVD of Ti and TiN Films on Si Substrates

Ti and TiN thin films are frequently deposited on Si substrates to serve as transitions for contact bonding or as dielectrics. Laser decomposition of precursors to yield free atoms is one means for fabricating the films. Understanding of the deposition process requires spectral diagnostics of numerous species including Si, Ti, Br, Cl, N, N_2, TiN, Br_2, Cl_2, $TiBr_x$ and $TiCl_x$ where x = 1 to 4. While some transition probability data are available for N_2, such data for all other molecular species are inadequate. Atomic data are available for Si[11], Ti[2,18], etc.[3] In addition to atomic and molecular transition data, collisional quenching data for all species in the pressure range 0.1 to 100 torr would be helpful.

6. Plasma Modeling

Models under development include those for plasma etching and deposition reactors, gas lasers, pulsed power devices and plasma remediation of toxic waste. Oscillator strengths and transition linewidths are used in these plasma chemistry models in two ways. The first use is in formulating the continuity equations for atomic and molecular species in the plasma. The knowledge of oscillator strengths leads directly to radiative lifetimes which, in some cases, is the dominant depopulating mechanism for excited states produced by electron impact in low pressure plasma etching reactors[19].

The second use is in calculating the small signal and saturated gain of plasma excited lasers. A system currently of interest is the electron beam excited Xe laser using Ar/Xe and He/Ar/Xe gas mixtures[20]. This laser operates on 6 infrared transitions (1.73 fm to 3.65 fm) between the 5d and 6p manifolds of Xe I (see Figure 1). The dominant laser transitions are, in order of efficiency, 1.73 fm ($5d[3/2]_1 \rightarrow 6p[5/2]_2$), 2.03 fm ($5d[3/2]_1 \rightarrow 6p[3/2]_1$), and 2.63 fm ($5d[5/2]_2 \rightarrow 6p[5/2]_2$). The upper laser levels of the Xe laser are populated by a collisional radiative cascade following dissociative recombination of dimer ions such as $ArXe^+$. For example, direct excitation of the Xe(7p) manifold by dissociative recombination leads to pumping the Xe(5s) manifold by a collisional radiative cascade. The lower laser levels are depopulated by radiative decay to the Xe(6s) and Xe(6s') levels and by heavy particle quenching collisions.

Since the Xe laser is usually operated in high pressure gas mixtures (> 0.5 - 1 atm), collisional broadening of the laser transitions are exceedingly important in calculating the gain of the system. In spite of the fact that this is a rare gas atomic laser, there have been surprisingly few measurements of broadening coefficients by either heavy particle or, more importantly, electron collisions. Recent measurements of the broadening of the 1.73 fm transition by collisions with He, Ne and Ar yielded values of 20.3, 12.7 and 19.7 MHz/Torr respectively, with uncertainties of approximately ±(10-25%)[21]. These yield broadened linewidths of ≃ 20-30 GHz at normal operating pressures. Broadening coefficients for the other laser transitions have only been implied from measurements of saturation intensity.

Perhaps the most important issue in scaling this laser is the broadening and quenching of the laser transitions by electron collisions[20]. The scaling of the optimum pump rates for the xenon laser lead one to conclude that electron collisions (either dephasing or quenching) lower gain and lead to termination of the laser. For example, the premature termination of lasre gain in a fission fragment excited laser is believed to be a result of electron collisions (see Figure 2)[22]. To date, there are no direct measurements of electron collision broadening coefficients of the laser transitions, which represents one of the greatest uncertainties in modeling and scaling the laser.

1. W. Whaling and J. Brault, *Phys. Scr.* 38, 707 (1989).
2. G. A. Martin, J. R. Fuhr, and W. L. Wiese, *NIST Atomic Transition Probabilities Data Files (Scandium through Nickel)*, Standard Reference Data Base No. 24 (also in *J. Phys. Chem. Ref. Data* 17, Suppl. 3 and 4 (1988).).
3. J. R. Fuhr and W. L. Wiese, "Atomic Transition Probabilities" in *CRC Handbook of Chemistry and Physics*, 73rd Ed., D. R. Lide, editor (CRC Press, Boca Raton, FL, 1992) P. 10-128 -- 10-179.
4. *NIST Spectroscopic Properties of Atoms and Atomic Ions*, NIST Standard Reference Database 38.
5. W. L. Wiese, J. W. Brault, K. Danzmann, V. Helbig, and M. Kock, *Phys. Rev. A*, 39, 2461 (1989).
6. J. Shumaker and C. Popenoe, *J. Op. Soc. Am.* 59, 980 (1969).
7. G. Garcia and J. Campos, *J. Quant Spectrosc. Radiat Trans.* 34, 85 (1985).
8. G. Garcia and J. Campos, *Phys. Scr.* 33, 321 (1986).
9. V. Vujnovic and W. L. Wiese, *J. Phys. Chem. Ref. Data* 21, 919 (1992).
10. J. E. Lawler and M. Salih, *Phys. Rev. A* 35, 5046 (1988).
11. T. R. O'Brian and J. E. Lawler, *Phys. Rev. A* 44, 7134 (1991).
12. D. K. Zerkle, S. Schwartz, A. Mertogul, X. Chen, H. Krier, and J. Mazumder, *J. Propuls. and Power* 6(1) (1990).
13. D. K. Zerkle and H. Krier, "Non-Local Thermodynamic Equilibrium in Laser Sustained Plasmas," AIAA 92-2991, *Proc. AIAA 23rd Plasmadynamics and Lasers Conf.* (1992).
14. M. Kwiatowski, P. Zimmermann, E. Biemont, and N. Grevesse, *Astron. Astrophys.* 112, 337 (1982).
15. K. S. Rao, *Nature* 170, 670 (1952).
16. K. S. Rao, *Nature* 173, 1240 (1954).

17. K. S. Rao, *Proc. Nat. Inst. Sci. India* 21A, 188 (1955).

18. W. L. Wiese and J. R. Fuhr, *J. Phys. Chem. Ref. Data* 4, 263 (1975).

19. L. E. Kline and M. J. Kushner, "Computer Simulations of Materials Processing Plasma Discharges", in *CRC Critical Reviews in Solid State and Materials Science*, 16, 1 (CRC Press, Florida 1989).

20. M. Ohwa, T. J. Moratz and M. J. Kushner, *J. Appl. Phys.* 66, 5131 (1989).

21. G. A Hebner and G. N. Hays, *Appl. Phys. Lett.* 59, 537 (1991).

22. J. W. Shon, G. A. Hebner, G. N. Hays, and M. J. Kushner, "Predictions for Gain in the Fission Fragment Excited Xe Laser", 2ubmitted to *J. Appl. Phys.*

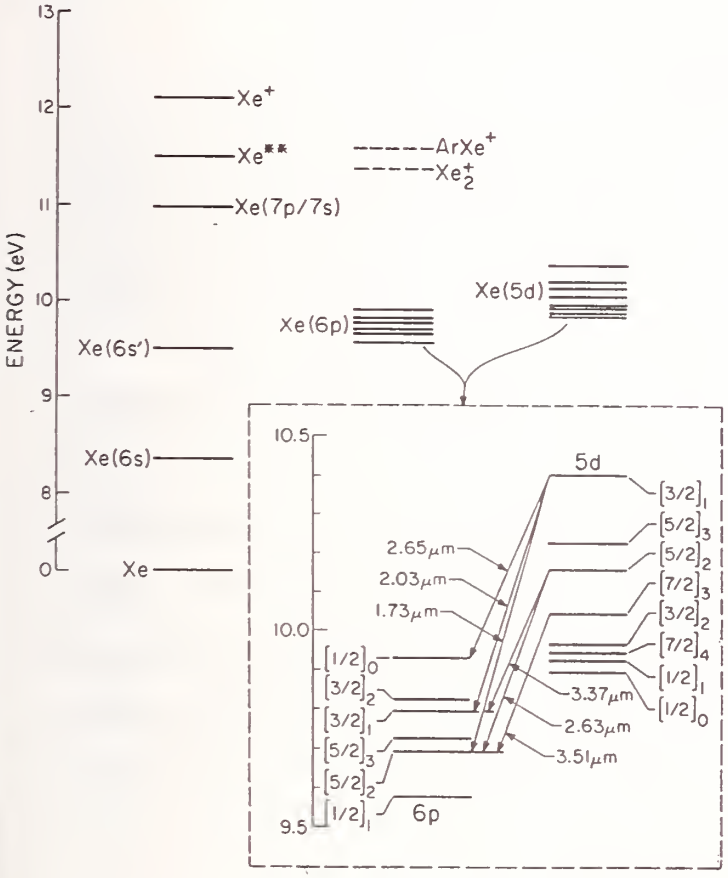

Figure 1. Energy levels and transitions in the atomic xenon (5d→ 6p) laser.

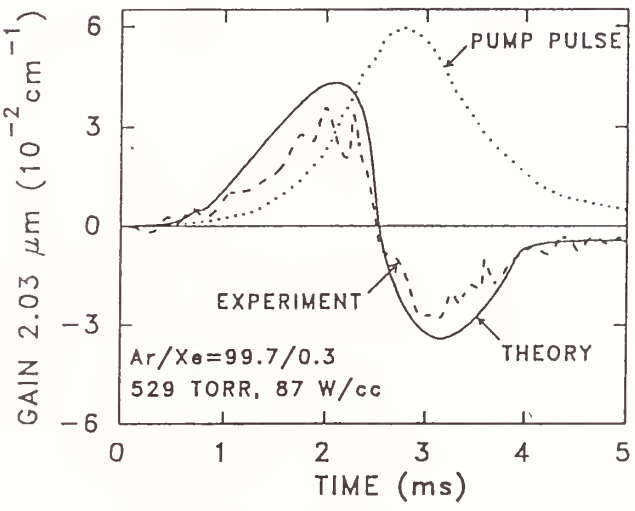

Figure 2. Experimental and modeling results for gain gain at 2.03μm in a fission fragment excited xenon laser. The termination in gain is believed to be a result of electron collisions.

New measurements in the spectrum of neutral lithium (Li I) by Fourier Transform Spectroscopy.

LEON J. RADZIEMSKI, Physics Department, Washington State University
ROLF ENGLEMAN, Chemistry Department, University of New Mexico
JAMES BRAULT, National Solar Observatory

The neutral lithium spectrum plays a pivotal role in modelling the solution for a four-body problem. Also it provides a good test for specific mass shift calculations (SMS), because SMS and the normal isotope shift are the only contributions. The most recent improvement in Li I energy levels appeared in the late 1950's. Since then energy level spacings due to electronic structure and electron-nuclear interactions have been measured by many spectroscopic techniques. The energy levels are of uneven accuracy due to variable wavenumber accuracy primarily due to the infrared data measured with 1950's grating technology. To remedy this situation we remeasured the ^{6}Li and ^{7}Li spectra (3,000 to 30,000 cm^{-1}) using the 1-meter McMath Fourier Transform spectrometer at Kitt Peak. The measurements have been completed but the level analysis has not been finished.

A by-product of the FT measurements will be a consistent set of relative oscillator strengths.

The Atomic Branching Ratio Project at NIST

J. Z. Klose and W. L. Wiese
National Institute of Standards and Technology
Gaithersburg, MD 20899

The Atomic Physics Division of the National Institute of Standards and Technology has a project underway to compile branching ratios for transitions in atomic ions of interest. So far, data have been published on H-, He-, Li-, Be-, and B-like ions, providing such ratios for transitions in ionic species of light elements. These elements (H, He, C, N, O, Ne) occur as impurity ions in high-temperature plasmas or may be conveniently introduced as trace elements for diagnostic studies. Further tabulations are planned to provide additional data on these elements.

Table 1, which contains branching ratios for the ion N II, is a typical presentation of such data. In the table the intensity ratio $I_{short}/I_{long} = A_{short}\lambda_{long}/A_{long}\lambda_{short}$.

References

[1] J. Z. Klose and W. L. Wiese, J. Quant. Spectrosc. Radiat. Transfer **42**, 337 (1989).

[2] J. Z. Klose, J. R. Fuhr, M. S. Price, and W. L. Wiese, J. Quant. Spectrosc. Radiat. Transfer **48**, 33 (1992).

[3] D. Luo and A. K. Pradhan, J. Phys. B **22**, 3377 (1989).

[4] K. L. Bell, C. A. Ramsbottom, and A. Hibbert, J. Phys. B **25**, 1735 (1992).

Table 1. Branching ratios for singly ionized nitrogen

Ion	λ_{short} (Å)	Multiplet	λ_{long} (Å)	Multiplet	A_{short} (10^8 s^{-1})	A_{long} (10^8 s^{-1})	$\frac{I_{short}}{I_{long}}$	Estimated Accuracy (%)	References (short; long)
N II	481.27	$2p^2\ ^1D - 6s\ ^1P^\circ$	525.17	$2p^2\ ^1S - 6s\ ^1P^\circ$	0.872	0.844	1.13	18	3;3
			1709.66	$3p\ ^1P - 6s\ ^1P^\circ$	0.872	0.186	16.7	18	3;3
			2044.76	$3p\ ^1D - 6s\ ^1P^\circ$	0.872	0.211	17.6	18	3;3
			2230.03	$3p\ ^1S - 6s\ ^1P^\circ$	0.872	0.0277	146	30	3;3
			4776.22	$4p\ ^1P - 6s\ ^1P^\circ$	0.872	0.103	84.0	18	3;3
			5631.72	$4p\ ^1D - 6s\ ^1P^\circ$	0.872	0.118	86.5	18	3;3
			6174.34	$4p\ ^1S - 6s\ ^1P^\circ$	0.872	0.0140	799	18	3;3
	485.85	$2p^2\ ^1D - 5d\ ^1F^\circ$	2130.18	$3p\ ^1D - 5d\ ^1F^\circ$	9.79	0.242	177	14	3;3
			6330.80	$4p\ ^1D - 5d\ ^1F^\circ$	9.79	0.0139	9180	14	3;3
	487.38	$2p^2\ ^1D - 5d\ ^1D^\circ$	1789.40	$3p\ ^1P - 5d\ ^1D^\circ$	6.32	0.126	184	14	3;3
			2159.93	$3p\ ^1D - 5d\ ^1D^\circ$	6.32	0.123	228	14	3;3
			6600.94	$4p\ ^1D - 5d\ ^1D^\circ$	6.32	0.0186	4600	14	3;3
	501.22	$2p^2\ ^1D - 5s\ ^1P^\circ$	549.03	$2p^2\ ^1S - 5s\ ^1P^\circ$	1.47	1.63	0.99	14	3;3
			1991.30	$3p\ ^1P - 5s\ ^1P^\circ$	1.47	0.369	15.8	14	3;3
			2461.27	$3p\ ^1D - 5s\ ^1P^\circ$	1.47	0.411	17.6	14	3;3
			2734.73	$3p\ ^1S - 5s\ ^1P^\circ$	1.47	0.0503	159	14	3;3
			7897.62	$4p\ ^1P - 5s\ ^1P^\circ$	1.47	0.227	102	14	3;3
			10546.76	$4p\ ^1D - 5s\ ^1P^\circ$	1.47	0.277	112	14	3;3
			12624.48	$4p\ ^1S - 5s\ ^1P^\circ$	1.47	0.0284	1300	14	3;3
	510.76	$2p^2\ ^1D - 4d\ ^1F^\circ$	2709.84	$3p\ ^1D - 4d\ ^1F^\circ$	18.7	0.264	376	14	3;3
	513.85	$2p^2\ ^1D - 4d\ ^1D^\circ$	2206.09	$3p\ ^1P - 4d\ ^1D^\circ$	12.4	7.04	7.56	14	3;3
			2799.22	$3p\ ^1D - 4d\ ^1D^\circ$	12.4	0.162	417	14	3;3
			12891.15	$4p\ ^1P - 4d\ ^1D^\circ$	12.4	0.211	1470	14	3;3

Table 1 - Continued-2

Ion	λ_{short} (Å)	Multiplet	λ_{long} (Å)	Multiplet	A_{short} (10^8 s^{-1})	A_{long} (10^8 s^{-1})	$\frac{I_{short}}{I_{long}}$	Estimated Accuracy (%)	References (short; long)
	530.34	$2p^2\ ^1S - 5d\ ^1P^o$	1765.68	$3p\ ^1P - 5d\ ^1P^o$	6.12	0.0110	1850	27	3;3
			2326.34	$3p\ ^1S - 5d\ ^1P^o$	6.12	0.183	147	14	3;3
			5240.86	$4p\ ^1P - 5d\ ^1P^o$	6.12	0.0062	9750	14	3;3
			6973.55	$4p\ ^1S - 5d\ ^1P^o$	6.12	0.0262	3070	14	3;3
	547.82	$2p^2\ ^1D - 4s\ ^1P^o$	605.44	$2p^2\ ^1S - 4s\ ^1P^o$	2.08	4.15	0.55	14	3;3
			3006.83	$3p\ ^1P - 4s\ ^1P^o$	2.08	0.956	11.9	14	3;3
			4227.74	$3p\ ^1D - 4s\ ^1P^o$	2.08	1.03	15.6	14	3;3
			5104.44	$3p\ ^1S - 4s\ ^1P^o$	2.08	0.0855	227	14	3;3
	559.76	$2p^2\ ^1S - 4d\ ^1P^o$	3023.67	$3p\ ^1S - 4d\ ^1P^o$	11.4	0.227	271	14	3;3
			10907.45	$4p\ ^1P - 4d\ ^1P^o$	11.4	0.132	1680	14	3;3
	574.65	$2p^2\ ^1D - 3d\ ^1F^o$	6610.57	$3p\ ^1D - 3d\ ^1F^o$	36.9	0.632	672	14	3;3
	582.16	$2p^2\ ^1D - 3d\ ^1D^o$	4447.03	$3p\ ^1P - 3d\ ^1D^o$	28.2	1.18	183	10	3,4;3,4
			7762.24	$3p\ ^1D - 3d\ ^1D^o$	28.2	0.855	440	12	3,4;3,4
	635.20	$2p^2\ ^1S - 3d\ ^1P^o$	3919.00	$3p\ ^1P - 3d\ ^1P^o$	22.9	0.693	204	12	3,4;3,4
			6284.33	$3p\ ^1D - 3d\ ^1P^o$	22.9	0.0726	3120	12	3,4;3,4
			8438.74	$3p\ ^1S - 3d\ ^1P^o$	22.9	0.207	1470	17	3,4;3,4
	660.29	$2p^2\ ^1D - 2p^3\ ^1P^o$	745.84	$2p^2\ ^1S - 2p^3\ ^1P^o$	34.1	12.1	3.18	12	3,4;3,4
	746.98	$2p^2\ ^1D - 3s\ ^1P^o$	858.38	$2p^2\ ^1S - 3s\ ^1P^o$	40.2	0.474	97.5	27	3,4;3

PRECISION MEASUREMENT OF THE MEAN LIFE OF THE Ar II 4p' $^2F^0_{7/2}$ LEVEL

Jian Jin and D. A. Church
Physics Department, Texas A&M University, College Station, Texas 77843

A variant of the collinear laser beam - ion beam spectroscopy technique has been used to measure the mean life of the 4p' $^2F^0_{7/2}$ level of Ar II to a relative precision of 3 x 10^{-3}. Our result is $\tau = 8.414 \pm 0.025$ ns, in excellent agreement with the recent result of Marger and Schmoranzer[1] $\tau = 8.41 \pm 0.03$ ns, obtained by a crossed laser-ion beam technique.

Our technique enables a measurement without either mechanical motion or laser sweeping. The apparatus is shown schematically in Figure 1. The beam from an etalon-stabilized ring dye laser is directed anti-parallel to a 30 keV Ar^+ ion beam. This ion beam contains metastable 3d' $^2G^0_{9/2,7/2}$ states produced in the ion source. With the laser fix-tuned to 6124.39Å, measured with a Burleigh wavemeter, and a voltage-controlled velocity change of the ions, the Doppler effect enables resonant excitation of the 4p' $^2F^0_{7/2}$ level from either of the lower levels. Optical decays of the upper level were observed near 4610 Å and 4906 Å, and a prompt cascade transition near 672 Å, which follows the 4610 Å decay, was observed as well. The fluorescence was collected perpendicular to the beam direction using a condensing lens for the visible transitions.

Precise electric field plates[2,3] were used to accelerate the ions in the observation region, resulting in laser excitation only in a limited spatial region. By adjusting the potential of the whole electric field plate assembly, this excitation region was scanned in space. The emissions of ions selectively excited upbeam from the detection region were collected after a delay determined by the distance between excitation and detection regions, and the ion velocity. This delay corresponded to times in the ns range, resulting in an ion intensity variation with accelerating potential from which the mean life was extracted. Figure 1 shows schematically this variation in space, or time relative to excitation.

The ion spectrum was obtained by setting the electric field to zero and scanning the potential of the field plate assembly. This spectrum is shown in Figure 2. The width is determined by the velocity distribution of the ions in the source, vari-

ations of the potentials, and the laser line width (about 30 MHz). Mean life measurements were initiated only when this spectrum was stable and reproducible.

Figure 3(a) shows the excitation as a function of scan voltage. Only that portion of the decay curve which is not influenced by the excitation distribution was useful for the mean life determination. The logarithm of the photon counts vs. scan voltage is shown in Figure 3(b), for this part of the intensity variation.

Measurements were made under various test conditions to define the possible existence of systematic effects. Since the laser light was partially polarized, and the residual magnetic field was not shielded, quantum beats were a possibility. Measurements with predominantly linearly and also circularly polarized light were completed, and found to result in mean lives which differed by slightly more than the standard deviation of the means of the measurements. This was the largest component of the error assigned to the final result. Table 1 shows other components of the error analysis. The 38 measurements made a statistical contribution of only 1.2×10^{-3} to the total error. Figure 4 shows the distribution of the results of these independent measurements. Only one measurement lies more than two standard deviations away from the mean result.

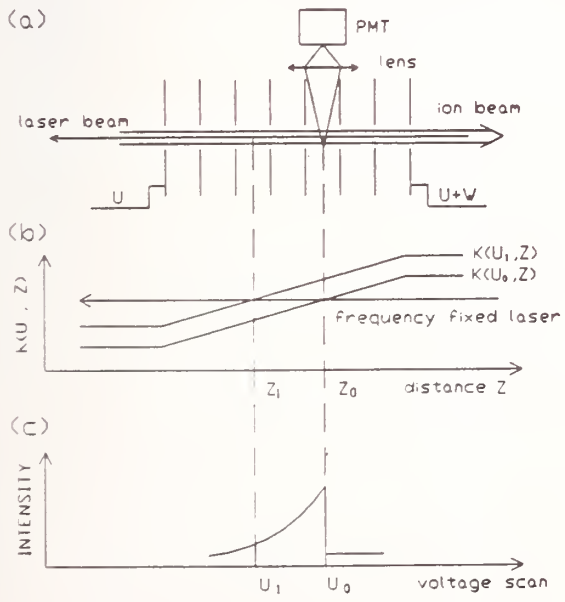

Fig. 1. Principle of the rapid Doppler switching technique. (a) Schematic of the apparatus. (b) Ion kinetic energy as a function of position between the field plates and the potential U. (c) Expected fluorescence intensity change as the potential U is scanned.

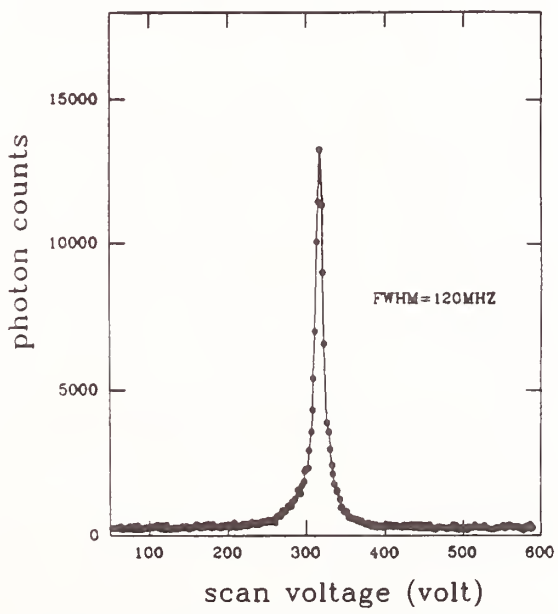

Fig. 2. *Ar II* $3d'\ ^2G_{9/2}$ - $4p'\ ^2F^0_{7/2}$ resonance spectrum.

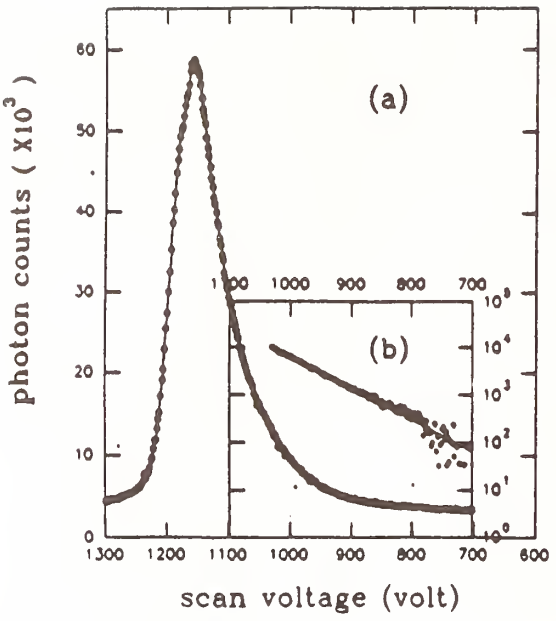

Fig. 3.(a) An example of data of the fluorescence decay curve of the *Ar II 4p' $F^0_{7/2}$* level. (b) The useful portion of the decay curve for extracting mean life information. The plot is semi-logarithmic with a constant background subtracted.

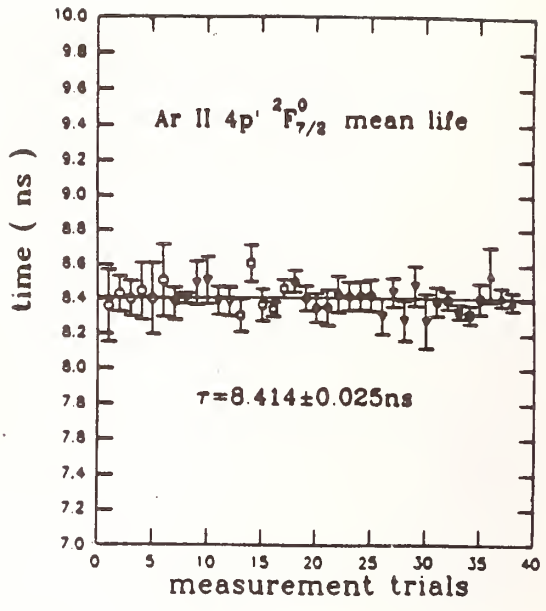

Fig. 4. Mean life measurement trials. All solid symbols represent the measurements done using partially linearly polarized laser light, and open ones for elliptically polarized light. Similar symbols designate trials made during a continuous sequence of measurements. The raw measurement result was τ = 8.409 ± 0.012 ns. After systematic corrections, the final result is τ = 8.414 ± 0.025 ns.

Table-1 List of systematic errors

source	correction (in 10^{-3})	error (in 10^{-3})
Collision with rest gas	+0.17	±0.17
E-field		±1.4
Alignment of ion-beam and E-field	+0.44	±0.44
U determination		±1.1
Stark effect	negligible	negligible
Quantum beat		±2
Statistics		±1.2
Total	+0.61 (in sum)	±3.0 (in quadrature)

References

1. D. Marger and H. Schmoranzer, Phys. Letters **A146**, 502 (1990).
2. M.L. Gaillard, D. J. Pegg, C. R. Bingham, H. R. Carter, R. C. Mlekodej, and J. D. Cole, Phys. Rev. A26, 1975 (1982).
3. D. J. Pegg, M. L. Gaillard, C. R. Bingham, H. R. Carter, and R. C. Mlekodej, Nucl. Instrum. Meth. 202, 153 (1982).

Accurate Oscillator Strengths for Interstellar Ultraviolet Lines of Cl I

R.M. Schectman, S.R. Federman, D.J. Beideck, and D.G. Ellis
Department of Physics and Astronomy, University of Toledo, Toledo, OH 43606

Work Supported in Part by NASA Grant NAGW-2457

We have recently begun a re-examination of the Cl chemistry in diffuse interstellar clouds, incorporating both older satellite UV data and recent HST results. As a preliminary to this work, we report here measured f-values for the astrophysically important lines of Cl I at 1088, 1097, and 1347 Å. For 1088 and 1097 Å, only f-values estimated from astronomical data or from theoretical calculations were previously available. However, the astronomical observations indicated that the f-value of λ1097 was significantly smaller than that of λ1088, while the calculations of Ojha and Hibbert, based upon the classification scheme of Radziemski and Kauffman, predicted the reverse.

VUV transitions were studied using the beam foil spectroscopy facility at the University of Toledo Heavy Ion Accelerator. Beams of Cl^+ ions at energies of 130 keV and 180 keV were neutralized and excited by traversal through thin (2 μg/cm^2) carbon foils. Time-resolved decay curves were obtained by recording the intensity of the radiation selected as a function of the distance between the exciter foil and the monochromator entrance slits.

Decay curves for transitions from the $3p^4(^3P)4s\ ^2P_{3/2}$ level to both the $3p^5\ ^2P^o_{3/2}$ ground state (1347.24 Å) and to the higher-lying fine structure level $3p^5\ ^2P^o_{1/2}$ (1363.45 Å) were measured. These decays were observed to be essentially single exponential for times after excitation of less than 10 ns, with deviations due to cascade repopulation observed only for longer delays. The value obtained for the meanlife of the $3p^4 4s(^3P)\ ^2P_{3/2}$ excited level was 1.51 ± 0.07 ns. To extract A-values for the two competing transitions, the branching ratio I(1347)/I(1363) was measured as 5.77 ± 0.23, independent of distance from the foil, as required. The detection efficiency of the monochromator-phototube combination varies by less than 1% over this small wavelength interval. The resulting f-values are shown in Table 1.

Next, the resonance transitions from the J = 5/2 levels at 1088.06 and 1097.37 Å were measured. The spectral feature at 1088.06 Å is strong and unblended. As for the two previous transitions, decay curves were measured at two energies and for different directions of travel. To improve the statistical accuracy, data from a number of decay curves measured with different foils were superimposed. The resulting experimentally determined meanlife was 3.3 ± 0.3 ns.
On the other hand, the line at 1097.37 Å is very weak. It appears only as a shoulder on the stronger transition 1098.07Å. The spectra were fit by a superposition of Gaussians and the ratio of the intensities of these two lines R(1088/1097) was obtained at a number of times after excitation. The ratio varied slowly with time and extrapolation to t=0 gave a value for R as the atoms exited the foil of R = 9.3 ± 1.1. Making the assumption that the two J=5/2 levels arising from the same $2p^4(^3P)3d$ configuration are equally populated initially results in a meanlife for the excited state leading to the 1097 Å transition of 31 ± 5 ns. The measured intensity of the 1097 Å line as a function of time is indeed consistent with a single exponential decay of 31 ns, qualitatively confirming the assumptions made concerning the nature of the foil excitation process. Because of the very small transition energies involved, the branching ratios to the lower-lying levels of the $3p^4(^3P)4p$ configuration are small and may be neglected when computing a transition probability for λ1088 from the measured meanlife. The f-values for λ1088 and λ1097 are compared with previous results in Table 2.

Conclusions:

Our f-values for λ1347 and λ1363 (f(1347) = 0.153±0.011 and f(1363) = 0.055±0.004) are the most precisely measured values available. They are systematically some 40% larger than those reported earlier, necessitating a re-evaluation of astrophysical conclusions based upon the older, less accurate, results. In particular, f-values obtained from astronomical observations which rely upon knowledge of f(1347) must be revised. Agreement between our measurements and the recent theoretical predictions of Ojha and Hibbert (1990) is, for these lines, quite satisfactory.

Our f-values for λλ1088, 1097 (f(1088) = 0.081±0.007 and f(1097) = 0.0090±0.0015) represent the first laboratory measurements for these lines. These results resolve the issue regarding the relative strengths for λλ1088, 1097 in favor of those indicated by astronomical measurements, showing that λ1088 is by far the stronger of the two lines.

We will discuss the consequences of these measurements for understanding the diffuse interstellar medium in a subsequent paper, where a study of the chlorine chemistry based upon our new f-values will be described.

Table 1
Oscillator Strengths

	1347.2Å	1363.Å
This Work	0.153 ± 0.011	0.055 ± 0.004
Previous Results:		
Schwab and Anderson	0.109 ± 0.010	---
Hofmann	0.090	0.035
Lawrence	0.113	0.039
Clyne and Nip	0.10 ± 0.03	0.038 ± 0.006
Ganas	0.138	0.028
Ojha and Hibbert	0.132(L)[a]	0.049(L)[a]
	0.117(V)[a]	0.041(V)[a]

[a](L) is length form and (V) is velocity form.

Table 2
Oscillator Strengths

	1088.06	1097.37
This Work	0.081 ± 0.007	0.0090 ± 0.0015[c]
Previous Results:		
Federman	0.069 ± 0.020[a]	...
Federman	0.094 ± 0.026[b]	...
Jura and York	...	0.014 ± 0.004
Jura and York	...	0.019 ± 0.005[b]
Ojha and Hibbert	0.016(L)[d]	0.042(L)[d]
Ojha and Hibbert	0.006(V)[d]	0.017(V)[d]

[a]redetermined from original data.
[b]revised using f(1347) obtained in this work.
[c]using assumed excitation.
[d](L) is length form and (V) is velocity form.

RELATIVE INTENSITIES OF RESONANCE TRANSITIONS IN B–LIKE IONS

J. Doerfert, E. Träbert, P.H. Heckmann, G. Möller, J. Granzow, C. Wagner
Experimentalphysik III, Ruhr–Universität Bochum
W–4630 Bochum 1, Germany

The relative intensities of the resonance transitions $2s^22p\ ^2P^o_{1/2,3/2} - 2s2p^2\ ^2S_{1/2}$ would be expected to show a ratio of 1÷2 for pure LS–coupling states. As especially the $^2S_{1/2}$ and $^2P_{1/2}$ levels are strongly mixed by spin–orbit–interaction, the intensity ratios deviate from these given ratios. We measured the intensity ratios of the fine fine structure components of the $2s^22p - 2s2p^2$ resonance transitions in the $^2P^o - ^2S$ case, where the effect should be strongest, and for the $^2P^o - ^2P$ transitions. Using the beam–foil technique, we thus follow up on a similar study on the Al–like ions [1], expecting that the effect of configuration interaction should be stronger in the homologous sequence of B I. As the configuration mixing varies with the nuclear charge of the ions, we undertook to study this B I isoelectronic trend as far as possible with our experimental set–up, i.e. from oxygen through chlorine. Some of our results are shown in fig. 1, alongside the theoretically predicted trends.

This particular case has been treated by theory before,e.g. using the Cowan Code and including only the mixing of the configurations within the n=2 shell [2] or using the Multi–Configuration Hartree–Fock method (MCHF) and including several configurations in the n=3 shell [3]. For low Z, the results of all these calculations agree with the experimental intensity ratios very well. For higher nuclear charges, however, there are some deviations; thus it seemed interesting to investigate whether the configuration interaction with some configurations in higher shells would be important as well.

Our own calculations were based on the Froese Fischer MCHF code. After first considering only configurations within the n=2 shell, we then included more and more configurations with one electron in the n=3 shell: at first only configurations with the electron core $2s^2$ were included, then configurations with the core $2s^2$ and 2s2p were added, and in the next step configurations with electron cores $2s^2$, 2s2p and $2p^2$. In the

most complex calculation we also took configurations into account with feature one electron in the n=4 shell with electron cores $2s^2$ and 2s2p. For all states of the same quantum number J the energy matrix was set up and diagonalized including the spin–orbit interaction.

In order to test for the influences of relativistic effects, we included all Breit–Pauli interactions in the most simple case of our calculations. It turned out, however, that even at higher nuclear charges these effects are negligible. As has already been observed by Dankwort and Trefftz [3], configuration mixing is more important for allowed transitions than relativistic effects.

Our calculations including the n=2 states only or configurations up to n=3 reproduced the results of the comparable earlier calculations [2, 3], respectively, fairly well. The effect of configurations of the n=4 shell, however,turned out to be smaller than we had expected and is rather insignificant. Therefore fig. 1 besides the experimental ones only shows the theoretical intensity ratios obtained from computations which included electrons up to the n=3 shell. For low nuclear charges it is apparently sufficient to include configuration mixing only within the n=2 shell, but for higher nuclear charges the mixing with configurations of the n=3 shell becomes important to match the experimental findings.

1. L. Engström, N. Reistad, C. Jupen and M. Westerlind, Phys. Scr. 39, 66 (1989).
2. B. C. Fawcett, At. Data Nucl. Data Tables 16, 135 (1975).
3. W. Dankwort and E. Trefftz, Astron. Astrophys. 65, 93 (1978).

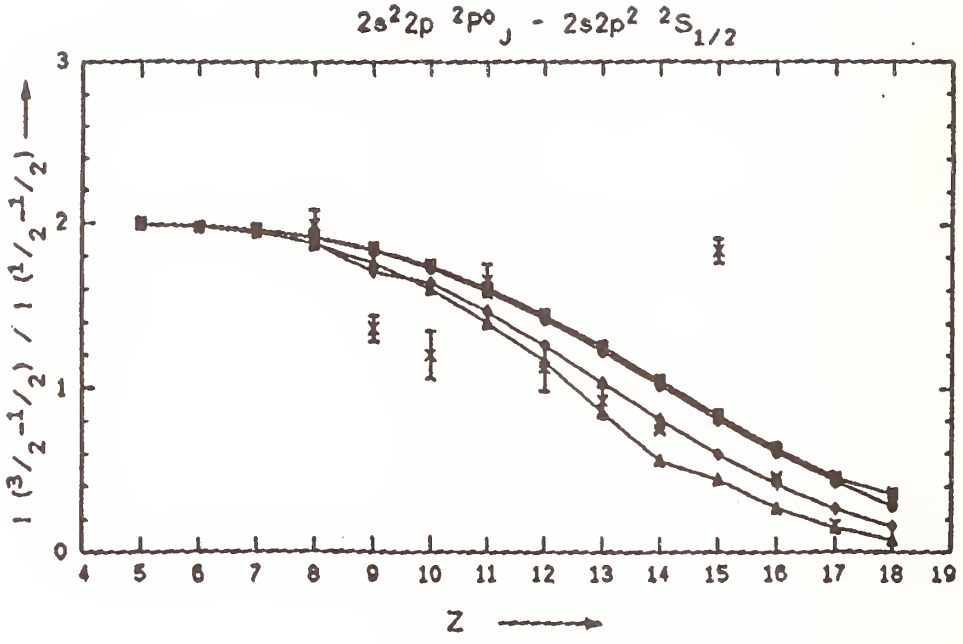

Fig. 1: Intensity ratio $I(^3/_2 - ^1/_2)/I(^1/_2 - ^1/_2)$ of the line pair $2s^2 2p\ ^2P^o_J - 2s2p^2\ ^2S_{1/2}$ as a function of nuclear charge Z.

(×) Experiment (Error bars reflect statistical uncertainties only.)

Theory

Results of our own MCHF calculations with varying numbers of configurations.

(•) Mixing within the n=2 shell only, (■) mixing with configurations of the n=3 shell with electron core $2s^2$, (▲) mixing with configurations of the n=3 shell with electron cores $2s^2$ and 2s2p, (◆) mixing with configurations of the n=3 shell with electron cores $2s^2$, 2s2p and $2p^2$.

ACCELERATOR-BASED SPECTROSCOPY PROJECTS AT BOCHUM

E. Träbert
Experimentalphysik III, Ruhr-Universität Bochum
D-4630 Bochum 1, Germany

The Bochum accelerator laboratory houses a 4 MV Dynamitron tandem accelerator capable of producing comparably high ion beam currents of many elements (about 40 have been tried so far) as well as a 400 kV single stage accelerator. Both machines can serve ion beams to the spectroscopy set-up which is run by P.H. Heckmann and E. Träbert. This permanent experimental set-up consists of a McPherson Mod. 247, R = 2.2 m, grazing-incidence spectrometer with four interchangeable gratings (300, 600, 1200 and 3600 l/mm), working best in the wavelength range λ = 4 to 80 nm. A mobile grazing-incidence spectrometer employs the same 1200 l/mm grating and covers the wavelength range λ = 1 to 13 nm. Foil and gas targets can be used. This contribution concentrates on data obtained since the previous conference at Amsterdam, in particular from intercombination decay studies done at Bochum and Argonne.

$2p^3\ {}^4S^o_{3/2}$ decay in He^-

The $2p^3\ {}^4S^o$ state can be considered as being triply excited, as none of the electrons are in an orbit occupied in the ground state configuration. Because of its particular symmetry, however, it does not disintegrate rapidly by autoionization, but is expected to emit narrow band radiation when decaying towards the $1s2p\ {}^3P^o + \varepsilon l$ continuum ([1] and refs. therein). In neutral Li and in the positively charged three-electron ions the $2p^3\ {}^4S^o$ level and the level it predominantly decays to, $1s2p^2\ {}^4P$, are both bound. This has been discussed e.g. by K.T. Chung ([2] and refs. therein), and it has been corroborated by wavelength and lifetime measurements in Li^0 and Be^+ [3,4] as well as by new experimental wavelength data for B^{2+} and C^{3+} [5,6].

In the case of He^- neither of the aforementioned levels is bound. The upper level, however, is narrow, because autoionization is suppressed for reasons of symmetry. The lower levels ($1s2p^2\ {}^4P$, $1s3p^2\ {}^4P$, $2s2p^2\ {}^4P$) autoionize rapidly and thus must be broadened. Of these lower levels, we consider only the lowest one, because the decay branch to this level is the dominant one. When a radiative transition from the $2p^3\ {}^4S^o$ level has populated the $1s2p^2\ {}^4P$ level (a shape resonance just above the $1s2p\ {}^3P^o$ ionization limit of the two-electron system), one might expect a radiationless transition, autoionization, to carry away the rest of the excitation energy of the upper level. Nicolaides, however, proposed a more complicated process to take place, radiative autoionization (RA) of the $2p^3\ {}^4S^o$ level, in which a photon would be emitted simultaneously with an electron. Nicolaides' prediction is that the photon energy distribution of

this transition has a peaked shape, with a notable maximum near the matching energy for reaching the $1s2p^2\ ^4P$ shape resonance, that is near a wavelength of λ=32.315 nm.

We have, indeed, observed a weak, line-like structure at λ=(32.32±0.02) nm, in spectra of foil-excited He ions at incident energies in the range 140 - 200 keV [7]. Our results agree with the results of a parallel study by E.J. Knystautas (Québec) [6]. This would be the first observation of this elusive decay in He^-. The present data are not sufficient, however, to distinguish between a radiative decay to the $1s2p^2\ ^4P$ resonance state and subsequent (immediate) autoionization on one hand and a truly simultaneous emission of a photon and an electron, as assumed in RA, on the other.

Intercombination transitions

The occurrence of spin-changing transitions is an indicator of the break-down of LS-coupling and its replacement by intermediate coupling. The transition rates of such transitions, compared to spin-conserving transitions between similar electron configurations, provide a direct measure of relativistic interactions like spin-orbit coupling which effects multiplet mixing. Our study of systems with only a few electrons outside of closed shells, but with different electron cores, aims at obtaining data for plasma diagnostics and at finding out about reliable calculations for such cases.

The only available method to measure such transition probabilities in highly charged ions is beam-foil spectroscopy. This technique, however, requires fast ion beams and thus works properly only for lifetimes shorter than, say, 50 ns. For intercombination transitions without a change of the principal quantum number, this typically is the case only for ionic charges higher than about 12.

The inherent time resolution of the beam-foil light source permits to record delayed spectra by simply displacing the exciter foil from the field-of-view of the detection system. In this way, spectra are obtained in which the bright lines from the decays of short-lived levels have lost out in comparison to the persistent decays from long-lived levels which are weaker per unit of length of ion beam observed [8]. In a number of cases, intercombination transitions have been identified first in such delayed spectra of foil-excited ions, which then could be singled out from laboratory or astrophysical plasma spectra yielding higher precision wavelength data [9].

Kr I sequence

The present experimental program at *Bochum* proceeded from two-, three- and four-electron ions with electrons in the n=3 shell (isoelectronic sequences Mg I, Al I and Si I) to those with electrons in the n=4 (Zn I, Ga I, Ge I sequences) or in the n=5 shell (Sm I, Eu I-like). Most recently, intercombination transitions in the rare-gas like spectra of the Kr I sequence have been added. In this sequence, there are two intercombination transitions within the lowest shell,

$4p^6\ {}^1S_0$ - $4p^5 4d\ {}^3P^o_1$ and ${}^3D^o_1$, with quite different dependences of the transition probabilities on the ionic charge. The measurements agree rather well with the predicted isoelectronic trends. In particular the long-lived level, ${}^3P^o_1$, the decay of which involves a much lesser degree of mixing (which even decreases again towards higher nuclear charges) stands out [10].

Mg I, Al I, Si I sequences

At *Argonne National Laboratory*, the EUV spectrum of 120 MeV foil-excited Br ions was studied close to and away from the exciter foil [11]. A multichannel detector was used which permitted to obtain sufficient data rather quickly. Clearly the appearance of the spectrum varies with the distance from the foil (time after excitation). The lifetime results for intercombination transitions in the spectra isoelectronic with Mg I, Al I, and Si I are shown on the poster.

Work on the intercombination transitions in the Zn I, Ga I and Ge I isoelectronic sequences and on $3d^9 4s^2$ - $3d^9$ 4s4p transitions in Cu I-like spectra (which feed the laser transitions in the Morley-Sugar laser scheme [12,13] is presently being continued by studying the spectra of Mo and Rh. Also, the intercombination decay of the $1s^2 2s3p\ {}^3P^o_1$ level in Be-like ions is being studied indirectly by searching for the 2s3s ${}^3S$ - 2s3p ${}^3P^o$ and $2p^2\ {}^3P$ - 2s3p ${}^3P^o$ transitions in the spectra of Na through Si [14].

References

1. C.A. Nicolaides, *J. Phys. B:***25** L91 (1992), Corr.: **25**, 2442 (1992).
2. B.F. Davis and K.T. Chung, *Phys. Rev.* A **42**, 5121 (1990).
3. M. Agentoft, T. Andersen , and K.T. Chung, *J. Phys. B:* **17**, L433 (1984).
4. S. Mannervik, R.T. Short, D. Sonnek, E. Träbert, G. Möller, V. Lodwig, P.H. Heckmann, J.H. Blanke, and K. Brand, *Phys. Rev.* A **39**, 3964 (1989).
5. E. Träbert, *DTL Annual Report* **18** (Bochum 1992, unpublished preliminary data)
6. E.J. Knystautas (private communication 1992).
7. E. Träbert, P.H. Heckmann, J. Doerfert, J. Granzow, J. Phys. B**25**, L353 (1992).
8. E. Träbert, P.H. Heckmann, R. Hutton, and I. Martinson, *J. Opt. Soc. Am.* B**5**, 2173 (1988).
9. E. Träbert, R. Hutton, and I. Martinson, *Mon. Not. R. astron. Soc.* **227**, 27p (1987).
10. E. Träbert, Physics Letters A **167**, 69 (1992), in collaboration with J. Doerfert, J. Granzow, P.H. Heckmann, G. Möller, and C. Wagner .
11. E. Träbert, H.G. Berry, R.W. Dunford, J. Suleiman, E.W. Kanter, C. Kurtz, S. Cheng, A.E. Livingston, K.W. Kukla, F.G. Serpa, A.S. Zacarias, and L.J. Curtis (work in progress).
12. P.D. Morley, J. Sugar, Phys. Rev. A**38**, 3139 (1988).
13. G. Möller, E. Träbert, P.H. Heckmann, J. Sugar, Physica Scripta **46**, 36 (1992).
14. J. Granzow, P.H. Heckmann, E. Träbert, J. Doerfert (work in progress).

WORK IN PROGRESS AT THE LUND VUV-FTS

Ulf Litzén and Sveneric Johansson
Lund University
Physics Department, Sölvegatan 14
S-223 62 Lund, Sweden
Tel 46-46-10 77 33

1. Introduction

A Fourier Transform Spectrometer specially designed for the UV and VUV regions is being used at the Lund University Atomic Spectroscopy Group. The instrument, manufactured by Chelsea Instruments Ltd., UK, was purchased thanks to a grant from the Swedish Natural Science Research Council. In the grant application, particular emphasis was put on the possibility to produce accurate laboratory data for astrophysical research, and investigations with this purpose have accordingly dominated during the first year. More general atomic spectroscopy and atomic physics work will, however, also be carried out at the instrument, and such projects have already been initiated.

Besides the VUV-FTS, other instruments are also being used in the work described here. Thus FTS spectra at longer wavelengths, recorded at the Kitt Peak NSO FTS, have kindly been put at our disposal for several years, and we look forward to continued collaboration. For wavelengths below the lower limit of our VUV-FTS, a 3-m normal incidence (NI) grating instrument is available at our laboratory. Numerous photographic spectra in the same region at higher resolution have been recorded in collaboration with the NIST (National Institute for Standards and Technology) atomic spectroscopists at the NIST 10.7-m NI spectrograph. A collaboration with the Observatoire de Meudon has just been started, comprising use of the Meudon 10.7-m NI spectrograph.

2. The Lund VUV-FTS

The Lund VUV-FTS, a Chelsea Instruments model FT500, is of the type developed at the Blackett Laboratory, Imperial College, London (Thorne et al. [1]). The instrument, which has a 20 cm maximum scan length, is equipped with a silica beamsplitter. This gives a short wavelength limit specified as 1750 Å. By making the mechanical and optical tolerances sufficiently narrow, the instrument has been prepared for [illegible] Å. A beamsplitter having sufficient transmittance and homogeneity for the region below 1750 Å is, however, not presently available.

Instrument control and data collecting is being handled from a standard PC, where the transform itself is being carried out on a transputer board.

3.Light sources

The spectra recorded at the FTS are emitted from hollow cathode (HC) discharges. Currents ranging from 200 mA to 8 A have been used with different types of lamps. By selecting proper mixtures of gases, charge transfer is used for enhancement of spectra from singly charged atoms (see below). A Penning type light source, originally designed for emission in the X-ray region, has also been tested. Using iron cathodes, it produced strong Fe I and Fe II spectra with good stability and reasonable noise when it was run at a low voltage mode. Attempts to produce higher charge states at high voltage, low pressure mode gave an enhanced Fe II spectrum and numerous Fe III lines, not present in a cw hollow cathode. However, the noise level was rather high. Further development of a source of this kind is planned.

4. Term analysis

Besides the work specially directed towards astrophysical applications, the FTS instrument is also being used for general term analysis. In particular the complex spectra of singly charged ions (and in some cases neutral atoms) of a number of the 3d-, 4d-, and 5d-elements are on our program. This far spectra of Ti, Mn, Ru, Pd, and Au have been recorded for this purpose. In most cases extensions to other wavelength regions are planned, by using the instruments mentioned above.

The term analysis is being performed by means of line identifications using already known energy levels, establishment of new levels, and derivation of highly accurate level values from the FTS wavenumbers. Classification of the levels and interpretation of the general term structure as well as predictions of unknown levels are made by means of extensive theoretical calculations.

5. Charge transfer at thermal energies

Charge transfer at thermal energies between noble gas ions and metal atoms, resulting in enhanced population of certain excited levels in singly charged metal ions, is a well known phenomenon. Extended experimental studies are, however, needed for a better understanding. A project has been initiated, where the population enhancement in a plasma (e.g. in a hollow cathode) will be studied through measurement of line intensities. The enhancement will be investigated as a function of the energy defect in the quasi resonant process. Complex systems with a high level density are expected to provide a possibility to derive the shape of this function. The FTS method is well suited for this kind of work, due to the high data collecting capacity and the possibility for accurate relative intensity measurements. No intensity calibration is needed, as the study only concerns changes of intensity at different noble gas mixtures.

6. Measurement of oscillator strengths

Preliminary studies have been made regarding use of the VUV-FTS for branching ratio measurements. In combination with lifetime measurements, this would yield absolute oscillator strengths. Our conclusion this far is that calibration of the FTS efficiency is best made by means of well measured branching ratios of groups of lines, emitted in the same light source and at the same time as the spectrum being measured. This will e.g. eliminate influence from wavelength dependent illumination of the entrance aperture and changing transmittance of the light source window, effects that are particularly pronounced and hard to check in the UV.

Branching ratios of groups of Ar II lines in the UV, suitable for efficiency calibration, have been measured e.g. by Adams and Whaling [2], Danzmann and Kock [3], and Hashiguchi and Hasikuni [4]. Further measurements, in particular extended to the region below 2000 Å are, however, badly needed.

References

1. A.P. Thorne, C.J. Harris, I. Wynne-Jones, R.C.M. Learner and G. Cox, J. Phys. E 20, 54 (1987).
2. D.L. Adams and W. Whaling, J.Opt.Soc.Am. 71, 1036 (1981).
3. K. Danzmann and M. Kock, J.Opt.Soc.Am. 72, 1556 (1982).
4. S. Hashiguchi and M. Hasikuni, J.Phys.Soc.Japan 54, 1290 (1985).

Radiative Decay Rates for the $3s3p^2(^4P)$ Metastable Levels of Si II

Anthony G. Calamai*, Peter L. Smith, V. H. S. Kwong† & William H. Parkinson

Harvard-Smithsonian Center for Astrophysics
60 Garden St., Cambridge, Massachusetts 02138

1. Introduction:

The Si II, spin-changing, 'intersystem' lines at ~234 nm, emitted as the fine-structure levels of the $3s3p^2(^4P)$ metastable term decay to the $3s^23p(^2P)$ ground term, are prominent features in astronomical UV spectra, *e.g.*, of the the solar chromosphere[1] and planetary nebulae[2]. Because the lifetimes of the metastable levels are comparable with the collision times in such regions, intensity ratios involving these Si II] lines can be applied to determination of plasma parameters, such as electron densities and tempertures, in solar and stellar atmospheres[3,4].

The accuracies of such diagnostic techniques depend critically upon accurate knowledge of the A-values for the allowed and forbidden transitions involved. At present, radiative decay rates of the $3s3p^2(^4P)$ metastable levels of Si II] are known only by theoretical means[4,5] that can be quite uncertain until tested by measurements. In this report, we present the first experimentally determined radiative decay rates for the $J = \frac{5}{2}$, $\frac{3}{2}$, and $\frac{1}{2}$ levels of the $3s3p^2(^4P)$ term of Si II.

2. Experimental Method:

Metastable Si^+ ions were produced by electron bombardment of SiH_4 vapor, at pressures ranging from 2 to 25 $\times$ 10^{-8} Torr, and stored in a cylindrical, radio-frequency, ion trap. Radiative decay rates for the metastable levels of the $3s3p^2(^4P)$ term of Si II were determined by measuring the time dependence of the intensity of ~234-nm photons emitted when the metastable ions decayed to the ground term. The photons were focused onto a 12-nm-bandwidth interference filter in front of a photomultiplier tube operated in photon-counting mode. Beginning ~80 μs after the end of the electron-impact interval, photons were detected using a data collection technique[6] that incorporates a real-time background correction.

A logarithmic plot of one of our 29 'decay curves' is shown in Fig. 1(a); the solid-curve represents the result of a nonlinear least-squares fit of three-exponentials plus a constant background, which was small relative to the other components, to the data. To ensure that the fits converged to a consistent set of 'best' parameters in the seven-parameter χ^2 space, each decay curve was fitted using three different sets of input seeds that varied by more than a factor of two. Generally, the χ^2_ν statistics of the nonlinear fits were $\leq$1.0 and the variations of fit results were within the expected uncertainties. Experimental parameters – including trap well depth, electron-impact excitation energy, and the silane source pressure – were varied for several of the accumulated decay curves. Plots of the mean decay rates *vs.* pressure for each of the three components are shown in Fig. 2. No other significant systematic effects were observed.

3. Discussion & Results:

The essentially pertubation-free environment of our low-energy rf ion trap, coupled with a negligible probability for systematic error from cascades and the outstanding signal-to-noise ratio for each decay component, permits unambiguous determination of the radiative decay rates of the Si II] ^4P levels. A measure of the accuracy of the results is evidenced by a decomposition of the data in Figure 1(a) using the decay-rate and initial-population values determined by the fits. Figure 1(b) shows the result of this procedure: The counts associated with the two fast-decay components and with the constant background have been subtracted from the data shown in Fig. 1(a). The logarithmic plot of the remaining signal clearly indicates that only a single-component is left in the data set. This is the result regardless of which two components are

subtracted from the data and is consistent from run-to-run. Moreover, if all three components are subtracted from the data sets, the residual counts are uniformly distributed about zero with an amplitude consistent with Poisson statistics.

Our results for the radiative decay rates of the $3s3p^2(^4P)$ metastable term of Si^+ are compared with calculated values in the Table below. The assignments of the measured decay rates to the various levels of the ^4P term are based on: *(i)*, good agreement with theoretical values[4,5] for the $J = \frac{5}{2}$ and $\frac{1}{2}$ levels, and, *(ii)*, agreement with the observed relative intensities from a laboratory spectrum[7].

Decay rates (sec^{-1}) for levels of the $3s3p^2(^4P)$ metastable term of Si^+.

Author	Method	$^4P_{5/2}$	$^4P_{3/2}$	$^4P_{1/2}$
Nussbaumer[5] (1977)	theory	2398	1634	7576
Dufton *et al.*[4] (1991)	theory	2703	1721	11236
this work	experiment	2460 ± 8.2%	1233 ± 9.5%	9615 ± 15.4%

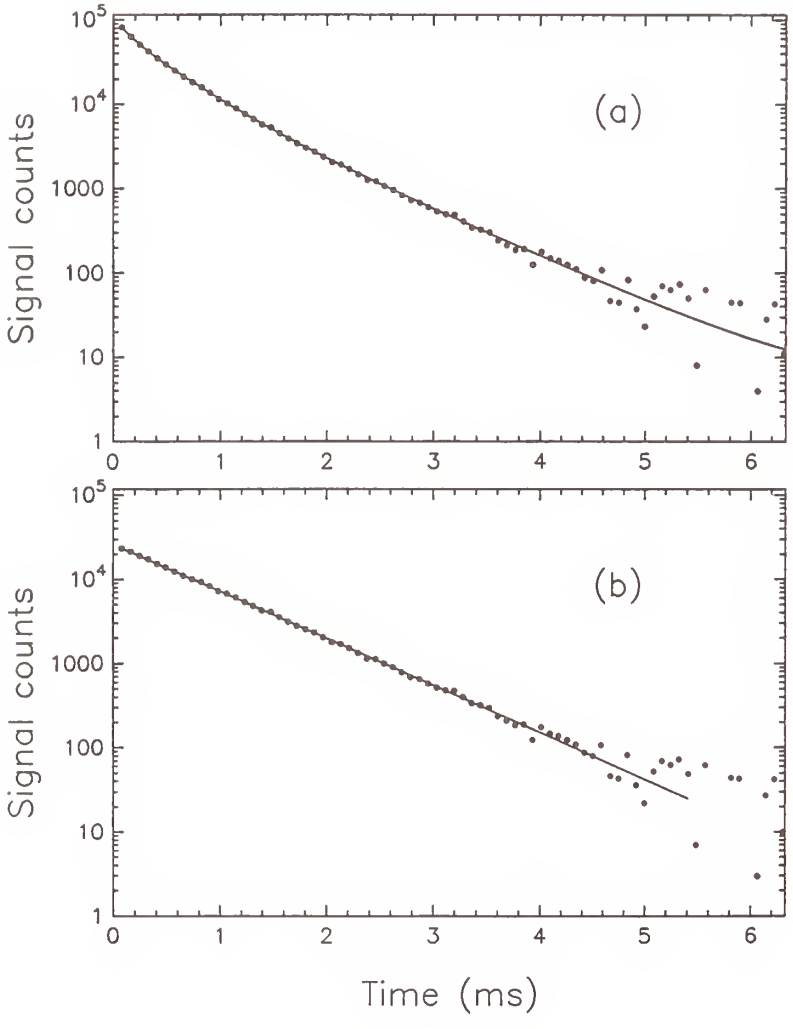

Fig. 1 Decay curves – **(a)** Logarithmic plot of the signal versus time as the $3s3p^2(^4P)$ $J = \frac{5}{2}$, $\frac{3}{2}$, and $\frac{1}{2}$ metastable populations of Si II decay. The solid-curve represents the results of a non-linear least-squares fit of three exponentials plus a constant background to the data. **(b)** Logarithmic plot of the resdiual signal counts in the data set after the results of the non-linear least-squares fit were used to extract the fast- and medium-rate components from the data. The straight-line behavior indicates only one exponentially decaying population remains in the modified data set.

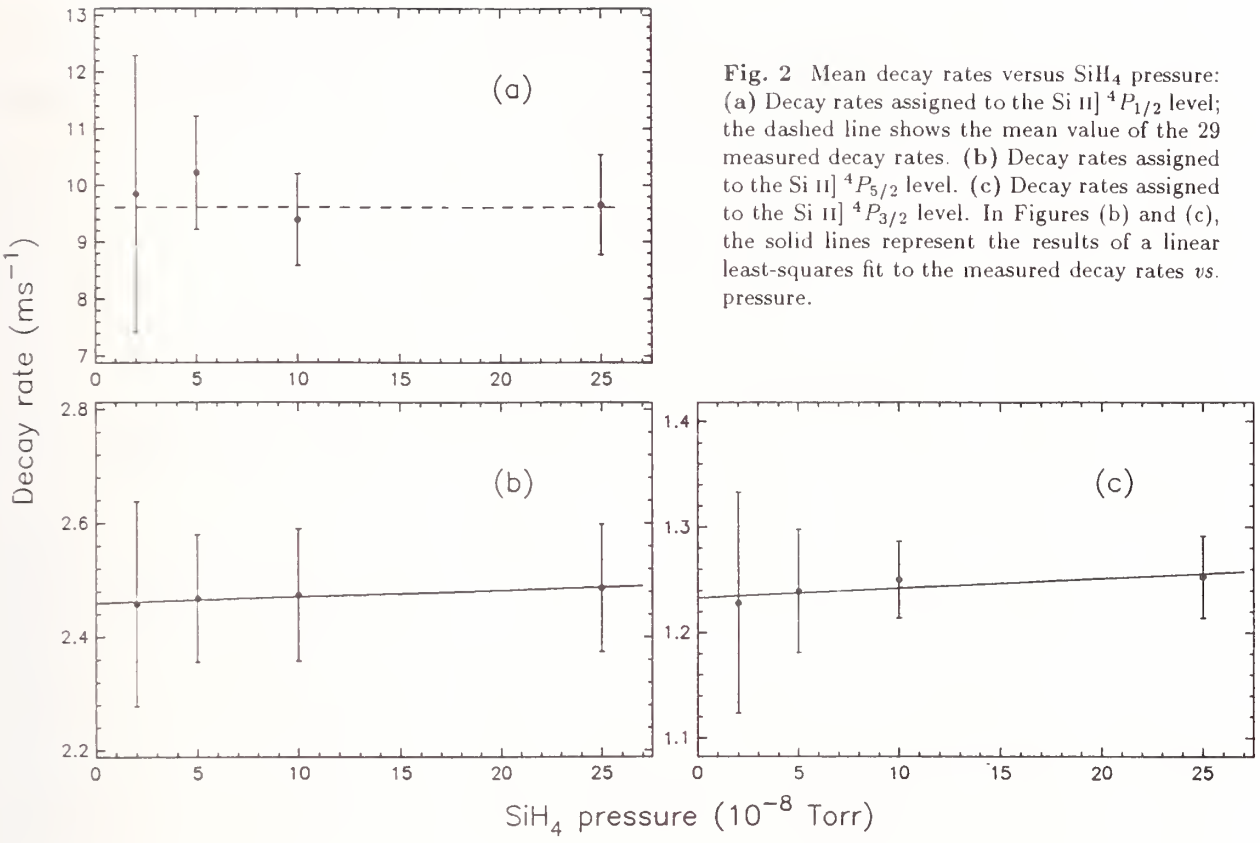

Fig. 2 Mean decay rates versus SiH_4 pressure: (a) Decay rates assigned to the Si II] $^4P_{1/2}$ level; the dashed line shows the mean value of the 29 measured decay rates. (b) Decay rates assigned to the Si II] $^4P_{5/2}$ level. (c) Decay rates assigned to the Si II] $^4P_{3/2}$ level. In Figures (b) and (c), the solid lines represent the results of a linear least-squares fit to the measured decay rates *vs.* pressure.

This work was supported in part by NASA Grants NAGW-1596 and -1687 to Harvard University.

[*] current address – Department of Mathematics & Physics, Philadelphia College of Pharmacy & Science
[†] permanent address – Department of Physics, University of Nevada at Las Vegas

References:

[1] G. A. Doschek *et al.*, Astrophys. J. Supp. **31**, 417 (1976).
[2] J. Köppen and L. H. Aller, *Exploring the Universe with the IUE Satelite*, ed. Y. Kondo, Reidel, Dordrecht, p.589 (1987).
[3] P. G. Judge *et al.*, Mon. Not. R. Astro. Soc. **253**, 123 (1991).
[4] P. L. Dufton *et al.*, Mon. Not. R. Astro. Soc. **253**, 474 (1991).
[5] H. Nussbaumer, Astron. Astrophys. **58**, 291 (1977).
[6] A. G. Calamai *et al.*, Phys. Rev. **A45**, 2716 (1992).
[7] A. G. Shenstone, Proc. R. Soc. London, Ser. A **261**, 153 (1961).

ATOMIC OXYGEN TRANSITION PROBABILITIES AND RECOMBINATION RATES OF ASTROPHYSICAL AND GEOPHYSICAL INTEREST

V. ESCALANTE[1], G. A. VICTOR[2], and A. GÓNGORA-T.[3]

[1] Instituto de Astronomía, UNAM, Ap. Postal 70-264, México, DF 04510, México
[2] Institute for Theoretical Atomic and Molecular Physics, Harvard–Smithsoninan Center for Astrophysics, 60 Garden St., Cambridge, MA 02138
[3] The University of Michigan, The Harrison Randall Laboratory of Physics, Ann Arbor, MI 48109–1120. Permanent address: Instituto de Física, UNAM, Ap. Postal 20-364, México, DF 01000, México

Dipole–allowed and spin–forbidden transitions of atomic O emit prominent lines in space and atmospheric plasmas, and accurate transition probabilities are needed to model and understand the excitation mechanisms that produce them. In the atmosphere at night and in the interstellar medium, these lines are excited by recombination of O^+ ions and thermal electrons, and information on recombination rates and transition probabilities for a large number of excited states is needed.

We present results of calculations using a model potential method to produce accurate wave functions of excited and continuum states with the ground core configuration $O^+(^4S^o)$ that allow the calculation of the recombination spectrum. Comparison with other theoretical calculations are shown. We have also carried out calculations of some allowed and spin–forbidden transitions using a multiconfiguration Hartree–Fock procedure that includes Breit–Pauli corrections (Froese Fischer 1991).

MODEL POTENTIAL CALCULATIONS

We used a one–electron semiempirical model potential (MP) to describe the interaction of the active electron with the core that includes a dipole polarization term and an additional term of the form

$$U_\gamma(r) = a_\gamma \exp(-k_\gamma r)$$

to account for exchange and other short–range corrections. The a_γ and k_γ parameters are calculated by a least squares procedure that fits the calculated energies to the observed values of the Rydberg series of a given symmetry γ. Experience with other open shell $2p$ core configurations indicates that the set of parameters for the $2p^3np$ series does not give an accurate description of the $2p^4$ terms due to the strong correlation between the 2p electrons. Thus a different set of parameters must be calculated for the ground configuration terms. Details of the calculations have been discussed by Escalante and Victor (1988, 1992a).

We have calculated transition probabilities for dipole–allowed transitions and photoionization cross sections for states with $n = 2$ to 12 and $\ell = 0$ to 2. Hydrogenic values needed for the calculation of the recombination cascade have been used for configurations with higher ℓ. Radiative recombination rates

have been calculated from the detailed balance relation for a thermal energy distribution of electrons. The effective recombination rate of a state is the rate of population of the state due to direct recombination, with rate α_i, plus cascades from all other states also populated by recombination:

$$\alpha_i^{\text{eff}} = \sum_{k \geq i} \alpha_k C_{k,i} \ , \quad C_{i,i} = 1$$

where $C_{k,i}$ is the probability of reaching state i from state k by successive transitions. The effective recombination coefficient times the branching ratio of a transition equals its emission rate. In calculating effective recombination rates we have included dipole-allowed transitions and recombination rates to triplet and quintet states of the ground core configuration. We also took into account some spin-forbidden (Egikyan 1984, Froese Fischer 1987), and dielectronic recombination rates (Nussbaumer and Storey 1984) that produce lines involving the ground configuration and states with the excited core configuration $O^+(^2D^\circ)$. Dielectronic recombination does not have a noticeable effect in the emission rates for electron temperatures below 1000 K.

In table 1 we compare our MP results for the case in which there is no absorption of resonant photons in the plasma with calculations of Julienne and Davis (1974), who used the quantum defect method (QDM), and Hartree–Fock (HF) calculations by Chung *et al.* (1991). The QDM values show significant discrepancies with the HF and MP results for low ℓ. However there is moderate or good agreement between the HF and MP results except for the $3s\ ^3S^\circ$ term where an order of magnitude disagreement exists. The difference in this case can be attributed to severe cancellation in the dipole matrix element. We have found a Fano–Cooper minimum in the $3s\ ^3S^\circ \rightarrow np\ ^3P^\circ$ photoabsorption cross section very near the continuum threshold. Thus the value of the recombination cross section is very sensitive to the details of the calculation. Decay of the $3s\ ^3S^\circ$ term produce strong lines at 130.217–130.603 and 164.131 nm and experimental determination of the cross section may help determine the correct value for the recombination rate.

MULTICONFIGURATION HARTREE–FOCK CALCULATIONS

Transitions between the ground state and excited states are important in the atmospheric dayglow and nightglow. When photons from resonant transitions are heavily scattered, spin–forbidden transitions must be taken into account. MCHF calculations for the transition probability of the $2p^4\ ^3P - 2p^3(^2D^\circ)3s\ ^3S^\circ$ multiplet at 130.217–130.603 nm (Froese Fischer 1987) is close to the the MP value. The value of Egikyan (1984) is a factor of 2 smaller than the value calculated by Froese Fischer (1987) for the transition probability of $2p^4\ ^1D - 2p^3(^2D^\circ)3s\ ^3S^\circ$ at 164.131 nm. Our MCHF calculations agree with the values of Froese Fischer (1987) even though we have used a smaller set of configurations. Nevertheless we have found some sensitivity in the choice of configuration list. For example, when $2s^2 2p^3 4f$ configurations are not included in the composition of the $2p^4$ states, the probability of the $\Delta S \neq 0$ transition at 164.131 nm decreases by a factor of 4 while resonant transition probabilities vary less than 15%.

Table 1. Comparison of direct and effective recombination rates (in $10^{-14}\,cm^3\,s^{-1}$) at 1160 K.

Term	α_{Term}[a]	α_{Term}[b]	α_{Term}[c]	α^{eff}_{Term}[a]	α^{eff}_{Term}[c]
$3s\ ^3S^o$	1.5(-3)[d]	1.24(-2)	9.00(-4)	4.89	7.1
$4s\ ^3S^o$	2.0(-3)	2.88(-4)	6.66(-3)	7.9(-1)	9.5(-1)
$5s\ ^3S^o$	3.2(-3)	8.29(-4)	7.31(-3)	2.9(-1)	3.3(-1)
$6s\ ^3S^o$	3.1(-3)	1.11(-3)	5.96(-3)	1.5(-1)	1.5(-1)
$3p\ ^3P$	6.1(-1)	1.05	6.08(-1)	4.51	7.0
$4p\ ^3P$	5.0(-1)	6.41(-1)	4.56(-1)	9.7(-1)	1.1
$5p\ ^3P$	3.5(-1)	4.01(-1)	3.10(-1)	4.6(-1)	4.8(-1)
$6p\ ^3P$	2.4(-1)	2.64(-1)	2.12(-1)	2.8(-1)	2.7(-1)
$3d\ ^3D^o$	3.00	2.98	3.23	1.56(+1)	2.4(+1)
$4d\ ^3D^o$	2.00	1.84	1.95	4.71	5.1
$5d\ ^3D^o$	1.18	1.11	1.16	2.05	2.2
$6d\ ^3D^o$	7.4(-1)	7.05(-1)	7.32(-1)	1.10	1.1
$3s\ ^5S^o$	1.3(-3)	3.95(-2)	5.05(-2)	4.93(+1)	4.8(+1)
$4s\ ^5S^o$	3.7(-3)	1.02(-3)	8.32(-4)	8.80	8.1
$5s\ ^5S^o$	5.9(-3)	8.85(-4)	3.31(-3)	2.32	2.5
$6s\ ^5S^o$	5.5(-3)	1.39(-3)	3.72(-3)	9.1(-1)	1.0
$3p\ ^5P$	2.85	2.53	2.50	4.77(+1)	4.8(+1)
$4p\ ^5P$	1.63	1.49	1.53	9.67	8.9
$5p\ ^5P$	9.6(-1)	9.00(-1)	9.26(-1)	3.24	3.1
$6p\ ^5P$	6.1(-1)	5.78(-1)	5.94(-1)	1.44	1.4
$3d\ ^5D^o$	4.90	5.24	5.62	2.68(+1)	2.8(+1)
$4d\ ^5D^o$	3.49	3.20	3.37	8.24	6.9
$5d\ ^5D^o$	2.02	1.91	1.98	3.53	3.2
$6d\ ^5D^o$	1.25	1.20	1.23	1.86	1.7

[a] Julienne and Davis (1974).
[b] Chung *et al.* (1991).
[c] Escalante and Victor (1992b).
[d] Numbers inside parenthesis indicate powers of 10.

References

Chung, S., Lin, C.C., and Lee, E.T.P., 1991, *Physical Review A*, **43**, 3433.
Egikyan, A.G., 1984, *Astrofizika*, **20**, 341 (English translation in *Astrophysics*, **20**, 185).
Escalante, V. and Victor, G.A., 1988, *Atomic Data and Nuclear Data Tables*, **40**, 203.
Escalante, V. and Victor, G.A., 1992a, *Atomic Data and Nuclear Data Tables*, submitted.
Escalante, V., and Victor, G.A., 1992b, *Planetary Space Sci.*, submitted.
Froese Fischer, C., 1987, *J. Phys. B*, **20**, 1193.
Froese Fischer, C., 1991, *Comput. Phys. Commun.*, **64**, 369.
Julienne, P.S. and Davis, J., 1974, *J. Geophysical. Res.*, **79**, 2540.
Nussbaumer, H. and Storey, P.J., 1984, *Astronomy and Astrophysics Supp.*, **56**, 293.

Transition Probabilities and Lifetimes of Ar I

V. Helbig
University of Kiel, Kiel, Germany

D. E. Kelleher and W. L. Wiese
National Institute of Standards and Technology, Gaithersburg, Maryland 20899

INTRODUCTION

Advances in modern atomic structure computer codes and reduced uncertainties in recent lifetime and branching ratio measurements have yielded extensive sets of high-accuracy atomic transition probabilities. However, most of these advances have been concentrated on spectra of the light elements. For the neutral argon spectrum, none of the modern atomic structure codes has provided theoretical data up to now nor have high precision lifetime values been provided by experimental investigations. Nevertheless, we have shown in a recent paper [1] that experiments done in recent years provide a greatly improved basis for the compilation for the Ar I 4s - 4p and 4s - 5p transition arrays and yield transition probabilities considerably more accurate than the most comprehensive earlier set of transition probabilities for Ar I [2]. We have undertaken the present compilation to extend the data given in [1] to the other prominent lines of argon.

METHOD

Following the routine discussed in detail in reference [1] we started by collecting all available lifetime values for levels of Ar I. Data have been published for 75 levels with main quantum numbers $n < 9$ (see table 1). While for some of the 4p and 5p levels up to 13 different experimental results are available, for most of the other levels only one or two experiments have been performed so far. Large differences between the data given by various authors are found for the $2s_5$, $3s_1$, $3d_2$, $4s_1$, $5d_2$, $5d_3$, $5d_5$, and $7d_2$ levels (Paschen notation). Complete sets of lifetimes are only available for the 4p, 5p and 4d configurations, as shown in Table 1. Additional measurements to augment the known lifetime data and to resolve the discrepancies in the data are therefore definitely needed. The experimental set-up at the University of Kiel (see e.g., [3]) is well suited to provide additional experimental data for a number of levels. Measurements for the 6p and 7p levels are in progress.

Table: Lifetime data available for Ar I. The numbers given after the designation of the valence electron indicate the percentage of levels measured with respect to the total number of levels (e.g., 2/4 means lifetimes for 2 out of 4 levels have been measured).

ns		np		nd	
4s	2/4	4p	10/10	3d	7/12
5s	3/4	5p	10/10	4d	12/12
6s	3/4	6p	3/10	5d	11/12
7s	1/4	7p	0/10	6d	8/12
8s	1/4	8p	0/10	7d	4/12
9s	1/4	9p	0/10	8d	0/12

To convert the lifetimes to absolute transition probabilities the respective branching ratios are required. With increasing main quantum number the branches in the infrared region of the spectrum resulting from transitions between higher quantum numbers become more and more important. This is inversely correlated to the availability of branching-ratio data. We have therefore decided to use theoretical data whenever experimental values are missing in literature. Though various papers have been published [4,5,6] that list transition probabilities, no tables exist with a complete set of the data necessary for our purpose. We therefore calculated the required transition probabilities using the Hartree-Fock code by Cowan [7]. With the help of this program the data for all transition arrays leading to levels for which experimental lifetime data are available have been calculated. These transition arrays are indicated in Fig. 1. A total number of 3 370 transition probabilities has been obtained in the course of our investigation. The accuracy of these theoretical transition probabilities is estimated by comparison with the values for the 4s - 4p and the 4s - 5p transition arrays. While for the 4s - 4p transitions very good agreement was observed, considerable differences occur for the 4s - 5p transitions, especially for the weak lines. This result was expected because of strong cancellation in the transition integral for these transitions. Attempts to improve the agreement by adjusting the energy levels to the observed ones and by including configuration interaction showed some promise, but were not yet successful.

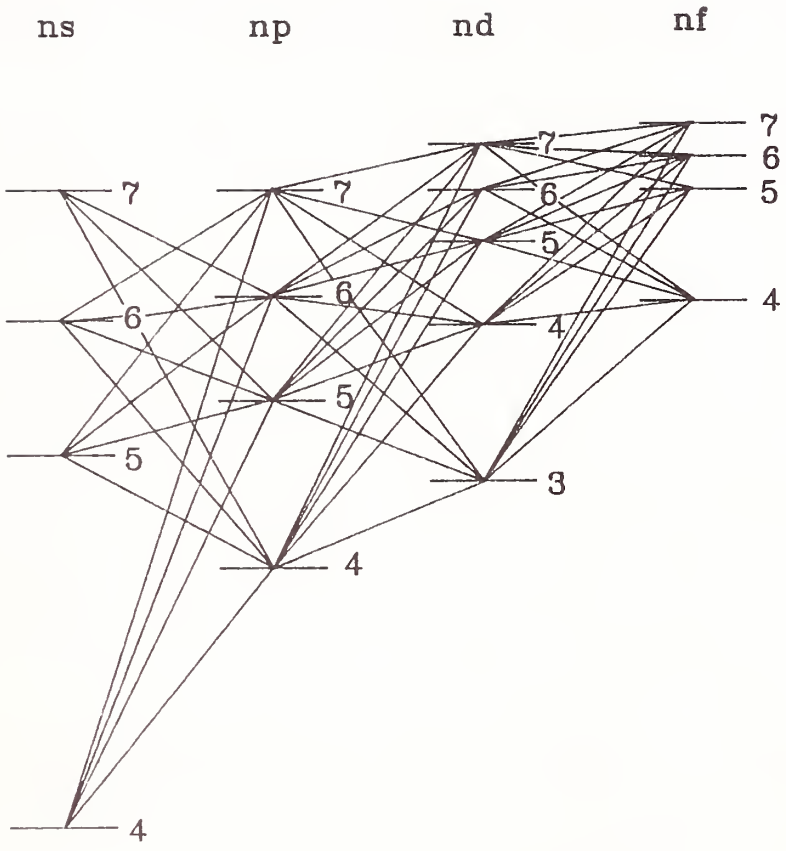

Fig. 1: Part of the Grotrian diagram for Ar I indicating those transition arrays for which calculations have been carried out.

REFERENCES

[1] W. L. Wiese, J. W. Brault, K. Danzmann, V. Helbig, and M. Kock, Phys. Rev. **A39**, 2461 (1989).

[2] W. L. Wiese, M. W. Smith, and B. M. Miles, Atomic Transition Probabilities, Vol. II, NSRDS-NBS 22 (1969).

[3] Z. Stryla, H. Pobee, W. Schade, and V. Helbig, Phys. Rev. **A41**, 512 (1990).

[4] R. A. Lilly, JOSA **66**, 245 (1976).

[5] P. E. Grudzev and A. V. Loginov, Opt. Spectroc. **38**, 411 (1975).

[6] N. V. Afanaseva and P. F. Grudzev, Opt. Spectrosc. **38**, 450 (1975).

[7] R. D. Cowan, "The Theory of Atomic Structure and Spectra," University of California Press, Berkeley (1981).

CALCULATED Ar XVII LINE INTENSITIES AND COMPARISON WITH SPECTRA FROM THE ALCATOR C TOKAMAK

K. J. H. Phillips,[1] F. P. Keenan,[2] L. K. Harra,[2] S. M. McCann,[2] E. Rachlew-Källne,[3] J. E. Rice[4] and M. Wilson[5]

Introduction: X-ray spectra from high-temperature plasmas such as those formed in tokamak devices or in solar flares are dominated by lines due to transitions in helium-like ions between the ground ($1s^2\,{}^1S_0$) level and $1s2l$ levels. The four most intense lines are due to transitions from the $1s2p\,{}^1P_1^o$, $1s2p\,{}^3P_2^o$, $1s2p\,{}^3P_1^o$ and $1s2s\,{}^3S_1$ levels to the ground level (called here w, x, y and z – see Gabriel 1972). The upper levels of these transitions are mainly populated by electron collisional excitation from the ground level, though cascade and recombination are also important. The intensity ratio $R = z/(x+y)$ is sensitive to electron density N_e for certain elements in a range that include those typical of tokamak plasmas (see Gabriel and Jordan 1969). Also, the intensity ratio $G = (x+y+z)/w$ has a rather weak dependence on electron temperature T_e. Both the R and G ratios are useful for diagnosing plasmas for which no direct measurements are available.

High-resolution spectra from helium-like argon (Ar^{+16}) have been obtained using argon-seeded plasmas in the Alcator C tokamak device at the MIT Plasma Fusion Center (e.g. Rice *et al.*, 1987). For the intermediate-Z element argon, dielectronic satellites due to $1s^2nl - 1s2pnl$ transitions in the lithium-like stage are fairly strong, and some of these satellites blend with the chief Ar XVII lines, so affecting the R and G intensities.

X-ray spectra from Alcator C: The experimental details of the Alcator C tokamak are described fully by Rice *et al.* (1987). The deuterium plasma typically has N_e in the range $1 - 2 \times 10^{14}$ cm^{-3}, $T_e = 1 - 2$ keV, and was seeded with argon atoms having a concentration of $10^{-5} - 10^{-4} \times N_e$. The X-ray emission was measured with a bent Bragg crystal spectrometer, with spectral range 3.9–4.4 Å, so including all the Ar XVII lines and Ar XVI dielectronic satellites of interest. Standard diagnostic techniques were used to find T_e and N_e.

For the spectra under discussion here, much of the emission originated from centre of the plasma, where T_e and N_e are highest, and for which any contribution from charge-exchange (see Kato *et al.* 1991) is very small.

Calculated Ar XVII spectra: Electron excitation rates from the argon ground level ($1s^2\,{}^1S_0$) to the $1s2l$ levels were calculated by Keenan, McCann, and Kingston (1987) by interpolating from results for other He-like ions obtained with the R-matrix code of Burke and Robb (1975).

[1] Astrophysics Division, Rutherford Appleton Laboratory, Chilton, Didcot, Oxon. OX11 0QX, U.K.
[2] Dept. of Physics, Queen's University, Belfast BT7 1NN, U.K.
[3] Dept. of Physics I, Royal Institute of Technology, S10044 Stockholm, Sweden
[4] MIT Plasma Fusion Center, Cambridge, Mass. 02139, U.S.A.
[5] Dept. of Physics, Royal Holloway and Bedford New College, Egham Hill, Egham, Surrey TW20 0EX, U.K.

Other atomic data required in this calculation are described by Keenan *et al.* (1987). Using these atomic data and a statistical equilibrium code, level populations were derived and hence Ar XVII line emissivities for a range of T_e and N_e.

Dielectronic excitation of the Ar XVI dielectronic satellites was calculated from the pseudo-relativistic Hartree–Fock (HFR) code, described by Cowan (1981). Collisional excitation is an important excitation mechanism for dielectronic satellites of the $1s^2\,2s - 1s2s2p$ array, and the rates for this were taken from the collision strengths calculated for Fe and Ca by Bely-Dubau *et al.* (1982a, 1982b).

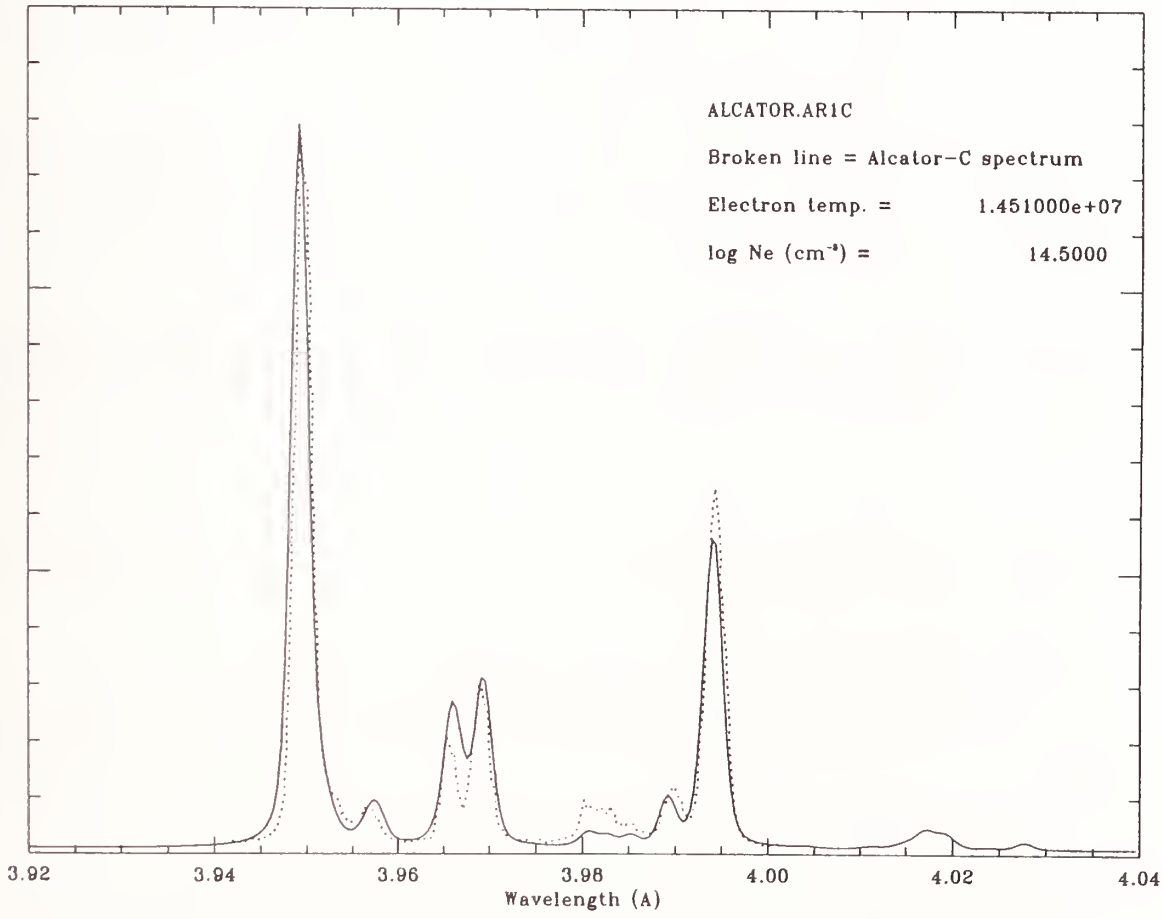

Figure 1. Calculated spectrum (solid line) compared with an argon X-ray spectrum obtained from the Alcator C tokamak, with central values of $T_e = 1.25$ keV and $N_e = 3 \times 10^{14}$ cm^{-3}.

Theoretical spectra were formed by giving each line in the spectrum a profile that is a convolution of the thermal Doppler profile and the spectrometer's instrumental width. The final spectrum is the addition of the profiles of all the lines considered. T_e and N_e are free parameters which can be chosen for any synthesized spectrum.

The Ar XVII line intensities alter with N_e through the R ratio and with T_e through the slightly varying G ratio, while the dielectronic satellites decrease in intensity with increasing T_e. As mentioned, some satellites blend with Ar XVII lines, so that any measurement of the R and G ratios to get densities of, e.g., solar-flare plasmas must take such blends into account.

Comparison of observed and calculated spectra: Several Alcator C spectra were used for comparison with theoretical spectra as calculated above. Fig. 1 shows the results of one such comparison. The values of T_e and N_e used in the calculated spectrum are those measured from diagnostic techniques, i.e. T_e and N_e have not been arbitrarily adjusted to obtain the best agreement between calculated and observed spectra. Usually these values refer to central values. Strictly, the theoretical spectrum should be formed by an integration across the plasma, taking into account the radial variation of T_e and N_e. This will be dealt with in a forthcoming paper, but meanwhile it can be said that taking central values for T_e and N_e is not expected to result in large errors as the emission from outer parts of the plasma contribute only a small amount to the intensity, the spectral intensity depending on N_e^2.

The agreement between the observed and calculated spectra is such that one can be confident of the accuracy of the atomic calculations. The chief disagreement is a difference between the calculated (too small) and observed intensities of the collisionally excited satellite known as q. Possibly this is due to the fact that coronal equilibrium, assumed in the calculations, is not adequate and that particle transport should be taken into account.

In summary, the good agreement between calculated spectra and those from a well-diagnosed tokamak plasma lead one to suppose that Ar XVII spectra can themselves be used as temperature and density diagnostics for plasmas without detailed measurements, such as solar-flare plasmas.

References

F. Bely-Dubau, J. Dubau, P. Faucher, and A. H. Gabriel, Mon. Not. R. Astron. Soc. 198, 239 (1982).

F. Bely-Dubau *et al.*, Mon. Not. R. Astron. Soc. 201, 1155 (1982).

P. G. Burke and W. D. Robb, Adv. Atom. Molec. Phys. 11, 143 (1975).

R. D. Cowan, *The Theory of Atomic Structure and Spectra*, Univ. California Press, Berkeley (1981).

A. H. Gabriel, Mon. Not. R. Astron. Soc. 160, 99 (1972).

A. H. Gabriel and Jordan, C., Mon. Not. R. Astron. Soc. 145, 241 (1969).

F. P. Keenan, S. M. McCann, and A. E. Kingston, Phys. Scr. 35, 432 (1987).

J. E. Rice, E. S. Marmar, E. Källne, and J. Källne, Phys. Rev. A, 35, 3033 (1987).

T. Kato *et al.*, Phys. Rev. A 44, 6776 (1991).

Comprehensive measurements of Fe I oscillator strengths

T. R. O'Brian, M. E. Wickliffe, J. E. Lawler
University of Wisconsin, Madison, WI
W. Whaling
California Institute of Technology, Pasadena, CA
J. W. Brault
National Solar Observatory, Tuscon, AZ

We describe an efficient method for measuring absolute oscillator strengths of moderate precision (generally 10% or better) for essentially every classifiable transition in an atomic spectrum [T. R. O'Brian *et al*, J. Opt. Soc. Am. B **8**, 1185 (1991)]. Both lifetimes and branching fractions are measured for 186 levels in Fe I, yielding absolute oscillator strengths for 1174 transitions in the range 225 to 2666 nm, most to 10% or better precision. Level lifetimes are measured using time-resolved laser-induced fluorescence on a slow beam of atomic Fe. Branching fractions are measured in emission with the one meter Fourier transform spectrometer at the National Solar Observatory. The upper level energies of the transitions with measured oscillator strengths densely span the range 30,000 to 61,000 cm^{-1}. The extensive set of oscillator strengths permits accurate interpolation of relative upper level populations in an emission source operating near Boltzmann equilibrium, thus allowing accurate determination of oscillator strengths for levels not directly interrogated for lifetimes or branching fractions. An additional 640 Fe I oscillator strengths are determined by this interpolation, for a total of 1814 accurately measured oscillator strengths.

Level lifetimes are measured using pulsed laser excitation of atoms in a beam generated by a modified hollow cathode discharge. A pulsed, tunable dye laser, with second harmonic generation in crystals when necessary, provides spectral coverage from about 205 to 700 nm. The laser is tuned to selectively excite a single upper level and the subsequent spontaneous fluorescence decay is detected with a photomultiplier tube and fast transient recorder. Fluorescence decays from several hundred laser shots can be recorded and analyzed in less than one minute. Selective laser excitation eliminates error from growing-in cascades from higher-lying levels, and potential cascade radiation from decays through lower levels is blocked with simple spectral filtering. The hollow cathode discharge source generates beams of neutral and singly-ionized atoms for virtually any element. The source has been used for more than 30 elements so far, including highly refractory metals non-metals. Systematic error from radiation trapping or non-radiative decay is eliminated by using the optically thin, collisionless beam. The beam also contains significant populations of atoms and ions in long-lived levels of both parities, as well as the ground level, so that many high-lying levels are accessible to excitation with photons of modest energy. In Fe, useful populations of long-lived levels occur with energies as high as 30,000 cm^{-1}, permitting excitation of upper levels up to the ionization limit (63,700 cm^{-1}) without the technical difficulties of using VUV or multiphoton processes.

Branching fractions are measured from emission spectra obtained with the one meter Fourier transform spectrometer (FTS) at the National Solar Observatory. The FTS provides rapid collection of extensive spectra with

excellent resolution, broad dynamic range, and accurate absolute frequency calibration. A million point spectrum covering the spectral range 2,000 to 44,000 cm^{-1} is collected in about 8 minutes with resolution 0.04 cm^{-1} (see Figure 1.). Several spectra are collected using hollow cathode Fe discharges in Ar, Ar + He, and Ar + Ne, and spectra are also recorded from an inductively-coupled plasma (ICP) source. The high temperature ICP source (about 7000 K) produces broad lines less prone to self-absorption, while the sharper hollow cathode lines are better suited for spectrophotometry of closely-spaced transitions of moderate or low intensity and for precise identification of peak transition frequencies. Relative intensities and peak positions are measured automatically with the DECOMP program, which fits a Voigt profile to all features with signal-to-noise ratios exceeding a specified value.

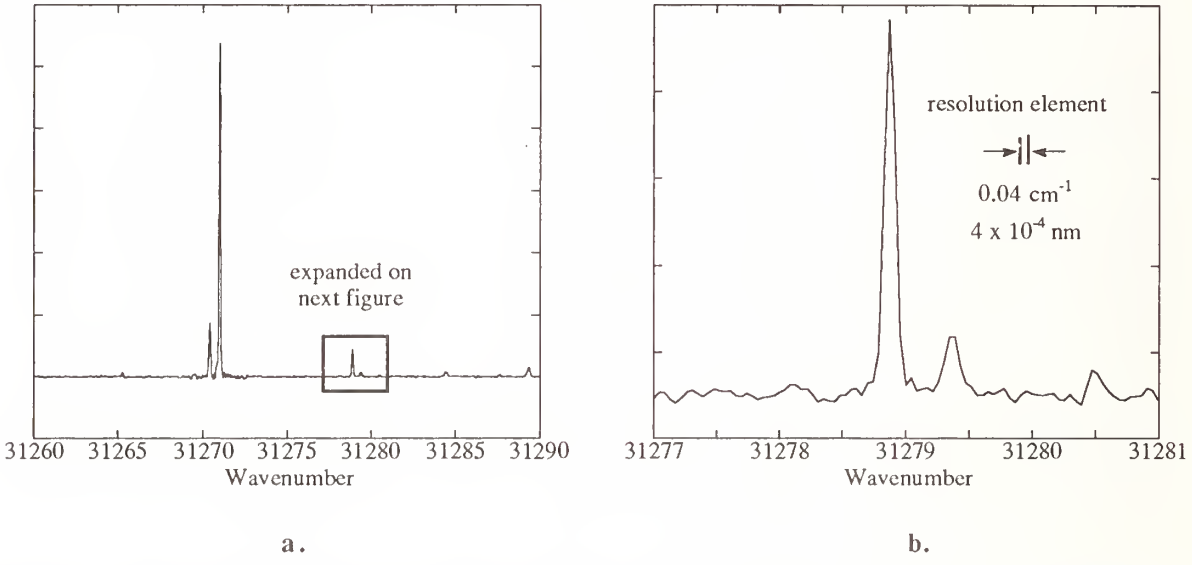

Figure 1. A very small portion of the Fourier transform spectrum of an Fe + Ar hollow cathode discharge used for measuring branching fractions showing the high resolution and wide dynamic range obtained.

Under appropriate operating conditions, the upper level populations in the ICP source approximate a Boltzmann distribution, although deviation from local thermodynamic equilibrium is seen in the populations of shorter-lived levels . Using oscillator strengths determined by measured level lifetimes and branching fractions, relative populations of upper levels can be determined from ICP spectral line intensities, and a smooth curve fit to the relative populations as a function of upper level energy. This curve deviates somewhat from the expected (Boltzmann) inverse exponential dependence on upper level energy (see Figure 2.). However, since oscillator strengths of transitions from 186 upper levels were measured, and since these upper levels densely span the excitation range 26,000 to 61,000 cm^{-1}, accurate interpolation can be made between relative level populations based on directly measured oscillator strengths. This interpolation determines the relative population of upper levels for which lifetimes were not measured, but for which branching fractions were measured. Interpolation of the relative upper level population combined with relative emission intensities from the FT spectra then determines the oscillator strengths of transitions out of these upper levels relative to the directly measured oscillator strengths.

Using this method, moderately precise (10 - 20% uncertainty) absolute oscillator strengths are determined for 640 additional transitions for which upper level lifetimes were not directly measured.

The Fe I spectrum provides a particularly stringent test of the accuracy of this interpolation method, since precise oscillator strengths for 163 of these transitions have been previously measured by Blackwell *et al* [Mon. Not. R. Astron. Soc. **201**, 595 (1982)]. For 133 oscillator strengths measured in this experiment by the lifetime-branching fraction technique and by Blackwell *et al*, the mean value of the ratio $gf_{\text{this experiment}} / gf_{\text{Blackwell}}$ is 0.95 with sample standard deviation 0.08. For 30 additional lines measured by the interpolation method, the corresponding ratio is 0.90 ± 0.08. The 8% spread in the ratios is consistent with the fractional uncertainty in the oscillator strength measurements in this experiment (typically about 10%). These results support the accuracy of the lifetime-branching fraction measurements and demonstrate no significant difference in the accuracy of the interpolation method compared to the lifetime-branching ratio technique.

The methods reported here are applicable to efficiently measuring and interpolating accurate absolute oscillator strengths in the UV through near IR for virtually any neutral or singly-ionized atomic species. Further understanding of departure from local thermodynamic equilibrium in ICP or other sources may lead to even greater efficiency by minimizing the number of lifetimes needed for normalization.

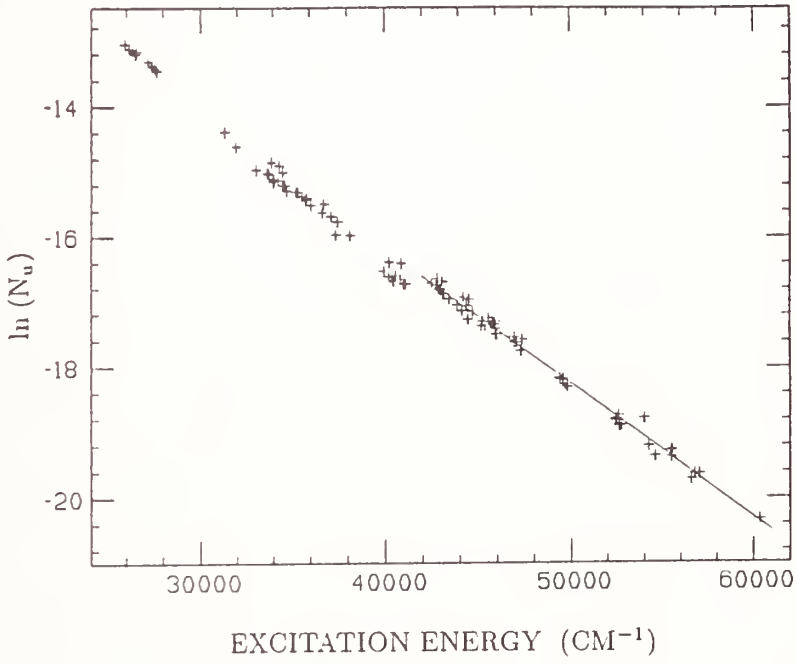

Figure 2. Relative upper level population (N_u) as a function of the upper level energy for Fe I levels, determined from relative line intensities in a Fourier transform spectrum of Fe in an ICP source and measured oscillator strengths. The solid line segment in a least-squares fit to populations of levels above 40,000 cm^{-1}.

MEASUREMENT OF LIFETIMES OF EXCITED STATES OF SELECTED VUV LINES OF NI, NII, AlII, AND AlIII

Santosh K. Srivastava
Jet Propulsion Laboratory, California Institute of Technology,
Pasadena, CA 91109, U. S. A.

Delayed coincidence technique has been employed to measure lifetimes of upper levels of transitions which give rise to spectral lines in the VUV region of spectrum of NI, NII, AlII, and AlIII. Two different instruments were used for these measurements. They are shown in figures 1 and 2. In the first instrument (fig. 1) a fast pulsed electron beam (Khakoo and Srivastava, 1984) with cut off times of the order of 0.5 nano seconds was employed to generate excited NI and NII states by dissociating N_2 which then emitted in the VUV. At the same time this electron pulse was also used to start a tme to pulse height converter (TPC). Emitted radiation was detected by a VUV sensitive fast channeltron. Output of this detector was amplified and sent to the stop teminal of the TPC. The TPC converted the time difference between start and stop pulses into an electrical pulse whose height was directly proprtional to the time difference. Pulses of varying heights corresponding to various times of arrivals of photons were stored in a pulse height analyzer (PHA). Collection of pulse height data over a period of time gave a time decay curve. A typical time decay curve is shown in fig. 3. Such decay curves were obtained for each spectral line of interest. At least five different sets of data were obtained to test the reproducibility of results. In the second instrument a fast pulse (100 ps wide) of a Nd:YAG laser was employed to generate a laser produced plasma of Al. This plasma emitted radiation in the VUV. Spectrum analysis of the emitted radiation showd that it contained well defined spectral lines of Al from its various stages of ionization. Details on the characteristics of the plasma and method of its production are given in our previous publication (Timmer et al., 1991). Method of obtaining the temporal decay curves for each spectral line was the same as described above for the first instrument.

The upper level of a transition of interest is generally populated by two mechanisms: one by the direct excitation from the ground state and the other by cascade transitions from higher levels. Therefore, the time decay curves such as shown in fig. 3 contain cascade contributions which lengthen the true lifetime of the excited state. In the past the effect of cascading has been estimated by plotting a log of the intensity of the spectral line as a function of time. Without the effect of cascade this plot should be a straight line. Any departure from a straight line shows the contribution due to cascading and its value can be estimated. For this purpose we have used the two component decay method described by Corney (1977). This method combines the cascading contribution of all of the upper levels into one and devides the exponential decay formula into two parts: one for the direct excitation and the other for the cascade contribution. The experimental decay curves are fitted to this formula by a ^{2} minimization technique. We have wrtitten programs (Srivastava and Nguyen, 1986) which use this technique to fit the present experimental curves to the two component formula of Younger and Wiese (1978).

Our experimental results for NI and NII are presented in Tables I and II along with previously reported ones. As is clear from these tables that the various results differ considerably from each other. We esimate that our results are accurate to within 20%. This error has been arrived at by estimating the spread in our measured data and fitted data. A typical fitted curve is shown by a solid line in fig. 3. We were able to fit our measured

data to the two component formula of Younger and Wiese well. The main reason for the differences in the results of various measurements lies in the fact that all previous and present measurements have serious cascade contributions which have been estimated differently by different investigators.

Values of lifetimes of AlII and AlIII lines are presented in TableIII. Previous experimental results are not readily available for these lines. Decay curves for each spectral line were fitted to the theoretical formula of Younger and Wiese (1978). A typical fitted curve is shown in fig. 3. It is estimated that the present results are accurate to within 20%.

Acknowledgements: The research described in this paper was carried out at the Jet Propulsion Laboratory, California institute of technology, and was sponsored by NASA. The help in acquiring and reducing the experimental data by C. Timmer and H. Nguyen is greatfully acknowledged.

References:

Corney, A., in "Atomic and Laser Spectroscopy", Clarendon Press, Oxford, England, pp160(1977).
Khakoo, M. A., and S. K. Srivastava, J. Phys. E: Sci. Instrum. **17**, 1008 (9184).
Srivastava, S. K. and H. Nguyen, "Paramtrization of Electron impact Cross Sections for CO, CO2, CH4, NH3 and SO2" JPL Report #87-2 (1987).
Timmer, C., S. K. Srivastava, T. I. Hall, and A. F. Fucaloro, J. Appl. Phys **70**, 1888(1991).
Younger, S. M. and W. L. Wiese, Phys Rev. **A17**, 1944(1978).

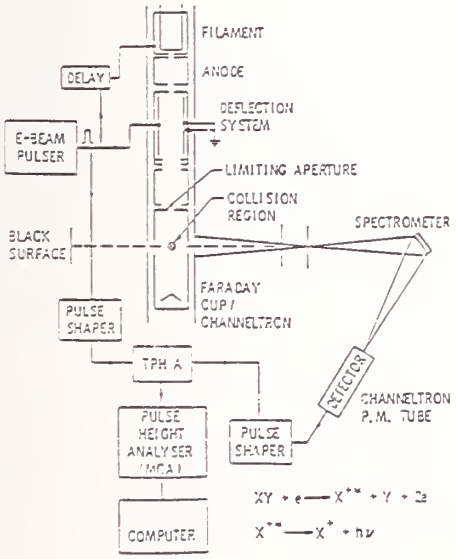

Fig. 1

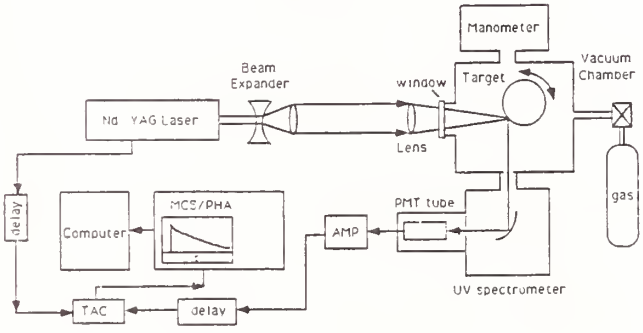

Fig. 2

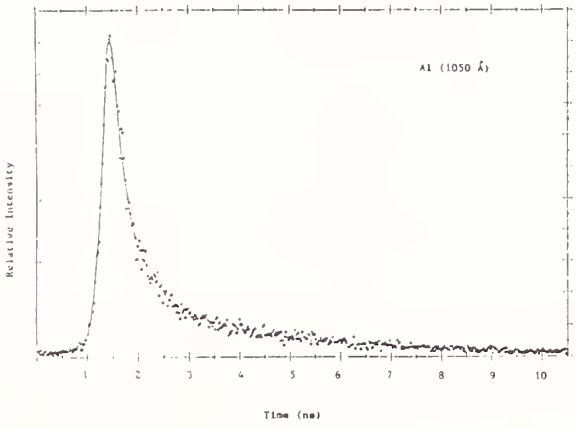

Fig. 3

TABLE I

Lifetimes for 1134.6 A° Line of NI

Reference	Lifetime (ns)	Method
Lawrence and Savage (1966)	7.2	Phase shift
Wiese et al. (1966)	4.348	
Smith et al. (1970)	7.4	Phase shift
Berry et al. (1971)	7.0	Beam foil
Hutchinson (1971)	9.9±1	Modified Phase shift
Chang (1977)	3.18	Beam foil
Hibbert et al. (1985)	8.264	
Present work	2.8±0.56	Delayed coincidence

Lifetimes for 1199.9 A° Multiplet of NI

Reference	Lifetime (ns)	Method
Lawrence and Savage (1966)	2.5±0.3	Phase shift
Wiese et al. (1966)	1.852	
Berry et al. (1971)	2.4±0.1	Beam foil
Hutchinson (1971)	2.2±0.4	Phase shift
Dumont et al. (1974)	2.35±	Beam foil
Brooks et al. (1977)	2.4±	
Chang (1977)	2.27±0.11	Beam foil
Hibbert et al. (1985)	2.32	Phase shift
Present work	3.2±0.64	Delayed coincidence

Lifetimes for 1243 A° Line of NI

Reference	Lifetime (ns)	Method
Wiese et al. (1966)	2.174	
Lawrence and Savage (1966)	2.2±0.3	Phase shift
Berry et al. (1971)	2.6	Beam foil
Hutchinson (1971)	6.9±0.8	Phase shift
Goldbach et al. (1986)	2.857	Arc
Present work	1.1±0.22	Delayed coincidence

TABLE II

Lifetimes for 671.48 A° Line of NII

Reference	Lifetime (ns)	Method
Buchet e tal. (1972)	0.82	Beam foil
Smith et al. (1970)	1.08	Phase shift
Hutchinson (1971)	1.08	Phase shift
Chang (1977)	0.67	Beam foil
Present work	1.3±0.26	Delayed coincidence

Lifetimes for 775.957 A° Line of NII

Reference	Lifetime (ns)	Method
Smith et al. (1970)	0.7	Phase shift
Chang (1977)	0.52	Beam foil
Present work	0.25±0.05	Delayed coincidence

Lifetimes for 748 A° Line of NII

Reference	Lifetime (ns)	Method
Hesser and Lutz (1968)	0.8±0.4	Phase shift
Knystautas et al. (1973)	0.43±0.01	Beam foil
Kernahan et al. (1974)	0.213±0.01	Beam foil
Dumont et al. (1976)	0.22±0.03	Beam foil
Sorenson (1979)	0.35±0.01	Beam foil
Baudinet-Robinet et al. (1990)	0.267	Beam foil
Tripp et al. (1991)	0.1125	Electron Impact
Present work	0.4±0.08	Delayed coincidence

Lifetimes for 1085 A° Line of NII

Reference	Lifetime (ns)	Method
Smith et al. (1970)	0.92	Phase shift
Hutchinson (1971)	2.7	Modified phase shift
Chang (1977)	2.8	Beam foil
Present work	3.0±0.6	Delayed coincidence

TABLE III

Lifetimes of upper levels of transitions listed below as measured by utilizing the laser produced plasma of Al

Species	Transition	Wavelength(Å)	Lifetime(ns)
AlII	3s3p-3s7s	990, 991	2.63
AlII	3s3p-3s5d	1049.9	3.45
AlII	3s3p-3s5s	1209, 1210	3.75
AlIII	4s-7p	1262	3.49

OSCILLATOR STRENGTH MEASUREMENTS OF NEUTRAL NITROGEN LINES IN THE 900 - 1200 Å RANGE

C. Goldbach[1], T. Lüdtke[2], M. Martin[1], G. Nollez[1]

[1] *Institut d'Astrophysique, Paris, France*

[2] *Institut für Experimentalphysik, Kiel, Germany*

The far UV range offers two main interests: first, most of the lines of the elements of astrophysical interest lie in this spectral range, second a given element exhibits often lines with very different oscillator strength values, which allows to analyse absorption features corresponding to complex lines of sight. On the other hand, the experimental techniques have greatly improved and it is possible to extend to the VUV the classical emission method of oscillator strength measurement without any dramatic loss of precision. The technical improvements relate to crucial experimental points: realisation of high resolution VUV spectrometers, of efficient differential pumping units, of VUV radiation standards, computer control in data acquisition and analysis. Also the accuracy reached now on the lifetime data allows the normalisation to an absolute scale of the measured relative f-values.

Having measured f-values of strong and weak lines of neutral nitrogen and carbon in the 1200-2000 Å range, we are now extending our measurements to the 900-1200 Å range. Neutral nitrogen lines of this region are of particular interest for interstellar medium and quasi-stellar object absorption system studies and no reliable laboratory data are available: we present hereafter the results of f- measurements for 19 lines of neutral nitrogen, belonging to 9 multiplets, between 950 and 1200 Å .

The experiment

The emission source is a wall stabilised arc operated in high-purity argon and at a 80 A current(T=13000 K; $n_e = 1.1\ 10^{17} cm^{-3}$). The arc radiation is observed axially through a three-stage differential pumping unit which reduces the atmospheric pressure down to 10^{-7} mbar. The first orifice (tungsten, 0.6 mm diameter, 0.6 mm length) is placed only 4 mm from the anodes to keep the cool plasma boundary layer as short as possible. The mirrors and the grating of the 2.5 m normal incidence monochromator are platinum coated. The entrance and exit slits are set to 50 μ and the spectral resolution is about 0.1 Å . A windowless multiplier serves as detector.

The method

The method, an advanced version of the emission method avoiding the difficulties associated with an absolute number density determination in a multi-component plasma, is based on relative f-measurements. A reliable and precise f-value of the line standing for reference is required; fortunately, the lifetime of the upper term of the NI multiplet at 1200 Å is known with a good accuracy: the lifetimes measured through different techniques ([1] to [6]) yield a weighted mean value of 2.35 $\pm$0.06 ns.

In the case of strong lines, and in particular of resonance lines, the line optical depth is not negligible. To take full account of this effect, the quantity we choose to determine is the optical depth profile of the line τ_λ (see [7] and [8]). The relative gf-value of a line is deduced from the ratio of the integrated optical depth of the investigated line (X) to that of a reference line (R) through

$$\frac{\int_L \tau_\lambda^X d\lambda}{\int_L \tau_\lambda^R d\lambda} = \frac{\lambda_X^2}{\lambda_R^2} \frac{(gf)_X}{(gf)_R} \exp\left(\frac{E_R - E_X}{kT}\right) \qquad (1)$$

where g and E are the statistical weight and the excitation energy of the lower level of both transitions. τ_λ is determined from the end-on measured spectral radiance I_λ through

$$\tau_\lambda = -\ln(1 - \frac{I_\lambda}{B_\lambda}) \quad (2)$$

where B_λ is the Planck function at the plasma temperature. The blackbody saturation level B_λ is measured at the top of the line by increasing the nitrogen concentration.

Most of the investigated transitions appear as multiplets of overlapping and blended lines of nearly Gaussian shape. The determination of the integral of τ_λ over the profile of each line (including wing contributions) is performed using least-squares fitting technique of digital data.

For all the measured lines, but multiplet *uv*3.06, we use as reference the 1200.71 Å line of multiplet *uv*1. For the weak forbidden multiplet *uv*3.06 at 952 Å , we choose as reference the 965.04 Å line of the multiplet *uv*3 with gf= 0.0131 ±5%, our present result.

For resonance lines, as the temperature disappears from Eq.(1), the uncertainty on the absolute gf-value is obtained by summing in quadrature the standard deviation of the distribution of the measured line ratios (between ±3 and ±10%), the uncertainty in the realisation of the blackbody plateau (±2%) and the uncertainty in the gf-reference value.

For other lines, an uncertainty of ±3% in the Boltzmann factor arising from the uncertainty in the temperature has to be added.

Results

The following table displays the results of our measurements, together with the largely used values given by Lugger et al. [9], the results of the calculation of Bell and Berrington [10], of Lennon and Burke [11] (Opacity Project) and the new results of Hibbert et al. [12].

Our absolute scale is only 2.5% lower than Lugger et al. and 15% higher than Hibbert et al., but discrepancies on forbidden lines may reach 50%. Comparison with the results of [10] concerns only the three allowed multiplets *uv*2, *uv*3 and *uv*3.05; because of LS-coupling departure exhibited by our measurements, the noteworthy agreement stated for the multiplet values would be significantly lower for the line values. The same remark applies also to the Opacity results with which our measurements agree very well with the noticeable exception of multiplet *uv*2.

A detailed comparison between our experimental values and the results of different theories [10], [11], [12] shows that the agreement level varies according to the data considered (multiplet- or line-values) and to the nature of the transitions (resonant or not, allowed or forbidden).

References

[1] Lawrence G.M., Savage B.D., 1966, Phys. Rev.,**141**, 67
[2] Berry H.G., Bickel W.S., Bashkin S., Desesquelles J., Schectman R.M., 1971, J. Opt. Soc. Am., **61**, 947
[3] Hutchison R.B., 1971, JQSRT, **11**, 81
[4] Dumont P.D., Biemont E., Grevesse N., 1974, JQSRT, **14**, 1127
[5] Chang M.W., 1977, ApJ, **211**, 300
[6] Brooks N.H., Rohrlich P., Smith W.H., 1977, ApJ, **214**, 328
[7] Goldbach C., Martin M., Nollez G., Plomdeur P., Zimmermann J.P., Babic D., 1986, A&A,**161**, 47
[8] Goldbach C., Nollez G., 1987, A&A, **181**, 203
[9] Lugger P.M., York D.G., Blanchard T., Morton D.C., 1978, ApJ, **224**, 1059
[10] Bell K.L., Berrington K.A.,1991, J. Phys. B, **24**, 933
[11] Lennon D.J., Burke V.M., 1992, private communication
[12] Hibbert A., Biemont E., Godefroid M., Vaeck N., 1991, A&AS, **88**, 505

Table 1. Absolute gf-values for neutral nitrogen resonance lines. Length and velocity values are given for theoretical results.

λ (Å)	g_{lo}	g_{up}	This work gf	HBGV[12] gf	BB[10] gf	LYBM[9] gf	Opacity[11] gf
uv3.06 $2s^22p^3\ ^4S^0 - 2s^22p^23d\ ^4D$							
952.3037	4	6	$0.0075 \pm 7\%$	0.0160-0.0144		$0.010 \pm 12\%$	
952.4151	4	4	$0.0068 \pm 6\%$	0.0172-0.0156		$0.008 \pm 16\%$	
952.5231	4	2	$0.0024 \pm 10\%$	0.0076-0.0068		$0.0017 \pm 12\%$	
uv3.05 $2s^22p^3\ ^4S^0 - 2s^22p^23d\ ^4P$							
953.8	4	12	0.30	0.264-0.239	0.312-0.277	0.27	0.28-0.26
953.4150	4	2	$0.057 \pm 8\%$	0.0444-0.0400		$0.048 \pm 8\%$	
953.6548	4	4	$0.108 \pm 7\%$	0.0852-0.0772		$0.084 \pm 5\%$	
953.9698	4	6	$0.135 \pm 7\%$	0.134-0.122		$0.14 \pm 9\%$	
uv3.04 $2s^22p^3\ ^4S^0 - 2s^22p^23d\ ^2F$							
954.1040	4	6	$0.027 \pm 25\%$	0.0008-0.0004		$0.034 \pm 9\%$	
uv3 $2s^22p^3\ ^4S^0 - 2s^22p^24s\ ^4P$							
964.4	4	12	0.109	0.126-0.118	0.103-0.104	0.120	0.128-0.124
963.9904	4	6	$0.059 \pm 8\%$	0.0644-0.0600		$0.056 \pm 7\%$	
964.6258	4	4	$0.037 \pm 5\%$	0.0416-0.0388		$0.040 \pm 10\%$	
965.0415	4	2	$0.013 \pm 5\%$	0.0204-0.0192		$0.024 \pm 7\%$	
uv2 $2s^22p^3\ ^4S^0 - 2s^22p^4\ ^4P$							
1134.7	4	12	0.34	0.322-0.446	0.349-0.378	0.322	0.092-0.124
1134.1651	4	2	$0.061 \pm 6\%$	0.0552-0.0760		$0.054 \pm 2\%$	
1134.4147	4	4	$0.114 \pm 7\%$	0.109-0.150		$0.107 \pm 2\%$	
1134.9801	4	6	$0.162 \pm 6\%$	0.158-0.220		$0.161 \pm 2\%$	
uv41 $2s^22p^3\ ^2P^0 - 2s^22p^23s\ ^2S$							
1143.6458	2	2					
			}$0.35 \pm 8\%$				
1143.6508	4	2					
uv6 $2s^22p^3\ ^2D^0 - 2s^22p^23d\ ^2F$							
1167.9	10	14	0.32	0.45-0.30			0.34-0.31
1167.4484	6	8	$0.20 \pm 7\%$	0.258-0.175			
1168.4167	6	6		0.0066-0.0054			
			}$0.12 \pm 10\%$				
1168.5358	4	6		0.186-0.124			
uv6.01 $2s^22p^3\ ^2D^0 - 2s^22p^23d\ ^4P$							
1168.3344	4	6	$0.029 \pm 8\%$	0.0012-0.0008			
uv5.02 $2s^22p^3\ ^2D^0 - 2s^22p^24s\ ^2P$							
1176.9	10	6	0.13	0.05-0.15			0.125-0.120
1176.5097	6	4		0.0276-0.0864			
			}$0.088 \pm 8\%$				
1176.6304	4	4		0.0036-0.0096			
1177.6948	4	2	$0.044 \pm 11\%$	0.0184-0.0500			

Sun and Stars

OBSERVED REDSHIFT OF O V LINES IN SOLAR UV SPECTRA

P. BRÆKKE

Institute of Theoretical Astrophysics, of Oslo
University of Oslo, P.O. Box 1029, Blindern, N-0315 Oslo 3, Norway

Ultraviolet observations of the Sun show a net redshift near disk center in the emission lines from the transition region. During the last decades, this phenomenon has been observed with several UV instruments with different spatial resolution (e.g. Doschek, Feldman, & Bohlin 1976; Gebbie et al. 1981; Dere, Bartoe, & Brueckner 1986; Hassler, Rottman, & Orral 1991). Systematic redshifts have also been observed in stellar spectra of late type stars (e.g. Ayres, Jensen, & Engvold 1988). Both solar and stellar flows in the transition region have been most extensively studied at temperatures around $T = 10^5$ K. For the Sun, the typical value of the average downflow velocity, derived from the C IV lines at 1550 Å, is 5–10 km s^{-1}.

Measurements of the variation of the flow with temperature are somewhat ambiguous. However, the net downflow velocity has been observed to increase with temperature, reaching a maximum at $T= 10^5$ K and then decreasing again at higher temperatures. The O V lines at 1218 Å and 1371 Å define the highest observable transition region temperatures available in the wavelength range of most high resolution, normal incidence UV slit spectrometers. Of these two lines, which also form a density sensitive pair, the 1218 Å line is the one most readily available for observation. The reason being that the photographic density of the intrinsically weak line is lifted up by the wing of the neighboring strong Lyα line from hydrogen.

Some observers find no significant shift in the O V line at 1218 Å at disk center (e.g. Doschek et al. 1976). It should be noted that the commonly quoted average velocity variation with temperature above 10^5 K to a large extent depends on this particular observation of the 1218 Å line. The result of Doschek et al. (1976) has been used in comparison with numerical simulations of flows in the transition region, where the redshifted emission is replaced by blueshifted emission at temperatures around 2.5×10^5 K where O V is formed (e.g. McClymont & Craig 1987, Spadaro, Antiochos, & Mariska 1991).

However, results from the observed wavelength of this line, as presented by Doschek et al. (1976) should be regarded with some caution for the following reasons:

- The wavelength determination of the O V line may be influenced by the Lyα line from hydrogen at 1215.67 Å.
- The solar wavelength calibration is uncertain owing to few chromospheric reference lines in this wavelength region.
- The laboratory wavelength of the oxygen line at 1218 Å is uncertain.

The last point is crucial for the determination of absolute velocities. Doschek et al. (1976) tried to avoid this problem by comparing the measured wavelengths with measurements of the same lines outside the solar limb where they expected no net shift of the lines.

A detailed analysis of O V was presented by Bockasten & Johansson (1968). They recalculated the energy levels from measurements of 126 lines between 340 Å and 7700 Å observed with a theta-pinch discharge as the light source. Their wavelength value for the $2s^2\ {}^1S_0$—$2s2p\ {}^3P_1$ line was 1218.406 Å. The value of Bockasten and Johansson is commonly used in reference literature. It has been known for a long time that the observed solar wavelength of the 1218 Å line differs significantly from the wavelength reported by Bockasten & Johansson (1968).Using the NRL 6.6 m spectrograph Brown (1980) found the wavelength to be 1218.344 ± 0.010 Å, which is in better agreement with solar observations.

In this paper we present measurements of Doppler shifts in the O V lines at 1218 Å and 1371 Å obtained during two rocket experiments with the High Resolution Telescope and Spectrograph – HRTS. The result is compared with corresponding measurements of the Si IV line at 1402 Å and the O IV line at 1401 Å. We discuss variation of velocities in the O V lines over the entire field of view of the HRTS instrument, which extended from disk center to outside the solar limb.

The High Resolution Telescope and Spectrograph – HRTS – is described by Bartoe & Brueckner (1975). The particular strength of the HRTS instrument lies in its high spatial, spectral, and time resolution combined with the extensive wavelength and angular coverage. For this investigation we have used data from the two first HRTS rocket flights which took place in 1975 and 1978 respectively. During both missions the slit extended from the solar center to the limb covering both quiet and active regions.

The spectrograms were registered on photographic film. Microphotometry of the spectrograms has been carried out at the Institute of Theoretical Astrophysics in Oslo and at the US Naval Research Laboratory. A description of the photometry and of the various steps in the reduction process is given by Brekke et al. (1991).

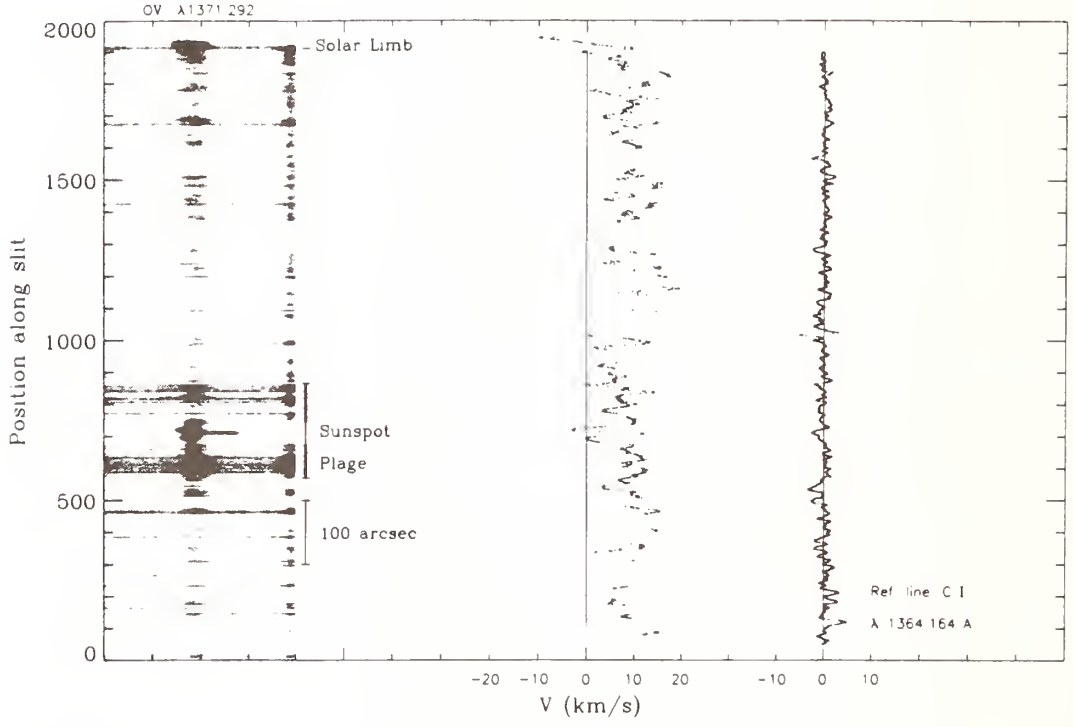

Figure 1. Spatial variation of line-of-sight velocities in the O V line at 1371 Å and a chromospheric reference line (C I λ1364.164 Å) observed with HRTS 1. To the left is a section of the HRTS 1 spectrogram showing the O V profile extending from approximately disc center to the solar limb. The active region McMath 13766 has been marked. The scale along the spectrograph slit is given in pixel units where 1 pixel corresponds to approximately 0.″5.

In Figure 1 the spatial variation of the observed line-of-sight velocities in the O V line at 1371 Å is displayed together with a section of the HRTS 1 spectrogram showing the O V profile. The image extends from approximately disk center ($\cos\theta = 0.99$) to the solar limb and the location of the active region McMath 13766, including a sunspot, has been marked. The scale along the spectrograph slit is given in pixel units where 1 pixel corresponds to approximately 0.″5.

The O V line is clearly redshifted at most positions along the slit corresponding to an average line-of-sight velocity of 8 km s^{-1} in the quiet regions. Close to Sun center the measured redshifts give a net radial downflow. There is considerable spatial variation along the slit, where the flow velocities are varying between −3 km s^{-1} to almost 20 km s^{-1} at the solar disk. The blueshift is located above the sunspot umbra and outside the limb. For comparison, the observed shift of a nearby chromospheric reference line (the C I line at 1364.164 Å) has been plotted on the same velocity scale. The measured redshift shows no strong center-to-limb variation.

When measuring the 1218 Å line we have adopted the laboratory wavelength from Brown (1980) of 1218.344 Å. Using this value we find an average net redshift of approximately 3 ± km s^{-1} in the quiet regions. This is approximately 5 km s^{-1} less than the value obtained from the line at 1371 Å. The difference is probably due to an error in the adopted laboratory wavelength of the 1218 Å line, which is an intersystem

line and thus, more difficult to measure in laboratory. The result suggests a laboratory wavelength close to 1218.325 Å if the two lines are to have the same redshift. The observed Doppler shifts in transition region and coronal lines has been summarized in Table 1. In addition to O V we have also measured Si IV, O IV, and Fe XII.

TABLE 1

Observed average redshifts in transition region; HRTS 1

Ion	Laboratory Wavelength (Å)	Temperature of Formation (K)	Line of Sight Velocity Quiet Region (km s^{-1})	Line of sight Velocity Plage (km s^{-1})
Si IV	1402.770[1]	7.0×10^5	5 ± 2	14 ± 2
O IV	1401.156[2]	1.4×10^5	6 ± 2	14 ± 2
O V	1371.292[3]	2.4×10^5	8 ± 2	8 ± 2
O V	1218.344[4]	2.3×10^5	3 ± 2	4 ± 2
Fe XII	1249.40[5]	1.3×10^6	—	7 ± 4

1 — Moore 1965, 2 — Bromander 1969, 3 — Bockasten & Johansson 1968
4 — Brown 1980, 5 — Sandlin et al. 1977, (Solar observation)

I am indebted to Drs. Guenter E. Brueckner and Kenneth P. Dere for making the excellent HRTS material available. I will also thank Drs. Philip G. Judge and Charles M. Brown for interesting discussions. I also wish to acknowledge support from the Norwegian Research Council for Science and the Humanities.

REFERENCES

Ayres, T. R., Jensen, E., & Engvold, O. 1988, ApJS 66, 51

Bartoe, J.-D. F., & Brueckner, G. E. 1975, J. Opt. Soc. Am., 65, 13

Bockasten, K., & Johansson, K. B. 1968, Arkiv f. Fys. 38, No 31. 563

Brekke, P., Kjeldseth-Moe, O., Bartoe, J.-D. F., & Brueckner, G. E. 1991, ApJS, 75, 1337

Bromander, J. 1969, Arkiv f. Fys., 40, 257

Brown, C. M. 1980, A&A. 88, 273

Dere, K. P., Bartoe, J.-D. F., & Brueckner, G. E. 1986, ApJ, 305, 947

Doschek, G. A., Feldman, U., & Bohlin, J. D. 1976a, ApJ, 205, L177

Gebbie, K. G., et al. 1981, ApJ, 251, L115

Hassler, D. M., Rottman, G. S., & Orral, F. Q. 1991, ApJ, 372, 710

McClymont, A. N., & Craig, I. J. D. 1987, ApJ, 312, 402

Moore, C. E. 1965, NSRDS-NBS, 3, Section 1

Sandlin, G. D, Brueckner, G. E., & Tousey, R. 1977, ApJ, 214, 898

Spadaro, D., Antiochos, S. K., & Mariska, J. T. 1991, ApJ, 382, 338

RUTHENIUM STELLAR ABUNDANCE DETERMINED FROM FTS BRANCHING RATIOS, LIF LIFETIMES AND HST OBSERVATIONS

S. Johansson, A. Joueizadeh, U. Litzén
Lund University
J. Larsson, A. Persson, S. Svanberg
Lund Institute of Technology
D.S. Leckrone, G.M. Wahlgren
Goddard Space Flight Center

1. INTRODUCTION

Selected intervals of the UV spectrum of the chemically peculiar B-star χ Lupi have been recorded with the Goddard High Resolution Spectrograph (GHRS) onboard the Hubble Space Telescope. In one of the intervals, two unidentified lines at 1939 Å were found to coincide with Ru II lines.

In order to firmly establish the Ru II identification and to determine the ruthenium abundance in χ Lupi, accurate wavelengths and oscillator strengths for the two lines are needed. The wavelength measurements are described in the contribution by Joueizadeh and Johansson (A Progress Report on the Analysis of VUV-FTS spectra of Ru I and Ru II).

For the oscillator strengths, lifetimes and branching ratios have to be measured.

2. LIFETIME MEASUREMENTS USING LASERINDUCED FLUORESCENCE

2.1 Generation of ruthenium ions

Ruthenium is an expensive and brittle metal, evaporating only at very high temperatures. A special method was therefore used for producing the ruthenium ions in a laser-produced plasma. A smooth ruthenium surface was formed by vibrating a container with ruthenium powder by means of a small loudspeaker. A ruthenium plasma was generated by focusing 10 - 50 mJ pulses from a Nd:YAG laser onto the powder surface. Due to the vibration, a new smooth surface was formed before the next laser pulse arrived 100 ms later.

2.2 Excitation and detection

The short, tunable laser pulse for the excitation was generated by using the second harmonic from a Nd:YAG laser to pump a dye laser. The output from the tuned dye laser was then mixed with the fourth harmonic of the pump laser to produce the radiation in the 1939 Å region. By optimizing the difference in optical path length between the dye laser radiation and the fourth harmonic from the Nd:YAG laser, a pulse length of 3 ns was obtained.

The fluorescence emitted when the exciting pulse was tuned to resonance with one of the Ru II lines was recorded with a microchannelplate photo-multiplier connected to the data collecting system. Lifetimes were extracted by fitting a convolution of the system response function and an exponential to the recorded fluorescence decay.

The lifetimes of the upper levels for the two Ru II lines were found to be 2.7 ns and 2.6 ns, with an estimated uncertainty of 10%.

3. BRANCHING RATIOS FROM FTS RECORDINGS

The Ru II spectrum emitted from a hollow cathode (Ni cathode + Ru powder + Ne and Ar carrier gas) was recorded at the Lund VUV FTS in the region 3000 - 1800 Å.

The two Ru II lines at 1939 Å have the upper levels $z^4D_{3/2}$ and $z^4D_{5/2}$. The decay schemes involve numerous decay channels, but only 5 and 6 respectively are strong enough to be observed, and to significantly influence the branching ratios.

Two different methods were used for the efficiency calibration of the spectrometer. In a separate recording an efficiency curve was obtained from a calibrated D_2 lamp. A disadvantage with this method is the fact that the hollow cathode window, which may be contaminated from cathode sputtering, is not included in the calibration. For this reason internal calibration points from accurately measured Ar II branching ratios were also used. In an attempt to extend the internal calibration to shorter wavelengths also Ge I lines were used. The Ge lines were emitted from a small amount of germanium powder placed in the cathode.

4. RESULTS

The branching ratios for the two 1939 Å lines are found to be very sensitive to the shape of the calibration curve at the short wavelength end. More accurately measured branching ratios for internal calibration below 2500 Å are expected to be available soon. Pending this information, we only state that the measured lifetimes and the preliminary branching ratios give the oscillator strengths 0.15 - 0.18, i.e. log gf in the range -0.82 to -0.74.

A synthetic spectrum fitted to the observed spectrum of χ Lupi, using the new laboratory wavelengths and the preliminary oscillator strengths, indicates that ruthenium is about 2 dex (100 times) more abundant in χ Lupi's atmosphere than in the sun.

Investigating the Pt III Spectrum in Chemically Peculiar Stars

Glenn M. Wahlgren[1], David S. Leckrone[2], and Sveneric Johansson[3]

[1] Computer Sciences Corporation/GHRS Team, Code 681, GSFC, Greenbelt, MD 20771

[2] Code 681, NASA/LASP, GSFC, Greenbelt, MD 20771

[3] Lund University, Department of Physics, Solvegatan 14, S-223 62 Lund, Sweden

1. INTRODUCTION

Recent advances in astronomical instrumentation and laboratory spectroscopy have made it possible to search for Pt III in stellar spectra. The chemically peculiar star χ Lupi (Bp, HgMn) is known to display strong spectral features of very heavy elements, such as Pt, Au, and Hg. Its extremely sharp spectral lines are due to minimal turbulence in its atmosphere and an inherently slow rotational velocity. Its projected rotational velocity of 1 km sec^{-1} is similar to that of the Sun, but is two orders of magnitude below that typical for stars of its spectral type. Our investigations of this star to date have been primarily concerned with determining the abundance and isotope mixture of Hg (Leckrone *et al.* 1991). However, it is clear that similar analyses are required for other heavy elements, as for example the 5d 6s configuration elements, to test theories of abundance enhancement in the atmospheres of chemically peculiar stars.

It has also become necessary to understand the platinuum spectrum as its many transitions are a non-negligible source of line opacity in the ultraviolet which can therefore be blended with other atomic lines of interest. The line-formation region temperature in the photosphere of χ Lupi is hot enough (6,500 - 11,000 K) to expect the Pt III number density to be up to a few percent of the total Pt present, and therefore produce observable lines in the stellar spectrum. A platinuum lamp, which provides standard wavelength calibrations for the Goddard High-Resolution Spectrograph (GHRS) on-board the *Hubble Space Telescope*, has been used to analyse the Pt I/II spectra (Reader *et al.* 1990) and serves as a map for the Pt II lines in the χ Lupi spectrum. But the lamp is not energetic enough to produce a Pt III spectrum. This has now been partially remedied by the laboratory Pt III analysis of Ryabstev *et al.* (1992). Pt III transitions can now be identified in high-dispersion ultraviolet spectra of Pt-rich stars, which will allow the observed line strengths to serve as constraints on theoretical calculations and atomic models.

2. STELLAR SPECTRA

The GHRS was used in its echelle mode, providing spectral resolving powers between 80,000 and 90,000. Spectra were obtained at three wavelength settings, centered at 1741, 1848, and 1942 Å, totalling approximately 30 Å of spectral coverage. Signal to noise levels varied between 60 and 100 at the stellar continuum level. Included in the standard data reduction procedures are wavelength corrections that account for spacecraft orbital motion, transformation of coordinates to the heliocentric rest frame, stellar radial velocity, and spectrum drifts across the detector array due to the spacecraft magnetic and thermal environments. The wavelength scale is established by Pt lamp spectra taken at standard wavelengths with an accuracy of 0.05 Å for echelle spectra. We have improved the accuracy of the absolute wavelength scale to ± 0.001 Å using Fe II and Mn II transitions appearing in the stellar spectrum, whose wavelengths were measured with the FTSs at Lund and Imperial College, London.

3. ATOMIC PARAMETERS

This study was initiated as a result of recent work by Ryabstev *et al.* on the Pt III spectrum. Their measurements of Pt spark spectra below 2020 Å resulted in cataloging 850 transitions. Their wavelength accuracy is quoted as 0.005 Å, set by the Pt II analysis of Sansonetti *et al.* (1992) for those transitions observable in our stellar spectra. The intensity calculations by Ryabstev *et al.*, using the Cowan code, produced values for gA which we have transformed into the gf-values required by our synthetic spectrum code. Line broadening by thermal, Stark, and van der Waals mechanisms is included in our synthetic spectra.

4. RESULTS

We have positively identified spectral lines resulting from Pt III transitions in the χ Lupi spectrum. A synthesized stellar spectrum was generated with the computer code SYNTHE (Kurucz, private communication) for comparison with the observed spectra. The Pt III lines were typically found at wavelengths near the *measured* values of Ryabstev *et al.*. Line strengths were matched by varying the stellar Pt abundance. A total of nine lines, determined to be relatively free of contaminant blending, were used in the abundance analysis. Averaging the best fit abundances from these lines yielded a Pt III abundance by number relative to hydrogen of [log N(Pt III) / log N(H)] = -5.75, which is nearly 30,000 times greater than in the solar photosphere. The Pt III abundance is similar to the Pt II abundance of -5.95 which we obtained in a similar manner from four Pt II lines, and which agrees with an earlier Pt II analysis for this star (Dworetsky *et al.*, 1984). The figure below displays a one angstrom segment of the χ

Lupi spectrum compared with synthetically derived spectra for the two cases: 1) the best fit Pt abundance, and 2) the solar Pt abundance.

The Pt analyses for χ Lupi will continue as further observations of this star are made, and will be extended to other stars. A valuable, but missing, piece of the analysis is the isotopic structure of Pt II/III lines found in the ultraviolet, which would provide additional clues to understanding the anomalous abundance enhancements.

ACKNOWLEDGEMENT: The authors thank J.-F. Wyart for sending to us a copy of the Pt III paper prior to publication.

REFERENCES

Dworetsky, M. M., Storey, P. J.., and Jacobs, J. M. 1984, *Physica Scripta*, T8, 39

Leckrone, D.S., Wahlgren, G. M., and Johansson, Se. G., 1991, *ApJ*, 377, L37

Reader, J., Acquista, N., Sansonetti, C. J., and Sansonetti, J. E. 1990, *ApJ Suppl.*, 72, 831

Ryabstev, A. N., Wyart, J.-F., Joshi, Y. N., Raassen, A. J. J., and Uylings, P. H. M., 1992 submitted to *Physica Scripta*

Sansonetti, J. E., Reader, J., Sansonetti, C. J., and Acquista, N. 1992, *J. Res. Natl. Inst. Stand. Tech.*, 97, 1

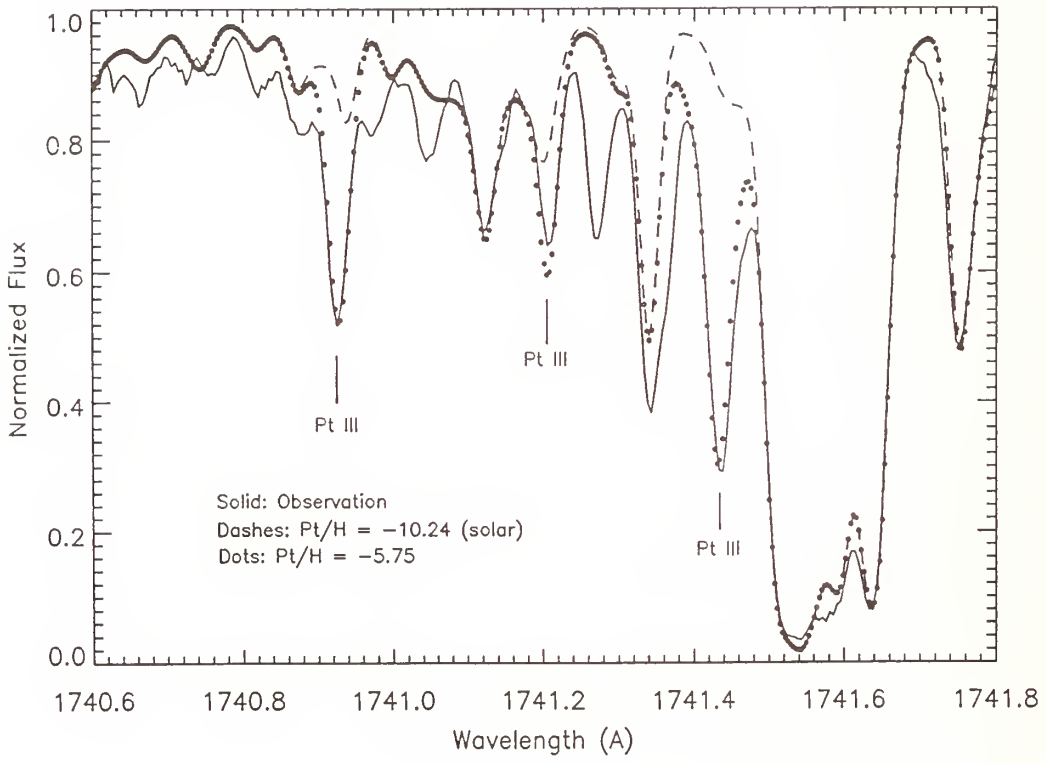

Burst Models for Line Emission in the Solar Atmosphere.

J. M. Laming, SFA Inc. Landover, MD 20785.

**U. Feldman, E. O. Hulburt Center for Space Research,
Naval Research Laboratory, Washington DC 20375-5000.**

Earlier papers (Laming & Feldman 1992, Feldman et al. 1992) have analyzed spectra which present problems of interpretation when the data are compared with model plasmas which assume thermal and ionization equilibrium. The Lyman series of hydrogen-like He II in an impulsive flare, and the resonance to intercombination line ratio R of magnesium-like Fe XV $\left(I\left(3s3p\ ^1P_1 - 3s^2\ ^1S_0\right)/I\left(3s3p\ ^3P_1 - 3s^2\ ^1S_0\right)\right)$, have both been understood in terms of a burst model, in which these ions emit their radiation from an ionizing plasma. The electron temperature is raised from some value at or below that where the ion in question is formed in ionization equilibrium, to a value, say, twice the equilibrium temperature.

In the case of He II, the fundamental problem regarding its observed strength, i.e. that much more radiation from He II is observed than predicted, is obviated in a burst model, since the increase in the Boltzmann factor produced by the increase in the electron temperature enhances the emission rate. Since the timescale of the increased temperature is short compared to the ionization equilibration timescale, this increased Boltzmann factor affects the emission before the He^+ is ionized to He^{++}, as it would be in ionization equilibrium at this raised temperature.

The ratio R in the spectrum of Fe XV is observed to be about 12 in photon units, but predicted to be a factor of two or so greater. This discrepancy is reduced in a burst model, when inner shell ionization of the aluminium-like Fe XIV is taken into account. This ionization from the $3s^23p$ configuration of Fe XIV to the $3s3p$ configuration of Fe XV will enhance the population of triplets relative to singlets, hence bringing the ratio closer to that observed. The effect is even bigger if one also postulates a non-Maxwellian electron distribution immediately following the burst, with an excess of electrons at or just above the Fe^{+13} ionization threshold. In fact, such a deviation of the electron distribution from a Maxwellian is required for absolute agreement between observations and theory.

Feldman (1992) has reviewed the effects of bursts on electron density diagnostics. In the work presented here, following in part the ideas of Parker (1988), that the solar corona, and presumably other solar regions as well may be thought of as being continuously heated by a population of bursts, we investigate the electron density diagnostics relevant to what has been called the Unresolved Fine Structures by Feldman (1983, 1987), otherwise known as the solar transition region. The densities inferred from line ratios formed at temperatures between 5×10^4 K and 2×10^5 K are evaluated to test the notion that this region obeys a constant pressure law, which would be most characteristic of a steady state plasma in ionization equilibrium. We also review the non-thermal mass motions associated with transition region lines formed over the same range of temperatures in ionization equilibrium.

In our analysis, it appears quite clear that the region of the Unresolved Fine Structures in the quiet sun and in the two active regions studied follows a constant density law much more closely than a constant pressure law, contrary to what has generally been assumed previously. Data from the 1973 June 15 flare are less conclusive, but there too, one can argue that at certain times during the decay phase of the flare, a constant density law is appropriate. We believe that this variation of density with temperature is another piece of evidence for the existence of bursts in the solar atmosphere. Moreover, it appears possible that these bursts compress material as they heat it rather than expand it as in something of an explosive nature. The morphology of this solar region, as observed by stigmatic slit spectra taken by the HRTS instrument, does not contradict such a conclusion. Features apparent in the image of lines formed at 5×10^4 K like Si III are also seen in images of lines formed at much higher temperatures, e.g. O V at 2.5×10^5 K.

Further, indirect, evidence for the existence of bursts comes from our analysis of the non-thermal mass motions present in the transition region. When the lines are assumed to be emitted from plasmas with temperatures about twice those where the lines would be formed in ionization equilibrium, the non-thermal mass motions are approximately independent of temperature. This is in contrast to the case of lines emitted at their ionization equilibrium temperatures, where the non-thermal velocities increase with temperature. This behaviour is harder to understand, if, according to the HRTS data, the morphology of transition region lines formed at different temperatures are very similar.

References

Feldman, U. 1983, ApJ, 275, 367

Feldman, U. 1987, ApJ, 320, 426

Feldman, U. 1992, ApJ, 385, 758

Feldman, U., Laming, J. M., Mandelbaum, P., Goldstein, W. H., & Osterheld, A 1992, ApJ, in press

Laming, J. M., and Feldman, U. 1992, ApJ, 386, 364

Parker, E. N. 1988, ApJ, 330, 474

Photoionization Resonances of Si II in the Spectrum of Ap Si Stars

T. Lanz[1], M.-C. Artru[2], M. Le Dourneuf[3], and I. Hubeny[4]

[1] NASA Goddard Space Flight Center, Code 681, Greenbelt, MD 20771, USA
[2] Ecole Normale Supérieure de Lyon, 46 allée d'Italie, F-69364 Lyon, France
[3] UPR 261 du CNRS et DAMAp, Observatoire de Meudon, F-92195 Meudon, France
[4] Universities Space Research Association, NASA/GSFC, Code 681, Greenbelt MD 20771, USA

ABSTRACT: We present a study of the photoionization of Si^+ in stellar atmospheres. New theoretical calculations provide detailed photoionization cross-sections, including autoionization resonances, for many energy levels of Si II. They are included in synthetic spectra calculations of the far UV spectrum of A and late B stars, and they increase dramatically the opacity when silicon is overabundant. The most characteristic features of the far UV spectrum of Ap Si stars can now be reproduced, as illustrated by a comparison with *IUE* data for HD 34452.

1. INTRODUCTION

The photoionization of Si^+ is expected to have a significant influence on the radiation transfer in the photosphere of A and late B stars ($T_{\rm eff}$ = 10000 to 15000 K), especially for the Ap Si stars which exhibit silicon overabundances (5 to 50 times solar). Silicon may become the third most abundant species beyond hydrogen and helium; moreover, the flux of the A and late B stars is maximum in the far UV, where the Si^+ cross-sections may be large. Besides the enhanced Si II lines, the UV spectra of Ap Si stars show characteristic depressions, with widths larger than 5 nm. It is likely that they may be due to autoionization resonances of Si II, as first suggested by Jamar *et al* (1978). The strongest one at 140 nm has been identified to an autoionization line from an excited level of Si II (Artru, 1986). Synthetic spectra including this transition with its theoretical natural line width reproduce well the observed flux depression (Artru & Lanz 1987). Other characteristic features in the ultraviolet (157 and 178 nm) and in the visible spectrum of silicon stars remained unexplained.

2. THE PHOTOIONIZATION OF Si^+

Very accurate calculations on the photoionization of the Si II ground state have been performed in 1984 by Taylor *et al*, using the standard $R-$matrix code (Burke and Taylor 1975, Berrington *et al* 1978), to calculate consistent close coupling expansions of the initial bound state and the final continuum states of Si^+ in terms of the 12 lowest states of Si^{2+}. These 12 states are represented by very accurate Configuration Interaction (CI) wave functions expressed in terms of 8 spectroscopic orbitals 1s, 2s, 2p, 3s, 3p, 3d, 4s, 4p and 2 correlation orbitals $\bar{4}d$ et $\bar{4}f$ optimised by Baluja and Hibbert (1974) and allowing all possible distributions of the 2 outer electrons in the $n = 3, 4$ shells. In the present extension of the photoionization calculation to all the excited states relevant to the analysis of the spectra of silicon stars, we have used the OPACITY $R-$matrix code (Berrington *et al* 1987), similarly to the other calculations of the OPACITY project. However, the present results are expected to be slightly more accurate than their OPACITY analogues, since they use more sophisticated L^2 expansions of the Si^{2+} and Si^+ states. Typically, the 50 lower bound states of Si^+ have been obtained in the experimental order, with relative energies accurate to within a few percents, and the agreement between the length and velocity forms of the oscillator strengths for the bound states of Si^+ and of corresponding photoionization cross-sections agree within a few percents, except for very small transitions subject to cancellation effects.

Several cross-sections have very strong broad resonances. In particular, a strong resonance from the level 3d ^{2}D occurs at 140 nm, which confirms the identification suggested by Artru (1986) and Artru & Lanz (1987). This cross-section is displayed in Fig. 1 and shows other wide resonances. A strong threshold is found at 129.6 nm from $3p^2$ ^{2}D (see Fig. 1). This cross-section corresponds to the ionization toward the ground state of Si^{2+}, which is only possible due to configuration mixing between 3d and $3p^2$. This limit has been observed by Artru & Lanz (1987) in the spectrum of Ap Si stars; moreover, they identified several

lines of the corresponding series. A strong resonance, due to the transition $3p^2\ ^3P - 4s''\ ^3P^o$, is calculated around 155 nm; an observed depression in Ap Si spectra can be attributed mainly to this resonance. So far, we have been unable to identify the depressions at 178 nm and in the visible spectrum; we may nevertheless note that if these depressions should be attributed to Si II, then the initial level would be highly excited and little populated.

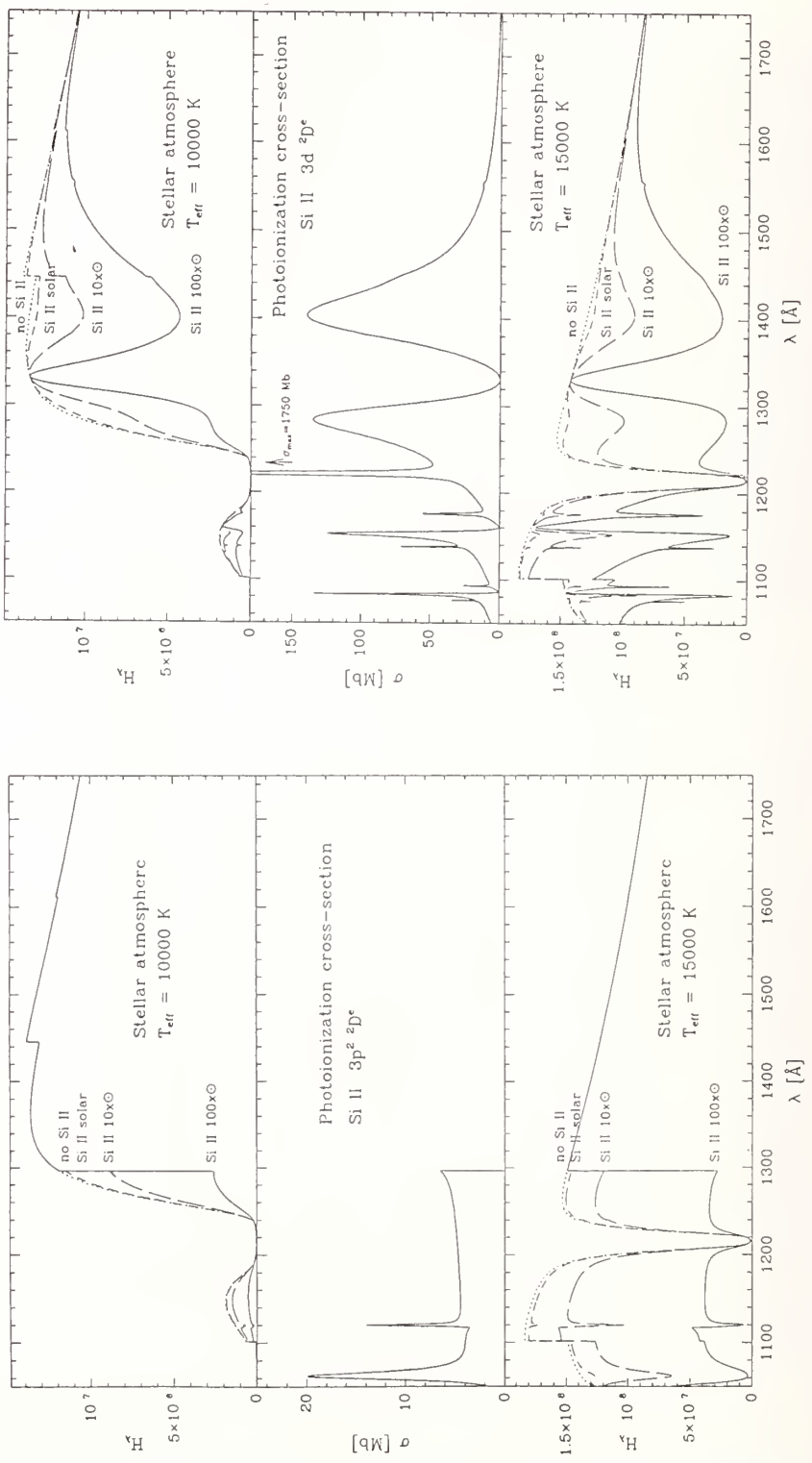

Fig. 1. Cross-sections for two low-excitation levels of Si II, and theoretical spectra for typical model atmospheres of A and late B stars, with a full range of silicon abundances.

3. ASTROPHYSICAL APPLICATION TO Ap Si STARS

We have computed some theoretical spectra for two model atmospheres typical of A and late B stars. We have included these new detailed cross-sections, assuming different silicon abundances. Fig. 1 displays such theoretical spectra, where a single cross-section is included at once to show its own effect. With a solar Si abundance, we found only rather small changes in the spectrum, but they could become dramatic for Ap Si stars with Si abundances larger than 10 times the solar abundance. We found observable effects only in the UV spectrum and for the cross-sections from levels with low excitation.

Fig. 2 displays a comparison with the observed *IUE* spectrum of HD 34452, an A0p Si star. We assumed the same stellar parameters than Artru & Lanz (1987): $T_{\rm eff}$ = 13650K, $\log g = 4$, $\epsilon(\mathrm{Si}) = 25\times\odot$, $\epsilon(\mathrm{ironpeak}) = 10\times\odot$. We have included the cross-sections of the six lowest Si II levels (up to 10.4 eV, without the ground state having a photoionization limit at 76 nm) and about 43000 metallic lines in the computation of the LTE theoretical spectrum. The agreement with the observed spectrum is striking! The depression at 140 nm and the region below 130 nm are very well reproduced, although the predicted flux below 118 nm is still too high. Attributing to Si II the depression between 155 and 160 nm is well supported. Several other calculated resonances are indeed observed in the stellar spectrum.

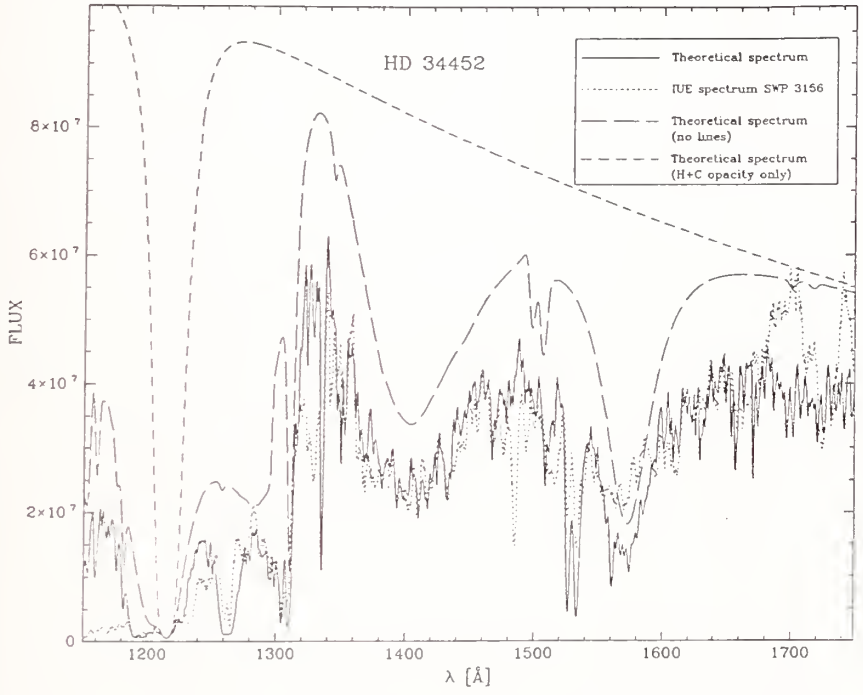

Fig. 2. Comparison of the observed *IUE* spectrum of HD 34452 and a theoretical spectrum calculated with the Si II photoionization cross-sections and about 43000 lines. The dashed lines show the dramatic effect of the Si II absorption.

REFERENCES

Artru M.-C., 1986, A&A **168**, L5.
Artru M.-C., Lanz T., 1987, A&A **182**, 273.
Berrington K.A., Burke P.G., Le Dourneuf M., Robb W.D., Taylor K. T., Vo Ky L., 1978, Comput. Phys. Commun. **14**, 367.
Berrington K.A., Burke P.G., Butler K., Seaton M.J., Storey P.J., Taylor K.T., Yu Y., 1987, J. Phys. B **20**, 6379.
Burke P.G., Taylor K.T., 1975, J. Phys. B 8, 2620.
Jamar C., Macau-Hercot D., Praderie F., 1978, A&A **63**, 155.
Seaton M.J., 1987, J. Phys. B **20**, 6363.
Taylor K.T., Zeippen C.J., Le Dourneuf M., 1984, J. Phys. B **17**, L157.

PHOTOSPHERIC HEAVY ELEMENTS IN HOT, HYDROGEN-RICH WHITE DWARFS (DA WD)

Stéphane Vennes and Stuart Bowyer
Center for EUV Astrophysics, University of California at Berkeley
2150 Kittredge St., Berkeley, CA 94720

1. Properties of Hot DA White Dwarf Stars

Hot, hydrogen-rich white dwarfs (spectral type DA) present extreme photospheric chemical composition. Their atmospheres, fully radiative, are largely dominated by hydrogen with, in some very hot stars, small heavy element traces ($Z \leq 10^{-5}$). As defined by the assigned spectral type, they show no traces of helium in optical and ultraviolet spectra ($Y < 10^{-3}$) in contrast with neighboring spectral types, DO ($Y > 10^{2}$) and DAO ($Y \approx 10^{-2}$). This pattern is usually explained in the context of chemical separation in a strong gravitational field, $g \approx 10^{8}$ cm s^{-2}, also known as *gravitational settling*. The presence of heavy elements (C, N, Si, Fe) in very hot DA white dwarfs ($T_{eff} \geq 50{,}000$ K) is naturally explained by *radiative levitation* in a strong radiation field (Chayer, Fontaine, & Wesemael 1989, 1991). The case of Feige 24 (WD 0232+035) is rather exemplary. Early high-dispersion spectroscopy with the *International Ultraviolet Explorer* revealed the presence of C IV, N V and Si IV absorption features attributed to the photosphere of the star (Dupree & Raymond 1982). The inferred abundances are in the range $5x10^{-7}$ - $5x10^{-6}$ (Wesemael, Henry, & Shipman 1984). Surprisingly the second most abundant element in Feige 24 was later found to be Fe (in the form of Fe V) with an abundance by number, $Fe/H \approx 10^{-5}$ (Vennes et al. 1992). These rather low trace element abundances as a whole help interpret one remarkable property of hot white dwarf stars: *all DA white dwarfs hotter than $T_{eff} \approx 25{,}000$ K are sources of extreme ultraviolet radiation* extending in some cases in the soft X-ray range. These EUV observations initiated with *Apollo-Soyuz* (Feige 24; Margon et al. 1976), were later refined and extended to a large group (~25 stars) of DA white dwarfs with *EXOSAT* (Paerels & Heise 1989; Vennes & Fontaine 1992). More recently the EUV all-sky survey performed in two EUV bandpasses (labelled S1 and S2) by the UK *Wide Field Camera* (Pounds et al. 1992) has extended EUV detections of DA white dwarf stars to about 100 objects. With this new data set we confirm one basic conclusion achieved with *EXOSAT*, i.e. the apparent EUV/soft X-ray flux deficiency relative to the predictions of *pure hydrogen atmospheres* found in most DA stars hotter than about 40,000 K (Fig. 1). This property can be understood if one postulates a direct filiation of the hot DA white dwarfs with the DO/DAO spectral types (DO —> DAO —> DA). In this context He and H are separated in two distinct layers with hydrogen floating on top the helium envelope. The thickness (i.e. transparency) of the hydrogen layers then determines the optical/UV properties (He II λ4686, He I λ4471, H I Balmer series) of the DO/DAO stars as well as the EUV/soft X-ray flux from DA stars which then departs strongly from pure H atmospheres (Vennes et al. 1988; Vennes & Fontaine 1992). The applicability of this model to EUV/soft X-ray properties of DA stars is debatable, however, because, as we have seen above, heavy elements are possibly dominating the EUV/soft X-ray spectra of these objects. This is clearly the case of Feige 24, for which *EXOSAT* low-dispersion spectroscopy is available (Paerels et al. 1986). Paerels et al.'s spectrum clearly shows the signature of heavy element photoionization opacities (Vennes et al. 1989) *probably from ionized species of Fe.* A more definitive answer may come from forthcoming medium-dispersion EUV spectroscopy by the *Extreme Ultraviolet Explorer.*

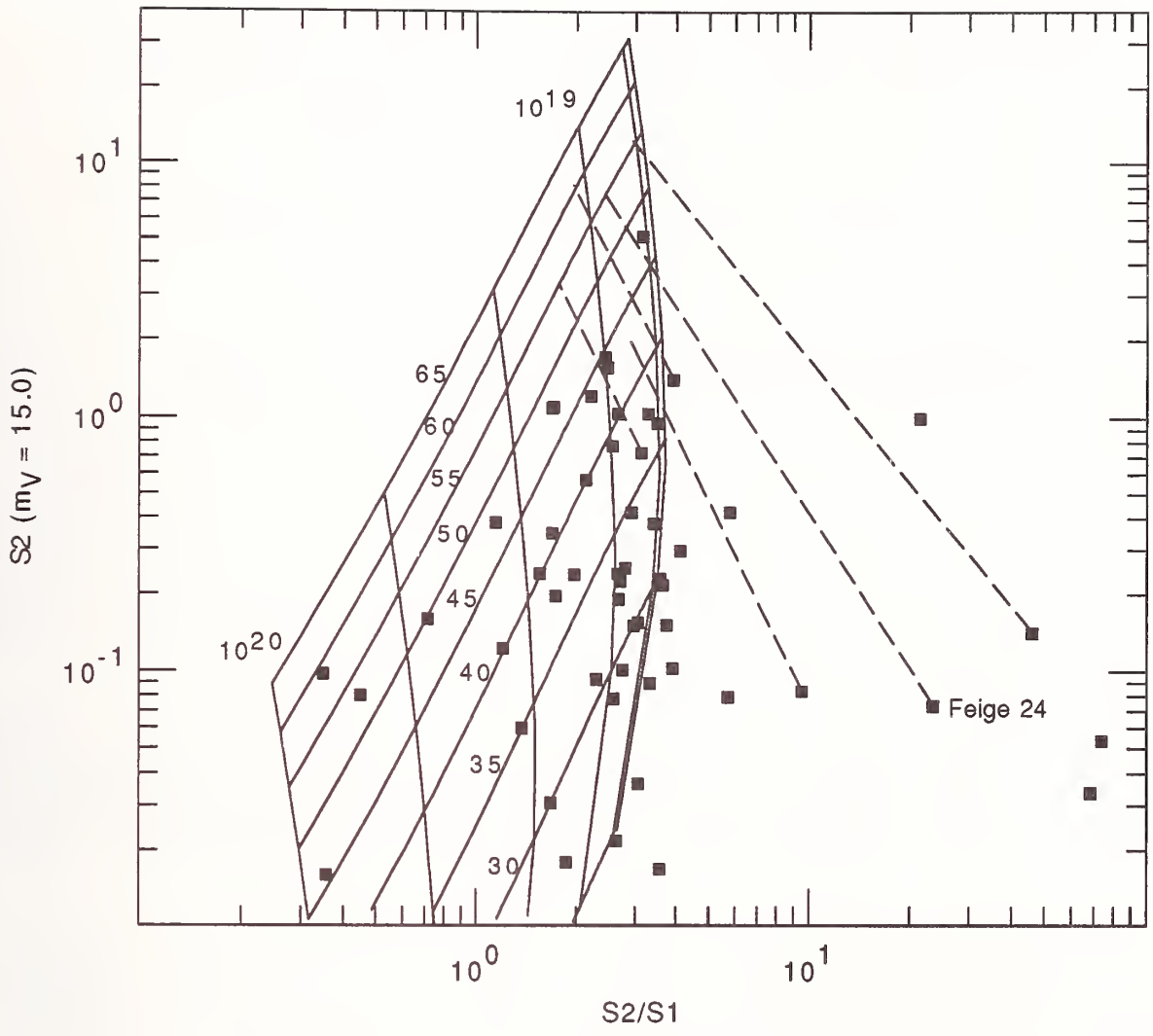

Figure 1. Interpretation of the *WFC* observations (S2 normalized to an apparent magnitude V = 15.0 vs S2/S1) of DA white dwarfs with *pure hydrogen model atmospheres* (log g = 8, T_{eff} = 25, 30, 35, 40, 45, 50, 55, 60, 65x10^3 K) also normalized to V = 15 and attenuated by ISM neutral hydrogen column density, n_H = 0.1, 1.0, 10.0, 30.0, 60.0, 100.0 x 10^{18} cm^{-2}. The likely presence of heavy elements (C, N, Si, Fe) shifts the apparent location of most hot ($T_{eff} \geq$ 40,000 K) DA stars to a *very soft* location in the diagram (shown for representative cases with broken lines pointing toward the lower right corner) unaccountable for with pure hydrogen models.

2. Far Ultraviolet Synthetic Spectra for Hot DA White Dwarfs

Most of the information about the chemical composition of hot DA stars is currently obtained in the far ultraviolet range using *IUE* as well as the *Hubble Space Telescope* (Sion et al. 1992). In Fig. 2 we present synthetic spectra of the FUV range for different chemical compositions: hydrogen rich atmosphere (T_{eff} = 55,000 K, log g = 7) with traces of Ni and Fe compared with the *IUE* spectrum of Feige 24. We confirm the predominant role played by Fe in this star as Ni remains undetected. Similarly we found no traces of Ca in Feige 24.

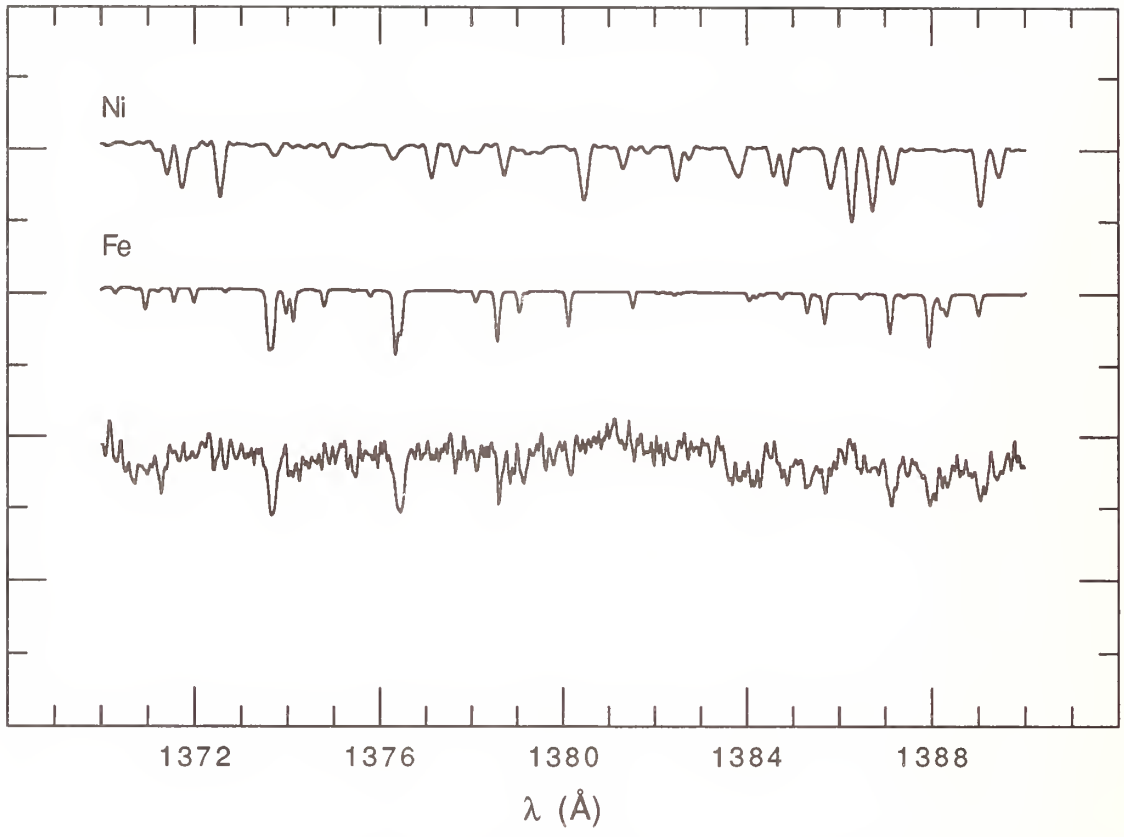

Figure 2. Far ultraviolet synthetic spectra of Fe (IV, V, VI) and Ni (IV, V) for a model atmosphere at T_{eff} = 55,000 K, log g = 7 (oscillator strengths from Kurucz, R.L. 1991, private communication) compared with *IUE* high-dispersion spectroscopy of Feige 24.

3. Conclusion

1. Extreme ultraviolet spectroscopy in the range 70-800 Å is necessary to fully investigate the chemical composition of DA white dwarfs. The apparent flux deficiency alluded to in *EXOSAT* and *WFC* photometric observations can be accounted for by either stratified H/He models *and/or* photospheric heavy elements. The *Extreme Ultraviolet Explorer* will fulfill this need.

2. Heavy elements, mainly Fe, are contaminating the UV, and most likely, the EUV/soft X-ray photospheres of hot DA white dwarfs. Modeling of these spectral ranges expose the need for accurate oscillator strengths and photoionization cross-sections of species like Fe V. This requirement can be extended to several light elements (C, N, Si) as well as other elements of the iron group.

Chayer, P., Fontaine, G., & Wesemael, F. 1989, White Dwarfs, (Berlin: Springer), 253
———. 1991, White Dwarfs, (Dordrecht: Kluwer), 249
Dupree, A.K., & Raymond, J.C. 1982, ApJ, 263, L63
Margon, B., Lampton, M., Bowyer, S., Stern, R., & Paresce, J. 1976, ApJ, 210, L79
Paerels, F.B.S., Bleeker, J.A.M., Brinkman, A.C., & Heise, J. 1986, ApJ, 309, L33
Paerels, F.B.S., & Heise, J. 1989, ApJ, 339, 1000
Pounds, K., et al. 1992, MNRAS, in press
Sion, E.M., Bohlin, R.C., Tweedy, R.W., & Vauclair, G.P. 1992, ApJ, 391, L30
Vennes, S., Chayer, P., Fontaine, G., & Wesemael, F. 1989, ApJ, 336, L25
Vennes,S., Chayer,P., Thorstensen, J.R., Bowyer, S., & Shipman, H.L. 1992, ApJ, 392, L27
Vennes, S., Pelletier, C., Fontaine, G., & Wesemael, F. 1988, ApJ, 331, 876
Vennes, S., Fontaine, G. 1992, ApJ (Dec. 10 issue)
Wesemael, F., Henry, R.B.C., & Shipman, H.L. 1984, ApJ, 287, 868

ATOMIC DATA NEEDS FOR OPTICAL REGION STUDIES OF EARLY A TYPE STARS

Saul J. Adelman*
Department of Physics, The Citadel, Charleston, SC 29409 USA

and

Austin F. Gulliver*
Department of Physics and Astronomy, Brandon University, Brandon, Manitoba R7A 6A9 Canada

* Guest Investigator, Dominion Astrophysical Observatory

If there are any types of stars for which we should be able to derive reliable elemental abundances, it is the early A stars. The atmospheric modeling is now straightforward as the atmospheres are in radiative equilibrium with hydrogen as the dominant opacity source. The line opacities for the light through the iron peak elements are reasonably well calculated. Hotter stars exhibit strong non-LTE effects. Cooler stars have substantial convection zones as well as molecules in their atmospheres, situations which involve more complicated physics.

With model atmospheres which have the proper opacities and physics included such as those calculated by the ATLAS9 program of Dr. Robert L. Kurucz, it should be possible to deduce high quality abundances of many elements. As A type star lifetimes are much less than the age of the Sun, the A type stars we see must have formed relatively recently on a cosmological time scale. Comparison of their abundances with solar values should yield important information about the chemical history of matter in our Galaxy during the last five billion years.

In the last decade with electronic detectors such as Reticons and CCDs replacing photographic plates for spectroscopy, the signal-to-noise ratio of typical high dispersion astronomical observations has tended to increase from 20 to 100 or more. This suggested that a detailed comparison of a high dispersion spectra with minimal noise of a prototype A star with the best spectral synthesis would be useful. As A type stars with effective temperatures of order 10000 K represent sources which are hotter than typical atomic laboratory sources, considerable atomic physics information can also be extracted from this data (see Leckrone et al. 1992).

The atomic line lists which one can realistically use for spectrum synthesis calculations are primarily the work of Dr. Robert L. Kurucz, whose generous policy of making them able to other workers has lead to much of the progress that has been made in this area. Also of importance are the critical compilations made at NIST by Fuhr, Wiese, and associates. When one performs a calculation, one finds that most spectral features are blends, even those which are often attributed to one primary line in line identification studies. Blending can be avoided to some extent by working with the sharpest lined stars, but these are only a small fraction of the known stars. For these calculations one can only use lines with good wavelengths and calculated or measured oscillator strengths which in practice means one works with classified lines. Potentially there are many still to be classified lines which also could make contributions to spectrum synthesis calculations. Excluding them means that the derived abundances may be overestimates.

Optical region line identification studies with high signal-to-noise data often reveal lines which are not in *A Multiplet Table of Astrophysical Interest* (Moore 1945). By using more recently published atomic spectra studies, one can identify a number of these features. Other methods of attack are to predict the wavelengths of lines to complete multiplets or even to predict wavelengths of lines between known energy levels (Dworetsky 1971, Adelman 1987).

Beyond the identification of a line, one can use its profile (or equivalent width) to deduce an elemental abundance. For an unblended line one needs to know its atomic parameters, in particular, its lower excitation potential, its oscillator strength and (for non-weak lines) its line damping constants as well as the ionization potentials and partition functions for the atom.

For these reasons we decided to compare as well as we could the spectrum of some relatively sharp-lined A type star with the predictions of a state of the art spectrum synthesis code, SYNTHE of Dr. Robert L. Kurucz. This we expected would allow us to assess the quality of the comparison, including lines in the star missing in the code and systematics in the oscillator strengths. For the spectrum synthesis input parameters we use stellar parameters derived from fine analyses of the same data. In some cases hyperfine structure and isotopic shifts can also be important and detectable if not included in the spectrum synthesis calculations.

We obtained Reticon spectra of Vega, one of the brightest stars in the sky, with the coudé spectrograph of the Dominion Astrophysical Observatory at a reciprocal dispersion of 2.4 Å mm^{-1} to produce a high quality spectral atlas. After considerable experimentation we have achieved signal-to-noise ratios of 3500 or more. Figure 1 illustrates the type of improvement in spectral quality which has been achieved. Besides showing at certain wavelengths the telluric spectrum which is weak or absent in most of the photographic region, the high signal-to-noise data have revealed some important clues about the nature of Vega. Most importantly the line profiles of Vega are not those expected from classical model atmospheres theory. There are a large number of weak flat bottom lines. This may be evidence that this star is a fast rotator seen pole on according to one interpretation of the non-classical line profiles. This interesting astrophysical observation means that we are now working to model these profiles before we can examine the atomic physics aspects of this data.

Thus, we selected another early A star which did not show peculiar line profiles for a second atlas. The star Omicron Pegasi is one of the sharpest-lined stars, v sin i about 6 km s^{-1}. It is about 100 times fainter than Vega and thus we can achieve signal-to-noise ratios of about 500 to 750 at best. Its effective temperature is 9600 K and its surface gravity log g = 3.60. We now have observations covering λλ4050-4880 and plan to extend these observations both longward and shortward as long as we can achieve a signal-to-noise ratio of 500 in two hours. The must recent abundance analysis is by Adelman (1988ab) based on coadding 12 IIaO nitrogen baked 2.4 Å mm^{-1} photographic region spectra obtained with the long camera of the DAO coudé spectrograph. The maximum signal-to-noise ratio of this data was about 80.

Figure 2 shows a comparison between the observations of o Peg (solid line) and a synthesized spectrum (dashed line) for λλ4380 - 4390. Many of the defects of the comparison can be fixed by changes in the oscillator strengths and/or assumed elemental abundances by factors of two or less. We would expect slightly better agreement if our synthesized spectrum was calculated based on parameters derived from a fine analysis of the Reticon S/N>500 data instead of the coadded photographic data. The instrumental profile might need to be slightly broader in the wings. However, we also see evidence for oscillator strengths being absent from the code and for errors in the laboratory wavelengths. Study of the later may be useful in improving the values of atomic energy levels. We would like to work with atomic physicists to improve the atomic data needed to synthesize such spectra.

REFERENCES

Adelman, S. J. 1987, PASP 99, 515
Adelman, S. J. 1988a, MNRAS 230, 671
Adelman, S. J. 1988b, MNRAS 235, 749
Dworetsky, M. M. 1971, PhD thesis, University of California at Los Angeles
Leckrone, D. S. et al. 1992, ApJ, in press
Moore, C. E., 1945. A Multiplet Table of Astrophysical Interest, Princeton University Observatory

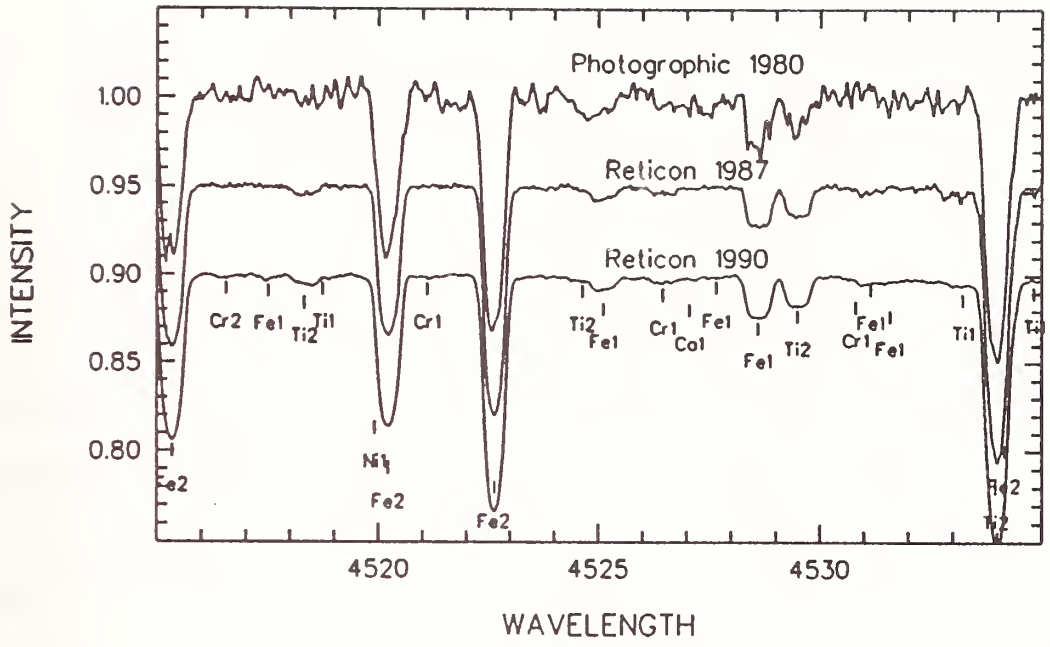

Figure 1. The spectrum of Vega as obtained with the long camera of the coudé spectrograph of the 1.4-m telescope of the Dominion Astrophysical Observatory. The three spectra illustrate how the improvement in the signal-to-noise ratio has resulted in revealing important details.

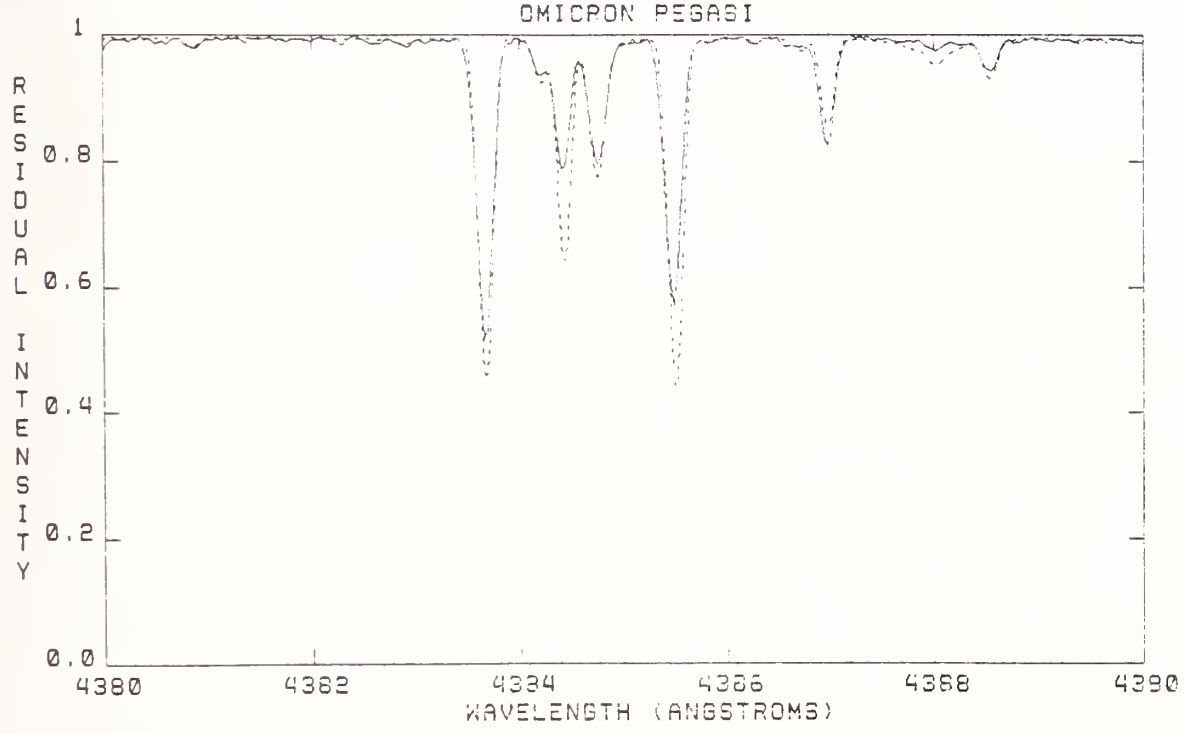

Figure 2. The spectrum of Omircon Pegasi λλ4380-4390 as observed with the long camera of the coudé spectrograph of the 1.4-m telescope of the Dominion Astrophysical Observatory (solid line) compared with a synthetic spectrum based on stellar parameters from an analysis by Adelman (1988b) (dashed line). On the whole the agreement is quite good. However, we can see that if one shifts stellar spectrum so that it agrees with the wavelength of the Fe I (41) λ4383.547, the wavelength of Fe II (27) λ4385.381 is not in good agreement. The blend dominated by Fe II (32) λ4384.33, which is a predicted line, also shows a wavelength shift.

EXPERIMENTAL ISOTOPE SHIFTS IN NI II AND FE II

Maria Rosberg, Ulf Litzén and Sveneric Johansson

Lund University, Department of Physics, Sölvegatan 14, S-223 62 Lund

This work reports about measurements of isotope structure in Ni II and Fe II. We have used spectra from hollow-cathode lamps that have been recorded with the Fourier Transform Spectrometer at Kitt Peak National Observatory. Measurements of isotope shifts yield useful information about atomic and nuclear properties. With high-resolution spectroscopy at modern telescopes it is also possible to observe isotope shifts in stellar spectra (Leckrone *et al.* 1991). The importance of a general knowledge about isotope structure for studies of the solar spectrum has recently been pointed out (Kurucz 1992). This is especially true for elements having line-rich spectra and a high solar abundance. Ignoring isotope structure when constructing synthetic spectra may introduce systematic errors in the calculation of line profiles and may therefore affect e.g. abundance determinations.

The nickel spectrum used covers the wavelength region 5800-7100 Å and it was emitted by a hollow-cathode lamp run at a current of 0.5 Amps with argon as a carrier gas at a pressure of 2.5 Torr. The iron spectrum we used covers the region 8600-14200 Å and in this case the light source was run at 1.0 Amps DC with neon as a carrier gas at a pressure of 4 Torr.

Some of the lines in the spectra show a nearly resolved isotope structure. These lines correspond to the transitions in Ni II $3d^8(^3F)4p\text{-}3d^74s^2$ (Shenstone 1970) and $3d^6(^5D)4p\text{-}3d^54s^2$ in Fe II (Johansson 1978). For both nickel and iron the measured isotope shifts

are negative, i.e. the heavier isotope is shifted towards smaller wavenumbers.

Thirteen Ni II lines in the red region have been studied in detail, see Figure 1. Natural nickel has the following isotope composition: 68% ^{58}Ni, 26% ^{60}Ni, 1% ^{61}Ni, 4% ^{62}Ni and 1% ^{64}Ni. However, in the spectrum we can only see four peaks for each line, as the ^{61}Ni isotope exhibits hyperfine structure and its intensity is therefore spread out on a number of undetectable components. The measured splittings ^{64}Ni-^{62}Ni, ^{62}Ni-^{60}Ni, ^{60}Ni-^{58}Ni are of the order of -100 mK with the largest spread in the first one. The intensity distribution among the components of the strongest $3d^8(^3F)4p$-$3d^74s^2$ lines show a good agreement with relative abundances of natural nickel.

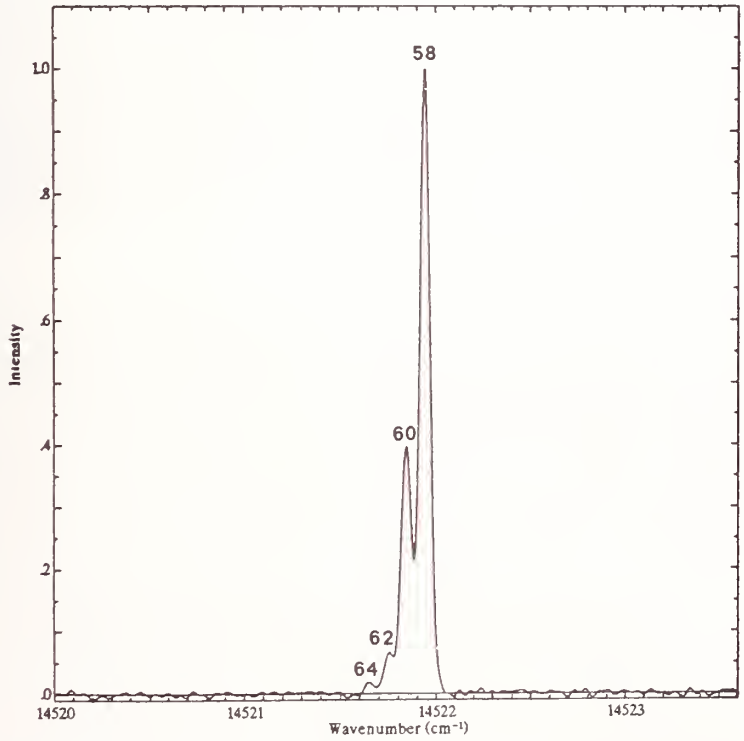

Figure 1 Isotope structure in Ni II λ6884.

Natural iron consists of 6% ^{54}Fe, 92% ^{56}Fe, 2% ^{57}Fe and 0.3% ^{58}Fe. However, we can only see the two most abundant isotopes, ^{54}Fe and ^{56}Fe, which is illustrated by the strong Fe II line at 9997 Å in Figure 2. This line is very strong in emission in spectra of various stars and extragalactic objects, probably due to fluorescence induced by H Lyα (Johansson 1990). We have studied the isotope structure of nine Fe II lines in the near-infrared region, giving an average value of the isotope shift of about -105±3 mK.

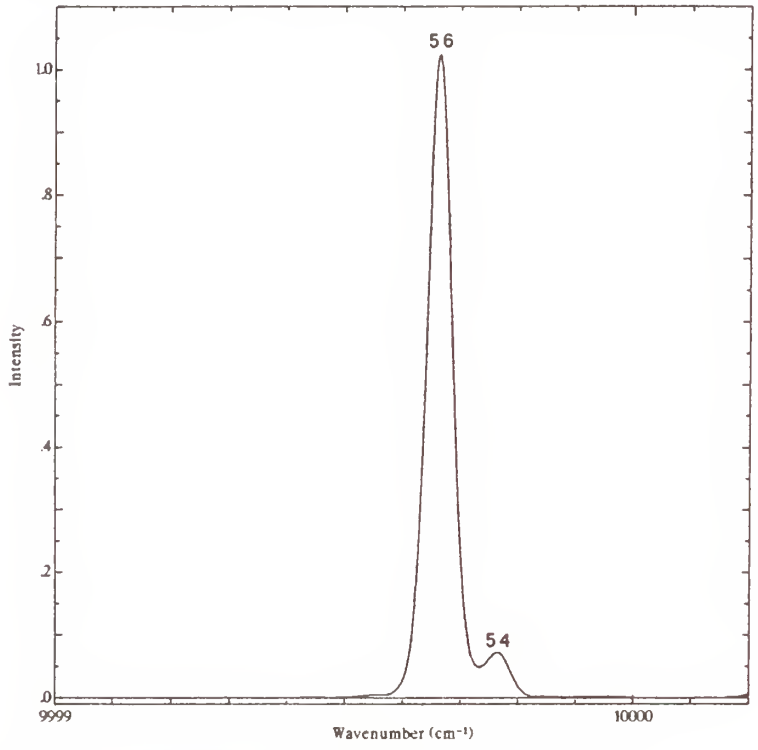

Figure 2 Isotope structure in Fe II λ9997.

References

Johansson S., 1990, ed. G. Wallerstein, in *Cool stars, stellar systems and the sun*, ASP Conf. Ser. **9**, 307.

Johansson S., 1978, *Physica Scripta* **18**, 217.

Leckrone D. S., Wahlgren G. M., Johansson S., 1991, *Ap. J.* **377**, L37.

Kurucz R. L., 1992, submitted to *Ap. J.*

Shenstone A. G., 1970, *J. Res. Nat. Bur. Std.* **74A**, 801.

Accurate Wavelengths and Isotope Shifts for Lines of Doubly-Ionized Mercury (Hg III) of Astrophysical Interest

Craig J. Sansonetti and Joseph Reader

National Institute of Standards and Technology
Gaithersburg, MD 20899

For thirty years it has been known from observations of the 3984 Å line of Hg II that Hg is much more abundant in the atmospheres of some chemically peculiar stars than in the sun. The wavelength of this line is seen to vary slightly from star to star, and Bidelman[1] suggested that these variations resulted from differing isotopic compositions. The most extreme isotope anomaly occurs in the star chi Lupi[2] where the observed wavelength is consistent with nearly pure ^{204}Hg.

Michaud et al.[3] have proposed a diffusion model to explain both the enhanced abundance of Hg and the isotope anomalies observed in Hg-rich stars. In this model the balance between radiation pressure and gravity causes heavy isotopes to concentrate in a thin layer of the stellar atmosphere as neutral and singly-ionized Hg, while the lighter isotopes exist at higher altitudes as doubly-ionized Hg or are driven away from the star by the radiation pressure. To test this model it is necessary to determine elemental and isotopic abundances for Hg by using lines of different stages of ionization.

Using the Goddard High Resolution Spectrograph (GHRS) on the Hubble Space Telescope, Leckrone and co-workers have made observations of the Hg III lines at 1738.4, 1738.5, 1740.2, and 2354.2 Å in chi Lupi. To derive abundances from these data, accurate wavelengths and isotope shifts are needed. The accuracy of the best available wavelength data by Johns[4] and Foster[5] is not adequate for the analysis. Although Foster[6] in a subsequent paper reported isotope shifts for 21 Hg III levels, no data were given that apply to the lines observed with GHRS.

The present work was undertaken to provide accurate wavelengths and isotope shifts for these lines of Hg III to permit reliable interpretation of the spectrum of chi Lupi. A full description will be published elsewhere.[7]

EXPERIMENT

The spectrum of doubly-ionized Hg was excited in sealed electrodeless-discharge lamps by using a pulsed radio-frequency oscillator. Four lamps of identical dimensions were used: two containing ^{198}Hg and one each containing natural Hg and ^{204}Hg. Each lamp was filled under high vacuum with a few mg of Hg and no carrier gas. The lamp design is shown in Fig. 1.

Rf power at a frequency of 13.5 MHz was coupled into the Hg discharge by a capacitively tuned resonant circuit. Excitation of the Hg III spectrum was optimized by adjusting the duration of the rf pulses, their repetition rate, and the peak pulse power. The metallic Hg was kept concentrated at the rear of the lamp by a gentle stream of air. The entire body of the lamp was cooled by diffuse air from a small fan. Under these conditions the lamp operated stably and emitted a strong Hg III spectrum with sharp unperturbed lines.

The spectrum was photographed with the 10.7-m normal-incidence vacuum spectrograph at the National Institute of Standards and Technology. Spectra of Pt I and II[8] and of Ar II[9] were used as wavelength standards.

The observations were used to determine wavelengths of the four lines of ^{198}Hg III, given in Table I. Small shifts between the Hg spectrum and the

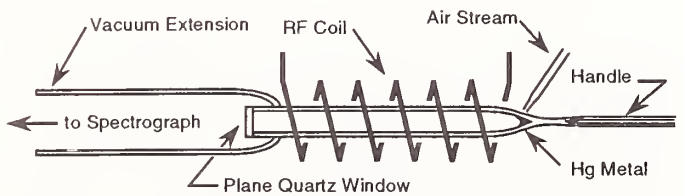

Fig. 1. Schematic of Hg pulsed rf lamp.

Pt and Ar reference spectra due to slightly different grating illumination were removed by using accurate values for several ^{198}Hg II lines given by Reader and Sansonetti.[10] The final uncertainty in our Hg wavelengths is attributable approximately equally to the uncertainty in the general calibration based on the reference spectra and to the uncertainty in determining the shift between the Hg and reference spectra.

Special exposures were made to measure the isotope shifts between lines of the 204 and 198 isotopes. For these exposures spectra from the ^{198}Hg, ^{204}Hg, and Ar lamps were photographed sequentially. By means of adjustable masks in front of the plate holder, the spectra were arranged as shown in Fig.2. The position of the plate in the spectrograph was not disturbed between exposures.

The isotope shifts were determined by measuring two parallel tracks on the photographic plate as shown in Fig. 2. These tracks were defined by masks in the optical system of the comparator so that the position of a line could be measured in either track without moving the comparator cross feed. The Ar lines served as a reference to define zero isotope shift.

Fig. 2. Exposures for isotope shift measurements.

For each Hg line, the displacement between the two isotopes was found as the difference of the positions measured in the upper and lower tracks. The result was corrected by subtracting the average displacement between the upper and lower track positions of the Ar lines. The corrected displacement was multiplied by the plate factor to obtain the isotope shift. The measured $^{204-198}$Hg isotope shifts are given in Table I.

Shifts between natural Hg and ^{198}Hg were determined by the same technique described above. The results are given in Table I. As the profile of the 2354-Å line of natural Hg was broadened and slightly asymmetric, the uncertainty of its shift was increased to ±0.003 Å.

SHIFTS FOR OTHER Hg ISOTOPES

For heavy elements, where mass-dependent effects are negligible, the relative shifts between isotopic components of a spectral line depend only on the size and shape of the nucleus and are independent of the combining energy levels and the stage of ionization. By using relative isotope shifts derived from lines of Hg I[11,12] and our measurements of the $^{204-198}$Hg shifts, we are able to calculate shifts for the remaining stable isotopes. We have also calculated the shift for natural Hg from the relative shifts by using the known abundances[13] for the stable isotopes.

In Table II we summarize the wavelengths for all stable isotopes obtained from our measured $^{204-198}$Hg shifts and the relative isotope shifts. The wavelengths for natural Hg in this table are those calculated from the relative isotope shifts and isotopic abundances, which we consider to be more reliable than the directly measured values for natural Hg.

Table I. ^{198}Hg III wavelengths and isotope shifts. Wavelengths shorter than 2000 Å are vacuum.

Wavelength	Wave Number	^{204}Hg - ^{198}Hg Shift[a]		Natural Hg - ^{198}Hg Shift[b]	
(Å)	(cm^{-1})	(Å)	(cm^{-1})	(Å)	(cm^{-1})
1738.4560(20)	57 522.31(7)	0.0218(20)	-0.72(7)	0.0091(20)	-0.30(7)
1738.5207(20)	57 520.17(7)	0.0190(20)	-0.63(7)	0.0078(20)	-0.26(7)
1740.2556(20)	57 462.82(7)	0.0221(20)	-0.73(7)	0.0093(20)	-0.31(7)
2354.2160(20)	42 463.99(4)	0.0398(20)	-0.72(4)	0.0201(30)	-0.36(5)

a The wavelength for ^{204}Hg is longer than for ^{198}Hg.
b The wavelength for natural Hg is longer than for ^{198}Hg.

Table II. Wavelengths (Å) for natural Hg and stable Hg isotopes. Results for odd isotopes are the center-of-gravity of the magnetic hyperfine structure.

Species	Hg III Line			
	1738	1738	1740	2354
^{196}Hg	.4501(21)	.5156(21)	.2496(21)	.2052(21)
^{198}Hg	.4560(20)	.5207(20)	.2556(20)	.2160(20)
^{199}Hg	.4569(20)	.5215(20)	.2565(20)	.2177(20)
^{200}Hg	.4628(21)	.5267(21)	.2625(21)	.2285(21)
natural Hg	.4647(22)	.5283(22)	.2644(22)	.2319(22)
^{201}Hg	.4651(22)	.5286(22)	.2648(22)	.2326(22)
^{202}Hg	.4704(24)	.5332(24)	.2702(24)	.2422(24)
^{204}Hg	.4778(28)	.5397(28)	.2777(28)	.2558(28)

ASTROPHYSICAL IMPLICATIONS

Based on our present measurements, Leckrone et al.[14] have analyzed the two lines of Hg III at 1738 Å in the GHRS spectra of chi Lupi. Their analysis shows the same isotope anomaly that was found previously with the lines of Hg II; that is, the spectrum is consistent with pure ^{204}Hg. They conclude that this result, which disagrees with some predictions of the diffusion model,[4] reveals a need for a new or refined model to explain the elemental and isotope abundance anomalies for Hg in chemically peculiar stars.

ACKNOWLEDGEMENT

This work was supported in part by the National Aeronautics and Space Administration.

REFERENCES

1. Sky and Tel., **23**, 140 (1962).
2. R. E. White, A. H. Vaughan, Jr., G. W. Preston, and J. P. Swings, Astrophys. J. **204**, 131 (1976).
3. G. Michaud, H. Reeves, and Y. Charland, Astron. & Astrophys. **37**, 313 (1974).
4. M. W. Johns, Can. J. Res. A **15**, 193 (1937).
5. E. W. Foster, Proc. Roy. Soc. London A **200**, 429 (1950).
6. E. W. Foster, Proc. Roy. Soc. London A **208**, 367 (1951).
7. C. J. Sansonetti and J. Reader, submitted to Phys. Rev. A (1992).
8. J. E. Sansonetti, J. Reader, C. J. Sansonetti, and N. Acquista, J. Res. Natl. Inst. Stand. Technol. **97**, 1 (1992).
9. G. Norlén, Phys. Scr. **8**, 249 (1973).
10. J. Reader and C. J. Sansonetti, Phys. Rev. A **33**, 1440 (1986).
11. S. Gerstenkorn and J. Vergès, J. Physique **36**, 481 (1975).
12. S. Gerstenkorn, J. J. Labarthe, and J. Vergès, Phys. Scr. **15**, 167 (1977).
13. D. R. Lide, ed., **Handbook of Chemistry and Physics**, 73rd Edition (CRC Press, Inc., Boca Raton, Florida, 1992).
14. D. S. Leckrone, G. M. Wahlgren, S. G. Johansson, and S. J. Adelman, "High Resolution Ultraviolet Spectroscopy of Chemically Peculiar Stars with the HST/GHRS," in Proceedings of I.A.U. Colloquium no. 138, M. M. Dworetsky, ed. (P.A.S.P. Conference Series, in press 1992).

LINE BLANKETING IN NOVA ATMOSPHERES

P. H. Hauschildt and S. Starrfield
Dept. of Physics and Astronomy
Arizona State University
Tempe, AZ 85287-1504

Introduction

We are currently using a spherical, expanding, non-LTE stellar atmosphere code to analyze the early spectra of novae in outburst. We have found that nova atmospheres are dominated by an enormous number of overlapping spectral lines. These lines originate from a large number of species in very different ionization stages due to the large temperature gradients found in nova photospheres. The features which appear to be 'emission lines' are actually "holes in the iron curtain". The conditions inside the line forming regions of these photospheres imply very large deviations from LTE and, therefore, the line formation process is a complicated multi-level non-LTE problem in a rapidly expanding shell. Spectral synthesis and analysis of these spectra demonstrate the importance of line blanketing in the early and late spectra of novae and require the best and most complete atomic data in order to obtain accurate abundances for the elements in nova ejecta.

In the following sections we describe briefly the model assumptions, parameters, and the model construction. We then show an example for the influence of line blanketing on nova spectra.

Model Assumptions

- steady state, i.e., $\partial/\partial t \equiv 0$,
- power law density, i.e., $\rho(r) \propto r^{-n}$,
- constant mass loss rate, $\dot{M} \equiv const.$, with respect to time and radius,
- radiative equilibrium in the Lagrangian frame,
- full non-LTE treatment of H I (10 levels), Mg II (3 levels), and Ca II (5 levels),
- LTE occupation numbers for the ionization stages I–III of He, C, N, O, Si, S, Fe, Al, Na, K, Ti, Sc, Mn and Cr (treated consistently with the non-LTE species),
- all relevant b-f, f-f and b-b transitions are included (b-f, f-f: Mathisen 1984; b-b: Kurucz & Peytremann 1978, Kurucz 1988)

Model Parameters

- the reference radius R, which refers to the radius where either the optical depth in absorption or extinction at 5000Å is unity,
- the effective temperature $T_{\rm eff}$, which is defined by means of the luminosity, L, and the reference radius ($T_{\rm eff} = (L/4\pi R^2\sigma)^{1/4}$ where σ is Stefan's constant),
- the density parameter, n, ($\rho(r) \propto r^{-n}$),
- the maximum expansion velocity, v_∞,
- the density, $\rho_{\rm out}$, at the outer edge of the envelope,
- the metal line threshold ratio, Γ,
- the albedo for line scattering (metal lines only),
- the element abundances.

Model Construction

Numerical Methods:

- Approximate Λ-operator iteration (ALI) method for the solution of the spherically symmetric, special relativistic equation of radiative transfer (SSRTE) for continua, LTE, and non-LTE lines (see Hauschildt 1992a),
- ALI method for the solution of the special relativistic, multi-level, non-LTE continuum and line transfer problem using a direct extension of the method of Rybicki & Hummer (1991) including overlapping lines and active continua (Hauschildt, submitted to JQSRT),
- a hybrid method (ALI combined with partial linearization) for the self-consistent solution of the radiative equilibrium equation in the comoving frame (see Hauschildt 1992b).

Model Computation:

- solve $dr/d\tau = -1/\chi_{5000}$ to obtain the connection between the radius, r, and the optical depth in extinction at 5000Å, τ, so that $r(\tau = 1) = R$,
- select relevant metal lines from the line list of Kurucz & Peytremann (1978) and Kurucz (1988) (typically 10^5 lines are treated explicitly),
- solve the SSRTE for, typically, 2000–4000 wavelength points and up to 13–25 additional wavelength points per non-LTE line,
- update departure coefficients and temperature structure,
- repeat the previous steps if the required accuracy is not reached,
- for a converged model, compute a high-resolution observer's frame spectrum (typically 5000–12000 wavelength points).

Acknowledgements: We thank S. Shore, R. Wehrse and G. Shaviv for stimulating discussions. This work was sponsored, in part, by NASA grants to Arizona State University.

References

Hauschildt, P. H. 1992a. JQSRT, **47**, 433.

Hauschildt, P. H. 1992b, Astrophys. J., **398**, 224.

Hauschildt, P. H., Wehrse, R., Starrfield, S., & Shaviv, G. 1992, Astrophys. J., **393**, 307.

Kurucz, R.L. 1988, private communication.

Kurucz, R.L. & Peytremann, E. 1975, "A Table of Semiempirical gf Values", Smithsonian Astrophysical Observatory, Special Report 362.

Mathisen, R. 1984, "Photo Cross-sections for Stellar Atmosphere Calculations — Compilation of References and Data", Inst. of Theoret. Astrophys. Univ. of Oslo, Publ. Series No. 1.

Rybicki, G. B. & Hummer, D. G. 1991, Astron. Astrophys., **245**, 171.

Figure 1: Example of the influence of line blanketing on nova spectra. The upper panel shows the continuum energy distribution of a nova model with the parameters $T_{\rm eff} = 10000\,{\rm K}$, $L = 20000\,{\rm L}_\odot$, $v_\infty = 2000\,{\rm km\,s^{-1}}$ and solar abundances (the structure was taken from a non-LTE, line-blanketed model). Only H I and Mg II (h+k) lines are considered in this spectrum. In the subsequent panels the number of lines is roughly increased by a factor of 10, respectively.

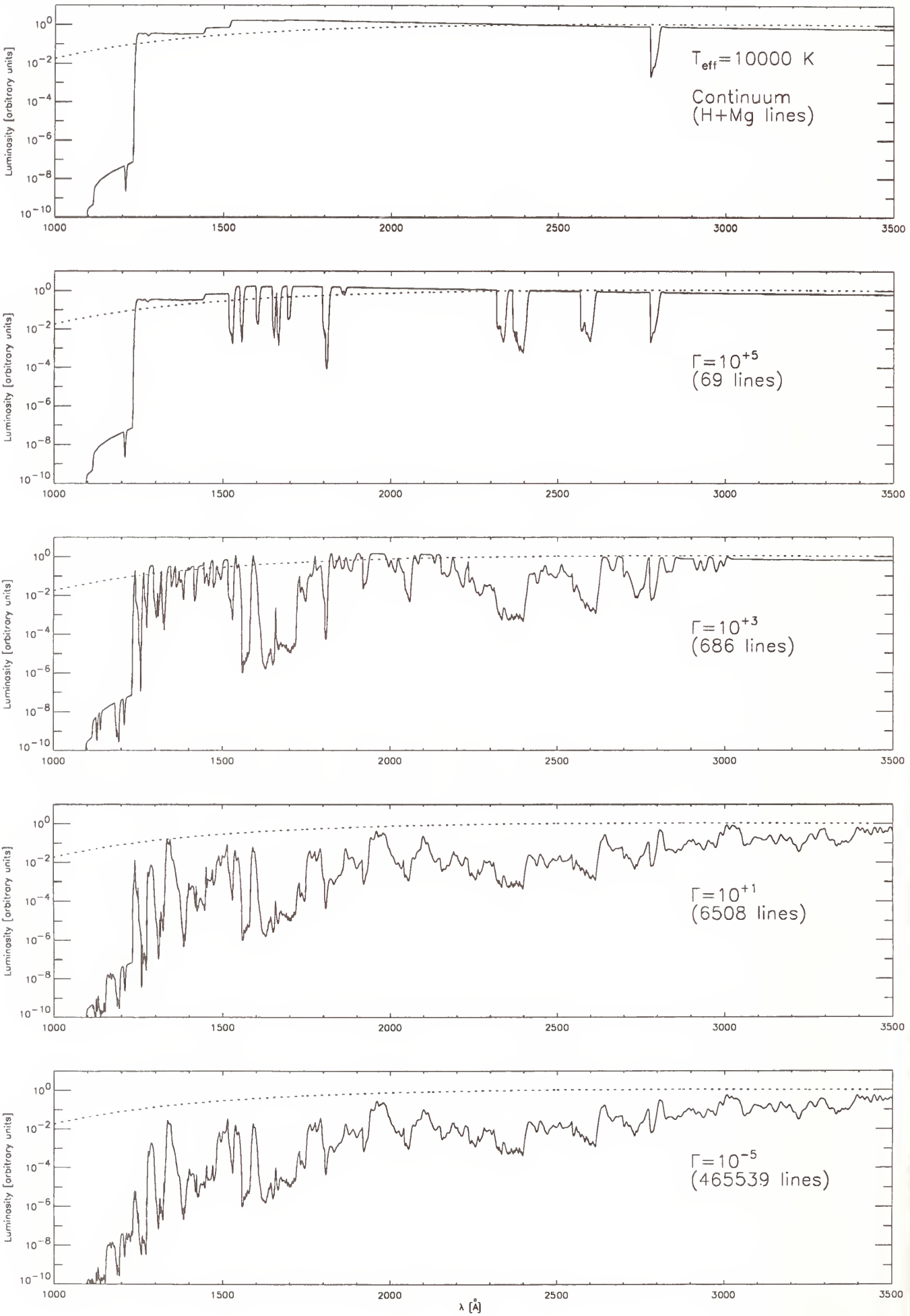
Luminosity [arbitrary units]
10^{0}
10^{-2}
10^{-4}
10^{-6}
10^{-8}
10^{-10}
1000
1500
2000
2500
3000
3500
T_{eff}=10000 K
Continuum
(H+Mg lines)
Γ=10^{+5}
(69 lines)
Γ=10^{+3}
(686 lines)
Γ=10^{+1}
(6508 lines)
Γ=10^{-5}
(465539 lines)
λ [Å]

DENSITY SENSITIVE LINES OF BORON-LIKE IONS OF C, N AND O

PHILIP JUDGE, High Altitude Observatory, National Center for Atmospheric Research[1]
RONG LU, Middlebury College, VT.
PAAL BREKKE, Institute of Theoretical Astrophysics, University of Oslo.
ANIL PRADHAN, Department of Astronomy, Ohio State University.

INTRODUCTION

Lines from ions of the $ns^2\ np$ isoelectronic sequences ($n = 2$:Boron, $n = 3$:Aluminum) have proven to be extremely useful as spectral diagnostics of electron densities in certain astrophysical plasmas (e.g. Feldman & Doschek 1979; Stencel *et al.* 1981). These include low density ($N_e \leq 10^{12}$ cm^{-3}) plasmas at temperatures between $\sim$ 5000 and 2×10^5K, regimes which are typical of stellar chromospheres and transition regions. In this paper we discuss calculations of the UV spectra of the astrophysically abundant B-like ions C II, N III and O IV, using new Maxwellian-averaged collision rates (Blum & Pradhan 1992). These rates were computed in the close-coupling approximation using a 10 state eigenfunction basis set and should be of high accuracy ($\pm$10%). Our aim is to compare these calculations with earlier theoretical results and with observations of a variety of astrophysical objects, to determine the value of these lines as diagnostics of plasma electron densities.

WHY UV LINES OF BORON-LIKE IONS ARE VALUABLE

The ground term of B-like ions is $2s^2\ 2p\ ^2P^o$. The lowest excited term is $2s\ 2p^2\ ^4P$ (the other terms of this configuration are $^2D\ ^2S\ ^2P$). Parity-changing transitions between the two lowest terms are therefore *spin-forbidden.* There are five lines within the multiplet $2s\ 2p^2\ ^4P_{5/2,3/2,1/2} \rightarrow 2s^2\ 2p\ ^2P^o_{3/2,1/2}$ (see Table 1). These lines are useful for studying certain properties of astrophysical plasmas because: (i) B-like ions of C, N and O are abundant, and they are quite easily observed; (ii) The multiplets are usually optically thin, and are excited by electron collisions from the ground term; (iii) Hence ratios of line intensities within the multiplets themselves are simply dependent on the electron densities of the emitting plasmas, when collision rates between the levels are comparable with the Einstein A-values (between 10^8 and 10^{12} cm^{-3} for C II, N III and O IV); (iv) The line ratios are almost independent of the electron temperatures and abundances; (v) the lines are close together in wavelength, and they are of similar strength so that calibration problems are minimized.

ANALYSIS

We wish to estimate the accuracy of electron densities derived from line ratios within the $2s\ 2p^2\ ^4P \rightarrow 2s^2\ 2p\ ^2P^o$ multiplet, and then to apply the results to the analysis of astrophysical plasmas. An important step is to check the theoretical atomic data used against available measurements. In the absence of experimental collisional and radiative data, we make comparisons with spectra of astrophysical sources (Table 3).

Since there are three upper levels in the $2s\ 2p^2\ ^4P$ term, there are just three independent line intensity ratios which can be derived from the five lines. The other two ratios are from lines sharing a common upper level (Table 2), whose intensities should remain fixed in the absence of blending or radiative transfer effects.

We proceed proceed as follows: (i) We examine line ratios in selected objects; (ii) We construct atomic models and solve the statistical equilibrium equations to obtain line emissivities and hence intensities; (iii) We compute the sensitivity of line intensity ratios as a function of N_e, T_e; (iv) We identify objects in which lines are formed in the high density ($N_e C_{ji} \gg A_{ji}$) and low density ($N_e C_{ji} \ll A_{ji}$) limits; (v) We identify blends from disagreements of observed line ratios in certain

[1] The National Center for Atmospheric Research is sponsored by the National Science Foundation

objects; (vi) We compare low (high) density limits with observations, yielding constraints on the ratios of acceptable collision rates (Einstein A-values).

RESULTS AND NEEDS FOR BETTER ATOMIC PARAMETERS

For the C II] lines, the results are essentially identical to earlier work of Lennon *et al.* (1985) who also performed close coupling calculations. Available spectra which sample the high density regime (Table 3) are consistent with the atomic data used here. For N III] the new collisional data yield N_e a factor of 2 lower than earlier work (Nussbaumer & Storey 1979), because of increased collision rates between the ^4P levels. Blends are a problem at least in the solar atmosphere (e.g. Feldman & Doschek 1979, also see Fig. 1). Disagreements between density-sensitive line ratios suggest that a new calculation of the Einstein A values is warranted (Fig. 1). For O IV] the new data yield N_e factor of 3-5 lower than earlier work, again because of increased collision strengths between the ^4P levels. These lines are unblended in most spectra, with the exception of a well-known blend with S IV line which is easily treated (Feldman & Doschek 1979).

In summary, we believe that the C II and O IV density sensitive multiplets are practical and simple density diagnostics. Ratios of lines of N III and O IV are sensitive at lower densities than previously thought, near 10^9 cm^{-3}, an important regime for the quiet sun (Doschek 1987).

REFERENCES

Blum, R.D., & Pradhan, A.K., 1992, ApJS, 80, 425

Carpenter K.G., Robinson R.D., Wahlgren G.M., Ake T.B., Ebbets D.C., Linsky J.L., Brown A., & Walter F.M., 1991, ApJ, 377, L45

Doschek, G.A., 1987. In *Theoretical Problems in High Resolution Solar Physics II*, eds. G. Athay, D.S. Spicer, NASA CP 2483, p. 37

Doschek G.A., Feldman U., Van Hoosier, M.E., and Bartoe, J.-D. F., 1976, ApJS, 31, 417.

Feldman, U., & Doschek, G.A., 1979, A&A, 79, 359

Hayes, M.A., & Nussbaumer, H., 1986, A&A, 161, 287

Judge, P.G., 1986a, MNRAS, 221, 119.

Judge, P.G., 1986b, MNRAS, 223, 239.

Lennon, D.J., Dufton, P.L., Hibbert, A. & Kingston, A.E., 1985, ApJ, 294, 200.

Nussbaumer, H., & Storey, P.J., 1979, A&A, 71, L8

Nussbaumer, H., & Schild, H., 1981, A&A, 101, 118

Sandlin, G. D, Brueckner, G. E., & Tousey, R., 1977, ApJ, 214, 898

Stencel R.E., *et al.* , 1981, MNRAS, 196, 47P

Table 1. Intersystem Lines of Boron like ions

Levels Upper	Lower	C II] λ(air)	N III] λ(vac)	O IV] λ(vac)
$2s2p^2\ ^4P_{5/2}$	$2s^22p\ ^2P^o_{3/2}$	2325.398	1749.674	1401.146
$^4P_{3/2}$	$^2P^o_{3/2}$	2326.930	1752.160	1404.812
$^4P_{3/2}$	$^2P^o_{1/2}$	2323.500	1746.822	1397.20
$^4P_{1/2}$	$^2P^o_{3/2}$	2328.122	1753.986	1407.386
$^4P_{1/2}$	$^2P^o_{1/2}$	2324.689	1748.646	1399.774

Table 2. Ratios of Lines in the $2s2p^2\ ^4P \rightarrow 2s^22p\ ^2P^o$ B-Like Multiplets

Name	Transition $J_u \rightarrow J_l$ / $J_u \rightarrow J_l$	$\lambda\lambda$(C II])	$\lambda\lambda$(N III])	$\lambda\lambda$(O IV])	Diagnostic
R_1	(5/2- 3/2)/(1/2- 3/2)	2325.4/2328.1	1749.7/1754.0	1401.1/1407.4	N_e
R_2	(5/2- 3/2)/(3/2- 3/2)	2325.4/2326.9	1749.7/1752.2	1401.1/1404.8	N_e
R_3	(1/2- 1/2)/(3/2- 3/2)	2324.7/2326.9	1748.6/1752.2	1399.8/1404.8	N_e
R_4	(3/2- 3/2)/(3/2- 1/2)	2326.9/2323.5	1752.2/1746.8	1404.8/1397.2	A-values, blends
R_5	(1/2- 3/2)/(1/2- 1/2)	2328.1/2324.7	1754.0/1748.6	1407.4/1399.8	A-values, blends

Table 3. Sources of Emission line data, and mean N_e and T_e

Object/type	Spectro-graph	Ion	*Log* P_e [cm^{-3} K]	*Log* N_e [cm^{-3}]	*log* T_e [K]	Source
Quiet Sun /Chrom.	S082B	C II]	15.3	11.3	4	1
Quiet Sun /Tr. Reg.	S082B	N III]	$\sim$ 15.0	10	4.85	2
Active Sun /Tr. Reg.	HRTS	O IV]	15-16	10-11	5.15	3
α Aur/G5 III+G0 III	GHRS	O IV]	14.8	9.75	5.15	3
α Boo /K1 III	IUE	C II]	13.15	9.3	3.85	4
α Tau /K5 III	IUE	C II]	12.8	9.0	3.8	4
	GHRS	C II]	12.8	9.0	3.8	5
β Gru /M5 III	IUE	C II]	12.3	8.5	3.8	4
RR Tel /Slow nova	IUE	C II]	12.0	$\sim$ 8.0	4.0	6
	IUE	N III]	10.9	$\sim$ 6.7	4.2	6
	IUE	C IV]	10.9	$\sim$ 6.7	4.2	6
V1016 Cyg /Symbiotic	IUE	N III]	10.9	6.5	4.2	7
/proto-PN	IUE	O IV]	10.9	6.5	4.4	7

References 1. Judge *et al.* in preparation. 2. Doschek *et al.* 1976. 3. This work. 4. Judge 1986. 5. Carpenter *et al.* 1991. 6. Hayes & Nussbaumer 1986. 7. Nussbaumer & Schild 1981.

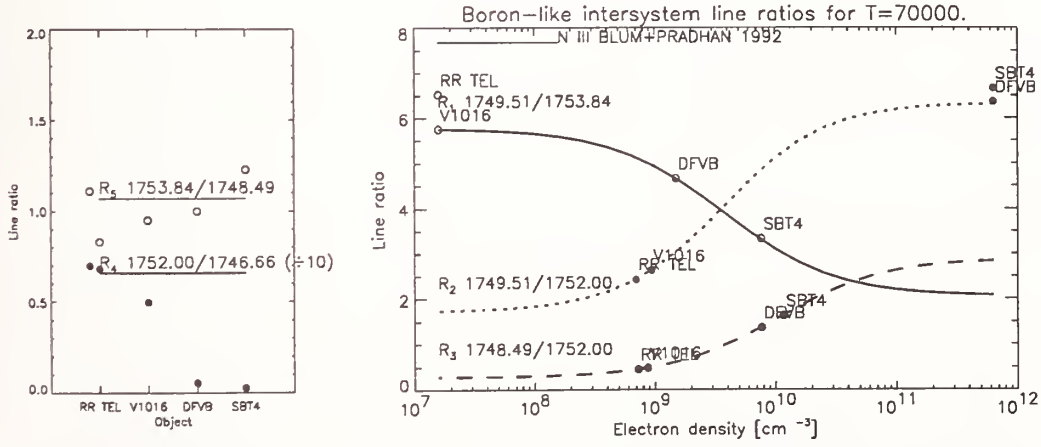

Fig 1. Ratios of N III lines sharing a common upper level (*left panel*) and those sensitive to electron densities (*right panel*). The lines are computed ratios, circles are observed ratios. The left panel shows that the weak λ1746 line is blended in solar data (DFVB= Doschek *et al.* 1976; SBT4 = Sandlin *et al.* 1977). The right panel suggests that, if the lines are unblended, then the Einstein A-values deserve further work (the adopted $A(\lambda 1749.5)$ may be too small).

THE NEED FOR ELECTRON / NEUTRAL-ATOM COLLISION CROSS SECTIONS AT THERMAL ENERGIES

PHILIP JUDGE, High Altitude Observatory, National Center for Atmospheric Research[1]
MATS CARLSSON Institute of Theoretical Astrophysics, University of Oslo.

INTRODUCTION

Analyses of UV emission line spectra of ionized atoms have led to enormous advances in our understanding of solar and stellar chromospheres, transition regions and coronae (reviews by Doschek 1987; Jordan & Linsky 1987). The gas in these plasmas is far from LTE, so that to analyze the emission line data requires electron-ion collision cross sections, for the processes of excitation (collisions between bound atomic states), ionization and recombination (between bound and free atomic states), as well as radiative data. A great deal of effort has been devoted to the determination of these cross sections, which can be accurate to ±10% at all energies of practical interest (e.g. Pradhan & Galagher 1992). **Much of the atomic data is now available to analyze lines of ionized species formed in transition regions and coronae.**

However, the situation is considerably worse for analyses of UV emission lines of complex neutral atoms, which are formed in stellar chromospheres, because:
(1) Chromospheric plasma has low electron temperatures ($T_e \leq 10^4$K [$\leq$0.81 eV]), an order of magnitude smaller than typical atomic energies at UV wavelengths. Collision cross sections for processes involving thermal electrons must therefore be determined accurately in the **low energy** regime ($kT_e << \Delta E$, where ΔE is the threshold energy for the collision). **Such cross sections are in general unavailable.**
(2) Point 1. casts doubt upon the reliability of calculations based upon the assumption of weak coupling (e.g. the Born approximations, distorted wave approximation). Such approximations (or semi-empirical cross sections based upon them) have almost always been used in quantitative analyses of chromospheric lines (e.g. Mauas *et al.* 1989).
(3) Unlike positively charged ions, excitation cross sections of neutrals approach zero as the outgoing electron energy approaches zero (e.g., Seaton 1962). Therefore excitation rate coefficients are sensitive to resonances in the cross sections. The figure shows the threshold behavior of the electron collision cross section for the transition $2p^4\ ^3P_{0,1,2} \rightarrow 2p^3 3s\ ^3S^o_1$ in O I.
(4) Chromospheric radiation often controls the excitation state of neutrals. Thus, other processes (photoionization, recombination, fluoresence, cascading) can control some lines of neutrals, especially in low gravity stars (Jordan & Judge 1984; Carpenter *et al.* 1992).

The purpose of this paper is to demonstrate the need for accurate electron-neutral atom collision cross sections at low energies in abundant atoms with high first ionization potentials (C,N,O). We argue that vital new clues to the elusive chromospheric heating mechanism might be obtained by studying UV spectra of neutral atoms, once accurate collision cross sections for important transitions become available.

ULTRAVIOLET SPECTRA OF NEUTRAL SPECIES: SOME PROBLEMS

The table lists prominent lines of neutral species observed in a variety of stellar chromospheres. We do not include lines for which other mechanisms are definitely responsible for the observed emission (e.g., some S I lines in low gravity stars which are photo-excited by H Lyα [Judge 1988]). Studies of the table, with additional data from a variety of sources, reveal several problems:
(1) The solar spectra cannot be accounted for by chance fluorescence processes, even though these can explain much of the emission seen in lower density stars (e.g., Jordan & Judge 1984).
(2) The Rydberg series of C I lines are trying to tell us something. Are they excited from above, via a large C II population, or from below, by electron collisions within C I?

[1] The National Center for Atmospheric Research is sponsored by the National Science Foundation

(3) Spatially resolved data from the HRTS and SKYLAB SO82B spectrographs reveal that most neutral emission lines listed do not behave very differently from collisionally excited lines of ionized species (see, e.g., Capelli *et al.* 1989). This suggests that electron collions are responsible for a large fraction of the neutral line emission (e.g., Athay & Dere, 1991).
(4) Carlsson & Judge (1992) studied in detail the O I resonance lines near 1304Å, and the intersystem lines near 1355Å. The only available low energy cross sections were computed in a three state close coupling calculation by Rountree (1977). They found that electron collisions from the ^3P ground term were very inefficient in exciting these lines, owing to small threshold collision strengths ($\bar{\Omega} \sim 0.5$), and that photo-excitation by H Lyβ dominates the exitation of λ1304.
(5) If H Lyβ is responsible for exciting O I λ1304, then what is exciting the other O I lines, and why do the λ1304 lines behave like collisionally excited lines?
(6) The HRTS data show tantalizing behavior of intensity ratios of O I intersystem lines to resonance lines (see also Cheng *et al.* 1980): if these lines are really influenced by electron collisions (in contradiction to present calculations), then valuable diagnostics of the chromospheric electron density may become available.

In summary, there exist UV data of neutral C, N, O and others, for which important questions remain unanswered. Many lines behave in HRTS data like collisionally-excited lines, and yet computed cross sections at thermal energies (available for O I only) are too small by perhaps an order of magnitude to account for the observed intensities. At least two important possibilities arise: (1) The available near-threshold collision cross sections are inaccurate, or (2) the chromospheric electron distribution is not Maxwellian. A small population of non-thermal electrons (which presumably result from the unknown chromospheric heating mechanism), at energies substantially higher than kT_e, might explain all of the above observations. Clearly, the possibility of putting quantitative estimates of populations of non thermal electrons in the solar chromosphere is of central interest to studies of the heating mechanism itself. **The only way to answer these questions is through calculations using accurate electron-atom collision cross sections.**

IMMEDIATE NEEDS FOR BETTER ATOMIC PARAMETERS

The accompanying table is a good starting point for a "wish list" for studies of solar and stellar chromospheres. With radiative data accurate to $\pm 10\%$ being routinely available for these transitions from the OPACITY project, collision cross sections from highly populated lower levels of C,N and O atoms (including metastable levels) are needed to a similar degree of accuracy.

REFERENCES

Athay, R.G. & Dere, K.,P., 1991, ApJ, 379, 776

Carlsson, M., & Judge, P.G., 1992. ApJ (in press)

Cappelli, A., Cerruti-Sola, M., Cheng, C.C., & Pallavicini, R., 1989, A&A, 213, 226.

Carpenter, K.G., Robinson, R.D., Wahlgren, G.M., Linsky, J.L., & Brown, A., 1992, In *Science with the Hubble Space Telescope*, in press

Cheng, C.C., Feldman, U., & Doschek, G.A., 1980, A&A, 377, 379

Doschek, G.A., 1987. In *Theoretical Problems in High Resolution Solar Physics II*, eds. G. Athay, D.S. Spicer, NASA CP 2483, p. 37

Doschek G., Feldman U., Van Hoosier M.E. & Bartoe J.-D.F, 1976, ApJS, 31, 417

Feldman, U., & Doschek, G., 1991, ApJS, 75, 925

Jordan C. & Judge P.G., 1984, Physica Scripta, T8, 43

Jordan, C. & Linsky, J.L. 1987, in *Exploring the Universe with the IUE Satellite*, Ed. Kondo Y., Reidel: Dordrecht, p. 259

Judge, P.G., 1986a, MNRAS, 221, 119

Judge, P.G., 1986b, MNRAS, 223, 239

Judge, P.G., 1988, MNRAS, 231, 419.

Mauas, P.J., Avrett, E.H., & Loeser, R., 1989, ApJ, 345, 1104

Pradhan, A.K., & Galagher, J.W., 1992, ADNDT in press

Robinson, R., *et al.* , 1992, *The Seventh Cambridge Workshop on Cool Stars, Stellar Systems and the Sun*, Eds. J. Bookbinder & M. Giampapa, PASP Conf. Series 26, p. 31

Rountree, S.P., 1977, J. Phys. B.: Atom. Molec. Phys., 10, 2719.

Seaton, M.J., 1962. In *Atomic and Molecular Processes*, ed. D.R. Bates, New York: Academic Press, ch. 11

SOME PROMINENT ULTRAVIOLET CHROMOSPHERIC LINES OF NEUTRAL ATOMS (914-1940Å)

Ion	Lines	Transitions	Object
H I	Lyman series (918-1215Å)	n=1 → n=2,12	Sun
C I	Rydberg series (1114-1158Å)	$2s^22p^2\ ^3P \rightarrow 2s^22p(^2P^o)nd, ns\ ^{1,3}P^o,^{1,3}D^o,^{1,3}F^o$	Sun
	Rydberg series (1256-1481Å)	$2s^22p^2\ ^1D \rightarrow 2s^22p(^2P^o)nd, ns\ ^1P^o,^1D^o,^1F^o$	Sun, AU Mic
	1329Å	$2s^22p^2\ ^3P \rightarrow 2s2p^3\ ^3P^o$	Sun
	1561Å	$2s^22p^2\ ^3P \rightarrow 2s2p^3\ ^3D^o$	Sun
	1657Å	$2s^22p^2\ ^3P \rightarrow 2s^22p3s\ ^3P^o$	Sun, Giants
	1931Å	$2s^22p^2\ ^1D \rightarrow 2s^22p(^2P^o)3s\ ^1P^o$	Sun
N I	1134Å	$2s^22p^3\ ^4S^o \rightarrow 2s2p^4\ ^4P$	Sun
	1143Å	$2s^22p^3\ ^2D^o \rightarrow 2s^22p^2(^3P)3d\ ^4P,^2D,^2F$	Sun
	1163-1170Å	$2s^22p^3\ ^2D^o \rightarrow 2s^22p^2(^3P)3d\ ^4P,^2D,^2F$	Sun
	1492Å	$2s^22p^3\ ^2D^o \rightarrow 2s^22p^23s\ ^2P$	Sun
O I	988Å	$2s^22p^4\ ^3P \rightarrow 2s^22p^3(^2D^o)3s\ ^3D^o$	Sun
	1152Å	$2s^22p^4\ ^1D^o \rightarrow 2s^22p^3(^2D^o)3s\ ^1D^o$	Sun
	1304Å	$2s^22p^4\ ^3P \rightarrow 2s^22p^33s\ ^3S^o$	(Many)
	1355Å	$2s^22p^4\ ^3P \rightarrow 2s^22p^33s\ ^5S^o$	(Many)

Sources: Solar data (914-1177Å)– Feldman & Doschek 1991. Solar data (1175-1940Å)– Doschek *et al.* 1976. AU Mic (dMe flare star) data from the *Hubble Space Telescope*– Robinson *et al.* 1992. Giant star data– Judge (1986a,b).

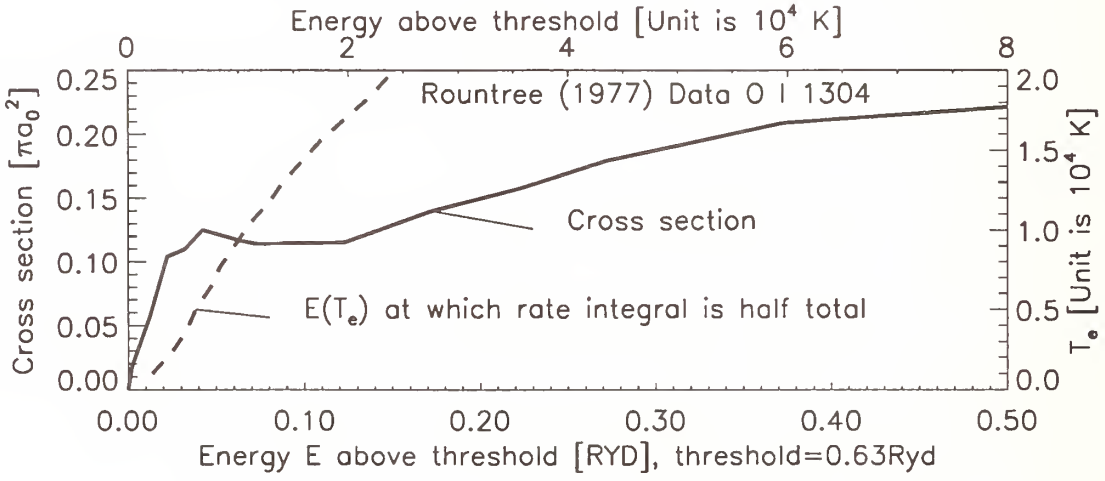

Cross section (*solid line*) for collisional excitation of the $3s\ ^3S^o_1$ level from the $2p^4\ ^3P$ ground term of O I, from Rountree (1977), and a locus (*dashed line*) of energies $E_{half}(T_e)$ at which $\int_0^{E_{half}} \Omega(E)exp(-E/kT_e)dE = 0.5 \cdot \int_0^{\infty} \Omega(E)exp(-E/kT_e)dE$. $\Omega(E)$ is the usual "collision strength" ($= \frac{\sigma_{ij}(E)}{\pi a_0^2} g_i \frac{E}{Ryd}$ [e.g., Seaton, 1962], where $\sigma_{ij}(E)$ is the cross section for transitions from level i to level j at energy E, and g_i is the degeneracy of level i). The excitation rate is proportional to these integrals. Notice that much of the excitation rate is determined at energies **very close to threshold**.

Laboratory Sources

Interpretation of the VUV Spectra of Some Iron Group Element Ions

W.-Ü L. Tchang-Brillet,[1] J.-F. Wyart,[2] V. Azarov,[3] L.I. Podobedova,[3] A. N. Ryabtsev[3]

[1] Département Atomes et Molécules en Astrophysique,* Observatoire de Paris-Meudon, 92190 Meudon, France

[2] Laboratoire Aimé Cotton,** CNRS II, Bâtiment 505, 91405 Orsay, France

[3] Institute of Spectroscopy Academy of Science, Troitsk, Moscow region, Russia

A great amount of observational data in the VUV wavelength region (1050-3000Å) is provided by the IUE satellite and the Hubble Space Telescope. The interpretation of the stellar spectra taken from space requires the knowledge of a large number of atomic spectra. The data needed include accurate wavelengths, oscillator strengths, collisional and photoionization cross sections etc. As an example, the research program concerning the chemical-peculiar stars for more accurate elemental abundance determinations requires improved data for the first ionization stages of all the iron group elements.

We are investigating the VUV spectra (380 - 2000Å) of three- and four-times ionized manganese Mn^{3+} (Mn IV) and Mn^{4+}(Mn V). Previous publications[1, 2, 3] concerned the transition arrays $3d^4$ - $3d^34p$ (478 - 847Å) in Mn IV, $3d^3$ - $3d^24p$ (380-547Å) and $3d^24s$ - $3d^24p$ (1086 -1915Å) in Mn V. The present work concerns the $3d^24p$ - $3d^24d$, 5s transitions in Mn V and the $3d^34s$ - $3d^34p$, $3d^34p$ - $3d^34d$, 5s transitions in Mn IV.

The spectrograms were obtained on photographic plates either in Meudon, with a vacuum triggered spark, using the 10.7-meter normal incidence vacuum spectrograph of the Paris-Meudon Observatory, or in Troitsk, using a 6.65-m normal incidence vacuum spectrograph, with a similar triggered spark source, which is operated in different conditions so as to enhance the emission of lower ionization stages.

The plates were measured on semi-automatic comparators. Selected impurity lines of oxygen, nitrogen, carbon and Mn^{2+} were used for wavelength calibration. The uncertainty of the relative positions of the lines is estimated to be ±0.005Å. About 250 lines of Mn V and about 800 lines of Mn IV are newly identified in the wavelength range 660-1900Å.

---

* Also associated with CNRS (URA 812)

** Also associated with Université Paris-Sud

The analysis, i.e., the identification and the classification of spectral lines by the energy levels involved, was guided by theoretical studies of the atomic structure, as developed in [4], which predict the level positions and the line strengths. Isoelectronic comparisons were also a useful support. An automatic search-for-level computer code was used, taking into account the theoretical relative intensities of the transitions. Then the results were checked to avoid fortuitous coincidences. 60 new energy levels, belonging to the $3d^2 4d$ and $3d^2 5s$ configurations of Mn V, and more than 100 levels, belonging to the $3d^3 4s$ and $3d^3 4d$ configurations of Mn IV, are determined. The determination of the $3d^3 5s$ configuration is in progress.

All the configurations were interpreted by parametric studies. In the case of the Sc-like Mn^{4+} ion, a GLS (Generalized Least Square) calculation was performed, by adding the data for Ti II[5], V III[6] and Cr IV[7] to the new Mn V levels. Independent studies of the $3d^2(4d+5s)$ group had shown that the Slater parameters P increase nearly linearly with Z_C, the charge of the ionic core, and that the constraint of the expansion $P = A + BZ_C + F/(Z_C + 2)$ does not increase substantially the deviations $E_{exp} - E_{th}$. The improvement of the ratio (number of experimental levels)/(number of parameters) allows a better determination of "small" parameters, i.e., the configuration interaction parameters R^2(3d4d, 3d5s) and R^2(3d4d, 5s3d). Earlier systematic studies of the $3d^N$ core configurations helped in fixing some parameters to reliable values[8]. The fitted parameter expansions are summarized in the Table. They are of interest for prediction of level positions, and thus transition wavelengths for higher members of the isoelectronic sequence. The extension of the present work to the isoelectronic ions of iron Fe^{4+} (Fe V) and Fe^{5+} (Fe VI) is also in progress.

References

1. W.-Ü L. Tchang-Brillet, M.-C. Artru and J.-F. Wyart, Physica Scripta **33**, 390 (1986).

2. V. I. Kovalev, A. A. Ramonas, A. N. Ryabtsev, Opt. Spectrosc. **43**, 4 (1977).

3. L. I. Podobedova, A. A. Ramonas, A. N. Ryabtsev, Opt. Spectrosc. **45**, 237 (1978).

4. R. D. Cowan, "The Theory of Atomic Structure and Spectra", University of California Press, (1981).

5. S. Huldt, S. Johansson, U. Litzén, J.-F. Wyart, Physica Scripta **25**, 401 (1982).

6. L. Iglesias, O. P. y Appl. **2**, 132 (1969).

7. J. O. Ekberg and L. Engström, Physica Scripta **25**, 611 (1982).

8. J.-F. Wyart, A. J. J. Raassen, P. H. M. Uylings, Physica Scripta **32**, 169 (1985).

Table Expansion of energy parameters fitted from 237 levels of the sequence Ti II - Mn V $3d^2$ (4d+5s)

$$P = A + B\,Z_c + C\,Z_c^2 + D\,Z_c^3 + E\,Z_c^4 + F/(Z_c + 2)$$

Parameter values and standard errors in cm^{-1}. Parameters without standard error have been fixed.

The r.m.s. deviation is 82 cm^{-1}

Parameter	A	B	C	D	E	F
$F^{(2)}(3d,3d)d^2d$*	44684 (455)	9505 (96)				-86240
$F^{(2)}(3d,3d)d^2s$*	45006 (501)	"				
$F^4(3d,3d)d^2d$ *	34053 (735)	5900 (156)				-83790
$F^4(3d,3d)d^2s$ *	35489 (808)	"				
$F^2(3d,4d)$	-1671 (303)	3594 (78)				
$F^4(3d,4d)$	-1657 (284)	1964 (79)				
$G^0(3d,4d)$	-416 (42)	1123 (11)				
$G^2(3d,4d)$	-551 (225)	1423 (60)				
$G^4(3d,4d)$	-145 (269)	955 (74)				
$G^2(3d,5s)$	-4835 (2375)	1140 (265)				16204 (7672)
$R^2(3d4d,3d5s)$	200	341 (75)				
$R^2(3d4d,5s3d)$	140	326 (77)				
α *	20.75	4.61				-45.02
β *	-105.25	0.				152.17
X^1	0	120 (14)				
X^3		80 (38)				
$\zeta_{3d}\ d^2d$ *	-24.82 (29)	2.271 (0.6)	0.6690	0.00506	0.00015	
$\zeta_{3d}\ d^2s$ *	-28.97 (31)	"	"	"	"	
ζ_{4d}	-21.9 (43)	14.33 (12)	1.			

* For those parameters relative to the core, Z_c is to be replaced by $Z_c + 1$ in the parameter expansion.

VUV-Lines of Low-Z Ions and Their Identification

H.H. Bukow, A. Bastert, G. Rieger and M. Krenzer
Ruhr-Universität Bochum, Experimentalphysik III
Postfach 102148 NB 3 D 463 Bochum

Introduction. At the last conference of this series, Kurucz [1] pointed out that "half of the lines in the solar spectrum are unidentified or unclassified". Laboratory observations of such lines are often hindered by the difficulty of establishing an environment capable to produce similar excitation conditions. The beam-foil technique [2] combines very strong interaction inside the foil and an interaction-free decay outside. The observation of numerous lines stemming from doubly-excited states [3], hardly accesssible with other light sources, indicates that beam-foil spectroscopy approaches certain photospheric conditions. Therefore a systematic spectroscopic study of the astrophysically important elements N, O and Ne at low ionization stages covering a wavelength range from 40 nm to 120 nm was performed. As a preliminary result we note a surprisingly large number of up-to-date unknown lines. In this report the experimental technique, the type of data and some selected results will be described.

Experimental Procedures. State-of-the-art beam-foil spectroscopy is used. A 400 keV accelerator yields μA beams of the ions in question. To get higher projectile energies some measurements are done using 2+ and 3+ ions, respectively. A 2-m normal-incidence monochromator, designed to match the requirements of fast-beam spectroscopy (refocalisation for all wavelengths [4]), is used to scan the light emitted at 90° to the beam axis. With 80 μm (equal) slits and a 2400 l/mm grating a linewidth (FWHM) between 0.025 nm and 0.040 nm depending on the projectile energy and mass and the foil thickness is realized. Once a spectrum is registered the

positions of the spectral lines are determined by fitting a Gaussian profile to each feature. Then a number of well-known lines (typically: 25) are identified and used for the calibration, yielding a wavelength accuracy of 0.004 nm (one standard deviation) for well resolved lines. The charge state of the emitting ion can be deduced approximatively from the variation of the individual line intensity as a function of the projectile energy. The confidence level of this procedure is good for most lines but deviations may occur up to an uncertainty of ± 1 unit. To exhaust all sources of information available with the beam-foil technique lifetime measurements are performed for a number of transitions. Lifetime data (typical accuracy: 10 % to 20%) are aimed as a supplementary information in the process of line identification. These measurements are evaluated using a multiexponential fitting program (DISCRETE [5]). Finally it may be helpful to have a measure of a line's intensity (photons.cm^{-2}.s^{-1}). To get meaningful numbers, the intensities of most of the unknown lines together with a suitable reference line are measured using a recent efficiency calibration [6].

If an identification for a line is proposed, the measured lifetime may be compared to what is expected theoretically. Calculating population numbers from the intensities the population of the state in question may be compared to the reference state if some assumptions are made concerning the dependence of the population on the main and angular quantum numbers n and l, respectively.

Results. The evaluation of the bulk of data being still under work we present only some results concerning neon.

Two decades ago, Edlén et al. [7] determined by extrapolation the relative positions of triplet and quintet spectra in Ne V, and of doublets and quartets in Ne IV [8]. Both numbers are the respective basis of the corresponding level system as tabulated by Kelly [9]. To our best knowledge they

have not been verified experimentally. We have directly measured the $2s^2 2p^2\ ^3P\text{-}2s2p^3\ ^5S^0$ ground state transitions in Ne V, estimated to 113.704 nm and 114.613 nm [7] and observed at (113.6273±0.008) nm and (114.5648±0.008) nm, respectively. Moreover we have identified other 16 transitions between those systems and one singlet-triplet transition. In Ne IV 44 doublet-quartet transitions have been observed. The difference in wavelength between the present work and the value calculated on the basis of Kelly's table [9] yields the uncertainty of the relative position of the spin-different systems, named X in the case of Ne V and E for Ne IV [9]. From the total of observed intersystem lines we have X=(0±25) cm^{-1} and E=(0±36) cm^{-1} thus confirming the estimates of Edlén [7,8].

To give an impression of the amount of identification work still to be done we quote approximate numbers of unknown (known) lines as oberved. They are: 460 (200) for neon, 50 (200) for oxygen and 80 (350) for nitrogen.

Acknowledgement. The authors wish to express their gratitude to F.J. Meijers (Amsterdam) for his help and encouragement in the identification of intersystem lines.

References

[1] R.L. Kurucz, in J.E. Hansen (Ed.): Atomic States and Oscillator Strengths for Astrophysics and Fusion Research, North Holland, Amsterdam 1990, p. 20
[2] for a review, see: H.J. Andrä, in W. Hanle and H. Kleinpoppen (Ed.): Progress in Atomic Spectroscopy, Plenum, New York 1979, part B, p. 829
[3] for a review, see: S. Mannervik, Phys. Scripta 40(1989)28
[4] J.O. Stoner, J.A. Leavitt, Optica Acta 20(1973)435
[5] S.W. Provencher, J. Chem. Phys. 64(1976)2772
[6] A. Bastert, H.H. Bukow, H.v. Buttlar, Appl. Optics (in print)
[7] B. Edlén, H.P. Palenius, K. Bokasten, R. Hallin, J. Bromander, Solar Phys. 9(1969)432
[8] B. Edlén, Solar Phys. 24(1972)356
[9] R.L. Kelly, J. Phys. Chem. Ref. Data 16(1987) Suppl.1

ANALYSIS OF THE ($5s5p^2$+$5s^25d$) - [$5p^3$+5s5p5d+5s5p6s] TRANSITIONS OF I V

A. Tauheed and Y. N. Joshi
Physics Department, St. Francis Xavier University,
Antigonish, NS, Canada B2G 1C0

Introduction and Experiment

The groundstate of four times ionized iodine (I V) is $5s^25p^2$. Kaufman et al [1] revised the earlier work of Even-Zohar and Fraenkel [2]. They established levels of the $5s^25p$, $5s5p^2$, $5s^2$ ns (n = 6-8), $5s^2$nd (n=5,6) configurations and the $5p^3$ ^4S. Ansbacher et al [3] investigated I V spectrum using Beam-foil technique and reported the $5s^26p$ ^2P levels, revised $5s5p^2$ ^4P levels of Kaufman et al [2] and rejected the $5p^3$ ^4S level. During our recent investigation of the I IV spectrum [4] we were able to achieve very reliable ionization discrimination between the I III, I IV, IV and I VI lines. We observed that the line at 1168.8 Å classified by Goslin et al [3] as $5s^25p$ $^2P_{1/2}$ - $5s5p^2$ $^4P_{3/2}$ was in fact an I III line. This lead us to study the $5s^25p^2$ ^2P - $5s5p^2$ ^4P transitions in the Cd I isoelectronic sequence from Sb III to La IX [5]. However, further confirmation of the ^4P system can be obtained only by studying the configuration systems containing quartet terms. These configurations are $5p^3$, 5s5p5d and 5s5p6s and consequently their investigation was undertaken. The preliminary results and presented here.

The spectrum of iodine was photographed in the 300 Å - 2000 Å region on a 3-m normal incidence spectrograph (plate factor in first order 1.385 Å/mm). The source used was a triggered spark in which Li I salt was packed into the cavity of an aluminum sample electrode. The second electrode was a pure aluminum electrode. By introducing various turns of an inductance coil in the discharge circuit we could enhance or suppress the lines of different ionization stages. The polarity exhibited by the lines of higher ionization was also a reliable criteria for the ionization discrimination. Further experimental details appear in our earlier paper [4]. Accuracy of wavelength measurements for sharp lines is ±0.005Å.

Results and Discussion

The $5p^3$,5s5p5d and 5s5p6s configurations contain five quartet terms which give rise to strong transitions to the $5s5p^2$ ^4P term. These three configurations were calculated using Cowan Code [6] with the scaling factors similar to the ones in other iodine spectra studied in our laboratory. The E_{av} (RHF) of the $5s^3$, 5s5p5d, $5s^26p$ and 5s5p6s configurations in Cd I isoelectronic sequence from Sb III to La IX are shown in Figure 1. It is clear that whereas the 5s5p6s configuration rises fast the $5p^3$ and 5s5p5d configurations collapse along the sequence. Soon it was noticed that the $5s5p^2$ - ($5p^3$+5s5p5d) transition array appeared very strong where as transitions arising out of the $5s5p^2$ - 5s5p6s array were relatively weak. All levels belonging to the $5p^3$ and almost 90% of the levels belonging to the 5s5p5d and 5s5p6s configurations have been established

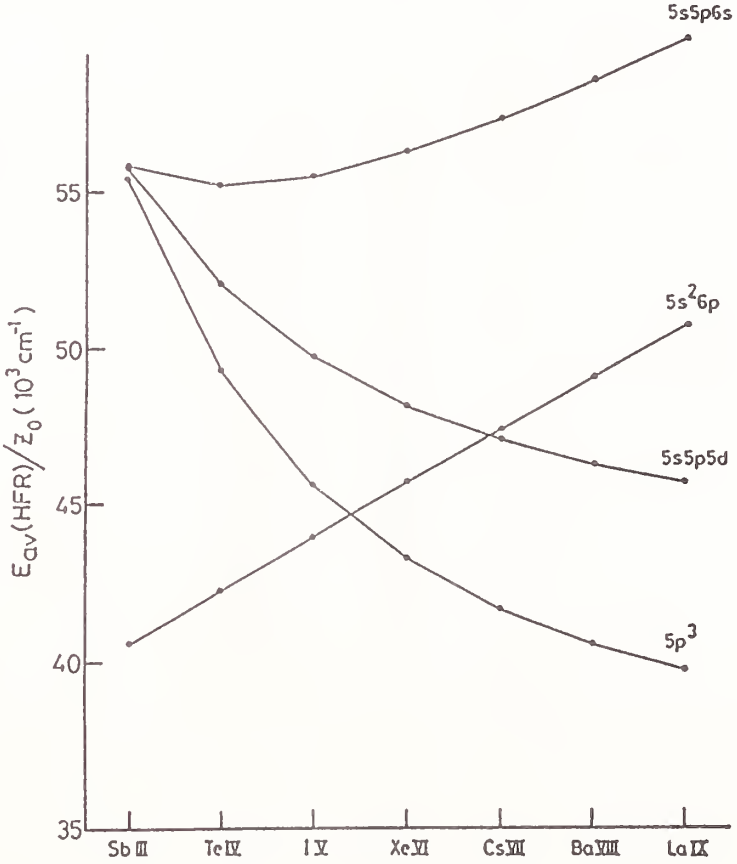

are listed in Table I. The $5p^3\ {}^4S_{3/2}$ level reported by Kaufman et al [1] and a revised value suggested by Ansbacher et al [3] were both incorrect. The levels marked (?) are based on definite I V lines but need some further checking. One also expects moderately strong lines arising out of $5s^25d$ - (5s5p5d+5s5p6s) transitions. We could not see any of these lines in our line list. On rechecking the data it was found that $5s^25d\ {}^2D$ identified earlier [1,2,3] was incorrect. New values of $5s^25p\ {}^2D$ are given in Table II. These levels gave transitions to the 5s5p5d, 5s5p6s, and to the $5s^26p$ levels reported form the beam foil study. Over 150 additional lines have been classified in the spectrum.

Complete analysis involving configuration interaction calculations will follow soon.

We wish to thank Natural Sciences and Engineering Research Council of Canada (NSERC) for the financial assistance.

References

1. V. Kaufman, J. Sugar and Y.N. Joshi, J. Opt. Soc. Am. B. 5, 619 (1988).
2. M. Even-Zohar and B.S. Iraenkel, J. Phys. B. 5, 1596 (1972).
3. W. Ansbacher, E.H. Pinnington, A. Tauheed and J. A. Kernahan, J. Phys. B: At Mol. Opt. Phys. 24, 587 (1991).
4. A. Tauheed, Y. N. Joshi and V. Kaufman, J. Phys. B: At. Mol. Opt. Phys.
5. A. Tauheed, Y. N. Joshi and E. H. Pinnington, J. Phys. B: At. Mol. Opt. Phys. (in press).
6. R. D. Cowan, Theory of Atomic Spectra and Structure and Cowan Code programs.

Table I

New energy level values (cm^{-1}) of I V belonging to the, $5p^3$, 5s5p5d and 5s5p6s configurations

Config	Desig	J	Level (cm^{-1})	Config	Desig	J	Level (cm^{-1})
$5p^3$	^4S	3/2	209984	5s5p5d		5/2	226526
	^2D	3/2	204472	5s5p5d		5/2	236379
		5/2	210092			5/2	245331
	^2P	1/2	228924			5/2	248068
		3/2	233038			5/2	251760
						5/2	274074
5s5p5d		1/2	237451			5/2	278712
5s5p6s		1/2	246459			5/2	281342
		1/2	261368			7/2	230308
		1/2	281051			7/2	244734
		1/2	304619			7/2	258571
		3/2	224080			7/2	278129
		3/2	237300				
		3/2	246966				
		3/2	249250				
		3/2	264136				
		3/2	277513				
		3/2	283800				
		3/2	306461				

Table II

New or revised level values (cm^{-1}) of the levels of the $5s5p^2\ ^4P$, $5s^25d\ ^2D$ and $5s^26p\ ^2P$ of I V

Config	Desig	J	Level (cm^{-1})
$5s5p^2$	^4P[a]	1/2	81003
		3/2	86899
		5/2	92554
$5s^25d$	^2D[b]	3/2	154050
		5/2	155462
$5s^26p$	^2P[c]	1/2	211216
		3/2	215054

[a] From ref, [5], included for completeness
[b] New levels
[c] Revised value of beam foil data

New High Excitation Fe I Levels determined by Fourier Transform Spectrometry

Gillian Nave, Sveneric Johansson
Department of Physics, University of Lund, Sölvegatan 14, S-223 62 Lund, Sweden

Abstract

Seven new subconfigurations in Fe I, ranging from 56000 – 60000 cm^{-1}, have been found using Fourier transform spectra. The total number of levels is 166, giving lines in both the infra-red and visible range. A summary of the methods of analysis, and comparisons with solar and grating spectra are described.

1 Introduction

The high quality of recent solar IR spectra obtained with the ATMOS space experiment [1] has illustrated the need for more identifications of atomic lines, with Fe I being particularly important. Recent discovery of lines due to $3d^6(^5D)4s4f - 5g$ transitions in both laboratory and solar spectra resulted in classifications of levels as high as 60300 cm^{-1}, which have been used in confirming the solar iron abundance [2]. The accuracy of the solar spectra means that high resolution Fourier Transform (FT) spectra must be used for laboratory identifications.

This paper describes levels from seven new subconfigurations of Fe I which have been analysed using FT spectra, which range in energy from 56000 $cm^{-1}$to 60000 cm^{-1}. Details of the levels and identifications will be published separately in the near future. The work will also form part of a new multiplet table for Fe I that is currently being prepared.

2 Laboratory Measurements

The spectra used in this analysis were recorded with the IR-visible FT spectrometer at the National Solar Observatory, Tucson, Arizona, and with the vacuum-ultraviolet FT spectrometer at Imperial College, London. A hollow cathode lamp of pure iron was used as a source, and was operated in neon or argon at pressures of 3 – 4 Torr, with a current of 400 – 1400 mA. The cathode was water cooled for one infra-red spectrum. Details of the experimental setup are given in [3]. The wavenumbers, intensities and widths of all the lines in each spectrum were determined with the DECOMP computer code [4], and the wavenumbers carefully calibrated from Ar II standard lines [3, 5].

3 Term Analysis

Terms arising from five even parity subconfigurations and two odd parity subconfigurations have been found, due to the lowest two parent terms, $3d^6(^5D)4s$ and $3d^7(^4F)$ in Fe II. They cover the energy range 56000 $cm^{-1}$to 60000 cm^{-1}. Figure 1 shows the energy ranges of the new levels, with the most important transitions.

Values for the lower levels of the transitions involved were taken from [6], or the atomic energy level table (AEL) [7]. Eight levels due to the $3d^6(^5D)4s5d$ subconfiguration were discovered by Brown et. al. [8], and levels from both this and the $3d^7(^4F)6s$ subconfiguration were found by Zhu and Knight using laser spectroscopy [9]. The accuracy of these levels has been substantially improved, and both subconfigurations are now almost complete. The (^5D) and (^5G) terms of $3d^6(^5D)4s(^4D)4d$ and one $3d^6(^5D)4s7s$ term are also listed in the AEL. No previous levels of the $3d^7(^4F)4f$, $3d^6(^5D)4s5f$, or $3d^7(^4F)5d$ are listed.

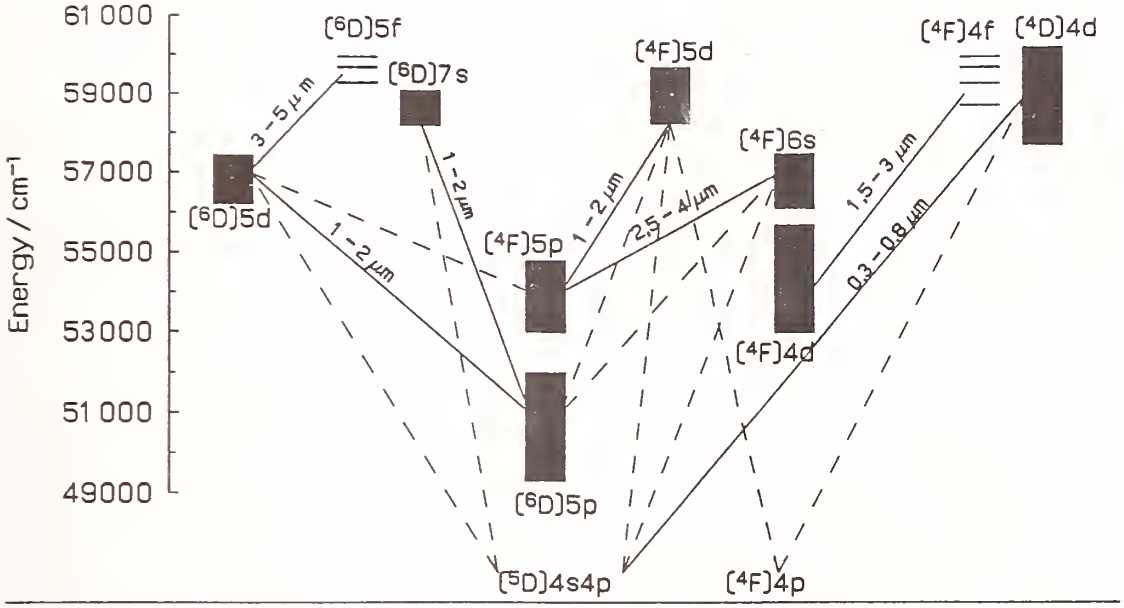

Figure 1: Partial Term diagram for Fe I showing energy ranges of the new levels, and major transitions. Solid lines represent the transitions used to find the levels, and broken lines indicate other important transitions. The terms $3d^6(^5D)4s4p$ and $3d^7(^4F)$ $4p$ are much lower in energy (19000 $cm^{-1}$to 40000 cm^{-1}), and hence their position is not shown.

The overlap of the configurations in Fe I results in strong configuration interaction. This means that many inter-parent transitions are seen, giving many lines throughout the visible and infra-red. The mixing is particularly strong between the $3d^6(^5D)4s5d$ and $3d^7(^4F)6s$ subconfigurations, and the $3d^6(^5D)4s7s$, $3d^7(^4F)5d$ and $3d^6(^5D)4s(^4D)4d$ subconfigurations. As no particular coupling scheme adequately describes these levels, LS designations have been assigned. The two odd parity subconfigurations - $3d^7(^4F)4f$ and $3d^6(^5D)4s5f$ - are best described in the JK coupling scheme. Levels have been assigned to each subconfiguration according to both the calculations of Kurucz, and according to the strongest expected transitions from each level. These transitions are marked with solid lines on figure 1. Other transitions are useful in confirming the identifications, and are marked with dotted lines.

Transitions to the $4d$, two $5d$, $6s$ and $7s$ subconfigurations from the lowest odd subconfigurations $3d^6(^5D)4s4p$ and $3d^7(^4F)4p$ fall in the ultraviolet and are not present in the FT spectra. Some evidence was present in grating [8] and solar spectra. Transitions between $3d^6(^5D)4s5f$ and $3d^7(^4F)4s$ were also observed in grating spectra, and work is continuing on these identifications.

Comparisons were also made with solar spectra. The $3d^6(^5D)4s5d - 5f$ transitions fall in the infra-red above 2 μm, where the high quality ATMOS spectra referred to earlier were used. Work is continuing in confirming the identifications. Between 1 and 2 μm, the Kitt Peak photometric atlas [11], was used, but proved less useful due to strong atmospheric absorption in many of the regions covered. The $3d^6(^5D)4s4p$ - $4s(^4D)4d$ are strong in the visible region, and the Kitt Peak Table of Photographic Solar Spectrum Wavelengths was used to obtain equivalent widths [10]. A plot of the equivalent width in the solar spectrum against the log of the laboratory intensity is useful in verifying transitions and detecting blended lines [12].

4 Summary

Even terms of Fe I have been found up to 60000 cm^{-1}, with only a few terms of low J in the described subconfigurations still to be found. Only one even subconfiguration - the $3d^6(^5D)4s6d$

remains to be found in this range. Work has commenced on the odd terms with the $3d^7(^4F)4f$ and $3d^6(^5D)4s5f$. The results of all this analysis will be published in the future as part of a new multiplet table for Fe I.

5 Acknowledgements

G. Nave gratefully acknowledges a Research Fellowship from the European Space Agency, under which this work was carried out. We also thank A. J. Sauval for his assistance with the solar identifications, and R. C. M. Learner and J. W. Brault for provision of the laboratory spectra.

References

[1] Farmer, C. B., Norton, R. H. , NASA Ref. Publ. 1224, NASA Scientific and Technical Information Division, Washington D. C. (1989)

[2] Johansson, S., Nave, G., Geller, M., Sauval, A. J., Grevesse, N., Schoenfeld, W. G., Chang, Ed. S., Farmer, C. B., (1992) in preparation.

[3] Nave, G, Learner, R. C. M., Thorne, A. P , Harris, C. J., J. Opt. Soc. Am. **B8** (1991) p 2028.

[4] Brault, J. W. , Abrams, M. A., vol 6 of 1989 OSA Technical Digest Series (Optical Society of America) p 110.

[5] Nave, G, Learner, R. C. M., Murray, J. E., Thorne, A. P., Brault, J. W., J. Phys. II France 2 (1992) pp 913

[6] O'Brien, T. R., Wickliffe, M. E., Lawler. J. E., Whaling, W., Brault, J. W., J. Opt. Soc. Am. **B8** (1991) p1185.

[7] Sugar, J., Corliss, C., J. Phys. Chem. Ref. Data **14** (1985) Suppl 2.

[8] Brown, C. M., Ginter, M. L., Johansson, S., Tilford, S. G., J. Opt. Soc. Am. **B5** (1988) p 2125.

[9] Yang Zhu, Knight, R. D, J. Opt. Soc. Am. **B9** (1992) p 27.

[10] Pierce, A. K., Breckinridge, J. B., Kitt Peak National Observatory contribution no. 559.

[11] Delbouille, L., Roland G., Brault, J. W., Testerman, L., "Photometric Atlas of the Solar Spectrum from 1850 to 10000 cm^{-1}". (Tucson:KPNO) (1981).

[12] Johansson, S., Learner, R. C. M., Astrophys. J.,**354** (1990) p755.

A PROGRESS REPORT ON THE ANALYSIS OF VUV-FTS SPECTRA OF RU I AND RU II

Ali Joueizadeh and Sveneric Johansson

Lund University, Department of Physics, Sölvegatan 14, S-223 62 Lund, Sweden

1. INTRODUCTION

High-resolution spectra of the chemically peculiar star χ Lupi obtained with the Goddard high-resolution spectrograph (GHRS) on board the Hubble Space Telescope (HST) have revealed the existence of singly ionized ruthenium in the stellar atmosphere [1]. Spectral lines at 1939 Å of Ru II in the stellar spectrum were shifted about 16 mÅ compared to laboratory data, and the difference seemed to be systematic. A revision of previous experimental results would help to clarify these wavelength shifts. The latest measurements of the Ru II spectrum were performed by A.G. Shenstone and W.F. Meggers [2].
In this paper we report on new recordings of the Ru spectrum, emitted by a hollow-cathode lamp, with the VUV-FTS at Lund.

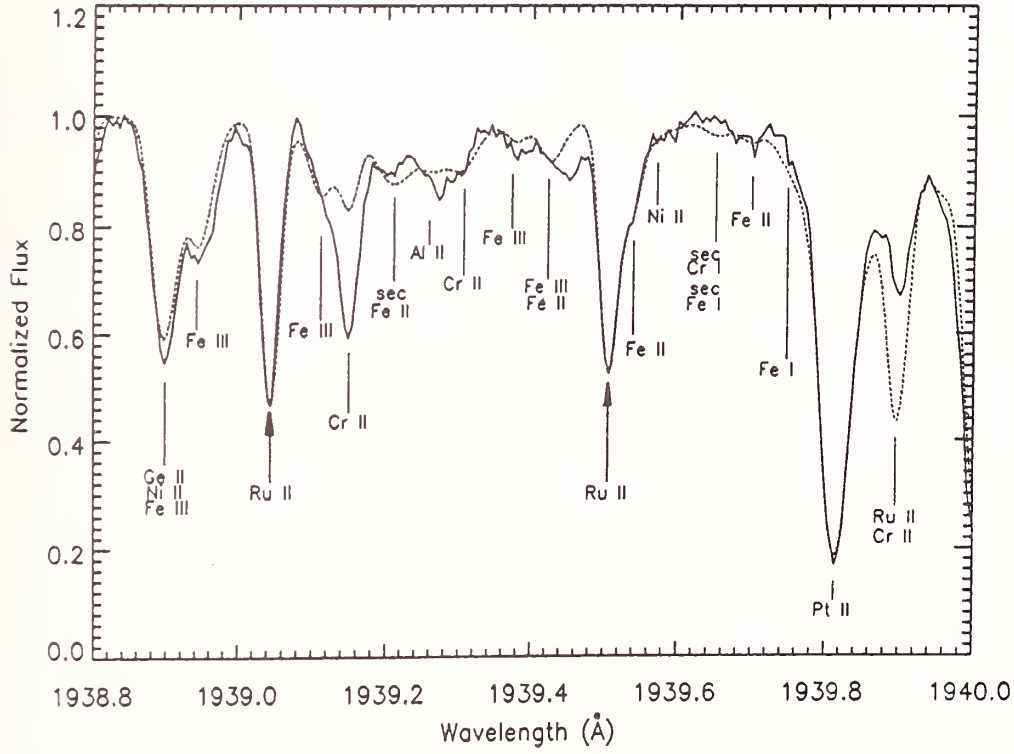

Figure 1. HST/GHRS spectrum of χ Lupi, showing the Ru II lines. Solid line = observed spectrum, dashed line = synthetic spectrum

2. MEASUREMENTS

We have registered Ru I and Ru II lines with the new VUV-FTS at Lund in the following regions: 1750-3162 Å, 2113-4215 Å, and 4160- 6325 Å. A hollow-cathode has been used as a light source. We inserted ruthenium powder in a nickel cathode and ran the source with neon. The spectrum, which contains emission lines of Ru I, Ru II, Ni I, Ni II, Ne II and Ne III, has been calibrated against Ni and Ne lines. The accuracy of the measurements is about 0.005 cm^{-1} (0.2 mÅ at 2000 Å). Totally 213 Ru II and 1053 Ru I lines have been measured.
In Table 1 we compare new FTS wavelengths with those from [2] for a number of Ru II lines to illustrate the systematic shift, which appears below 2230 Å.

When the new wavelength values were used in the calculation of the synthetic stellar spectrum of χ Lupi, a good agreement was obtained whith the observed spectrum, as illustrated in Figure 1.

Many energy level values have been improved for both Ru I [3] and Ru II [2], see table 2, where also some new levels are included. The analysis is in progress. The term analysis is guided by theoretical calculations of energy levels and line intensities of Ru II by means of the Cowan computer codes.

FTS wavelengths (Å)	Shenstone & Meggers [2] (Å)	difference (Å)
3177.0488	3177.048	0.001
2778.3888	2778.388	0.001
2687.4939	2687.494	0.000
2571.0899	2571.09	0.00
2455.5311	2455.53	0.00
2396.7103	2396.71	0.00
2281.7212	2281.72	0.00
2218.5333	2218.552	-0.019
2192.8634	2192.889	-0.026
2113.8708	2113.895	-0.024
2107.3074	2107.322	-0.015
2074.5518	2074.581	-0.029
2049.0912	2049.111	-0.020
1966.7313	1966.746	-0.015
1966.0660	1966.076	-0.010
1939.5053	1939.521	-0.016
1939.0432	1939.056	-0.013
1844.1340	1844.138	-0.004

Table 1. Improved Ru II wavelengths. Note the systematic shift below 2218 Å of the previously measured wavelengths.

Ru I			
Level		Energy(cm^{-1})	
		old	new
$4d^7(a^4F)5s$	a^5F_2	2713.24	2713.275
	a^5F_1	3105.49	3105.520
	a^3F_4	6545.03	6545.048
$4d^8$	c^3P_2	20933.75	20933.772
$4d^65s^2$	c^3F_4	21643.09	21643.071
$4d^8$	b^1D_2	23453.47	23453.377
$4d^7(a^4F)5d$	e^5D_3	47188.32	47188.348
	e^5G_5	48521.77	48521.860
	e^3G_4	48727.68	48727.749
$4d^65s6s$	e^7D_3	50016.70	50016.813
$4d^65s5p$	z^7D_4	*25464.49*	*25464.520*
$4d^7(a^4F)5p$	z^5D_3	*27506.59*	*27506.623*
$4d^65s5p$	z^5P_1	*35046.77*	*35046.814*
	y^5F_4	*35471.15*	*35471.206*
$4d^7(a^2D)5p$	x^3F_2	*41182.94*	*41182.951*
$4d^7(a^2H)5p$	x^3G_3	*43975.79*	*43975.830*
$4d^7(a^2P)5p$	u^3D_2	*43509.17*	*43509.209*

Ru II			
Level		Energy(cm^{-1})	
		old	new
$4d^7$	$a^4F_{7/2}$	1523.1	1523.269
	$a^4F_{5/2}$	2494.9	2493.937
	$a^4F_{3/2}$	3104.2	3104.267
$4d^6(^5D)5s$	$a^6D_{7/2}$	10150.4	10150.925
	$a^6D_{5/2}$	10851.7	10852.170
$4d^6(^5D)6s$	$e^6D_{9/2}$	84510.9	84511.455
	$e^6D_{7/2}$	—	85411.112
	$e^6D_{5/2}$	—	86137.668
	$e^6D_{3/2}$	—	86602.315
	$e^4D_{7/2}$	86440.4	86441.216
	$e^4D_{5/2}$	87523.4	87523.595
$4d^65d$	9/2	—	89347.373
$4d^65d$	7/2	—	91036.427
$4d^6(^5D)5p$	$z^6D_{9/2}$	*46471.9*	*46471.517*
	$z^6D_{7/2}$	*46711.5*	*46711.916*
	$z^6F_{11/2}$	*50758.3*	*50758.676*
	$z^4F_{5/2}$	*54794.3*	*54794.672*
	$z^4P_{3/2}$	*56664.9*	*56665.349*
	$z^4P_{1/2}$	*57263.8*	*57264.022*

Table 2. Examples of improved and new energy levels in Ru I and Ru II.

REFERENCES

1 D.S. Leckrone, S.G. Johansson, and G.M. Wahlgren,
in "The first year of HST observations",
Eds A.L. Kinney and J.C. Blades,
(Space Telescope Institute, Baltimore, 1991) p.83
2 A.G. Shenstone and W.F. Meggers, 1958, J.Res.NBS **61**, 373
3 K.G. Kessler, 1959, J.Res.NBS **63A**, 213

Diagnostics of Electron Temperature and Density in High Density Plasmas Using L-shell Xenon Emission Spectroscopy

C.J. Keane, B.A. Hammel, A.L. Osterheld, D.R. Kania
Lawrence Livermore National Laboratory

K- and L-shell x-ray spectra have long been of use in diagnosing the fuel conditions in both directly and indirectly driven ICF targets.[1] To date, spectral diagnosis of the fuel region of capsules indirectly imploded using the Nova laser has relied on K-shell emission from H- and He-like Ar.[2] K-shell Ar emission is used to diagnose the fuel region through Stark broadening of the Ar Ly-β and He-β lines (which gives fuel N_e) and the ratio of Ly-β to He-β (which gives fuel T_e). In these experiments Ar and Xe are placed as dopants in the deuterium fuel at the 0.02-0.1 atomic percent level. Typical fuel plasma conditions in current implosions inferred from Ar line emission are $N_e \sim 10^{24}$ cm^{-3} and $T_e \sim$1-2 keV; the latter depends strongly on laser energy.

While K-shell Ar emission has been of valuable diagnostic use in implosions to date, future implosion experiments are expected to achieve pusher opacities high enough to prevent Ar emission from escaping the capsule. The consequent need for higher photon energy diagnostics has motivated our work in developing L-shell Xe emission as a measure of electron temperature and density. Previous work[3] with Xe in direct drive implosions showed emission from ionization stages near Ne-like; a number of F-like transitions included in the model used here were identified. Using a state of the art Xe model[4] of the type originally developed for Ne-like ion x-ray laser research, we have developed spectral diagnostics of electron temperature and density based on ratios of clusters of Xe lines.[5]These methods require spectrographs with relatively low (~500) spectral resolving power. Specifically, ratios of F-like resonance lines and Ne-like satellites to Ne-like resonance lines and Na- and Mg- like satellites are found to be temperature and density sensitive. The temperature and density sensitivity reflects the changing ionization balance with plasma conditions. Experimental Xe spectra from Nova indirect drive implosions are in good qualitative agreement with calculated spectra; inclusion of spatial gradients in temperature and density is necessary before a full comparison with measurement can be made. Finally, pressure broadening of Xe 4-2 transitions also appears feasible as a electron density diagnostic for $N_e \sim 10^{25}$ cm^{-3}.[6] It is necessary to include ion motion effects here; this is in progress.

References

1. R.L. Kauffman, "X-ray Radiation from Laser Plasma", in *Handbook of Plasma Physics, Vol. 3: Physics of Laser Plasma*, A. Rubenchik and S. Witkowski, eds., North Holland Publishing Co., 1991.

2. B.A. Hammel, C.J. Keane, D.R. Kania, J.D. Kilkenny, R.W. Lee, R. Pasha, and R.E. Turner, to be published in Rev. Sci. Inst.
3 Y. Conturie, B. Yaakobi, U. Feldman, G.A. Doschek, and R.D. Cowan, J. Opt. Soc. Am. B 71, 1309 (1981).
4. A.L. Osterheld, B.K.F. Young, R.S. Walling, W.H. Goldstein, J.H. Scofield, M. Chen, G. Shimkaveg, M. Carter, R. Shepherd, B.J. MacGowan, L. DaSilva, D. Matthews, S. Maxon, R. London, and R.E. Stewart, in *Proceedings of the 3rd International Colloquium on X-ray Lasers*, Schliersee, Germany, May 1992.
5. C.J. Keane, B.A. Hammel, A.L. Osterheld, and D.R. Kania, to be submitted for publication.
6. C.J. Keane, R.W. Lee, B.A. Hammel, A.L. Osterheld, L.J. Suter, A. Calisti, F. Khelfaoui, R. Stamm, and B. Talin, Rev. Sci. Inst. 61, 2780 (1990).

Acknowledgment

Work performed under the auspices of the U.S. Department of Energy by Lawrence Livermore National Laboratory under contract No. W-7405-ENG-48.

120-keV Kr^{8+} - Li collisions studied by near UV and visible photon spectroscopy.

E. Jacquet*, P. Boduch*, M. Chantepie*, M. Druetta#, D. Hennecart*, X. Husson*, D. Lecler*, N. Stolterfoht* †, M. Wilson‡

* *Laboratoire de spectroscopie atomique CNRS-URA 19*
ISMRA Bd Maréchal Juin F-14050 CAEN CEDEX FRANCE

Laboratoire de traitement du signal et instrumentation CNRS-URA 842, Université de Saint-Etienne
23 rue du Docteur Paul Michelon F-42023 SAINT-ETIENNE CEDEX, FRANCE

† *Hahn-Meitner Institut, Gleinicker Strasse 100, D-1000 Berlin 39, GERMANY*

‡ *Department of Physics, Royal Holloway and Bedford New College*
University of London, Egham Hill, Egham, Surrey TW20 0EX, ENGLAND

Introduction.

Collisions of multiply charged ions on a neutral atomic or molecular target produce excited multiply charged ions following the reaction:

$$A^{q+} + B \rightarrow A^{(q-k)+} + B^{k+} + \Delta E$$

when k is the number of electrons which have been captured.

It has already been shown that near UV and visible photon spectroscopy is a convenient tool [1] to observe charge exchange collisions. Following previous work (Kr^{8+} - He, H_2 [2], Ar^{8+} - Li [3]), we present results for collisions between Kr^{8+} ions and lithium atoms at 120 keV. The three electrons lithium target allows us to study single, double and triple electron captures. The outermost 2s electron of the lithium target is very loosely bound and population of relatively high Rydberg states is therefore expected in Kr VIII. The 2s and one or two 1s electrons are transferred during double and triple electron captures. The relative population of the outgoing channels allow an estimates of the importance of correlation effects (electron-electron interactions) in the exchange process.

After a description of the experimental set-up, we present a detailed spectroscopic analysis of the recorded spectra. The analysis was made using collisional models (Niehaus [4], Landau-Zener [5] and Stolterfoht [6]) and spectroscopic ab initio pseudo-relativistic Hartree-Fock (HFR) calculation (Cowan [7]).

Experimental set-up.

120-keV Kr^{8+} incident ion beam provided by an ECR source of the GANIL* test bench is focused on an effusive jet of lithium. The ion beam current was of the order of 20 μA, the pressure in the collision chamber of the order of 10^{-6} mbar. The emitted photons were observed at right angles to the directions of the incident beam and of the lithium jet with a normal grating incidence spectrometer.

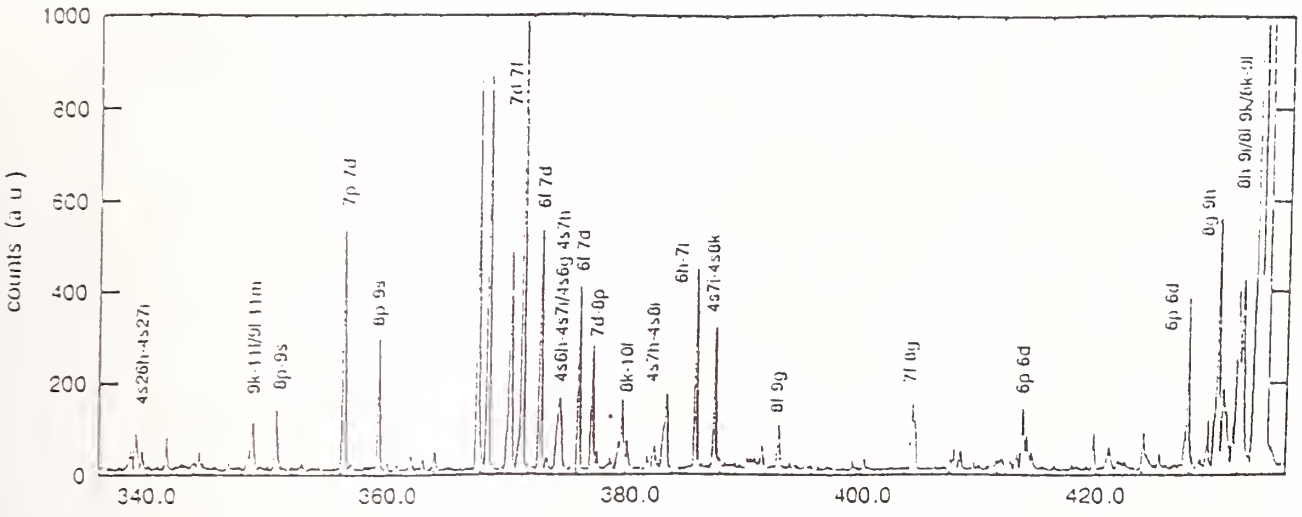

Spectral analysis.

Single electron capture lines.

The classical over-barrier model of Niehaus [5] predicts that the 2s electron of the target is preferentially captured into a n=9 orbital. Lines corresponding to $\Delta n=0$, $\Delta n=1$ and $\Delta n=2$ transitions are expected to be observed in the 200-600 nm wavelength range. Observed transitions are presented in Table I.

Double electron capture lines.

Observed lines corresponding to 4snl - 4sn'l' Rydberg transitions are indicated in Table II. The 4snl configurations in Kr VII are produced by a one-step process involving electron-electron interaction.

Triple electron capture lines.

We observed two lines corresponding to $4s^26h$ - $4s^27i$ and $4s^26g$ - $4s^27h$ transitions.

$4s^26g$ - $4s^27h$ λ=338.17 nm

$4s^26h$ - $4s^27i$ λ=339.47 nm

---

1 P. Boduch, M. Chantepie, M. Druetta, B. Fawcett, D. Hennecart, X. Husson, H. Kucal, D. Lecler, N. Stolterfoht, M. Wilson, Physica Scripta, 45, 203 (1992).
2 P. Boduch, M. Chantepie, M. Druetta, D. Hennecart, X. Husson, D. Lecler, M. Wilson, Physica Scripta, to be published (1992).
3 E. Jacquet, P. Boduch, M. Chantepie, M. Druetta, D. Hennecart, X. Husson, D; Lecler, N. Stolterfoht, M. Wilson, Physica Scripta, submitted (1992).
4 A. Niehaus, J. Phys. B: At. Mol. Phys., 19, 2925 (1986).
5 E.E. Nikitin, Theory of elementary Atomic and Molecular Processes in Gases, Clarendon Press, Oxford (1974).
6 N. Stolterfoht, K. Sommer, J.K. Swenson, C.C. Haveneur, F.W. Meyer, Physical Review A, 42, 5396 (1990).
7 R.D. Cowan, The Theory of Atomic Structure and Spectra, University of California Press, Berkeley (1981).

Transitions in Kr VIII	$_{exp}\lambda$ (nm) in air
$5f\ ^2F_{5/2}$ - $6d\ ^2D_{3/2}$ $5f\ ^2F_{7/2}$ - $6d\ ^2D_{5/2}$	227.65 225.93
$6d\ ^2D_{3/2}$ - $7p\ ^2P_{1/2}$ $6d\ ^2D_{5/2}$ - $7p\ ^2P_{3/2}$	229.22 225.64
$6f\ ^2F_{5/2}$ - $7d\ ^2D_{3/2}$ $6f\ ^2F_{7/2}$ - $7d\ ^2D_{5/2}$	375.90 372.74
6g - 7f	191.61
6h - 7i	192.84
$7p\ ^2P_{3/2}$ - $8s\ ^2S_{1/2}$	229.57
$7d\ ^2D_{3/2}$ - $8p\ ^2P_{1/2}$ $7d\ ^2D_{3/2}$ - $8p\ ^2P_{3/2}$ $7d\ ^2D_{5/2}$ - $8p\ ^2P_{3/2}$	377.07 367.78 370.29
7f - 8g	269.62 or 269.80
7g - 8f	318.94
7g - 8h	294.92
7h - 8i	297.04
7i - 8k	297.35
$8p\ ^2P_{1/2}$ - $9s\ ^2S_{1/2}$ $8p\ ^2P_{3/2}$ - $9s\ ^2S_{1/2}$	350.62 359.00
$8d\ ^2D_{3/2}$ - $9f\ ^2F_{5/2}$ $8d\ ^2D_{5/2}$ - $9f\ ^2F_{7/2}$	241.83 242.53
8f - 9g	392.92
8g - 9h	429.95
8h - 9i	433.27
8i - 9k	433.77
8k - 9l	433.81

$6s\ ^2S_{1/2}$ - $6p\ ^2P_{1/2}$ $6s\ ^2S_{1/2}$ - $6p\ ^2P_{3/2}$	355.88 333.74
$6p\ ^2P_{1/2}$ - $6d\ ^2D_{3/2}$ $6p\ ^2P_{3/2}$ - $6d\ ^2D_{3/2}$ $6p\ ^2P_{3/2}$ - $6d\ ^2D_{5/2}$	206.87 215.23 213.78
$6d\ ^2D_{3/2}$ - $6f\ ^2F_{5/2}$ $6d\ ^2D_{5/2}$ - $6f\ ^2F_{7/2}$	221.99 223.72
$7s\ ^2S_{1/2}$ - $7p\ ^2P_{3/2}$	584.88
$7p\ ^2P_{1/2}$ - $7d\ ^2D_{3/2}$ $7p\ ^2P_{3/2}$ - $7d\ ^2D_{3/2}$ $7p\ ^2P_{3/2}$ - $7d\ ^2D_{5/2}$	356.08 370.07 367.53
$7d\ ^2D_{3/2}$ - $7f\ ^2F_{5/2}$ $7d\ ^2D_{5/2}$ - $7f\ ^2F_{5/2}$ $7d\ ^2D_{5/2}$ - $7f\ ^2F_{7/2}$	368.41 371.05 371.27
9k - 10l 9l - 10m	605.63 606.58
8i - 10k 8k - 10l	252.78 252.99
9k - 11l 9l - 11m	348.35 348.69
10m -12n	466.79

Table I.

Transition in Kr VII	$_{exp}\lambda$ (nm)
4s6g - 4s7h 4s6h- 4s7i	249.44 249.63
4s7g - 4s8h 4s7h - 4s8i 4s7i - 4s8k	382.20 382.99 387.28
4s8i - 4s9k 4s8k - 4s9l	— 565.88

Table II

Photon and Auger Spectroscopy of Single and Double Electron Capture following 90-keV C^{6+} - Li Collisions

F.Fremont, E.Jacquet, P.Boduch, M.Chantepie, G.Cremer, D.Hennecart, S.Hicham, X.Husson, D.Lecler and N.Stolterfoht [a]

Laboratoire de spectroscopie atomique, ISMRA, bd du Maréchal Juin, 14050 CAEN

M.Druetta

Laboratoire de traitement du signal et instrumentation CNRS-URA 842, Université de Saint-Etienne 23 rue du Docteur Paul Michelon F-42023 SAINT-ETIENNE CEDEX, FRANCE

M.Wilson

Royal Holloway and Bedford New College, Department of Physics, University of London, Egham Hill, Egham, Surrey, TW20 0EX, LONDON, ENGLAND.

The system 90-keV C^{6+} - Li has been studied recently using an ECR ion source of the GANIL*. Lithium is an interesting target because it has three active electrons. The single electron capture of the outermost 2s electron, which is loosely bound produces configurations nl (n=7, 8) in C^{5+}. The states of these configurations are radiative states which give rise to photon emission in the visible and near UV wavelength range. Double electron capture is expected to produce 2l2l', 2lnl' (n=4, 5...) in C^{4+} (Figure 1) by the electron nucleus interaction and 2l3l', 2l4l', 3l3l' by the electron nucleus interaction (Figure 2) and the electron-electron interaction (correlated transfer capture). Most of the states of these configurations are autoionizing states and give rise to electron emission by Auger effects.

Single electron capture

The observed spectra in the 250-600 nm wavelength range is presented in Figure 3. According to the theoretical predictions, nl (n=7, 8) configurations in C^{5+} are produced. The experimental wavelengths and the emission cross sections are given below.

Transitions	Experimental wavelengths	Emission cross sections (10^{-17} cm^2)
n=7 → n=6	343.49 ± 0.04 nm	50
n=8 → n=7	529.21 ± 0.04 nm	9
n=9 → n=7	313.88 ± 0.04 nm	1.7
n=10 → n=8	450.00 ± 0.04 nm	0.3

Double electron capture

Photon spectroscopy

We observed lines corresponding to 1s5g - 1s6h and 1s6h - 1s7i or to 2p5g ^{1}G - 2p6h ^{1}H and 2p6h ^{1}H - 2p7i ^{1}I transitions. We cannot observe 2s5g - 2s6h and 2s6h - 2s7i transitions because 2s6h and 2s7i are autoionizing states. 1s5g - 1s6h and 1s6h - 1s7i transitions can correspond to the second step of radiative de-excitation.

---

[a] also Hahn-Meitner-Institut Berlin GmbH, Glienickerstr. 100 Berlin 39

* Grand Accélérateur National d'Ions Lourds, Caen, France.

Auger spectroscopy

As seen from the spectrum (Figure 4), we actually observed the expected configurations, but we also observed un-expected configurations. Between 0 and 20 eV, we can see 4lnl' configurations which were not expected. First, we thought that double collisions can contaminate the real double capture, but an estimate of the jet pressure excludes this possibility. No explanation can be given yet. We have a similar problem with 2121' configurations, which can come from double collisions as well as double capture.

In the range [20-80eV], we find 3lnl' (n=3,4,5) configurations. However, for a given intensity of the peaks corresponding to 3131' and 3151' configurations, the 3141' configurations intensity changes strongly with the pressure.

Between 300 and 380eV, we observed 2lnl' configurations. As expected, the peaks corresponding to 2131' and 2141' configurations are weak.The biggest peak corresponds to 2151' states.

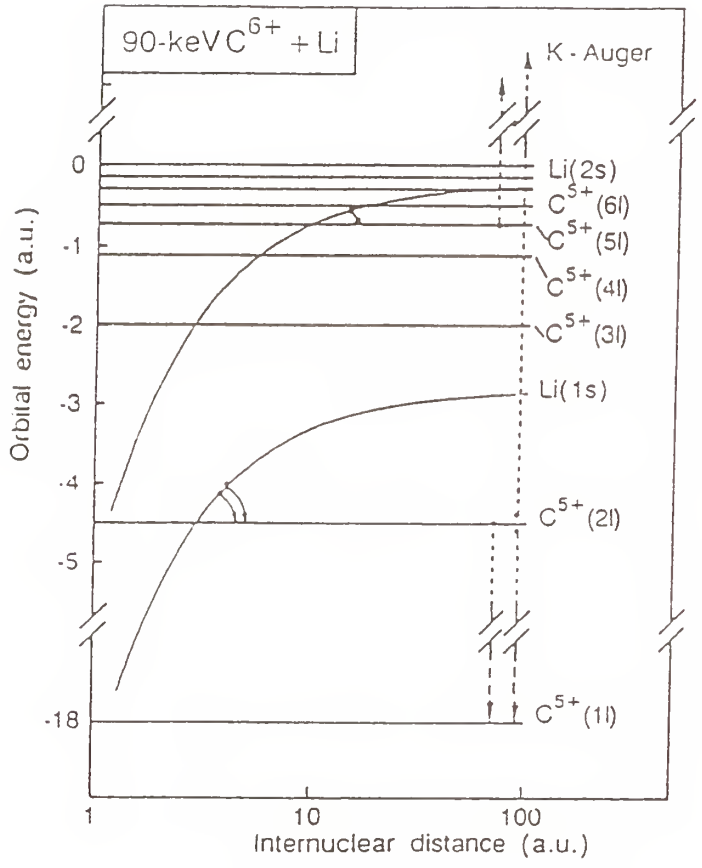

Figure 1

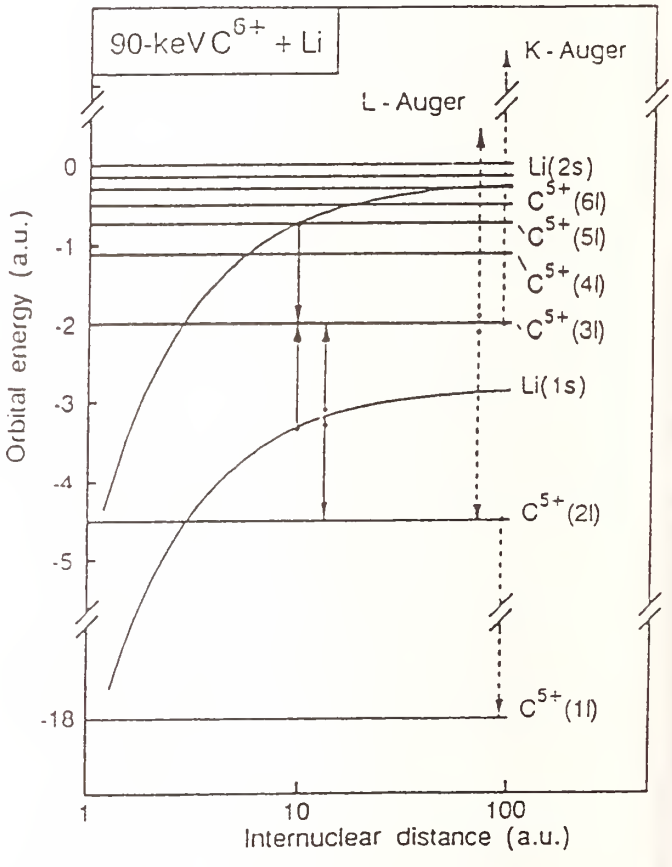

Figure 2

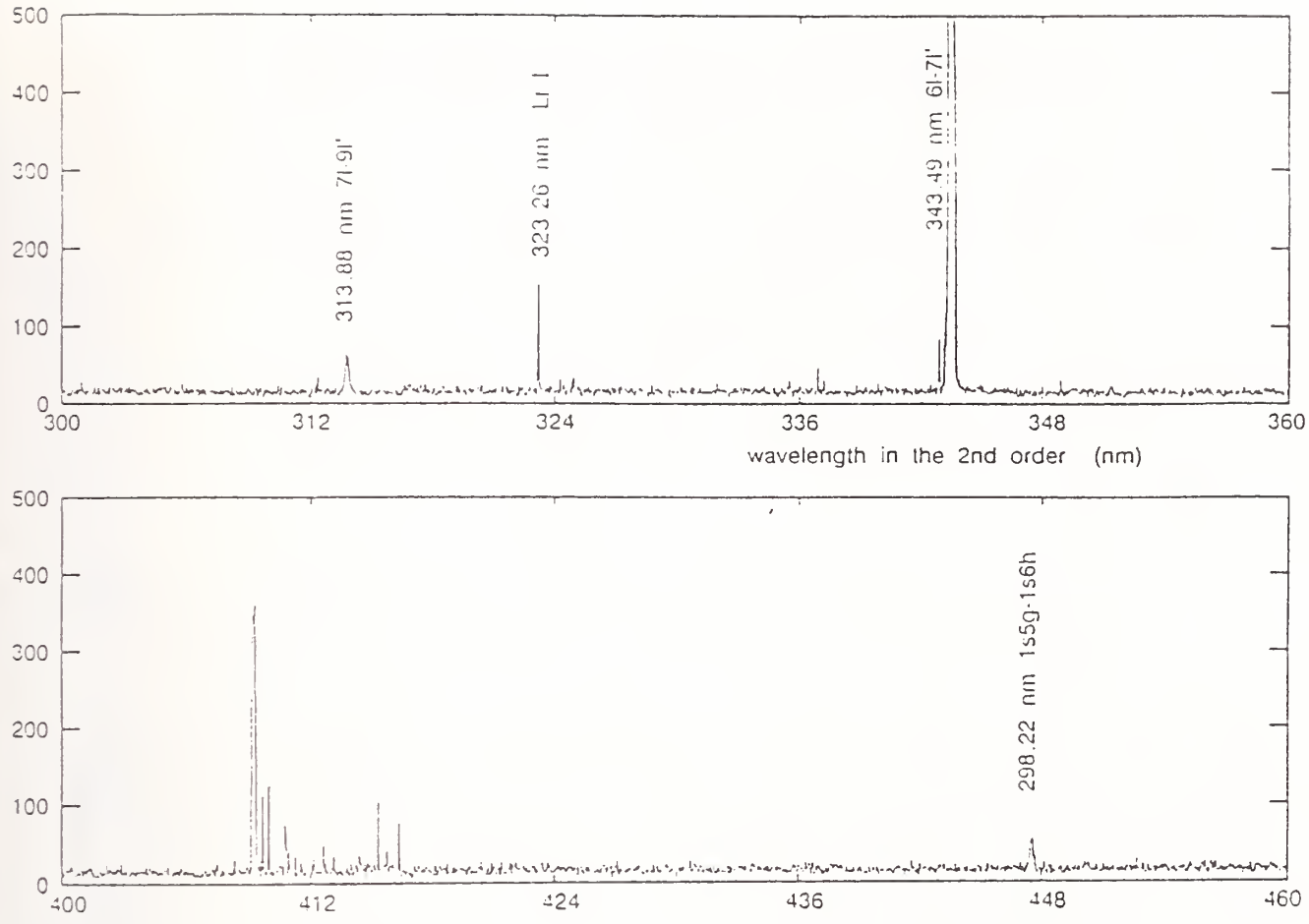

Figure 3

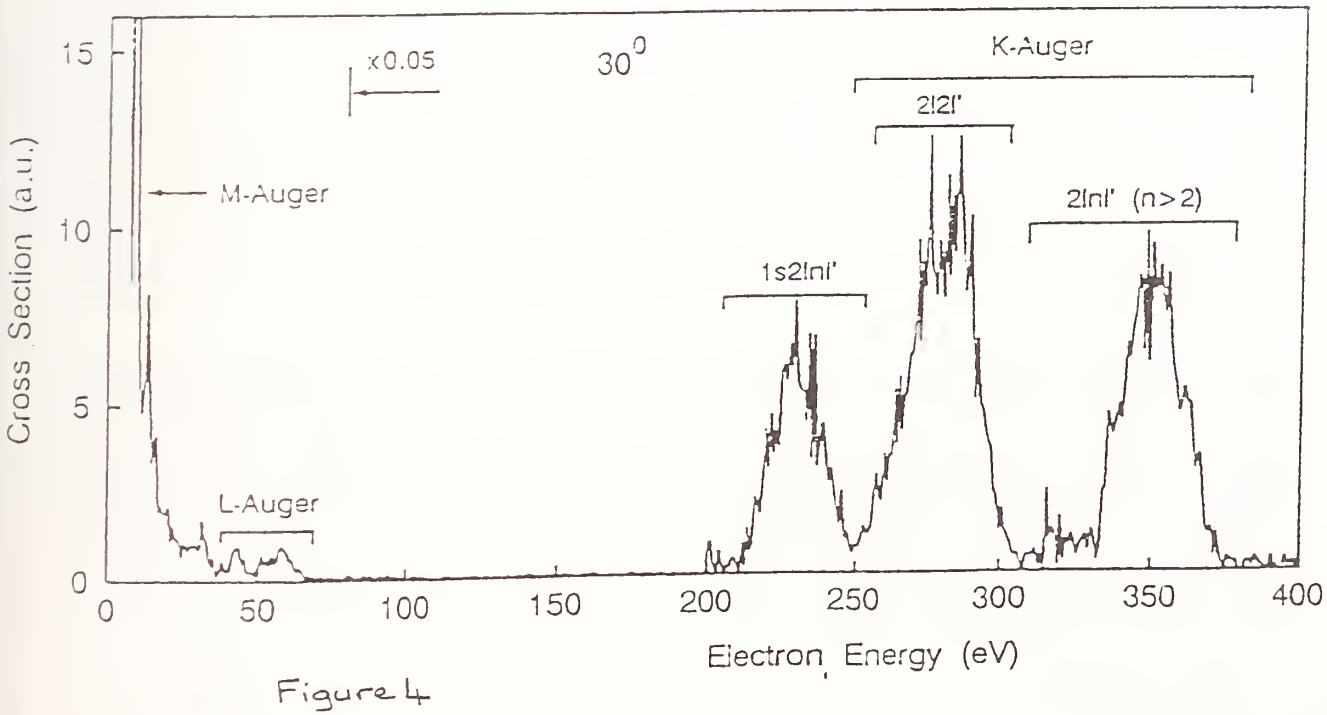

Figure 4

Measurements of Electron Emission From Collisions of MeV Energy N, C, and He Ions With He Gas

N. A. Guardala, J .L. Price, and D. J. Land
Naval Surface Warfare Center/White Oak, Silver Spring MD

M. F. Stumborg and D. G. Simons
The Catholic University of America

G. A. Glass
University of Southwestern Louisiana

1. Introduction

Experiments involving collisions between neutral gas targets and ion-beams produced by positive-ion accelerators have become a useful means of gathering information pertinent to the modeling and understanding of both astrophysical and laboratory plasmas[1]. Typical experiments may involve emergent projectile charge state distributions, energy loss and various spectroscopic measurements of both target and projectile excited states. Measurements of the electron emission spectra produced in collisions of energetic projectiles with relatively simple targets such as: H, H_2, and He gas have become a powerful tool in the study of the dynamics of ion-atom collisions[2].

This brief paper reports on measurements of electron emission spanning kinetic energies typically from 200-3000 eV and involving projectile energies that range from 0.20-1.40 MeV/u. Two types of emitted electrons are almost always observed regardless of the charge state and velocity of the projectile, these are: "cusp" electrons [3] which involve electrons moving with zero velocity in the projectile's reference frame and therefore have the same velocity in the laboratory frame as the projectile and Binary Encounter electrons [4] which originate from bound target electron states. The cusp electron peak can be due to either capture of a target electron to a Rydberg-like state of the projectile, this process is referred to as Electron Capture to the Continuum (ECC) or to the excitation of a projectile bound electron to a similar excited state. This later process is known as Electron Loss to the Continuum or ELC.

A third kind of electron transition is possible when the projectile is capable of forming a Li-like i.e. a three electron excited-state configuration, that excited state will have some probability of decaying via the Auger emission process. Typically, this excited state involves a K-shell vacancy so that the emitted electron represents some type of K-shell Auger transition. Figure 1 shows an ejected electron spectrum involving 0.92 MeV/u C^{+3} ions colliding with He gas. Cusp, KLL, KLM and Binary Encounter electrons are clearly identifiable.

2. Experimental

In order to measure discrete transitions such as Auger lines and cusp electrons without significant Doppler broadening this series of electron measurements were carried out at 0° with respect to the beam axis [5]. Therefore, the peaks have observed widths that are determined primarily by the instrumental resolution which is ca. 2 % .

The measurements were carried out using the 3 MeV Tandem Pelletron at the Naval Surface Warfare Center/White Oak Lab. Beams of N^{+4}, C^{+3}, He^{+1} and He^{+2} were produced from the accelerator and were mass, charge and energy analyzed magnetically before being focused through the target interaction chamber. This chamber contained a gas jet which allowed pressures of 1-4 torr to be maintained in the jet with a background chamber pressure of typically 2×10^{-5} torr. The electrons were energy analyzed using a double-focusing, hemispherical electrostatic analyzer coupled to a channeltron electron detector[6]. The gas jet was positioned at a distance from the entrance to the analyser which approximated the entrance focal point. Integrated beam currents were collected in a Faraday cup.

3. Conclusion

Measurements of ejected electron spectra involving MeV energy projectiles and neutral He gas have begun at NSWC/White Oak. These measurements are preliminary to a proposed collaboration between NSWC and the University of Maryland's Laboratory for Plasma Physics to perform similar measurements which will substitute a laboratory generated plasma target for a neutral gas target. The scientists at NSWC/WO acknowledge the Independent Research Fund of the U. S. Navy in supporting this work.

References

[1]. G. Hoffmann, A. Muller, K. Tinschert and E. Salzborn, Z. Phys. D 16, 113 (1990).

[2]. K. Tinschert, A. Muller, G. Hoffmann, E. Salsborn and S. M. Younger, Phys. ReV A 40, (1991).

[3]. R. Shakeshaft and L. Spruch, Phys. Rev. A 20, 367 (1978).

[4]. D. H. Lee, P Richard, T. J. M. Zouros, J. M. Sanders J. L. Shinpaugh and H. Hidmi, Phys. Rev. A 41, 816 (1990).

[5]. A. Itoh, D.Schneider, T.Schneider, T. J. M. Zouros, G. Nolte, G. Schwieitz, Z. Zeitz and N. Stolterfoht, Phys. Rev. A 31, 684 (1985).

[6]. K.D. Sevier, Low Energy Electron Spectrometry, Wiley, New York 1972.

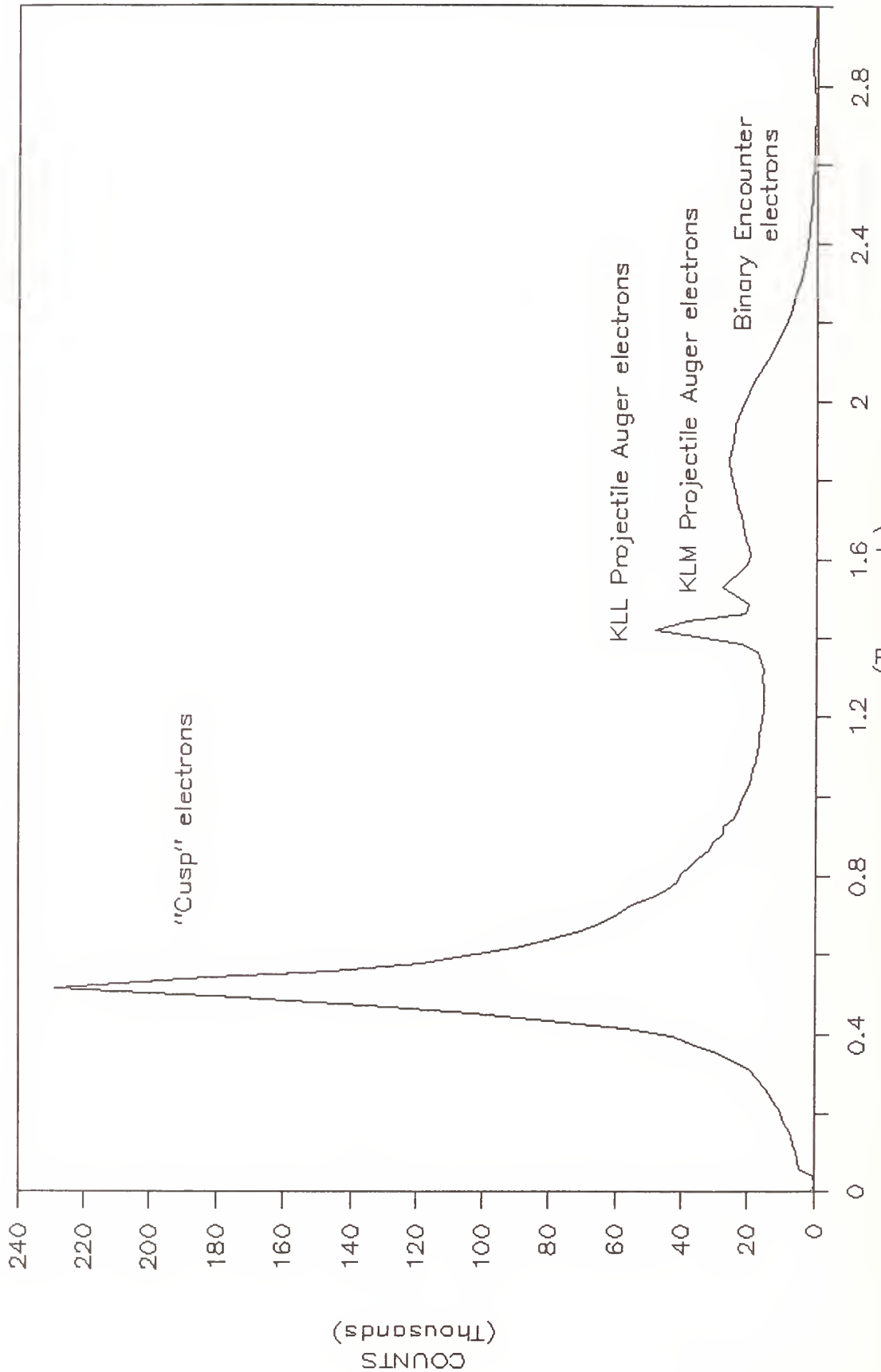

Figure 1. Electron emission spectra taken at 0^0 with respect to the beam axis involving 0.92 MeV/u C^{+3} projectiles incident on He gas

UPDATE ON THE NIST EBIT

J.D. Gillaspy* and J.R. Roberts
National Institute of Standards and Technology
Atomic Physics Division, Gaithersburg, MD 20899
and
C.M. Brown and U. Feldman
E. O. Hulburt Center for Space Research
Naval Research Laboratory, Washington, D. C. 20375

I. Introduction to EBIT.

A decade ago, the Electron Beam Ion Source (EBIS) was hailed as the most advanced method for producing highly charged ions [1]. A few years later, the EBIS concept was reevaluated and optimized for use as a spectroscopic source. The new device, the Electron Beam Ion Trap (EBIT) [2], produced a high density of ions in a relatively small volume with radial access ports. With this new geometry, plasma instabilities were removed and very high electron beam densities were achieved. These improvements boosted both the spectral brightness and the maximum attainable charge state, and furnished the atomic spectroscopy community with an important new laboratory source.

The spectra produced with an EBIT are very pure, consisting of lines from only a few charge states of essentially a single atomic species. The choice of charge state can be continuously varied by adjusting the electron beam energy. The ability to literally "dial up" a particular charge state greatly simplifies the identification of spectral lines. Virtually any highly charged state of any atom on the periodic table is accessible in this way.

In addition to operating the EBIT in a static mode where the electron beam energy is held constant and a spectrum is collected in order to determine accurate wavelengths, one can also use the precise and rapid control of the electron beam energy to carry out temporal studies of the emitted photons. This feature allows one to directly determine excited state lifetimes and to map out dielectronic recombination cross-sections.

A summary of the advantages of EBIT over conventional sources include:

1. Relatively few charge states.
2. No Doppler shifts
3. Insignificant Doppler broadening.
4. Insignificant density effects.
5. Very high charge states attainable.
6. Control over dielectronic satellites.
7. Slit-like source dimensions (60 um x 2 cm) ideally suited to spectrometers.
8. Very little background signal.

9. High accuracy (21 ppm) wavelength measurements demonstrated.
10. Ultrahigh vacuum (10^{-10} Pa) maintained by cryogenic environment.
11. No cascade contamination in lifetime studies.

Although the spectral brightness of an EBIT is much weaker than that from powerful sources such as Tokamaks, the photon flux from an EBIT is nevertheless quite adequate for spectroscopic work when reasonable effort is taken to make use of efficient modern detection methods. A typical x-ray spectrum recorded with a solid state detector on an EBIT may only take a few seconds to collect. Very high precision studies of weak lines using crystal detectors may require many hours of data collection, however. Even in such cases the brightness is not usually of overriding concern since the source is under local control and operates reliably for long periods of time. Because the source is run by computer control, ions can be dumped from the trap and reloaded automatically at periodic intervals.

II. Present status of superconducting EBIT facilities.

The only full-scale EBIT devices in operation at this time are those at Livermore. The mechanical components for the NIST EBIT were made in Oxford England where an identical device is being put into operation [3]. The NIST EBIT will go into operation in Gaithersburg, Maryland during the coming year through a collaborative effort with the Naval Research Laboratory. An EBIT project is reportedly underway in Japan, although information about this project is scarce. A major EBIT project has been underway in the former Soviet Union at Dubna.[4]

Charge states as high as fully stripped Uranium are being actively pursued at Livermore where the prototype EBIT has been upgraded to operate above 150 keV. The NIST EBIT will begin operations under 50 keV, with possible upgrades in the future. Even at 50 keV, most of the states of any ion can be accessed.

The design of the NIST EBIT was developed by M. Levine and is based on his highly successful original work with the Livermore prototype. Detailed drawings, a discussion of the improvements that have been made, and a table of the projected operating conditions will be published in the proceedings of the VIth International Conference on the Physics of Highly-Charged Ions (HCI-92).

*Bitnet: Gillaspy@NBSenh, Internet: Gillaspy@enh.NIST.gov

[1]. H. Winter, "The Production of Multiply Charged Ions for Atomic Physics Experiments" in Atomic Physics of Highly Charged Ions, R. Marrus (Ed.), 1983.

[2]. M.A. Levine, R.E. Marrs, J.R. Henderson, D.A. Knapp, and M.B. Schneider, "The Electron Beam Ion Trap: A New Instrument for Atomic Physics Measurements," *Phys. Scr.*, **T22**, 157 (1988).

[3]. J. Silver, private communication.

[4]. Y. Aglitskiy, private communication.

PERFORMANCE AND RESOLVING POWER OF CONCAVE MULTILAYER-COATED GRATINGS OPERATING NEAR NORMAL INCIDENCE IN THE 136-300 Å REGION

J. F. Seely[1], M. P. Kowalski[1], W. R. Hunter[2], J. C. Rife[1], T. W. Barbee, Jr.[3], G. E. Holland[2], C. N. Boyer[4] and C. M. Brown[1]

[1]Naval Research Laboratory, Washington DC 20375
[2]SFA Inc, 1401 McCormick Drive, Landover MD 20785
[3]Lawrence Livermore National Laboratory, Livermore CA 94550.
[4]USRA, 409 Third Street SW, Washington, DC 20024

Owing to the low reflectance of materials for wavelengths below 300 Å and near normal incidence, most grating spectrometers operate at grazing incidence in the XUV and soft X-ray regions. These instruments typically have low throughput because of the small geometrical collection factor and tend to be costly and difficult to focus. Newly-developed multilayer coatings, that have high reflectance below 300 Å, have opened the possibility of building high-throughput spectrometers that operate near normal incidence. The multilayer coating can be matched to the blaze angle of the grating substrate so that the grating operates on-blaze in wavebands of spectroscopic interest with an efficiency that can be orders of magnitude higher than that of a similar gold-coated grating. These are important advantages for instruments intended to observe weak sources such as EBIT.

Multilayer coatings were applied to two sister replica grating substrates that were made from a ruled master by Hyperfine Inc. The grating substrates were concave with 2.2 meter radius of curvature, had 2400 g/mm, and nominal blaze angle of 2°. The multilayer coatings were sputter deposited at the Lawrence Livermore National Laboratory and consisted of alternating layers of Mo and Si. Witness optical flats were coated simultaneously with each grating substrate. The reflectances of the witness flats and the efficiencies of the multilayer-coated gratings were measured using the NRL reflectometer-monochromator at the National

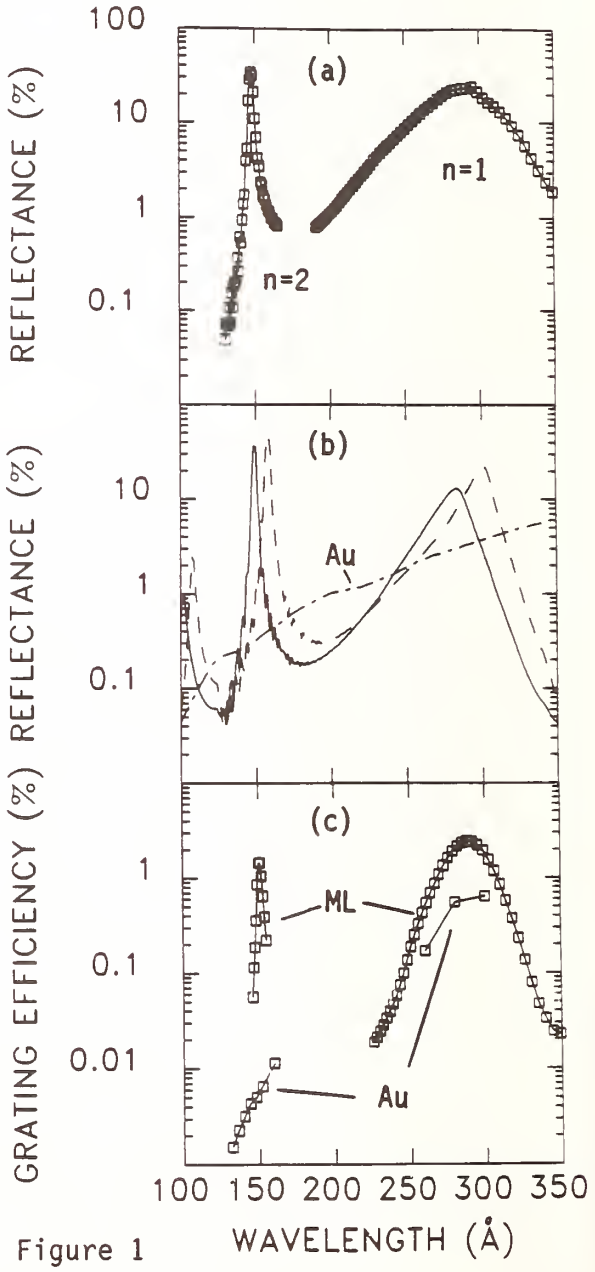

Figure 1

Synchrotron Light Source. The resolving powers of the gratings were determined by mounting the gratings in a 2.2 meter McPherson normal-incidence spectrograph. Similar measurements were made using a sister replica grating that had a gold coating.

Multilayer grating #1 had 30 Mo/Si periods with a d-spacing of 162.5 Å. The multilayer coating was designed to have high reflectance in both the first and second Bragg orders. As shown in Fig. 1(a), the reflectance of the witness flat measured at an angle of incidence of 20° was 24% at a wavelength of 290 Å and in the first multilayer order (n=1) and 33% at 148 Å in the second multilayer order (n=2). The calculated reflectances of the witness flat at 20° and 4° angles of incidence are shown by the solid and dashed curves in Fig. 1(b), respectively, and this illustrates how the reflectance wavebands shift with angle of incidence. For comparison, the normal-incidence reflectance of a gold coating is shown by the dot-dashed curved in Fig. 1(b). The measured efficiencies of the multilayer and gold gratings are shown in Fig. 1(c) for an angle of incidence of 14.5° and in the first outside grating order. The peak efficiencies were 2.5% and 1.5% at wavelengths of 290 Å and 151 Å. These efficiencies were factors of 4 and 200 greater than the corresponding efficiencies of the gold grating.

The multilayer coating for grating #2 was designed so that the grating would operate on-blaze with high efficiency in the second grating order and at a wavelength of 140 Å at normal incidence. The multilayer coating was composed of 40 Mo/Si periods with a d-spacing of 73 Å. The reflectance of the witness flat was 55% near normal incidence. For an angle of incidence of 14.5°, the grating efficiency in the second outside order was highest for a wavelength of 136 Å, as shown in Fig. 2, and the efficiency of the multilayer grating was a factor or 150 higher than that of the gold grating. Figure 3 shows the efficiency in the outside orders at a wavelength of 136 Å and at 14.5° incidence, and the

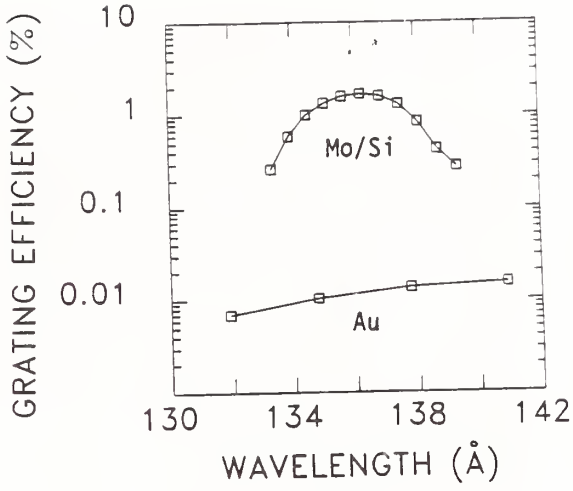

Figure 2

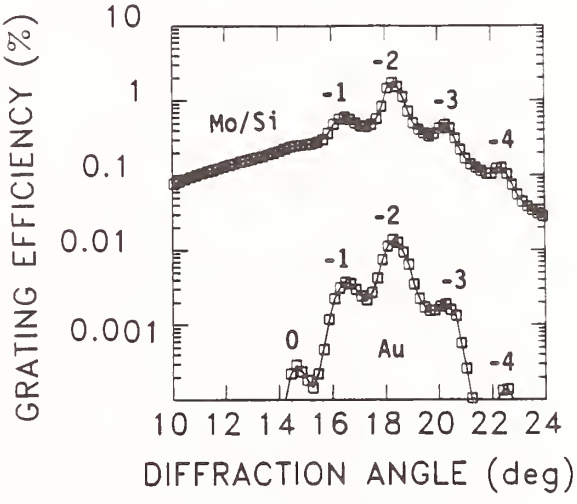

Figure 3

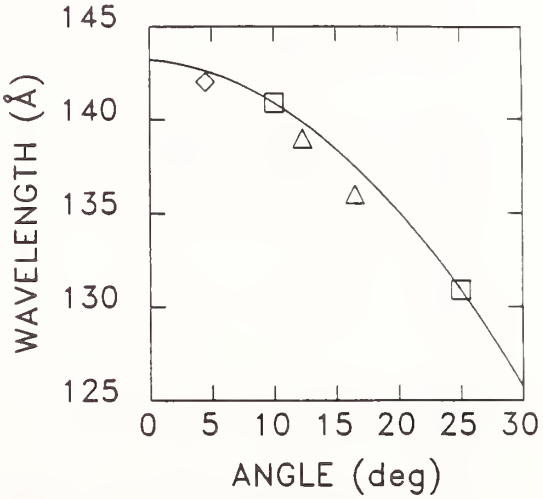

Figure 4

efficiency is highest in the second order.

Figure 4 illustrates how the wavelength of peak reflectance of the witness flat (squares) and peak efficiency of the grating (diamond and triangles) vary with angle of incidence.

The McPherson spectrograph operated with an angle of incidence of 6° and a 20 μm entrance slit. The spectra from a vacuum spark source were recorded on Kodak 101 plates. The higher grating orders were observed by using a 1 μm beryllium filter to attenuate the longer wavelength radiation. The transmittance of the filter is shown in Fig. 5(a), and the spectra recorded from a tungsten electrode without and with the filter are shown in Figs. 5(b) and (c), respectively. The first, second, and third grating orders are clearly visible in Fig. 5(c) at wavelengths near 140 Å, 280 Å, and 420 Å. The periodic structure on the long wavelength side of the orders results from the periodicities in the off-peak reflectance of the multilayer coating.

The resolving power of multilayer grating #1 is illustrated in Fig. 6. This is the second-Bragg-order spectrum of a vanadium electrode in the first, second, and third grating orders. Using the V VII transition at 156.608 Å, the resolving power is 14,000 after removing the broadening caused by the 20 μm entrance slit. Comparisons between the multilayer and gold gratings indicated that the application of the multilayer coating did not affect resolving power.

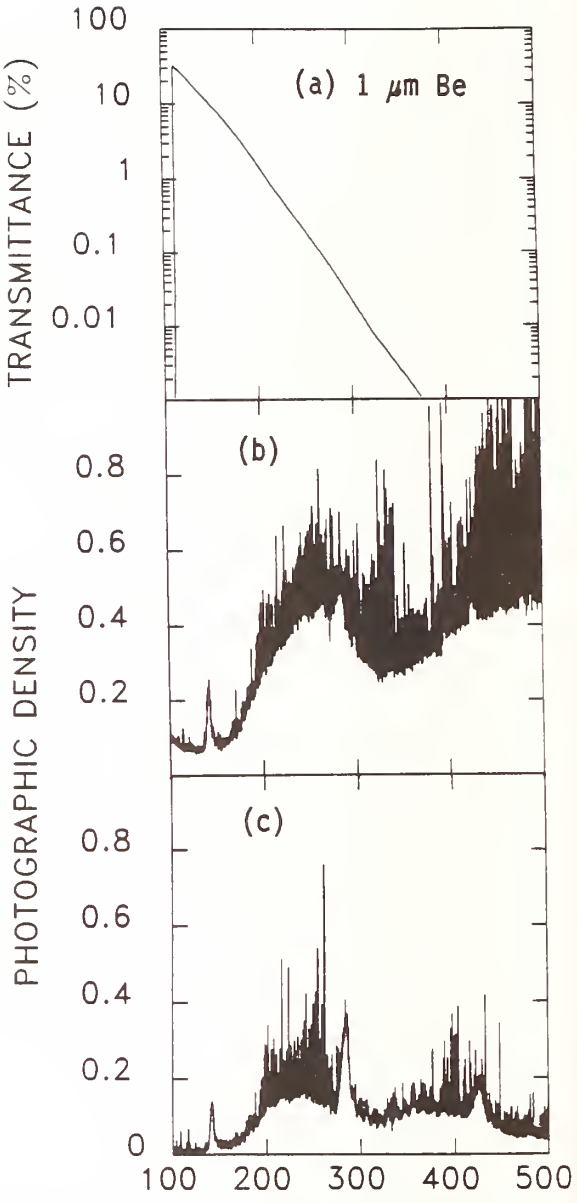

Figure 5

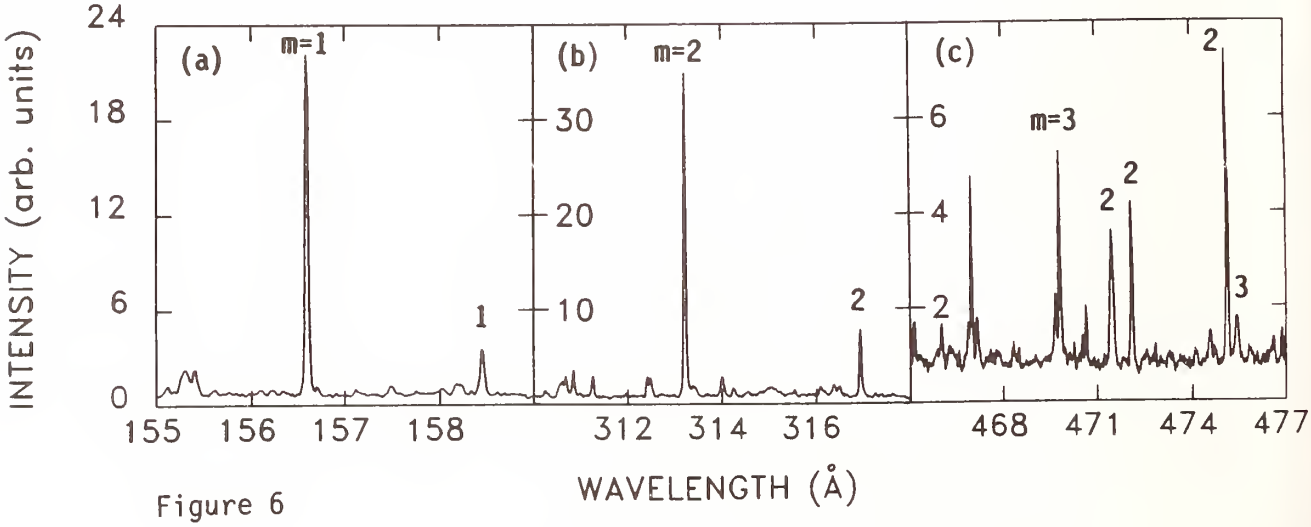

Figure 6

New line identifications in XeVIII and XeVII

M. DRUETTA
Laboratoire de Traitement du Signal et Instrumentation
URA CNRS 842
Université Jean Monnet, 42023 SAINT-ETIENNE Cedex, France

D. HITZ, P. LUDWIG
DRFMC/PSI Centre d'Etudes Nucléaires de Grenoble
85X 38041 GRENOBLE Cedex, FRANCE

ABSTRACT

XeVIII and VII spectra have been observed in the 30 - 90 nm spectral region by charge exchange collision. New lines are identified.

Introduction

Charge exchange collision spectroscopy between multicharged ions and neutrals is a good technique to obtain new spectra [1] of these multicharged ions. The particularity of this excitation, is suitable for line identification :
- selectivity of the capture and possible prediction of the populated nl sublevels [2,3],
- possible discrimination between one and two electron capture by the maximum level n excitated, or with double collision by pressure variation ,
- variation the selective n level excitated by change of the target (ionisation potential).
We present here our preliminary results on XeVIII and XeVII obtained by this method.

$Xe^{8+, 7+}$ ions produced by a 10 GHz E.C.R. ion source at an energy of 160 - 140 kev, are sent after magnetic selection, in a charge exchange chamber filled with He or H_2 . A 3m - VUV grazing incidence spectrometer equipped with a 300 lines/mm grating blazed at 51.2 nm and a channel electron multiplier, analyse the light emitted at 90° of the incident ion beam.

Results and discussion

For line identification we have used the results obtained in a theta pinch plasma [4,5] or by beam foil spectroscopy [6,7].
In XeVIII we have observed the already classified 5s - 5p, 5p - 6s, 5p - 5d, 5d - 5f, 4f - 5g transitions. New observed lines (Table I) are identified as the 5d - 6f,

5f - 5g and 6p - 7s transitions. These measurements permit to deduce the energy of the 6f and 6g levels in XeVIII respectively to 593910 cm^{-1} and 656850 cm^{-1}.
In XeVII the known $5p^3P^\circ$- $5d^2D$, $5p^3P^\circ$ - $6s^3S$ transitions are observed. We have also observed the λ 81.6 - 79.8 - 73.7 - 72.3 nm components of the $5s5p^3P^\circ$ - $5p^2\ ^3P$ multiplet. But we did not observe the λ 71.4 nm line and a weak line may be the λ 66.0 nn line.The line observed at λ 82.8nm[6] is the second order of the λ 41.47nm component of the$5p\ ^3P^\circ$ - $6s^3S$ transition.
In the singlet system of XeVII only the λ 69.81 nm 5s - 5p transition is known. The two lines at λ 45.77 and 60.80 nm observed both during the collisions of Xe^{8+} and Xe^{7+} with He or H_2 are identified as XeVII lines. In the collisions of Xe^{8+} a two electron capture process is involved with spin conservation. Predictions with the MCDF code[8] show that the λ 45.77nm line may be identified as the $5p^1P$ - $6s^1S$ transition and the λ 60.80 nm line may be the $5d^1D$ - $5f\ ^1F$ transition instead of the 5p - 5d transition which is blend with the 5s - 5p transition.

Table I New lines in XeVIII and VII

	λ (nm) ± 0.05	identification
XeVIII		
	35.21	$5d\ ^2D_{5/2}$ - $6f\ ^2F^\circ_{7/2}$
	35.57	$5d\ ^2D_{3/2}$ - $6f\ 2F^\circ_{5/2}$
	62.86	$5f\ ^2F^\circ$- $6g^2\ G$
	82.00	$6p\ ^2P^\circ_{1/2}$ - $7s\ ^2S_{1/2}$
	87.30	$6p\ ^2P^\circ_{3/2}$ - $7s\ ^2S_{1/2}$
XeVII		
	45.77	$5p\ ^1P_1$ - $6s\ ^1S_0$
	60.80	$5d\ ^1D_2$ - $5f\ ^1F_3$

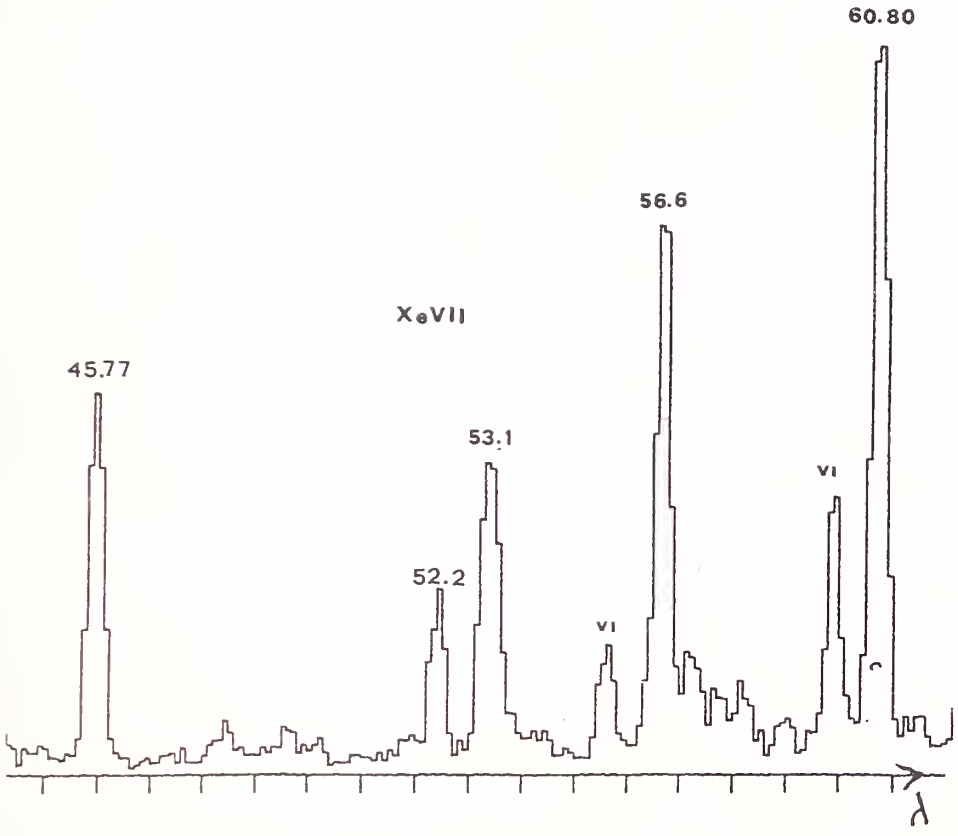

Part of the Xe7+ + He spectrum

References

1 M. Druetta, S.. Martin and J. Desesquelles
Nucl. Instrur. Meth B23, (1987), 268

2 A. Niehauss Phys. B 19, (1986), 2929

3 J. Burgdörfer, R. Morgenstern and A. Niehauss Phys B 19, (1986), L507

4 J.R. Roberts, E.J. Knystautas and S. Sugar J. opt. Soc. Am. 69, (1979), 1620

5 E.J. Knystautas, S. Sugar and J.R. Roberts J. opt. Soc. Am. 69, (1979), 1726

6 J.A. Kernahan, E.H. Pinnigton, J.A. O'Neill, J.L. Bahr and K.E. Donnelly
J. opt Soc. Am 70, (1980), 1126

7 S. Bashkin, R. Hallin, J. Leavitt, V. Litzenard and D. Walker
Phys. Scipta 23, (1981), 5

8 J.P. Desclaux Comp. Phys. Comm. 2, (1975), 31

Transition element spectra by high resolution Fourier transform spectrometry

Jon. E. Murray*, J. Pickering, G. Nave+, R. C. M. Learner & A. P. Thorne
Blackett Laboratory, Imperial College, London SW7 2BZ
(now at Harvard-Smithsonian Center for Astrophysics, Cambridge MA 02138)*
(+ now at Lund university, Department of Physics, Solvegatan 14, Lund Sweden)

Introduction

The needs of astrophysicists for new and improved atomic data have been emphasised in the previous meetings in this series and in many published papers. High resolution Fourier transform spectroscopy (FTS) is making an important contribution to both the accuracy and the completeness of the spectra of neutral and singly ionised atoms over a wavelength range that has now been extended from the near infra-red to 180 nm in the VUV.

The FTS advantages of linear ($\sim 1 : 10^8$) wavenumber scale, high resolution, and good light throughput combine to offer accurate wavenumbers (0.001 cm^{-1} for strong lines), with quantifiable errors, and the ability to make observations on weak lines and to resolve hyperfine structure. At Imperial College, in association also with the National Solar Observatory and Lund University, work has been proceeding on the astrophysically important transition element spectra. This paper describes the current status of this work.

The existing data base

The need for reliable f-values is well known. What is more surprising is the age and uncertainty of much of the wavelength data. Many spectra have not been measured since the publication of the Revised Multiplet Tables [1] in 1952. Moreover, closer examination of these tables reveals that they are in many cases a republication of very much earlier values, some of them obtained before 1910 - see, e.g., [2]. The uncertainties associated with the published wavelengths are rarely known, and many weak lines are missing.

The inadequacy of the data base has been highlighted by the results from the Hubble Space Telescope. In order to model the recorded spectra, data on weak lines of abundant elements and on isotope shifts and hyperfine structure are all required, in addition to more accurate wavelengths and f-values - see, e.g., [3].

Experimental

The spectra have been recorded on a Fourier transform spectrometer covering the range from about 900 nm to 180 nm, using either the prototype instrument developed at Imperial College [4] or the commercial version of it made by Chelsea Instruments. The maximum spectral resolution, 0.025 cm^{-1}, is sufficient to resolve fully the lines from the hollow cathode lamp used to excite the spectra. This lamp was run at currents up to 750 mA with carrier gas pressures of a few torr of Ne or Ar. Fig.1 shows examples from the Cr & Co spectra.

Wavenumber accuracy

The transformed and phase-corrected spectra were analysed by the DECOMP program developed by J.W.Brault, which allows a Voigt profile to be least-squares fitted to each line. The precision with which the centre of a symmetric line can be determined is given by its width divided by twice its signal-to-noise ratio. The high resolution ensures that the line width is actually the Doppler width, while the high light throughput maximises signal- to-noise ratio. The fact that the noise in our instrument is almost independent of wavenumber allows a quantitative value to be set on precision for each line.

Although the FTS wavenumber scale is accurately linear to within the stability of the monitoring laser (better than $1 : 10^8$), the absolute scale must be obtained from one or more standards (which do NOT need to be distributed through the spectral range as in grating spectrometry). A set of blue Ar II lines measured by Norlen [5] has been used to calibrate strong Fe lines in the same spectral

region, and the calibration has then been extended to both longer and shorter wavelengths by means of overlapping spectral regions. The procedure is fully described in three papers on recommended iron standards [6,7,8]. The calibration is accurate to a few parts in 10^8, corresponding to 0.001 cm^{-1} in the visible and 0.002 cm^{-1} in the UV. A stainless steel hollow cathode has been used to put strong lines of Cr and Ni on the same scale as the Fe.

Current state of work

Fe I and Fe II

The combination of our measurements with those taken in the IR at NSO with a similar source has resulted in a set of about 29,000 lines over the range 5.5μm to 180 nm, some 11,500 of which are still unassigned transitions. Compared with previous measurements, the number of lines in increased by a factor of about 5 and the wavenumber accuracy is in general improved by an order of magnitude. Work on assignment is in progress in collaboration with S.Johansson, and a revised multiplet table for Fe I is in preparation. The assignment of the high $4f$ [9] and $5g$ (in progress) states has particular relevance to solar observations. As mentioned above, three subsets of Fe I and Fe II lines have been selected as recommended wavelength standards for the visible [6], UV [7] and IR [8] respectively.

Cr I and Cr II

About 10,000 lines have been measured in the visible and UV a significant increase over previous data (Fig.1). Some 40% of these new observations are unassigned. These measurements have allowed us to revise over half of the currently known energy levels, 539 [10] , many of them derived from more than 50 lines, with an uncertainty of 0.001 cm^{-1}. There are significant differences from the AEL levels [10], in some cases as much as 0.1 cm^{-1} (Fig.2). A line list will shortly be submitted for publication, and a revised multiplet table is in preparation.

Co I and Co II

The visible and UV spectra have been recorded. Nearly all lines show hyperfine structure, the resolution of which is limited by Doppler rather than instrumental width. The old data, published in 1952 [1], are very incomplete and do not include hfs. For example in one 6 nm section centred on 232 nm we have measured 47 lines, of which 15 have resolved hfs and only 19 are included in previous data. The level analysis will be done in collaboration with colleagues at Lund, and meanwhile we are determining hfs splitting factors (Fig.3).

Ti I and Ti II

We have started to measure branching ratios in these spectra. These will be combined with lifetimes measured by Lawler's group by laser techniques to give absolute f-values.

References

1. C.E.Moore,*An Ultraviolet Multiplet Table*, NBS Circular 488, 1952
2. R.C.M.Learner, J.Davies & A.P.Thorne, *Accurate wavelengths for the Th-Nd chronometer*, Mon.Not.R.Astr.Soc.**248**, 414-418, 1991
3. D.S.Leckrone et al.,*First results from the GHRS*, Ap.J. **377**,L37-40, 1991
4. A.P.Thorne et al., *A Fourier transform spectrometer for the VUV*, J.Phys.E **20**, 54-60, 1987
5. G.Norlen,*Wavelengths and energy levels of Ar I and Ar II*, Phys.Scr. **8**, 249-268, 1973
6. R.C.M.Learner & A.P.Thorne,*Wavelength calibration of FT emission spectra with applications to Fe I* J.Opt.Soc.Am.**B5**,2045-59, 1988
7. G.Nave, R.C.M.Learner, A.P.Thorne & C.J.Harris,*Precision Fe I and Fe II wavelengths in the UV* J.Opt.Soc.Am.**B8**, 2028-43, 1991
8. G.Nave, R.C.M.Learner, J.E.Murray, A.P.Thorne & J.W.Brault, *Precision Fe I and Fe II*

wavelengths in the IR, J.Phys.II **2**, 913-929, 1992
9. S.Johansson & R.C.M.Learner, *The lowest 4f subconfiguration of Fe I*, Ap.J.**354**, 755-762, 1990
10. J.Sugar & C.Corliss, *Atomic Energy Levels: K through Ni*, J.Phys.Chem.Ref.Data 14, Supp.2, 1985
11. C.C.Kiess, *Description and analysis of the first spectrum of chromium*, J.Res.NBS.**51**, 247-305, 1953.
12. C.C.Kiess, *Description and analysis of the second spectrum of chromium*, J.Res.NBS.**47**, 385-426, 1951.

Acknowledgements
We would like to take this opportunity to thank the following for their help, advice or funding of this work. The Science and Engineering Research Council, the National Solar Observatory (J. W. Brault), Mr Geoff Cox of Imperial College and Dr Peter L. Smith at the Center for Astrophysics.

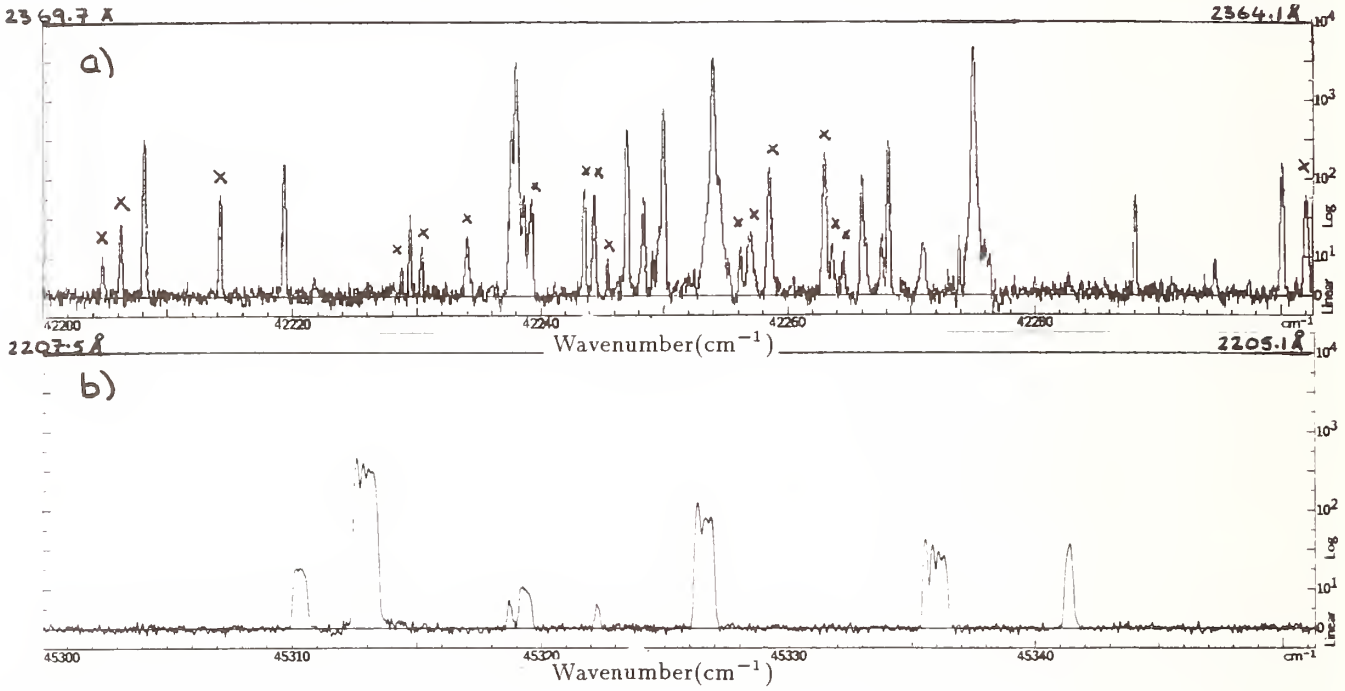

Fig.1: a) 5Å section of chromium spectrum centered on 2367Å. X marks those lines not seen in the work of Kiess [11][12].
b) 2.5Å section of cobalt spectrum centered on 2206Å.
The above intensities are arbitrary and plotted on a linear-log scale.

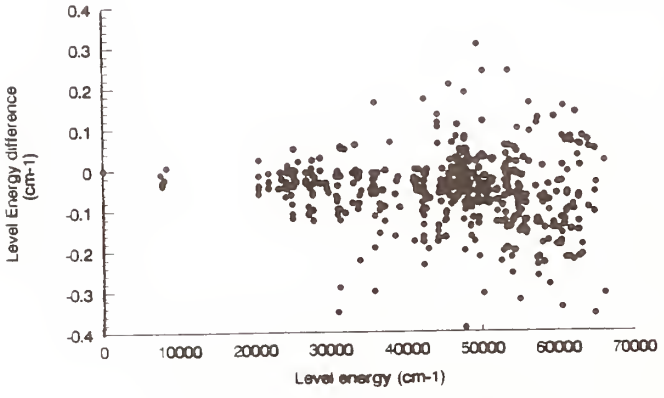

Fig.2 Cr level energy difference between this work and AEL[10]

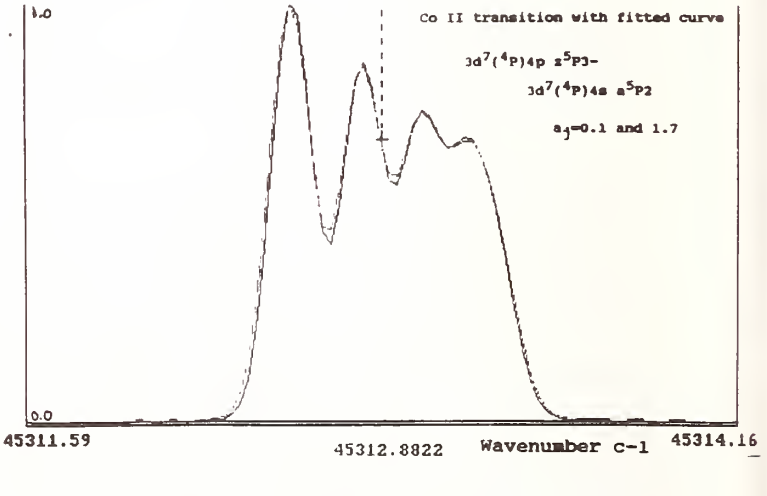

Fig 3. Example of fit to a Co II line with hfs.

Atomic Structure-theory

ATOMIC STRUCTURE IN ULTRASTRONG MAGNETIC FIELDS

E. P. LIEF and J. C. WEISHEIT

Space Physics & Astronomy Department, Rice University, Houston, TX 77251-1892, USA

Most previous studies of atoms in strong magnetic fields have been based on the assumption of a spherically symmetric shape, despite qualitative predictions of more complicated form. This paper presents equations for an approximate calculation of an axial charge density distribution in the Landau regime.

1. INTRODUCTION

Discoveries of magnetic white dwarfs and neutron stars in astrophysics, as well as developments in the physics of condensed matter and laser produced plasmas emphasize the issue of atomic behavior in strong magnetic fields.[1] Despite two decades' history of extensive work on the problem,[1-7] most quantitative approaches in the Landau regime were based either on a spherically symmetrical distribution of the charge density n, or a complete factorization, $n = n_\varrho(\varrho)n_z(z)$, in cylindrical coordinates (ϱ, z). In this paper we instead start with the Kadomtsev equation[2] and, using the factorization *ansatz*

$$n \equiv n(\varrho, z) = n_\varrho(\varrho)n_z(\varrho, z) \ , \tag{1}$$

with a parametric dependence of n_z upon ϱ, obtain an analytical solution for $n(\varrho, z)$. We also show that $n_\varrho(\varrho)$ is an almost uniform function of ϱ with a sharp fall at the edge, rather than a discrete set of coaxial cylinders, as was often assumed before. Our result has several features consistent both with Ruderman's[6] semi-quantitative treatment for multi-electron atoms and with some explicit computations for hydrogen.[8] By using the charge density distribution so obtained, one can calculate a Slater exchange term and then, after solving Hartree-Fock-Slater equations, derive energy levels and other spectroscopic information.

2. BASIC PRINCIPLES†

We consider a Z-electron atom in a high magnetic field $\vec{B}$ which is parallel to the z-axis. If $B \gg Z^{4/3}$ then the energy of the motion in $x - y$ plane is much greater than the energy of the motion in the z direction. This is the Landau regime, in which the z-distribution of the charge density can be treated in a one-dimensional Thomas-Fermi model. If, moreover, $B \gg Z^3$ there is only one electron in each magnetic sublevel m. We will consider this particular case.

Solving the Kadomtsev equation[2] for a one-dimensional, Thomas-Fermi model together with the Poisson equation, we get for n

$$\Delta n^2 = \frac{B^2 n}{2\pi^3} \ . \tag{2}$$

In cylindrical coordinates the non-linear equation for $n_z \equiv n_z(\varrho, z)$ can be written in the form

$$\frac{\partial^2 n_z^2}{\partial \tilde{z}^2} + \frac{\partial^2 n_z^2}{\partial \tilde{\varrho}^2} + C(\tilde{\varrho})\frac{\partial n_z^2}{\partial \tilde{\varrho}} = -A(\tilde{\varrho})n_z^2 + D(\tilde{\varrho})n_z \ , \tag{3}$$

where $\hat{\varrho} = \sqrt{2/B}$ is the quantum cyclotron radius, which serves as a natural unit of length in the problem, and where

$$\tilde{\varrho} = \varrho/\hat{\varrho} \ , \quad \tilde{z} = z/\hat{\varrho} \ , \quad A(\tilde{\varrho}) = \left(\frac{\partial^2 n_\varrho^2}{\partial \tilde{\varrho}^2} + \frac{1}{\tilde{\varrho}}\frac{\partial n_\varrho^2}{\partial \tilde{\varrho}}\right)/n_\varrho^2 \ , \quad C(\tilde{\varrho}) = \frac{1}{\tilde{\varrho}} + \frac{2}{n_\varrho^2}\frac{\partial n_\varrho^2}{\partial \tilde{\varrho}} \ , \quad D(\tilde{\varrho}) = 2/(\pi^3 \hat{\varrho}^2 n_\varrho) \ . \tag{4}$$

If we neglect the term $D(\tilde{\varrho})n_z$ in Eqn. (3), we will get a simple scaling relation: the magnetic field B determines the dimensions of an atom via $\varrho = \sqrt{2/B}$, but the form of the electron density distribution remains the same.

† We use atomic units. In particular, the unit of magnetic field is $B_0 = 2.35 \times 10^9$ Gauss

3. SOLUTION OF THE KADOMTSEV EQUATION IN CYLINDRICAL COORDINATES

We assume that the radial wavefunctions are just Landau wavefunctions,

$$\psi_{n=0,m}(\tilde{\varrho}) = \frac{e^{im\phi}}{\sqrt{\pi|m|!}} \frac{\tilde{\varrho}^{|m|}}{\dot{\varrho}} e^{-\tilde{\varrho}^2/2} \quad . \tag{5}$$

It has been shown by others that for the case $B \gg Z^3$ there is only 1 electron in each magnetic sublevel, m. This quantum number takes integer values from $-(Z-1)$ to 0. It therefore follows that

$$n_\varrho(\tilde{\varrho}) = \sum_{m=0}^{-(Z-1)} |\psi_{n=0,m}(\tilde{\varrho})|^2 = \frac{1}{\pi\dot{\varrho}^2} e^{-\tilde{\varrho}^2} \sum_{m=0}^{-(Z-1)} \frac{\tilde{\varrho}^{2|m|}}{|m|!} \simeq \frac{1}{\pi\dot{\varrho}^2} \quad (\tilde{\varrho} < \sqrt{Z}) \ , \tag{6}$$

$$\simeq 0 \quad (\tilde{\varrho} > \sqrt{Z}) \ .$$

The Landau wavefunctions Eqn.(5) strongly overlap, a fact that justifies the statistical treatment of the Thomas-Fermi type.

Complete factorization, $n(\varrho, z) = n_\varrho(\varrho) n_z(z)$, enables easy analytical solution of Eqn.(3), but such factorization is formally valid only if $A \equiv 0$ and $D = const.$

If we allow a parametric dependence of n_z on ϱ, we obtain a more realistic description of the atom in a strong field. Although we do neglect any explicit dependence on n_z on $\tilde{\varrho}$, such dependence is implicit, because of the forms $A(\tilde{\varrho})$ and $D(\tilde{\varrho})$ in the equation that can be obtained from Eqn. (3)

$$\frac{\mathrm{d}^2 n_z^2(\tilde{z})}{\mathrm{d}\tilde{z}^2} = -A(\tilde{\varrho}) n_z^2(\tilde{z}) + D(\tilde{\varrho}) n_z(\tilde{z}) \quad . \tag{7}$$

This equation also can be solved analitically, and explicit results for $n_z(\tilde{\varrho}, \tilde{z})$ are given in the following table, where C_2 is an arbitrary constant that can be calculated easily from the condition of normalization. The other integration constant, C_1 was chosen to get

$$\frac{\mathrm{d}n_z(\tilde{z})}{\mathrm{d}\tilde{z}}|_{\tilde{z}=-C_2(\tilde{\varrho})} = 0 \tag{8}$$

$A(\tilde{\varrho})$	$n_z(\tilde{\varrho}, \tilde{z})$	$C_2(\tilde{\varrho})$
< 0	$-\frac{4D(\tilde{\varrho})}{3A(\tilde{\varrho})} \sinh^2[\frac{(\tilde{z}+C_2(\tilde{\varrho}))\sqrt{-A(\tilde{\varrho})}}{4}]$	Computed for the normalization
$= 0$	$\frac{D(\tilde{\varrho})}{12}(\tilde{z} + C_2(\tilde{\varrho}))^2$	$-(\frac{18}{D(\tilde{\varrho})\tilde{\varrho}})^{1/3}$
> 0	$\frac{4D(\tilde{\varrho})}{3A(\tilde{\varrho})} \sin^2[\frac{(\tilde{z}+C_2(\tilde{\varrho}))\sqrt{A(\tilde{\varrho})}}{4}]$	Computed for the normalization

4. NUMERICAL RESULTS

Some calculations for a carbon atom in a field of $2 \times 10^{12} G$ are shown in Fig.2, which displays 3-dimensional and contour plots of the electron density. The graphs have features consistent with Ruderman's treatment[6] and with numerical calculations for hydrogen.[8]

Our next task is to solve numerically the full Eqn. (3) and to derive effects due to a point nucleus Z. Eqn. (3) also gives an opportunity to study weaker magnetic fields if instead of expresssion Eqn. (6) we substitute a corresponding form of n_ϱ in Eqn. (4).

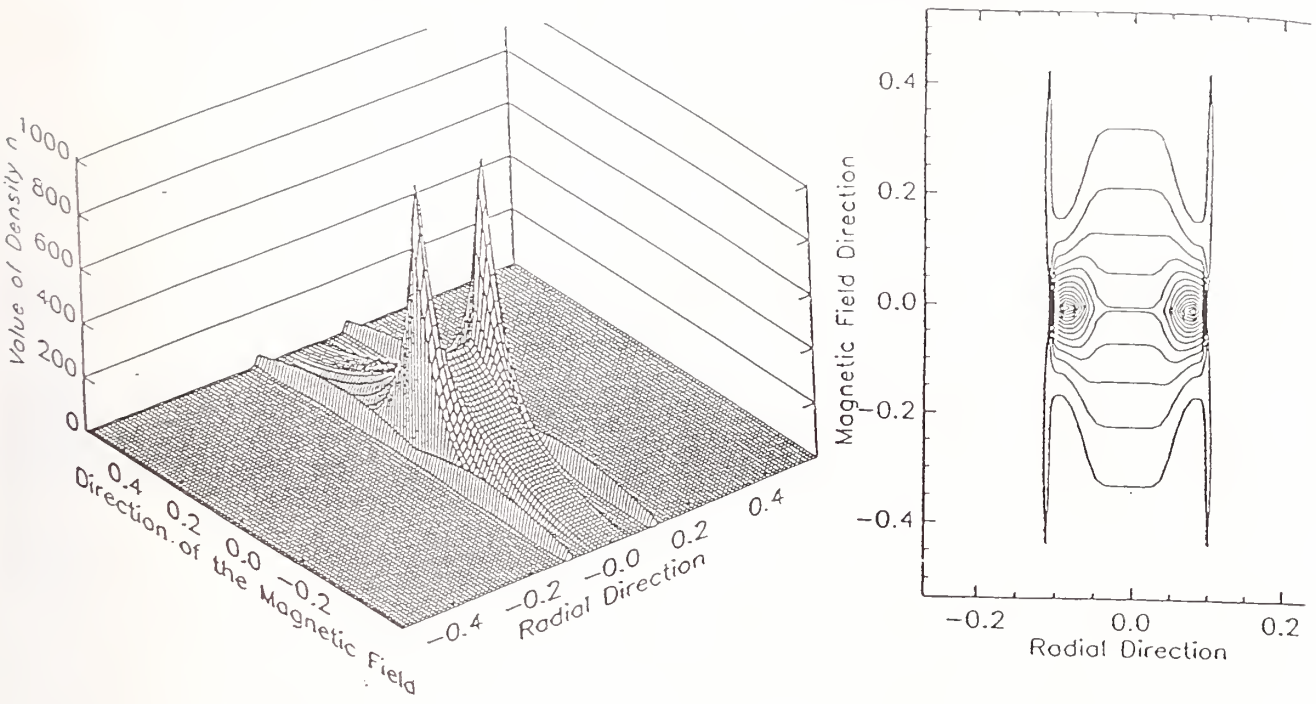

FIGURE 1

Electron density $n(\varrho, z)$ cross section in $\varrho - z$ plane passing through the center of the atom. Left: a 3-dimensional plot, right: a contour plot

5. SUMMARY

To this point our major conclusions are:

- For an atom in a strong magnetic field, the Kadomtsev equation can be rewritten in a general form with partial derivatives, Eqn. (3), using the factorization *ansatz* to reflect natural, axial symmetry.
- Under certain assumptions the equation obtained can be solved analytically. The solutions have an elongated form and are contracted both in length and width, as expected.
- Radial wavefunctions of individual electrons in a high magnetic field strongly overlap and lead to an almost uniform "radial" electron density that falls sharply at the edge.
- A solution of the simplified Eqn. (7) has features consistent with Ruderman's semi-quantitative predictions,[6] and with detailed numerical calculations for hydrogen.[8]

ACKNOWLEDGEMENTS

We thank the U.S. Department of Energy for supporting this research under grant DE-FG05-91ER14213.

REFERENCES

1) Garstang R. H. 1977, Rep. Progr. Phys. **40**, 105.
2) Kadomtsev, B. B. 1970, Soviet Phys. JETP, **31**, 945.
3) Rau, A. R. P., Mueller, R. O., Spruch, L. 1975, Phys. Rev. A **11**, 1865.
4) Neuhauser, D., Koonin, S. E., Langanke, K. 1987, Phys. Rev. A **36**, 4163.
5) Spruch, L. 1991, Rev. Mod. Phys. **63**, 151.
6) Ruderman, M. 1974, in *Physics of Dense Matter*, ed. C.J.Hanzen and L.H.Volsky (D.Reidel Publishing Company: Dodrecht, Holland / Boston, MA), p.117.
7) Lieb E.H., Solovej J.P., Yngvason J., Phys. Rev. Lett. **69**, 749 (1992).
8) Rösner, W., Wunner, G., Herold, H., Ruder, H. 1984, J. Phys.B: At. Mol. Phys. **17**, 29.

Fine Structure Splittings in the Ground State of B-Like Ions: Rb^{32+} --Xe^{49+}

M. A. Ali
Howard University, Washington, D.C. 20059

and

Y.-K. Kim
NIST, Gaithersburg, MD 20899

Forbidden lines due to transitions between ground levels of the n=2 "complex" in ions are of great interest for plasma diagnostics. Edlén[1] fitted the difference between experimental and multiconfiguration Dirac-Fock (MCDF) fine structure results of Cheng et al.[2] to a screening formula that includes nuclear charge Z and a few fitting parameters to allow for correlation and relativistic corrections partly missing in the theoretical values, and predicted unknown fine structure splittings of B-like ions up to Kr^{31+}. The original multiconfiguration Dirac-Fock level energies of Cheng et al.[2] were obtained by optimizing the relativistic radial orbitals and the configuration mixing coefficients (MCDF-OL) for each level separately. This procedure leads to a nonrelativistic offset[3], i.e., a nonvanishing (and spurious) fine structure splitting in the nonrelativistic limit between the levels arising from the same LS term. Edlén used for his fitting uncorrected fine structure splittings, which contained these spurious nonrelativistic offsets. Furthermore, Cheng et al.[2] used the $<r>$ method,[4] which uses expectation values of r of MCDF orbitals, in estimating the effect of screening in the self-energy part of the quantum electrodynamic (QED) corrections.

Since then other methods have been developed to estimate the self-energy screening. One of them is to use the charge density of MCDF orbitals near the nucleus; we shall refer to this as the ρ method. The ρ method leads to results on transition energies that agree better with experiment than the $<r>$ method, particularly for high-Z ions. Our MCDF codes use these newer methods to yield MCDF-OL energies. Moreover, new experimental results have also become available since Edlén published his recommended fine structure splittings. Also, Kim and Weiss[5] pointed out that, for the calculation of the fine structure splitting, MCDF calculations should include all j-j configurations which are degenerate in the limit of infinite Z and thus belong to the same "relativistic Coulomb complex."[5]

The difference between experimental and MCDF fine structure splittings may then be expected to be a smooth and slowly varying function of Z although the functional dependence may be a complicated polynomial in Z and Z^{-1} over an extended range of Z. This difference can then be used not only for identifying irregularities in experimental data, but also to interpolate and extrapolate to estimate unknown fine structure splittings.

We show the difference, Expt. − MCDF, between experimental and theoretical values of fine structure splittings corrected for nonrelativistic offsets for Z=19-36 in Fig. 1 using the ρ and $<r>$ methods to estimate QED corrections. We see that the curve with the ρ method varies almost linearly with Z while the curve with the $<r>$ methods rises sharply with Z. The

fine structure splitting for cobalt (Z=27) does not follow trends of the rest of the curves, suggesting that the experimental value might be in error. We fitted the ρ curve to a linear formula and obtained:

$$\Delta(\rho) = 26.444\ Z - 479.00 \quad (cm^{-1})$$

with a standard deviation of 37.08 cm^{-1}.

This fitted formula smooths fluctuations in experimental data, and hence fine structure splittings obtained from the formula should be more reliable than the original experimental data. We used this fitted formula to obtain predicted fine structure splittings for Rb^{32+} to Xe^{49+} in Table 1. The table also lists Edlén's predictions and known experimental values. Our predictions up to Mo^{37+} are probably accurate within 40 cm^{-1}. In the absence of experimental data for neighboring ions to define the difference curve, those for Tc^{38+} through Xe^{49+} are likely to be accurate within 80 cm^{-1}.

References

1. B. Edlén, Phys. Scr. **28**, 483 (1983).
2. K. T. Cheng, Y.-K. Kim, and J. P. Desclaux, At. Data and Nucl. Data Tables **24**, 111 (1979).
3. Y.-K. Kim and K.-N. Huang, Phys. Rev. A **26**, 1984 (1982).
4. Y.-K. Kim, D. H. Baik, P. Indelicato, and J. P. Desclaux, Phys. Rev. A **44**, 148 (1991).
5. Y.-K. Kim and A. W. Weiss, Bull. Am. Phys. Soc. **35**, 1188 (1990).

Fig. 1. FINE STRUCTURE SPLITTING IN B-LIKE IONS

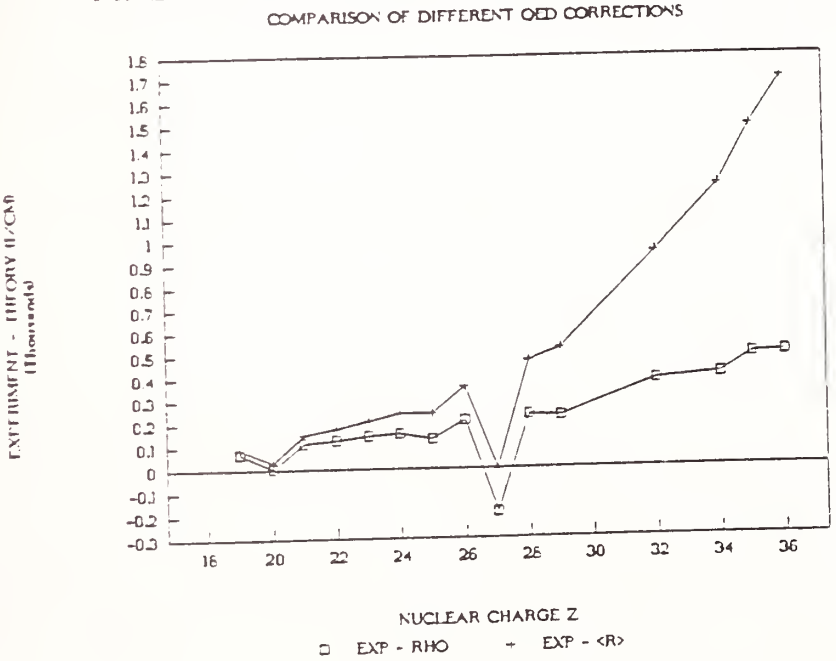

Table 1. MCDF-OL, fitted and experimental fine structure splittings in the ground state of boron-like ions (in cm^{-1}) using QED corrections for K^{14+} through Xe^{49+}.

Ion	Expt.	Edlén[1]	Theory	Ion	Theory
K^{14+}	28990	29004	28944	Rb^{32+}	555008
Ca^{15+}	36520	36611	36565	Sr^{33+}	623391
Sc^{16+}	45637	45634	45599	Y^{34+}	698071
Ti^{17+}	56240	56240	56216	Zr^{35+}	779449
V^{18+}	68610	68609	68595	Nb^{36+}	867946
Cr^{19+}	82926	82933	82927	Mo^{37+}	963997
Mn^{20+}	99360	99412	99413	Tc^{38+}	1068058
Fe^{21+}	118270	118260	118268	Ru^{39+}	1180599
Co^{22+}	139290	139702	139713	Rh^{40+}	1302109
Ni^{23+}	163960	163975	163988	Pd^{41+}	1433095
Cu^{24+}	191280	191328	191341	Ag^{42+}	1574094
Zn^{25+}		222021	222032	Cd^{43+}	1725648
Ga^{26+}		256329	256335	In^{44+}	1888334
Ge^{27+}	294551	294539	294536	Sn^{45+}	2062739
As^{28+}		336950	336937	Sb^{46+}	2249480
Se^{29+}	383833	383876	383850	Te^{47+}	2449199
Br^{30+}	435644	435644	435602	I^{48+}	2662565
Kr^{31+}	492560	492596	492537	Xe^{49+}	2890260

COMPLEX QUANTUM DEFECT AND SCREENING PARAMETERS FOR AUTOIONIZING STATES OF TWO- AND THREE-ELECTRON ATOMS FROM LOWEST-ORDER PERTURBATION THEORY

Lonnie W. Manning and Frank C. Sanders
Department of Physics, Southern Illinois University-Carbondale
Carbondale, IL 62901-4401

In the usual quantum defect theory, the energies for a Rydberg series of autoionizing states of an N-electron atom can be written as a sum of the threshold energy for the series, E_{th} plus the energy of the Rydberg electron,

$$E_r = E_{th} - \frac{(Z-\sigma)^2}{2(n-\mu)^2}.$$

Here σ is the screening of the nuclear charge, Z, by the core electrons, n is the principal quantum number of the Rydberg electron, and μ is the quantum defect. By making μ (or σ) complex one can also include the width of these autoionizing states in the method. In practice, σ and/or μ are generally obtained by fitting to experimental and theoretical data for a few members of the Rydberg series.

In recent work on autoionizing states of two- and three-electron atoms, we have found that the lowest-order perturbation expansion coefficients of the energy and width provide useful information for the classification of such Rydberg states over a broad range of Z and n. These coefficients can also yield reasonably accurate values of the resonance positions and widths. In the present work, we make use of these coefficients within the quantum defect method to obtain quantitatively useful data for such states of two- and three-electron atoms lying below the n=2 ionization threshold. The parameters of the method, and even the appropriate choice of approximant for a particular Rydberg series, are entirely determined by these lowest-order coefficients. Hence, the method is *"ab-initio"*, requiring no additional input.

In Z-dependent perturbation theory, the Hamiltonian is written as $H_0 + \lambda H_1$ where

$$H_0 = \sum_i^N (-\tfrac{1}{2}\Delta_i - \tfrac{1}{r_i}); \quad H_1 = Z^{-1} \sum_{j>i}^N \tfrac{1}{r_{ij}}.$$

The energy and width are given as expansions in $\lambda = 1/Z$: $E = \sum_{n=0}^{\infty} Z^{2-n}\epsilon_n$; $\Gamma = \sum_{n=2}^{\infty} Z^{-n}\Gamma_n$. σ can also be expanded in powers of λ, $\sigma = \sum_{k=0}^{\infty} \sigma_k \lambda^k$. The coefficients, σ_k, can thus be expressed in terms of the conventional perturbation coefficients of E_r and E_{th}. Hence, $\sigma_o = n^2(\epsilon_1 - \epsilon_1^{th})$ which, as expected, will approach $N-1$ in the limit of infinite n. Similar relations can also be obtained for the quantum defect, μ. The lowest-order contribution is just $\mu_1 = n[N - 1 - n^2(\epsilon_1 - \epsilon_1^{th})]$.

There are several alternative approaches that could be attempted at this point. For those states with $\sigma_o \lesssim N-1$, σ is represented with sufficient accuracy by its zeroth-order value, σ_o, and a good approximant for the energy of such states is,

$$E_r \approx E_{th} - \frac{(Z-\sigma_o)^2}{2n^2}. \tag{1}$$

This expression is equivalent to truncating E_r to second-order in λ and approximating ϵ_2 by $\epsilon_2^{th} - \frac{\sigma_o^2}{2n^2}$. Thus, for large values of Z, the error in E_r is a term constant in Z and of $O(1/n^3)$. For highly excited states, this difference rapidly becomes negligible.

Physical considerations tell us that σ must be less than or equal to $N-1$ for all Z and n. Therefore, in those cases where $\sigma_o > N-1$, the usual quantum defect theory with $\mu \approx \mu_1$ and $\sigma = N-1$ is used,

$$E_r \approx E_{th} - \frac{(Z-N+1)^2}{2(n-\mu_1\lambda)^2}. \tag{2}$$

In actual practice, it was found that these two approximants could be more effectively replaced by two alternative formulae which yield improved results over a wide range of n and Z. Replacing the first of the above approximants (screening), we have utilized

$$E_r \approx E_{th} - \frac{(Z-N+1)^2}{2n^2} + \frac{(Z-N+1)(\sigma_o-N+1)}{n^2}. \tag{3}$$

As an alternative to the second of these approximants (quantum defect), we have utilized

$$E_r \approx E_{th} - \frac{(Z-\sigma_{qd})^2}{2(n-\mu_1\lambda)^2}. \tag{4}$$

where $\sigma_{qd} = N-1+[n^2(\epsilon_1 - \epsilon_1^{th}) - N + 1]\lambda$

To obtain the total width of these states, we let $n \rightarrow n - i\frac{\gamma}{2}$ while keeping the screening parameter a purely real number. The resonance position and width are then given by

$$E_r - i\frac{\Gamma}{2} = E_{th} - \frac{(Z-\sigma)^2}{2(n-i\frac{\gamma}{2})^2}.$$

and the total width is given by $\Gamma = \frac{\gamma}{n^3}(Z-\sigma)^2\,(1+(\frac{\gamma}{2n})^2)^{-2}$. γ, the "reduced width", can also be written as an expansion in λ, and relations between these

and the Γ_n yield a simple approximant to the third-order width: $\Gamma_3 \approx -2\sigma_o\Gamma_2$. Thus, the total width is approximated here by,

$$\Gamma \approx \Gamma_2(1 - 2\tfrac{\sigma_o}{Z}), \tag{5}$$

Results are presented for the 36 lowest $^{1,3}S^e$ and 48 lowest $^{1,3}P^o$ autoionizing states for two-electron atoms, and the 36 lowest ^2S autoionizing states for three-electron atoms lying between the first and second ionization thresholds. Exact values for ϵ_1 and Γ_2 are presented, together with the corresponding values of σ_o and μ_1. Estimates of the resonance positions and widths for these states are compared with some recent experimental and theoretical values available in the literature. This comparison indicates that these lowest-order values are not only useful in the high-Z and n limit, but are also capable of giving reasonable estimates of both the resonance position and width for fairly low values of Z and n.

The three electron, doublet S-states presented here are all four-fold degenerate. Classification of these states is complicated by the fact that the mixing coefficients of the individual components of the zero-order wave functions behave erratically for the first few members of this rydberg sequence. Similarly, the lowest-order widths also exhibit this erratic behavior. These states can be classified into four unambiguous series, however, based on their first-order energies. These first-order energy expansion coefficients exhibit very smooth behavior with increasing degree of excitation. Of particular interest are two of these series of states, which become nearly degenerate in first-order at $n = 6$. This near degeneracy is the source of the erratic behavior of the mixing coefficients noted above. These particular states correspond to autoionizing states of the atom which, for high n, decay to the $(1s2s)^1$S and $(1s2p)^3$P states, respectively. At $n = 6$ each of these two states shows a significant enhancement of the component of the other state, so that each state becomes less "pure" and more of a mixture of the two components. Nevertheless, these states can be unambiguously classified by their first-order energies. Although this near degeneracy has little apparent consequence for the resonance position of these states, the effect on the widths is marked. Note that this irregular behavior of the widths along the Rydberg series is essentially due to the individual perturbation expansion coefficients, ϵ_1 and Γ_2, and can therefore be expected to persist over a range of values of Z.

Finally, it should be noted that there is little information available in the literature for the widths of many of these states. Of particular interest are those states where the total widths are extremely small. This is the case for all the Rydberg series considered here as the level of excitation increases. For such states, it becomes very difficult to calculate such widths variationally with any precision. Since the extent to which the Γ_2 accurately represent Γ improves rapidly as Z and n increase, the present results can be quantitatively useful, especially in the absence of other reliable results.

PAIR FUNCTION CALCULATIONS FOR SCREENED COULOMB POTENTIALS[1]

ZHENGMING WANG, YONG YAN, HONGBIN ZHAN and PETER WINKLER
Department of Physics, University of Nevada, Reno.

ABSTRACT

The results of pair function calculations of ground and excited state energies of H^- and He in various plasma environments are compared to very accurate calculations. The stability of the negative hydrogen ion in screened Coulomb potentials has been studied in particular.

1 INTRODUCTION

Numerical pair functions[1] have become an important tool in the study of atomic structure. For helium-like systems they offer a rather convenient way to obtain accurate, numerical bound-state wave functions. For larger systems the construction of pair functions is a feasible alternative to the correlation of single particle functions[2,3] .While the ultimate goal of an *ab initio* theory of general plasmas is still a development of the future considerable progress has been made for non-ideal hydrogen plasmas[4] and to some extent for helium plasmas[5]. A welcome alternative is offered by two-component plasma calculations based on density functional theory[6]. Such calculations determine distribution functions for ion-ion and ion-electron pairs. Potentials derived from such quantities allow the inclusion of plasma effects into atomic structure and scattering calculations in some average way.

Here we have studied, in particular, the stability of the negative hydrogen ion in various screening environments. We proceed from the simple Debye screening model to more realistic potentials obtained from pair distribution functions of two-component plasma simulations.

---

[1] Work supported by the Division of Chemical Sciences, Office of Basic Energy Sciences, Office of Energy Research, U.S. Department of Energy.

2 THE ATOMIC PAIR FUNCTION

Details of the theory of atomic pair functions can be found in a publication by Mårtensson[7]. We have developed a modified computer code that allows the inclusion of plasma screening.

For two-electron systems the equation for the pair function ρ_{ab} is given by

$$[\epsilon_a+\epsilon_b-h_0(1)-h_0(2)]|\rho_{ab}\rangle = \sum_{rs\in D} |rs\rangle\langle rs|V|ab+\rho_{ab}\rangle - \sum_{cd\in D} \rho_{cd}\langle cd|V|ab+\rho_{ab}\rangle \qquad (1)$$

Here D is the model space spanned by a subset of eigenfunctions of an approximate Hamiltonian consisting of a sum of single-particle operators $h_0(i)$. Starting with an initial guess for ρ on the right we use the function obtained in the (n-1)st step as input for the n-th iteration. The one-electron problem connected with h_0 has to be solved first (here given for Debye screening):

$$h_0(i) = -\nabla_i^2/2 - Z\exp(-r_i/D)/r_i. \qquad (2)$$

More realistic choices for u(r) have been studied also.

3 RESULTS

In Table 1 we present results of the present calculation for inreasing screening comparing the ground state energy of H^- to the binding energy of H. Both values decrease with D. We notice that at values of $D \approx 34$ the two-electron system ceases to be bound. What happens when we go beyond the bound regime? Does the system emit the second electron immediately into the continuum or do features of the bound system survive ? Our calculations yield electron densities in the continuum that are not much different from those of bound states. Similar findings for screened one-electron systems have been reported previously[8]. In table 2 we show results for the 1s3s - states of the helium atom near the critical screening value for which the system becomes unbound.

D	H-atom	H^--ion (N=45)	H^--ion (extrapolated)	H^--ion (exact)
∞	-0.500000	-0.527613	-0.527322	-0.527750
100	-0.490074	-0.508135	-0.508118	-0.508018
35	-0.472049	-0.472854	-0.472540	-0.472745
34.25	-0.471430	-0.471702	-0.471535	-0.471588
34	-0.471225	-0.471305	-0.471249	-0.471191
33.5	-0.470848	-0.470543	-0.470343	-0.470343
32	-0.469668	-0.468149	-0.467981	-0.468699

TABLE 1 The ground-state energy of the H^--ion for some values of the Debye parameter D is compared to the ground state energy of the neutral atom . Columns 3 and 4 show the results of the present calculation obtained on a grid of 45 by 45 points and the values of the Richardson extrapolation.

D	He-atom $\|1s3s\ ^1S\rangle$	He-atom $\|1s3s\ ^3S\rangle$	Orbital Energies 1s	3s
∞	-2.061907	-2.067574	-2.000000	-0.222222
100	-2.022529	-2.029193	-1.980074	-0.202088
50	-1.990510	-1.998564	-1.960298	-0.184795
20	-1.899884	-1.902935	-1.908184	-0.137318

TABLE 2 The energies of the 1s3s - states of the He-atom for some values of the Debye parameter D are shown together with the electron energies of the atom.

4 REFERENCES

1 Lindgren I. and Morrison J. 1986, *Atomic Many-Body Theory* (Heidelberg: Springer Verlag, 2nd edition).

2 Morrison J., J. Phys. B.: Atom.Molec.Phys. 6,2205 (1973).

3 Winkler P., Int. J. Quant. Chem. S 19, 201 (1986).

4 Lehmann H. and Ebeling W.,Z. Naturforsch. 46a, 583 (1991).

5 Förster A., Kahlbaum T., and Ebeling W. 1991, in *Proc. XX. Int. Conference on Phenomena in Ionized Gases* (in press).

6 Dharma-wardana M. W. C. and Perrot F., Phys.Rev.A26, 2096 (1982).

7 Mårtensson A., J.Phys.B.: Atom.Molec.Phys. 12,3995 (1979).

8 Wang Z., Winkler P., Pickup B. T., and Elander N., Chem. Phys. 135, 247 (1989).

Atomic properties from large-scale relativistic calculations

F. A. Parpia and C. F. Fischer

Computer Science Department
Box 1679, Station B
Vanderbilt University
Nashville, Tennessee 37235

The RSCF (relativistic self-consistent-field) and RCI (relativistic configuration interaction) programs are derivatives of the GRASP2 multiconfiguration Dirac-Fock package. RSCF and RCI are expressly designed for the construction of atomic models with large configuration state function bases [$O(1000)$ and up]. In addition to the atomic properties that can be computed using GRASP2 — level energies using the Dirac-Coulomb operator, corrections due to higher-order relativistic effects, and radiative transitions — nuclear motional corrections to level energies and diagonal hyperfine constants may be calculated with RCI. We describe RCI, RSCF, and a set of associated utility packages, and present examples of atomic properties computed using this approach to atomic structure.

The Multiconfiguration Dirac-Fock approach

The multiconfiguration (MC) Dirac-Fock (DF) method is based on the Dirac-Coulomb Hamiltonian:

$$H^{\mathrm{DC}} = \sum_{i=1}^{N} \left[c\boldsymbol{\alpha} \cdot \mathbf{p} + (\beta - 1)c^2 \right]_i + \sum_{i=1}^{N-1} \sum_{j=i+1}^{N} R_{ij}^{-1}$$

for an N-electron atomic system. Here $\mathbf{R}_{ij} = \mathbf{r}_i - \mathbf{r}_j$ and we use Hartree atomic units. The natural generalisation of the nonrelativistic orbital is the four component function,

$$\langle \mathbf{r} | nljm \rangle = \begin{pmatrix} P_{nlj}(r)\, \chi_{ljm}(\hat{\mathbf{r}}) \\ \mathrm{i} Q_{nlj}(r)\, \chi_{\bar{l}jm}(\hat{\mathbf{r}}) \end{pmatrix}.$$

We refer our readers to review articles [1, 2] for the details of the formalism, the trends of relativistic corrections, and an introduction to the literature. For our purposes it will suffice to note that all relativistic effects to order $1/c^2$ are included if the Dirac-Coulomb Hamiltonian is augmented by the Breit Hamiltonian,

$$H^{\mathrm{B}} = -\sum_{i=1}^{N-1} \sum_{j=i+1}^{N} \frac{1}{2R_{ij}} \left(\boldsymbol{\alpha}_i \cdot \boldsymbol{\alpha}_j + \frac{\boldsymbol{\alpha}_i \cdot \mathbf{R}_{ij}\ \boldsymbol{\alpha}_j \cdot \mathbf{R}_{ij}}{R_{ij}^2} \right).$$

The programs described in the remainder of this presentation are based on such a relativistic formalism.

RCI, RSCF, and the utility programs

The GRASP2 MCDF program [3] is a major revision of GRASP [4], in turn a major revision of MCDF+MCBP/BENA [5].

Extensive testing of GRASP2 has demonstrated that it is appreciably more stable than its predecessors. We attribute this to the relatively straightforward adaptation to the relativistic problem of the self-consistent-field (SCF) algorithms developed by Fischer and coworkers [6] for the nonrelativistic MC Hartree-Fock (HF) model, as well as to improved numerical integration, quadrature, and interpolation procedures.

It is natural to attempt to construct more sophisticated models of atoms as programs become more stable and computers become more powerful. Large-scale MCHF calculations have been carried out by Fischer and coworkers using the MCHF_ASP suite of programs [7] and derivatives. Here we describe revisions of the GRASP2 program carried out with the same scope.

Extensions to FORTRAN 77 permitting the run time allocation and deallocation of storage to arrays have been implemented in several compilers. Such *dynamic memory allocation* has been employed in RSCF [8] and RCI [8]. The elements of the lower triangle of the Hamiltonian matrix are stored in a sparse representation that reduces memory requirements when $\approx 33\%$ or more of the elements are zero.* In contrast to GRASP2, only the eigenvalues and eigenvectors (together, eigenpairs) of interest are computed and stored in RSCF and RCI. Eigenpairs are determined using the Davidson procedure [9] as implemented in a package due to Stathopoulos and Fischer [10]. These modifications have significantly reduced storage requirements and computational effort. Further improvements in efficiency in RSCF result from the elimination of all modules not required for the MCDF SCF problem. Similarly, in RCI all modules that apply only to the SCF problem have been eliminated.

The *normal* and *specific mass shifts* that result from nuclear translational motion can be estimated using RCI [11], as can the diagonal hyperfine constants A and B [12]. These capabilities go beyond those of GRASP2. The properties of radiative transitions could be estimated with GRASP2 and GRASP. This feature continues to be available in RCI.

Several utility packages are associated with GRASP2: a complete active space (CAS) [13] generator, JJCAS [14], programs for visualising atomic structure, and programs for computing coefficients for higher order numerical methods for the GRASP2 family of codes have been prepared. With few exceptions, CAS calculations are prohibitively expensive. A new package, GENASJJ, generates lists of configuration state functions (CSFs) associated with subspaces — referred to as *active spaces* (ASs) — of the CASs. Another new utility, MERGEORB, may be used to extract and combine orbital wavefunctions from GRASP2 or RSCF ORBOUT Files into a new ORBOUT File. Finally, MERGEJJAS, in preparation, will permit the merging of two or more CSF lists from GENASJJ.

Together, RSCF, RCI, GENASJJ, MERGEORB and MERGEJJAS form a fairly complete suite of programs for the computation of atomic properties using the MCDF formalism.

Large-scale relativistic calculations

With few exceptions, MCDF models of atoms have been constructed with substantially fewer than 1000 CSFs. We shall understand *large-scale* calculations to be those involving models with several hundred or more CSFs. Computations with a few thousand CSFs are now routinely carried out at Vanderbilt University using Sun workstations with 64MB or less of memory and 200MB or less of disk storage.

New approaches to the systematic study of atomic structure become possible using large-scale calculations. Different ASs may be used to construct models, the properties of which, in comparison with measurements, may be used to establish trends. This knowledge may then be applied to improve the reliability of theoretical models in other contexts.

An earlier modification of the GRASP2 program along the lines of RSCF was prepared by V. M. Umar, Z. Cai, and C. F. Fischer, and applied successfully to the prediction of the low-lying spectrum of the Pr IV ion [15]. This work, involving between 354 and 1708 CSFs in each of the largest calculations, was carried out on a network of Sun workstations.

We are currently studying the hyperfine structure of the $3d^2\,{}^3P_{1,2}$ levels of the Sc II ion using the programs described in the previous section. As observed first by Young *et al.* [16], the simplest DF and MCDF models cannot account for the measured value [17] of the diagonal hyperfine magnetic dipole parameter A. A summary of calculations completed to date appears in Table 1 below. New abbreviations used are: OL — optimal level calculation; S — single; D — double; R — replacement. The largest of these [a 3487 CSF CI calculation for the lowest level (1)] required less than 20 MB of storage and less than 12 hours of CPU time on a Sun SPARCstation 2.

* This applies to computers with 32-bit architectures; for 64-bit architectures the sparse representation is more efficient than a packed full representation when $\approx 50\%$ or more of the elements of the Hamiltonian are zeros.

Table 1: Measurement and calculations for the diagonal magnetic dipole hyperfine parameter of the $3d^2\,{}^3P_1$ level of Sc II.

Experiment [17]	$A = -107.3(6)$ MHz
1 OL 1: Reference CSF: $1s^2 2s^2 2\bar{p}^2 2p^4 3s^2 3\bar{p}^2 3p^4 3\bar{d} 3d\, J = 1$	-1.8
77 OL 2: $1s,\ldots,3d$ from 1 OL 1; $4s,\ldots,4f$ from SRAS of $3s,\ldots,4f$	-7.0
3487 CI 1: $1s,\ldots,4f$ from 77 OL 2; SDRAS of $3s,\ldots,4f$	-10.9
157 OL 2: $1s,\ldots,4f$ from 77 OL 2; $5s,\ldots,5g$ from SRAS of $3s,\ldots,5g$	-55.1
250 OL 2: $1s,\ldots,5g$ from 157 OL 2; $6s,\ldots,6h$ from SRAS of $3s,\ldots,6g$	-56.2
148 OL 2: $1s,\ldots,3d$ from 1 OL 1; $4s,\ldots,4f$ from SRAS of $2s,\ldots,4f$	-13.3
167 OL 2: $1s,\ldots,3d$ from 1 OL 1; $4s,\ldots,4f$ from SRAS of $1s,\ldots,4f$	-13.3
343 OL 2: $1s,\ldots,4f$ from 167 OL 2; $5s,\ldots,5g$ from SRAS of $1s,\ldots,5g$	-83.9

Future developments

We are currently revising the RSCF and RCI programs and associated utilities with a view to improving their computational efficiency and user interfaces. Experience gained from the parallelisation of the MCHF_ASP suite will be brought to bear in the preparation of parallel versions of RCI and RSCF for distributed and shared-memory parallel processors.

Acknowledgments

This work has been supported by the Department of Energy, Office of Basic Energy Sciences; and the National Science Foundation, under grant ASC-9005687.

References

[1] I. P. Grant, *Methods in Computational Chemistry* **2** (1988) 1
[2] P. Pyykkö, *Chemical Reviews* **88** (1988) 563
[3] F. A. Parpia, I. P. Grant, and C. F. Fischer, 1990, unpublished; most features of GRASP2 have been described in: F. A. Parpia and I. P. Grant, *Journal de Physique IV, Colloque C1, supplément au Journal de Physique* **1** (1991) C1-33
[4] K. G. Dyall, I. P. Grant, C. T. Johnson, F. A. Parpia, and E. P. Plummer, *Computer Physics Communications* **55** (1989) 425
[5] I. P. Grant, B. J. McKenzie, P. H. Norrington, D. F. Mayers, and N. C. Pyper, *Computer Physics Communications* **21** (1980) 207; B. J. McKenzie, I. P. Grant, and P. H. Norrington, *Computer Physics Communications* **21** (1980) 233
[6] C. F. Fischer, *Computer Physics Reports* **3** (1986) 273
[7] C. F. Fischer, *Computer Physics Communications* **64** (1991) 369; *ibid.* 399; *ibid.* 431, *ibid.* 473; C. F. Fischer and B. Liu, *ibid.* 406; A. Hibbert and C. F. Fischer, *ibid.* 417; A. Hibbert, R. Glass, and C. F. Fischer, *ibid.* 455; C. F. Fischer, M. R. Godefroid, and A. Hibbert, *ibid.* 486; C. F. Fischer and M. R. Godefroid, *ibid.* 501
[8] F. A. Parpia, I. P. Grant, and C. F. Fischer, 1992, unpublished
[9] E. R. Davidson, *Journal of Computational Physics* **17** (1975) 87
[10] A. Stathopoulos and C. F. Fischer, in preparation
[11] F. A. Parpia, M. Tong, and C. F. Fischer *Physical Review A*, in press.
[12] P. O. Jönsson, F. A. Parpia, and C. F. Fischer, 1992, unpublished
[13] This terminology was introduced in quantum chemistry by B. O. Roos, P. R. Taylor, and P. E. M. Siegbahn, *Chemical Physics* **48** (1980) 157; the first description of the underlying idea may be found in the article of K. Ruedenberg and K. Sundberg in *Quantum Science: Methods and Structure; A tribute to P.-O. Löwdin*, edited by J.-L. Calais, O. Goscinski, J. Linderberg, and Y. Öhrn; Plenum, NY 1976
[14] F. A. Parpia, W. P. Wijesundera, and I. P. Grant, in preparation
[15] Z. Cai, V. M. Umar, and C. F. Fischer, *Physical Review Letters* **68** (1992) 297
[16] L. Young, W. J. Childs, T. Dinneen, C. Kurtz, H. G. Berry, L. Engstrom, and K.-T. Cheng, *Physical Review* **37** (1988) 4213
[17] A. Arnesen, R. Hallin, C. Nordlins, Ö. Staaf, L. Ward, B. Jelénkovic, M. Kisielinski, L. Lundin, and S. Mannervik, *Astronomy and Astrophysics* **106** (1982) 327

Convergence Studies of Atomic Properties from Variational Methods: Total Energy, Ionization Energy, Specific Mass Shift, and Hyperfine Parameters for Li and Be

Ming Tong, Per Jönsson* and Charlotte Froese Fischer
Vanderbilt University
Nashville, TN 37235 USA

* Present address: Department of Physics, Lund Institute of Technology, P.O. Box 118, S-221 00 Lund, Sweden

In this paper we report on the study of systematic approaches for MCHF wave function calculations for both Li and Be, and the convergence patterns that are observed for a number of atomic properties. Since the variational procedure is based on the expression for the total energy of the system, the convergence pattern of the energy is of great importance. Other properties may rely on different parts of the wave function and may converge more rapidly than the total energy. The ionization energy, $E(Li^+) - E(Li)$, for example, relies more on the outer portion of the wave function as does an oscillator strength (or f-value) for the resonance transition, whereas the hyperfine contact term depends almost entirely on the wave function near the nucleus. The specific mass shift (SMS) has not been studied nearly as extensively as some other atomic properties. For some states of light atoms, the mass polarization correction may be larger than relativistic effects. Its dependence on the wave function is more like that of the energy, except that, being a smaller effect, it does not need to be computed to as many significant digits.

1 Results for Lithium

The lithium ground state is an excellent test case for our studies. Very accurate non-relativistic energies are available for comparison obtained from Hylleraas type of calculations which explicitly include the inter-electronic distance in the series expansion for the wave function (e.g. [1]). Unlike our MCHF approach, the latter cannot readily be extended to many-electron systems.

We use the n-expansion method to compute the wave function along with the other atomic properties, as shown in Table I. The column denoted "n" indicates the largest n values, in other words, all of the orbitals with n up to the given value are included in the calculation. The configuration list is generated from an active set of electrons.

We see in Table I that the computed total energies show convergence, but clearly, the procedure has not converged to the desired accuracy, although our *computed* total energy is the lowest among the known variational calculations so far.

Also included in Table I are the ionization energy (IE), specific mass shift (SMS), and Fermi contact term as a function of n. The former was computed as $E(Li^+) - E(Li)$, using the same orbital basis for the positive ion as for the neutral atom. This leads to an uneven increase in IE. The SMS (from the gradient form, in cm^{-1}) shows a generally decreasing trend whereas the Fermi contact term (a_c) is increasing.

Table I: The total energy (E_{tot}), the ionization energy (IE), the specific mass shift (SMS) and the Fermi contact term (a_c) from different n sequences for $1s^2 2s\ ^2S$ in ^7Li.

n	E_{tot} (a.u.)	IE (a.u.)	SMS (cm^{-1})		a_c (a.u.)
			Gradient	Slater	
2	−7.454 565 28	0.196 436 28	5.544 94	9.624 35	2.073 08
3	−7.473 184 27	0.196 512 54	5.147 33	10.109 27	2.827 43
4	−7.476 203 01	0.197 739 32	5.199 29	6.279 26	2.826 28
5	−7.477 159 95	0.197 941 52	5.208 56	5.072 19	2.907 37
6	−7.477 579 74	0.198 078 16	5.205 35	5.303 60	2.888 79
7	−7.477 772 41	0.198 105 70	5.200 00	5.188 70	2.905 66
8	−7.477 874 32	0.198 125 16	5.197 13	5.221 48	2.903 98
9	−7.477 932 61	0.198 131 76	5.195 27	5.195 62	2.904 85
10	−7.477 968 61	0.198 136 79	5.194 15	5.203 60	2.905 13
∞	−7.478 060 9	0.198 146 1	5.192 5	—	2.905 3
other	−7.478 060 1[a]	0.198 142 7[b]	5.192 4[c]		2.906 02[d]

[a] Ref. [1]
[b] Ref. [2]
[c] Ref. [3]
[d] Ref. [4]

A similar study is carried out for the $1s^2 2p\ ^2P$ state. We obtain a value of 0.130 229 2 a.u. for the ionization energy; 4.2484 cm^{-1} for the SMS. The convergence is similar to that of Table I.

The oscillator strength for the resonance $1s^2 2s\ ^2S$ — $1s^2 2p\ ^2P$ transition is computed with the same n-expansion, as shown in Table II. Our calculated transition energy is 0.067 908 8 a.u. We obtain an f-value of 0.7472 (length form). This is similar to other recent theoretical predictions, but, is still larger than the experimental values.

2 Results for Beryllium and Negative Lithium

Similar n-expansion calculations are performed for the $1s^2 2s^2\ ^1S$ ground state of Be and Li^-. Now, because of the rapid increase in the number of configuration states with n, rules based on the observed patterns of significant configuration states are employed to restrict the wave function expansion. At the same time, small contributors are omitted.

Our extrapolated total energy is −14.667315 hartrees for Be and −7.500758 hartrees for Li^-. The former agrees well with the "exact" non-relativistic energy estimated by Lindroth *et al.* [5] of −14.667353 hartrees.

The electron affinity for Li is predicted to be 0.61760±0.00004 eV which is identical to the experimental value of Dellwo *et al.* [6], although the latter has larger error bars. The affinity is

Table II: The Transition energy (ΔE) in a.u., the line strength S in a.u., and f-value for the $2s - 2p$ resonance transition from different n sequences.

n	ΔE (a.u.)	S (a.u.)		f-value	
		Length	Velocity	Length	Velocity
2	0.074 442 3	33.788 1	28.694 5	0.838 42	0.712 03
3	0.068 596 6	33.806 8	32.787 0	0.773 01	0.749 70
4	0.068 352 0	33.230 0	33.994 1	0.757 11	0.774 52
5	0.067 992 9	33.029 2	33.017 5	0.749 89	0.749 41
6	0.067 935 3	33.029 2	33.017 5	0.747 95	0.747 68
7	0.067 915 6	33.015 2	33.008 7	0.747 42	0.747 27
8	0.067 908 8	33.008 8	32.998 3	0.747 20	0.746 97
other	0.067 904 7 [a]				

[a] Obtained by subtracting the total energies (as reported by Pipin and Bishop [1]).

slightly larger than the value reported by Chung and Fullbright [7].

The change in the specific mass shift parameter in going from Be $1s^2 2s^2$ to Be^+ $1s^2 2s$ is 0.00723 a.u. in excellent agreement with the experimental value of 0.006741 a.u. reported by Wen *et al.* [8].

Acknowledgments

This research was supported by a grant from the U.S. Department of Energy, Office of Basic Energy Sciences.

References

1. J. Pipin and D.M. Bishop, Phys. Rev. A **45**, 2736 (1992).
2. K.T. Chung, Phys. Rev. A **44**, 5421 (1991).
3. F.W. King and M.P. Bergsbaken, J. Chem. Phys. **93**, 2570 (1990).
4. A. Beckmann, K.D. Böklen and D. Elke, Z. Phys. **270**, 173 (1974).
5. E. Lindroth, H. Persson, S. Salomonson, A-M Mårtensson-Pendrill, Phys. Rev. A **45**, 1493 (1992).
6. J. Dellwo, Y. Liu, D.J. Pegg, and G.D. Alton, Phys. Rev. A **45**, 1544 (1992).
7. K.T. Chung and P. Fullbright, Physica Scripta **45**, 445 (1992).
8. J. Wen, J.C. Travis, T.B. Lucatorto, C. Johnson, and C.W. Clark, Phys. Rev. A **37**, 4207 (1988).

PROSPECTS FOR RELATIVISTIC MULTICONFIGURATION DIRAC-FOCK-BREIT CALCULATION USING GAUSSIAN BASIS SET METHOD

Farid A. Parpia* and Ajaya K. Mohanty

IBM Corporation

Supercomputing Systems, High Performance

Supercomputing Systems Lab.

Kingston, New York 12401

* Present address: Department of Computer Science

Vanderbilt University, Nashville, TN 37235

Atomic properties from relativistic basis-set calculations

Two programs from IBM. Based on kinetically-balanced geometric Gaussian basis sets.

GDFB: Dirac-Fock-Breit (DFB) program. Only for closed-shell atoms and ions. "Step" or "Fermi" nuclear charge distribution.

- F. A. Parpia, A. K. Mohanty, and E. Clementi, *J. Phys. B: At. Mol. Opt. Phys.* **25** (1992) 1
- F. A. Parpia and A. K. Mohanty, *Phys. Rev. A*, in press
- A large DFB calculation for the ground state of Hg has just been completed.

MCGDFB: Multiconfiguration DFB program. Integral generation packages for one-electron (overlap, kinetic-energy, and electron-nucleus interaction) integrals and for Coulomb two-electron integrals completed and tested. These packages were carefully designed for efficient execution on IBM 3090 and ES/9000 computers equipped with the Vector Facility. Execution times are roughly 1/20 of comparable modules in GDFB.

- F. A. Parpia and A. K. Mohanty, *IBM DSD Technical Report*, 14 August 1991.

The many-body problem of electronic structure physics may be cast in a form that is "embarassingly parallel" and are ideal candidates for distributed memory parallel processors.

Efficient generation of one-electron integrals

The one-electron integrals most difficult to compute are the electron-nucleus interaction integrals. These involve incompleta Gamma functions,

$$\gamma(a,x) = \int_0^x dt\, e^{-t}\, t^{a-1}.$$

All incomplete Gamma functions required in MCGDFB may be obtained from two sets of Gamma functions using the recurrence relation

$$\gamma(a,x) = \frac{1}{a}\left[\gamma(a+1,x) + x^a\, e^{-x}\right]$$

which is stable as written. Our procedures for the generation of the two initial sets of incomplete gamma functions, as well as our use of the recurrence relation, *vectorise*.

Databases

CRITICALLY EVALUATED DATA ON ATOMIC SPECTRA – ENERGY LEVELS, WAVELENGTHS, AND TRANSITION PROBABILITIES*

W. C. Martin, A. Musgrove, J. Reader, and J. Sugar
Atomic Energy Levels Data Center

W. L. Wiese and J. R. Fuhr
Data Center on Atomic Transition Probabilities and Line Shapes

G. R. Dalton
Standard Reference Data Program

National Institute of Standards and Technology (NIST),
Gaithersburg, MD 20899, USA

and

T. Shirai
JAERI Nuclear Data Center
Japan Atomic Energy Research Institute (JAERI),
Tokai-Mura 319-11, Japan

The Atomic Energy Levels Data Center (NIST), the Data Center on Atomic Transition Probabilities and Line Shapes (NIST), and the Nuclear Data Center (JAERI) critically review, compile, and disseminate data on energy levels, wavelengths, and transition probabilities for the spectra of atoms and atomic ions in all stages of ionization. The NIST data centers also publish annotated bibliographies and maintain files on bibliographic references categorized by element, stage of ionization, and technical content.

Energy-level data have been compiled during the past fifteen years for all spectra of the elements Na through S (Z=11–16) [1–6], the iron-period elements K through Ni (Z=19–28) [7], all spectra of Cu, Kr, and Mo (Z=29, 36, 42) [8–10], and 63 spectra of the rare-earth elements La through Lu (Z=57–71) [11]. New energy level compilations are being completed for O II (Z=8) and all spectra of Cl, Zn, and Ge (Z= 17, 30, 32).

---

*Work is supported in part by the Office of Fusion Energy of the U.S. Department of Energy and the Astrophysics Division of the U.S. National Aeronautics and Space Administration.

New wavelength compilations based on these energy level data have been published for all spectra of Mg [12], Al [13], and Sc [14], in all wavelength regions from x-rays to the far infrared being covered. Work is now in progress on O II (Z=8), Na, Si, and S (Z=11,14,16).

Recent critical compilations of atomic transition probabilities cover the iron-group elements Sc through Ni (Z=21–28) [15,16]. Also, a recent update of the tables previously published in the CRC Handbook of Chemistry and Physics [17] contains about 8300 selected lines of all elements for which reliable data are available, mostly for neutral and singly ionized atoms. A critical compilation of prominent lines of neutral and singly ionized heavy atoms is now being updated, and work is also continuing on evaluating data for the light atoms and ions, H through Ne (Z=1–10). For these spectra, calculations from the "Opacity Project" [18] play a major role.

In collaboration with JAERI, new compilations containing energy levels, wavelengths, transition probabilities, and Grotrian diagrams have been published for the higher spectra of V (V VI–XXIII) [19], Fe (Fe VIII–XXVI) [20], Co (Co VIII–XXVII) [21], Ni (Ni IX–XXVIII) [22], Cu (Cu X–XXIX) [23] and Mo (Mo VI–XLII) [24]. Work has been completed on Cr and Mn and will be published soon.

An interactive PC database [25] has been developed by the Standard Reference Data Program at NIST containing prominent air or vacuum wavelengths and ionization potentials for neutral through quadruply ionized atoms. The wavelength data originally appeared in NSRDS–NBS **68** [26] and are reprinted annually with updates in the "CRC Handbook of Chemistry and Physics" [27]. Also, a PC database containing the NIST transition probability tables for Sc through Ni [15,16] is available [28]. Work is continuing at NIST on a general atomic spectroscopic database containing evaluated data on atomic energy levels, wavelengths, line classifications, and transition probabilities, covering many atoms and ions of laboratory and astrophysical interest.

References

[1] W. C. Martin and R. Zalubas, J. Phys. Chem. Ref. Data **10**, 153–195 (1981).
[2] W. C . Martin and R. Zalubas, J. Phys. Chem. Ref. Data **9**, 1–58 (1980).
[3] W. C. Martin and R. Zalubas, J. Phys. Chem. Ref. Data **8**, 817–864 (1979).
[4] W. C. Martin and R. Zalubas, J. Phys. Chem. Ref. Data **12**, 323–380 (1983).
[5] W. C. Martin, R. Zalubas, and A. Musgrove, J. Phys. Chem. Ref. Data **14**, 751–802 (1985).
[6] W. C. Martin, R. Zalubas, and A. Musgrove, J. Phys. Chem. Ref. Data **19**, 821–880 (1990).
[7] J. Sugar and C. Corliss, J. Phys. Chem. Ref. Data **14**, Suppl. No. 2 (1985).
[8] J. Sugar and A. Musgrove, J. Phys. Chem. Ref. Data **19**, 527–616 (1990).
[9] J. Sugar and A. Musgrove, J. Phys. Chem. Ref. Data **20**, 859–915 (1991).

[10] J. Sugar and A. Musgrove, J. Phys. Chem. Ref. Data **17**, 155–239 (1988).
[11] W. C. Martin, R. Zalubas, and L. Hagan, Natl. Stand. Ref. Data Ser., Natl. Bur. Stand. (U.S.) 60, (1978).
[12] V. Kaufman and W. C. Martin, J. Phys. Chem. Ref. Data **20**, 83–152 (1991).
[13] V. Kaufman and W. C. Martin, J. Phys. Chem. Ref. Data **20**, 775–858 (1991).
[14] V. Kaufman and J. Sugar, J. Phys. Chem. Ref. Data **17**, 1679–1789 (1988).
[15] G. A. Martin, J. R. Fuhr, and W. L. Wiese, J. Phys. Chem. Ref. Data **17**, Suppl. No. 3 (1988).
[16] J. R. Fuhr, G. A. Martin, and W. L. Wiese, J. Phys. Chem. Ref. Data **17**, Suppl. No. 4 (1988).
[17] J. R. Fuhr and W. L. Wiese, *Atomic Transition Probabilities*, CRC Handbook of Chemistry and Physics, 72nd Edition (CRC Press, Boca Raton, FL, 1991).
[18] M. J. Seaton, J. Phys. B **20**, 6363 (1987) and later Opacity Project papers in that journal.
[19] T. Shirai, T. Nakagaki, J. Sugar, and W. L. Wiese, J. Phys. Chem. Ref. Data **21**, 273–390 (1992).
[20] T. Shirai, Y. Funatake, K. Mori, J. Sugar, W. L. Wiese, and Y. Nakai, J. Phys. Chem. Ref. Data **19**, 127–275 (1990).
[21] T. Shirai, A. Mengoni, Y. Nakai, J. Sugar, W. L. Wiese, K. Mori, and H. Sakai, J. Phys. Chem. Ref. Data **21**, 23–122 (1992).
[22] T. Shirai, K. Mori, J. Sugar, W. L. Wiese, Y. Nakai, and K. Ozawa, At. Data Nucl. Data Tables **37**, 235–332 (1987).
[23] T. Shirai, T. Nakagaki, Y. Nakai, J. Sugar, K. Ishii, and K. Mori, J. Phys. Chem. Ref. Data **20**, 1–81 (1991).
[24] T. Shirai, Y. Nakai, K. Ozawa, K. Ishii, J. Sugar, and K. Mori, J. Phys. Chem. Ref. Data **16**, 327–377 (1987).
[25] NIST Spectroscopic Properties of Atoms and Atomic Ions, NIST Standard Reference Database 38.
[26] J. Reader, C. H. Corliss, W. L. Wiese, and G. A. Martin, Natl. Stand. Ref. Data Ser., Natl. Bur. Stand. (U.S.) 68 (1980).
[27] J. Reader and C. H. Corliss, *Line Spectra of the Elements*, CRC Handbook of Chemistry and Physics, 72nd Edition (CRC Press, Boca Raton, FL 1991).
[28] NIST Atomic Transition Probabilities (Scandium through Nickel), NIST Standard Reference Database 24.

Need for Complete Spectroscopic Tables*

Vivek Bakshi, Tom D. Boone, Jr., and William C. Nunnally
The Applied Physical Electronics Research Center
The University of Texas at Arlington
Arlington, TX 76019 (817) -- 794- 5100

(1) Abstract

This paper discusses the need for complete spectroscopic tables, i.e., for a given species, listing of all transition arrays and the transitions, combined with the values of transition probabilities and the line shape information, if possible. The presently available tables list only prominent transitions and transition probability values for only some of these transitions. However, in the case of spectra from some plasma devices one needs to analyze the weaker transitions for the estimation of plasma properties and hence arises the need for complete spectroscopic tables.

(2) Background

(2.1) Need for Atomic Data Base

Plasma spectroscopy is a commonly used and powerful diagnostics tool for the estimation of the plasma properties in various laboratory plasmas, e.g., plasma jets, low pressure discharges, plasma armature railguns, and astrophysical plasmas. We, at The Applied Physical Electronics Research Center, The University of Texas at Arlington, have been interested in the development of spectroscopic diagnostics of the railgun plasma armatures. The railgun operates at atmospheric pressure and the plasma emits spectra that are a combination of optically thin and thick regions. The major constituents of the plasma have been copper, aluminum, oxygen, and nitrogen in various ionization stages. In a recent publication[1], we have shown that prominent transitions are optically thick in our experiment and the attention must be turned to otherwise weaker transitions, which are still optically thin. Such transitions allow us to use the relations of emission spectroscopy for the estimation of the plasma parameters, which are less involved than the optically thick plasma calculations. The importance of weaker transitions can be important even in the case of optically thin plasmas where they may distort the line shapes of prominent transitions being used for the calculation of electron density, e.g., distortion of line shapes of hydrogen beta transitions by the transitions of O II and Si III, which can cause the error in the order of magnitude in the electron-density measurements[2]. For the same reasons, the presence of such transitions can also be important in the choice of transitions in the optically thick spectra.

In short, the presence of such weak transitions can distort the line shape of the prominent transitions and also introduce error in the measurements of the area under the transitions. In order to detect the presence of such weaker transitions and to be able to use them one needs their listing. Also, in order to obtain plasma parameters from the spectra the transition probability and line shape information is necessary.

In some experimental situations, where spectral data must be acquired in a single shot, one tries to cover the wide wavelength region in order to be able to use a Boltzmann plot with reasonable accuracy and may lose the resolution in this process. For example, in our experiment the wavelength resolution is only 0.6 Angstrom. At this resolution and in the presence of four or five elements in various ionization stages the acquired spectra have at least two hundred overlapping lines in the 40 nm wavelength region and are quite complex. For such spectra, in order to have a reliable identification of the weaker transitions it is quite important to have the complete spectroscopic information for Cu I and II and Al I and II.

(2.2) Present state of data bases

The atomic energy center at NIST provides, at user's request, a bibliography of all the published work on energy levels, wavelengths, transitions probability, and line shapes which is

* Paper presented at 4th International Colloquium on Atomic Spectra and Oscillator Strengths for Astrophysical and Laboratory Plasmas, September 14 - 17, 1992, National Institute of Standards and Technology, Gaithersburg, MD, USA

quite complete and very helpful. Some NIST publications[3] and CRC handbook [4] give listings of the prominent transitions of many elements. MIT press also has an extensive but not complete listing of wavelengths for many atoms and their atomic species which is useful [5]. There exists in some cases a close to complete listing of all the transitions in the literature, e.g., Shenstone's work for copper [6].

At present, atomic transition probability values are listed for prominent transitions only in NIST [3] publications or CRC handbook[4] and NIST may provide more of such tables in the coming years.

(3) Complete Spectroscopic Tables for Cu I and II

(3.1) Procedure for compilation

As explained in the section (2.2), we needed to have complete spectroscopic tables for Cu I and II in the wavelength region of 300-350 nm. We have compiled such tables. We started with Shenstone's tables[6] and numbered all the multiplets and transition arrays. The next step was to correct the energy levels by the new level information [7] and then predict the other possible transitions. The new wavelengths were also predicted according to the new energy levels. The forbidden transitions were listed separately. The transition probability values were then calculated according to Coulomb approximation. Stark widths of the transitions were estimated by using a SE formulation, however, the results are not included in this presentation.

(3.2) Some results

Table I gives the typical results for some transition array of Cu I. Entire table in the wavelength region (300 - 350 nm) will be published soon.

(4) Conclusions

(4.1) Summary of needs

There exists a need for complete spectroscopic tables. The best way will be to have a computerized data base combined with curve fitting and calibration programs. These data bases will give a definite boost to the application of plasma spectroscopy in the study of various plasma devices and astrophysical plasmas.

Table 1 : Example of Proposed Tables for Copper I.

No.	Transition Array	Multiplet	λ (Å) observed	λ (Å) calculated	$E_i(cm)^{-1}$	$E_k(cm)^{-1}$	g_i	g_k	strengths (multiplet)	strengths (line)	$A_{ki}(s)^{-1}$
1	$3d^9(^2D)4s4p(^3P^o)$ - $3d^94s(^3D)6s$	$^2D^o$ - ^2D	3498.938	3498.99	46598.34	75170.25	6	6	10	0.5600	3.60E+06
			3447.59	3447.64	46172.84	75170.25	4	6	10	0.0400	2.50E+05
			3362.12	3362.24	46598.34	76332.30	6	4	10	0.0400	4.90E+04
			3314.82	3314.81	46172.84	76332.30	4	4	10	0.3600	3.60E+05
2	$3d^9(^2D)4s4p(^3P^o)$ - $3d^94s(^3D)4d$	$^4D^o$ - ^4F	3498.063	3498.10	43513.95	72093.08	8	8	112	0.0407	7.50E+06
			3475.999	3476.04	44544.15	73304.67	4	6	112	0.0029	2.40E+05
			3474.578	3474.62	44544.15	73316.46	4	4	112	0.0400	4.80E+06
			3459.428	3459.46	44406.27	73304.67	6	6	112	0.0521	4.20E+06
			3599.140	3599.17	43513.95	71290.54	8	10	112	0.3571	7.80E+07
			3610.809	3610.84	44406.27	72093.08	6	8	112	0.0021	3.90E+05
			P	3355.84	43513.95	73304.67	8	6	112	0.2450	1.90E+07
			P	3458.05	44406.27	73316.46	6	4	112	0.1607	1.90E+07
			3520.031	3520.06	44915.61	73316.46	2	4	112	0.1000	1.20E+07

(4.2) Suggestions for Future Work in the Area of Atomic Data-Base

(1) The first step would be the compilation of energy levels for all of the useful atoms and their ions. The experimental and theoretical studies contributing to this step are very important.
(2) When energy levels are available, one can proceed to the second step of predicting all of the transitions in a transition array. Such predictions for allowed transitions are straightforward in the case of LS coupling but in other cases they are quite complex. There is no reliable technique for the prediction of forbidden transitions that works for all elements. In our work the compilation of forbidden transitions is restricted to observed transitions only.
(3) The next step will be the theoretical calculation and experiment measurement of the transition probabilities and line shape information for these transitions and critical evaluation of transition probability and line shape information
(4) The availability of such information for convenient user interaction is also very important.

(5) Acknowledgement

This work is sponsered under SDIO-US ARMY-SDC contract No. DASG60-90-C-0133

(6) References

[1] Vivek Bakshi et al, " Spectroscopic Diagnostics of Railgun Plasma Armature," To be published in IEEE Trans. Magnetics, Jan 93.
[2] Vivek Bakshi et al, "Plasma Diagnostics of Railgun Armatures," Resubmitted to IEEE Trans. Plasma Science, August 1992.
[3] (a) Joseph Reader and Charles H. Corliss (Part I: Wavelength) and W. L. Wiese and G. A. Martin (Part II Transition Probability), *Wavelength and Transition Probability for Atoms and Atomic Ions*, NSRDS-NBS 68, Institute of Basic Standards, NBS, Washington, DC., December 1982.
(b) W. L. Wiese, M. W. Smith, and B. M. Miles, *Atomic Transition Probability , Volume I : Hydrogen Through Neon*, NSRDS-NBS 4, Institute of Basic Standards, NBS, Washington, D. C., October 1969.
[4]Robert C. Weast and Melvin J, Astle, *CRC Handbook of Chemistry and Physics*, CRC Press Inc., Boca Raton, Florida 1982.
[5]*MIT Wavelength Tables*, vol. I by George R. Harrison (1969), vol. II by Federic M. Phelps (1982), MIT Press, Cambridge Press, Cambridge, MA.
[6]"The first Spectrum of Copper (Cu I)," A. G. Shenstone, Phil. Trans. R. Soc. London, Ser. A, **241** 37 (1948).
[7]"Energy Levels of Copper, Cu I through XXX," J. Sugar and A. Musgrove, J. Phys. Chem. Ref. Data **19**, 527-616 (1990).

Spectral Atlas of the Inductively Coupled Plasma

R.K. Winge, D.E. Eckels, and S.J. Weeks
Ames Laboratory, Iowa State University, Ames, IA 50011
and
J.C. Travis and M.L. Salit
National Institute of Standards and Technology, Gaithersburg, MD

ABSTRACT

Introduction - Needs: Analytical atomic spectrometry and astrophysics share common needs. Both fields require a means of positive identification of spectral lines, lines that are often masked or blended with other lines. Both fields also require line intensities and often other analytic information, e.g., temperatures and line widths that define the excitation characteristics of the source. Sample elements in the inductively coupled plasma (ICP) experience temperatures similar to those existing in the photospheres of our sun and cool stars, thus suggesting diagnostic applications for the ICP in astrophysics.

The ICP is used extensively as a high-temperature atomization-excitation source for atomic emission spectrometry (AES) and elemental mass spectrometry (ICP-MS). The ICP is an efficient source of spectral lines arising from the singly ionized state (M^+) and this characteristic provides many strong ion lines suitable for the measurement of trace concentrations of the elements in AES [1]. The enhancement of ion line intensities relative to atom line intensities in the ICP is only one among a number of differences that lead to the need for a new compilation of spectral data. Existing spectral line compilations include deficiencies in one or more of the following qualities in relation to the ICP:

1. Spectral line coverage. Gaps exist in wavelength coverage for many elements [2]. Deficiencies in weak line coverage exist throughout the spectrum.
2. Availability in machine readable form.
3. Capability for graphical representation of spectra.
4. Wavelengths, intensities, and peak widths relevant to the ICP.
5. Wavelength accuracy sufficient so that specific spectral lines can be located reliably within a narrow window in computer controlled routines.

The present work addresses these needs for >70 elements. The project combines the wavelength accuracy of Fourier Transform Spectrometry (FTS) at NIST with the dynamic range of wavelength dispersive spectrometry at the Ames Laboratory. The latter employs a conventional scanning spectrometer with a photodiode array detector.

ICP as an Emission Source: The ICP employed for analytical emission spectrometry is typically operated at 27 MHz or 40 MHz at power levels of approximately 1 to 1.2 kW. Elements of interest are introduced into the axial channel of the ICP as aerosols of liquid or solid samples. The aerosols are desolvated (liquids), vaporized, atomized, and excited, or ionized and excited as they progress along the axial channel where gas kinetic temperatures reach 5000 to 7000 K. The degree of ionization of elements in the ICP has been estimated from the Saha equation by Houk [3]. These calculations indicate some 54 elements are expected to reach the first ionization level M^+ with efficiencies at 90% or higher. The calculations also indicate appreciable fractions of doubly ionized species M^{++} in the ICP for elements with relatively low second ionization energies. The results of these calculations coincide closely with experimental observations, that the most prominent lines for many elements in the ICP arise from singly ionized species and that lines from doubly ionized species are observed for the predicted elements. The axial sample channel in the ICP is surrounded by an annular induction region with a temperature of approximately 10000 K. Thus, the ICP is an optically thin emission source exhibiting excellent linearity between intensity and concentration over approximately five orders of magnitude.

Experimental Facilities: Spectral data for each element are collected with a 1 m scanning spectrometer equipped with a 3600 grooves/mm grating and a 1024 pixel, photodiode array. The spectrometer is stepped through a fixed series of computer controlled

grating angles that allow coverage of the 187 to 434 nm range in 62 overlapping windows (25% overlap). The wavelength range included in the window changes with grating angle from ~6.4 nm at 189 nm to ~3.9 nm at 432 nm. The 1024 pixel array thus samples the spectrum at intervals varying from 6 pm to 4 pm (0.06 to 0.04 Å) as the spectrometer progresses through its stepped sequence of windows. Peak positions (interpolated diode array pixel positions), intensities, and widths (FWHM) are obtained from a three-point Gaussian curve fitting routine. Wavelengths corresponding to peak pixel positions are obtained from the grating equation, which, in contrast to polynomial curve fitting, requires only one reference wavelength per diode array window. Wavelength accuracies on the order of 0.1 pm are obtained, relative to NIST FTS wavelengths, after correction for an optical aberration associated with off-axis rays. Another small but systematic error (tenths of a picometer), arising presumably from another optical aberration, occurs at one end of the wavelength range. It is presently under investigation. The dynamic range of measurable intensities is extended to 5 to 6 orders of magnitude by a combination of three diode-array measurement conditions (exposure times of 0.03, 0.3, and 3.0 s; total integration time of 15 s each) and three elemental concentrations (10, 100, and 1000 mg/L) for each element.

Summary of Results: Table 1 provides an example of the wavelength accuracy, expressed as wavelength differences, achieved with the Ames Laboratory instrumentation with respect to NIST FTS wavelengths. The 12 iron lines, measured within one diode array window with a sample concentration of 1000 mg/L, yielded an RMS error of 0.08 pm. The RMS error values for 100 and 10 mg/L iron were 0.09 and 0.12 pm, respectively. Thus, excellent wavelength accuracy is maintained over a wide intensity range.

A segment of the ICP iron emission spectrum is compared with an absorption spectrum of star **R 81** [4] in Fig.1. The relative intensities and positions of the major features in the ICP spectrum correlate closely with the major absorption peaks in the star spectrum. The need and usefulness of an ICP atlas is apparent for analysis in astrophysical measurements, as it is in the field of analytical chemistry.

References

1. Winge, R.K., Fassel, V.A., Peterson, V.J., and Floyd, M.A., "Inductively Coupled Plasma-Atomic Emission Spectroscopy: An Atlas of Spectral Information," Elsevier (1985).
2. Boumans, P.W.J.M., Spectrochim. Acta, 43B, 5 (1988)
3. Houk, R.S., Anal. Chem. 58, 97A (1986).
4. Zickgraf, F.-J., "Fe II in Luminous Hot Stars", p.125 in "Physics of Formation of Fe II Lines Outside LTE", Viotti, R., Vittone, A., and Friedjung, M., Eds., D. Reidel Publishing Company, Dordrecht (1988).

Table 1. Differences between Ames Laboratory calculated wavelengths and NIST FTS wavelengths

NIST λ (nm)	NIST Rel. Int.	$\Delta\lambda$[1] (pm)
256.69133	41	-.06
257.79225	45	.10
258.25838	65	-.03
258.58762[2]	764	0.
259.15435	67	.07
259.83696	876	.15
259.93958	2470	.04
260.70875	727	.14
261.18740	1045	.04
261.38247	432	.07
261.76178	302	.02
262.16695	110	.01
RMS error[3]		**.08**

[1] $\Delta\lambda = \lambda_{AL} - \lambda_{NIST}$

[2] Reference wavelength with inherent zero error.

[3] The zero error value for the reference wavelength is excluded.

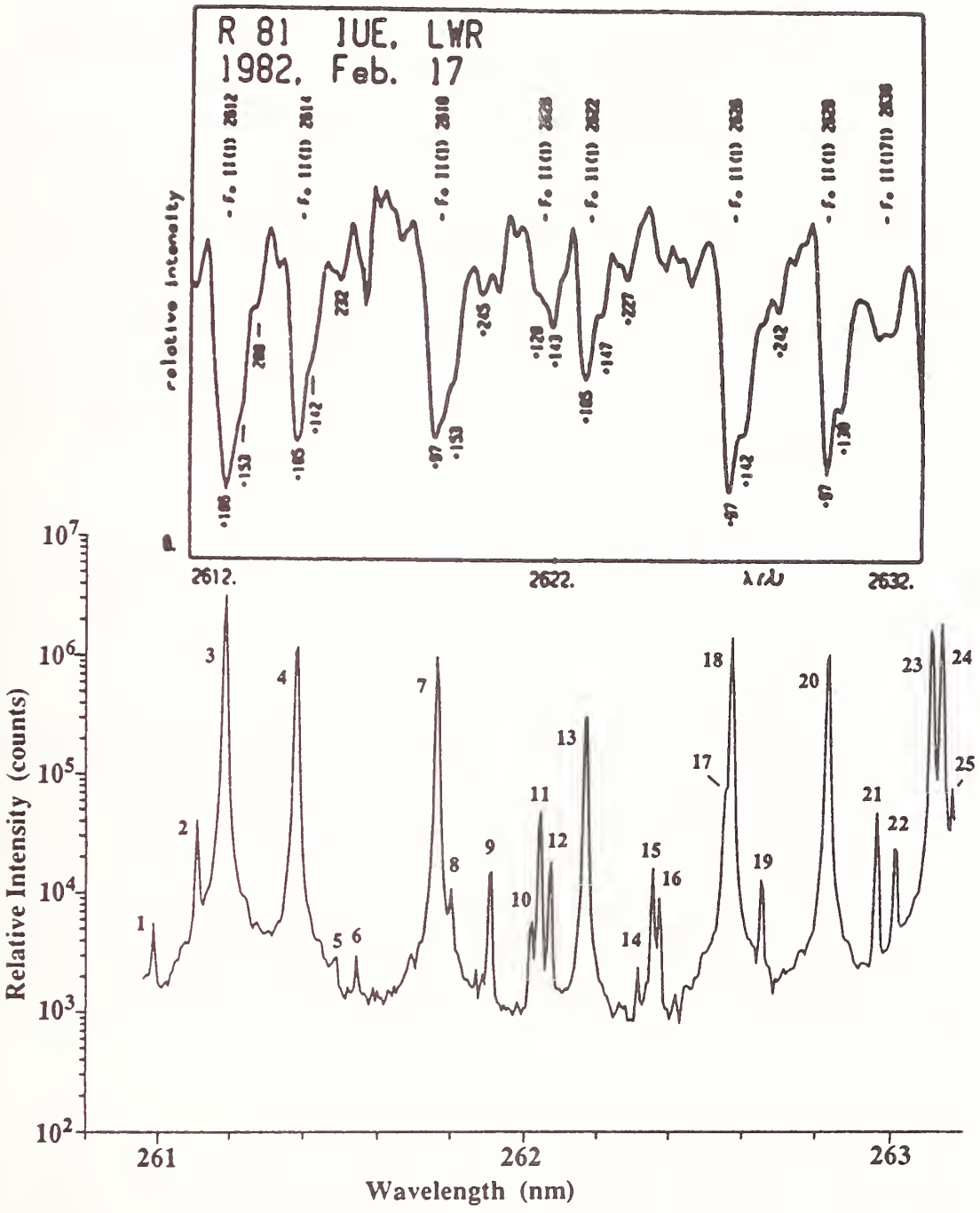

Figure 1. Comparison of the ICP emission spectrum of iron (bottom) with the absorption spectrum of R 81 (top). MIT table wavelengths are listed below for the lines numbered in the ICP spectrum. Upper part of figure reproduced with permission of author and publisher [4].

1. II 260.9866
2. II 261.1072
3. II 261.1872
4. II 261.3823
5. II 261.4872
6. 261.5422
7. II 261.7616
8. I 261.8017
9. II 261.9076
10. II 262.0173
11. II 262.0407
12. II 262.0695
13. II 262.1668
14. 262.3123
15. I 262.3532
16. II 262.3727
17. 262.5490
18. II 262.5666
19. II 262.6500
20. II 262.8292
21. I,II 262.9587
22. II 263.0066
23. II 263.1051
24. II 263.1323
25. II 263.1609

Atomic Data Center for Astrophysical and Laboratory Plasmas

K. T. Lu, Dennis Baba and Aria Kohshkhou
Atomic Engineering Corp., P. O. Box 3342, Gaithersburg, MD. 20885-3342

The astrophysical and laboratory plasmas scientists rely on atomic spectra to determine temperature, electron density and element abundance. The scientists often spend hours leafing through pages of wavelengths and energy levels in atomic data books, seeking an unidentified spectral line. Unfortunately, the usual wavelength tables are not fully adequate . They are too incomplete compared to the actual spectra. The wavelength lists and intensities available from different sources are not consistent with each other because they are measured under different experimental conditions. Furthermore, the tabulated data on wavelength, transition probability and energy level are not integrated. All these problems make the evaluation and compilation of data using traditional methods difficult, if not impossible.

This paper describes a software program, Atomic Engineering System (AESystem)[1], which can be used as a data center for astrophysical and laboratory plasmas. The AESystem can analyze and identify spectroscopic data. Furthermore, it can integrate and evaluate atomic/ionic data, model experiments, and plot a variety of data.

o **Automated Spectroscopic Analysis** :
AESystem can perform element identification and analysis of the spectra. The basic idea is to model a complete reference wavelength spectra using Atomic Engineering System. This complete reference wavelength spectra will be compared with the actual spectra. Atomic selection rules will be used to control the type of lines generated (e.g., allowed, forbidden, multiphoton). The user can enter a single line from keyboard or a list of lines from a file. The software program searches the database which consists of evaluated experimental data and the complete reference spectra for pairs of energy levels that can produce the frequency within a specified tolerance. This search can be done over many elements or ions at once. It is a useful feature for astrophysics and plasma spectroscopy where the source may include many elements/ions. A demonstration will be presented at this conference.

o **Computer Modeling of Absorption and Emission Spectra** :
The AESystem contains an integrated database. The data processed include: energy levels, ionization limits, oscillator strengths, intensities, Lande-g-factors, photoionization cross sections, frequencies or wavelengths, life-times. The source of these data are NIST compilations of atomic data, Kelly's tables on wavelengths, and the open literature. The basic data unit of this data management is the "channel," which includes a series of related energy levels plus information common to all members of the channel. The program organizes all channels of a given element or ion into a "super file" for easy access. The mathematical algorithm characterizes an atom or ion in terms of a small sets of structural parameters and a finite number of channel sets. The structural parameters are determined either by semi-empirical method (fitting to the data) or by first principle calculations. Many new data types can be calculated, once the structural parameters are known. Subsequently, only the structural parameters of each atom need to be stored in a modeling experiment. This step makes it unnecessary to use a

mainframe computer in managing and manipulating the vast amounts of data. Thus it is possible to use PC as data center. A computer modeling of absorption and emission spectrum will be demonstrated.

o **Evaluation and Integration of Data :**
The quantitative application of the AESystem in element identification and analysis of the spectra depends on the reliability and completeness of the database. The data of Fe I from NIST[2], Kelly's wavelength table[3], and NRL[4] as well as the latest data of life-time and transition probabilities[5] will be used as a case study to examine the reliability and completeness of various data. A generic data format has been developed to integrate the non-compatible data format of wavelengths vs. transition probabilities with the data format of energy levels vs. life-time. A user-friendly display allows user to select the desired data field to display. The following is the procedures of evaluation and integration of data:

1. Convert each data files, such as reference 2 to 5, into a generic data file,
2. The algorithm compares each data field in different data files. For example, wavelength 2345.67 A from data file a is checked and compared to the same value within a certain error with all the other data files, b, c etc. This procedure will be continued until all the data in one file are evaluated.
3. The evaluated wavelength data files are used as input to the automated spectroscopic analysis module. The "spectra lines" are chemically analyzed and identified according to its element or ion origin, upper/lower energy levels, allowed or forbidden transitions and etc.
4. The data with different data fields are integrated by merging all the evaluated data files under the generic data format. For example, data of wavelength vs. intensity, oscillator strength and transition probability from data files a and b are integrated with data of energy levels vs. upper/lower energy levels and upper/lower life-time from files c and d.

Sample data of life-times, transition probabilities, and level energies and wavelength in Fe I are shown in the following tables to demonstrate the evaluation and integration of data. Reference 5 provides the most reliable and consistent data on transition probabilities and life time, because data was taken under similar experimental conditions.

1. J. J. Wynne and C. M. Brown, "Atomic Data Center on Your PC", p. 42, Optics and Photonics News/July (1992).
2. (a) J. R. Fuhr, G. A. Martin, and W. l. Wiese, "Atomic transition probabilities: Fe through Ni," J. Phys. Chem. Ref. Data 17, Suppl. 4 (1988).
   (b) J. Sugar and C. Corliss, "Atomic energy levels of the iron-period elements: K through Ni," J. Phys. Chem. Ref. Data 14, Suppl. 2 (1985).
3. R. L. Kelly, "Atomic and Ionic Spectrum Lines Below 2000 A: Hydrogen through Krypton," J. Phys. and Chem. Ref. Data, 17, Suppl. 1, (1987).
4. C. M. Brown, M. L. Ginter, S Johansson and S. G. Tilford, "Absorption spectra of Fe I in the 1550-3215 A region," J. O. S. Am. B 5, (1988).
5. T. R. O'Brian, M. E. Wickliffe, J. E. Lawler, W. Whaling and J. W. Brault, J. O. S. A. B., V. 8, 1185, (1991).

	Elm Spec#	Wl(air) Wl(air)	Ref	EUx10^3cm-1 ELx10^3cm-1	UTerm LTerm	ju jl	Trans. Prob. ref.	tu(ns) tl(ns)
	Fe	11689.973		26479.3770	z5D*	1.00	1.39E+05(11%)	86.300
	1			17927.3770	a5P	1.00		
	Fe	11638.256		26140.1777	z5D*	3.00	4.30E+04(10%)	81.100
	1			17550.1758	a5P	3.00		
	Fe	11607.574		26339.6934	z5D*	2.00	9.70E+04(11%)	84.500
	1			17726.9863	a5P	2.00		
	Fe	11593.584		26550.4746	z5D*	0.00	1.77E+05(15%)	88.500
	1			17927.3730	a5P	1.00		
	Fe	11439.120		31686.3496	z3D*	2.00	1.81E+05(9%)	245.000
	1			22946.8105	b3P	1.00		
	Fe	11422.322		26479.3770	z5D*	1.00	3.40E+04(11%)	86.300
	1			17726.9844	a5P	2.00		
	Fe	11374.079		26339.6934	z5D*	2.00	6.00E+03(13%)	84.500
	1			17550.1797	a5P	3.00		
	Fe	11298.854		31686.3496	z3D*	2.00	2.70E+04(10%)	245.000
	1			22838.3164	b3P	2.00		
	Fe	11251.111		31937.3223	z3D*	1.00	1.13E+05(10%)	237.000
	1			23051.7441	b3P	0.00		
	Fe	11119.789		31937.3223	z3D*	1.00	1.13E+05(11%)	237.000
	1			22946.8086	b3P	1.00		
*	Fe	9889.042		50703.8633	e5G	5.00	2.22E+06(26%)	11.500
	1			40257.3086	x5F*	4.00		2.000
	Fe	9861.735		50979.5742	e5G	4.00	5.49E+06(26%)	12.800
	1			40842.1484	x5F*	3.00		2.000
	Fe	9763.380		51370.1406	e5G	2.00	5.42E+06(21%)	10.300
	1			27559.5801	z5F*	2.00		2.000
	Fe	9738.573		50522.9414	e5G	6.00	7.65E+06(30%)	13.000
	1			40257.3086	x5F*	5.00		2.000
	Fe	9626.494		50979.5742	e5G	4.00	4.51E+06(26%)	12.800
	1			40594.4258	x5F*	4.00		2.000
*	Fe	9569.909		50703.8633	e5G	5.00	2.50E+06(21%)	11.500
	1			40594.4258	x5F*	5.00		2.000
	Fe	9443.803		51604.1016	f5F	3.00	6.39E+06(21%)	14.800
	1			41018.0469	x5F*	2.00		2.000
	Fe	9414.041		51461.6680	f5F	4.00	3.98E+06(35%)	12.700
	1			40842.1484	x5F*	3.00		2.000
*	Fe	9401.112		51228.5469	e7G	5.00	2.64E+06(21%)	7.800
	1			34039.5117	y5F*	4.00		7.700
	Fe	9372.897		31307.2422	z3F*	4.00	2.05E+04(13%)	
	1			20641.1094	b3F	4.00		
	Fe	9362.360		29056.3203	z5P*	3.00	7.66E+03(31%)	
	1			18378.1836	a3P	2.00		

* Revised Data
Transition Probabilities and Life-Times are from reference 5.

Author Index

☆ U.S. GOVERNMENT PRINTING OFFICE 1993 — 341-832/83033

NIST Technical Publications

Periodical

Journal of Research of the National Institute of Standards and Technology—Reports NIST research and development in those disciplines of the physical and engineering sciences in which the Institute is active. These include physics, chemistry, engineering, mathematics, and computer sciences. Papers cover a broad range of subjects, with major emphasis on measurement methodology and the basic technology underlying standardization. Also included from time to time are survey articles on topics closely related to the Institute's technical and scientific programs. Issued six times a year.

Nonperiodicals

Monographs—Major contributions to the technical literature on various subjects related to the Institute's scientific and technical activities.

Handbooks—Recommended codes of engineering and industrial practice (including safety codes) developed in cooperation with interested industries, professional organizations, and regulatory bodies.

Special Publications—Include proceedings of conferences sponsored by NIST, NIST annual reports, and other special publications appropriate to this grouping such as wall charts, pocket cards, and bibliographies.

Applied Mathematics Series—Mathematical tables, manuals, and studies of special interest to physicists, engineers, chemists, biologists, mathematicians, computer programmers, and others engaged in scientific and technical work.

National Standard Reference Data Series—Provides quantitative data on the physical and chemical properties of materials, compiled from the world's literature and critically evaluated. Developed under a worldwide program coordinated by NIST under the authority of the National Standard Data Act (Public Law 90-396). NOTE: The Journal of Physical and Chemical Reference Data (JPCRD) is published bimonthly for NIST by the American Chemical Society (ACS) and the American Institute of Physics (AIP). Subscriptions, reprints, and supplements are available from ACS, 1155 Sixteenth St., NW, Washington, DC 20056.

Building Science Series—Disseminates technical information developed at the Institute on building materials, components, systems, and whole structures. The series presents research results, test methods, and performance criteria related to the structural and environmental functions and the durability and safety characteristics of building elements and systems.

Technical Notes—Studies or reports which are complete in themselves but restrictive in their treatment of a subject. Analogous to monographs but not so comprehensive in scope or definitive in treatment of the subject area. Often serve as a vehicle for final reports of work performed at NIST under the sponsorship of other government agencies.

Voluntary Product Standards—Developed under procedures published by the Department of Commerce in Part 10, Title 15, of the Code of Federal Regulations. The standards establish nationally recognized requirements for products, and provide all concerned interests with a basis for common understanding of the characteristics of the products. NIST administers this program in support of the efforts of private-sector standardizing organizations.

Consumer Information Series—Practical information, based on NIST research and experience, covering areas of interest to the consumer. Easily understandable language and illustrations provide useful background knowledge for shopping in today's technological marketplace.

Order the **above** *NIST publications from: Superintendent of Documents, Government Printing Office, Washington, DC 20402.*

Order the **following** *NIST publications—FIPS and NISTIRs—from the National Technical Information Service, Springfield, VA 22161.*

Federal Information Processing Standards Publications (FIPS PUB)—Publications in this series collectively constitute the Federal Information Processing Standards Register. The Register serves as the official source of information in the Federal Government regarding standards issued by NIST pursuant to the Federal Property and Administrative Services Act of 1949 as amended, Public Law 89-306 (79 Stat. 1127), and as implemented by Executive Order 11717 (38 FR 12315, dated May 11, 1973) and Part 6 of Title 15 CFR (Code of Federal Regulations).

NIST Interagency Reports (NISTIR)—A special series of interim or final reports on work performed by NIST for outside sponsors (both government and non-government). In general, initial distribution is handled by the sponsor; public distribution is by the National Technical Information Service, Springfield, VA 22161, in paper copy or microfiche form.

U.S. Department of Commerce
National Institute of Standards and Technology
Gaithersburg, MD 20899